Energetics, epigenetics, and memory as acclimation strategies of marine bacteria in subzero brines

Georges Kanaan

A dissertation

submitted in partial fulfillment of the

requirements for the degree of

Doctor of Philosophy

University of Washington

2025

Reading Committee:

Jody W. Deming, Chair

John A. Baross

Randelle M. Bundy

Program Authorized to Offer Degree:

Oceanography

University of Washington

ABSTRACT

Energetic and epigenetic acclimation strategies of marine bacteria in subzero brines

Georges Kanaan

Chair of the Supervisory Committee:
Jody W. Deming

School of Oceanography

Memory is familiar to us all. Our memories structure our beings and inform how we respond to the present. The principle that memory alters an individual's response to a given stimulus structures the work conducted in this thesis. I ask: why do bacteria respond the way they do to environmental stressors in the Arctic? I set out to enable the study of memory in subzero brines and investigate its existence in a model sea-ice bacterium. As the Arctic transforms at an unprecedented pace, understanding memory in this ecosystem is urgent. Larger fluctuations in environmental conditions will select for organisms with well-suited acclimation mechanisms. Memory appears to be precisely such a mechanism, allowing organisms capable of encoding, storing, and recalling information about past conditions to be more fit in the face of change. Despite the diversity of functions, mechanisms, and timescales in bacterial memory, its ecological role remains obscure. Two Arctic ecosystems provide complementary natural laboratories to investigate the ecological function of memory: cryopeg brines and sea ice. Cryopeg brines are volumes of hypersaline subzero liquid water isolated in permafrost for millennia and relatively stable until the Anthropocene. Sea ice is shorter-lived and fluctuates significantly more. With respect to variability and timescale, they offer a natural contrast in which to study memory.

In Chapter 1, I reconstructed the environmental history of heterotrophic bacterial communities in cryopeg brines by developing a model relating cell density, enzyme kinetics, energetic requirements, and available energy. I estimated cell-specific metabolic rates to be higher than those in marine sediments despite lower temperatures, challenging expectations. This high energy cost suggests substantial investment in producing extracellular enzymes to liberate organic carbon and synthesizing protective compounds for cryoprotection

and osmoprotection. These results provide context for considering memory: if these bacteria possess memory of a more variable past, does that memory remain after 40,000 years of environmental stability? What are the implications for their capacity to acclimate as permafrost thaws? Such questions motivate an investigation of memory in these and related Arctic environments. The fluctuations experienced by sea ice, especially in a changing Arctic, make it a promising environment in which to begin searching for memory. In Chapter 2, I searched for bacterial memory in *Colwellia psychrerythraea* strain 34H, a model sea-ice bacterium. Culturing 34H in alternating salinity conditions showed acclimation to repeated stress evidenced by changes in growth rates and lag times, phenotypic evidence suggestive of bacterial memory. I used DNA sequencing to determine whether DNA methylation might serve as an underlying mechanism. DNA methylation clearly regulated gene expression in response to osmotic stress. However, DNA methylation did not clearly emerge as the mechanism for memory in 34H, though further investigation is warranted. Chapter 3 extended this work to the environment by studying DNA methylation patterns of entire sea-ice bacterial communities in situ. Comparing the thermally variable top ice with the more stable bottom ice, I found differential methylation across temperature and salinity gradients in various community members. DNA methylation served multiple roles: immune defense through restriction-modification systems, gene regulation across environmental gradients, and novel roles in prophage-host interactions. The abundance of orphan methyltransferases suggests that much of this methylation was serving purposes beyond classical immune defense. These chapters show the different acclimation mechanisms used by bacteria in subzero brines, from energetic strategies to memory. By understanding what allows bacteria to thrive in these extreme environments on Earth, we push the boundaries for what can be considered habitable, with implications for ice-bound brines on Europa, Enceladus, and Mars. This dissertation lays foundational work for further investigations of memory's ecological role in bacterial communities facing rapid environmental change.

TABLE OF CONTENTS

ACKNOWLEDGMENTS

I would like to thank my advisor and mentor Dr. Jody Deming who took in a young computer scientist wanting to do anything but the things he knew. She took a chance I could learn all the skills and knowledge to become a marine microbiologist. I had never seen a pipette before enrolling in the program, yet Jody believed in me. Her belief and support of me have been a constant throughout my PhD, without which I would not have completed this dissertation. Advising me first, she always supported the decisions I've made. In matters personal, professional, and scientific Jody's thoughts have always enriched my thought process. Her office has been a space for crazy ideas, exciting results, conversations about God, grammar lessons, and often comfort from the sadder parts of life. I am incredibly grateful to her for her compassion, time, energy, intellectual openness, knowledge, and humor. For the last 4 years and 4 months our weekly meetings have been the highlights of my week. Never shorter than an hour, many over three, these times have been awesome. I always leave more knowledgeable and more excited about science than I do coming in. Jody has nurtured my curiosity for the natural world. I was given the opportunity to perform field work which I dreamed of as an undergraduate student. My time in the Arctic has shown me unprecedented beauty and confronted me with unprecedented loss. I am now forever in love with the icy landscapes that float 3000 m above our ocean's seafloor. Jody has instilled in me a love and fascination for bacteria which has permeated my view of our planet and life. From the bacteria that fix nitrogen in symbiosis with the trees of our forests, to those which may exist in the oceans of Europa, they are everywhere doing so much out of sight and out of mind of so many on this microbial planet. Thank you, Jody, for believing in me.

I would be remiss if I did not acknowledge Dr. Jodi Young, who equally took a risk when co-advising my masters thesis and whose support allowed me to enroll in the program in the first place. Jodi's enthusiasm for my research and endeavors was crucial in the early years of my career as a scientist, and her lab provided a place to learn about the eukaryotic life within and around Antarctic ice. My committee members Dr. John Baross, Dr. Randelle Bundy, Dr. Baptiste Journeaux, and Dr. Drew Gorman-Lewis , have given me the trust and support to follow my interests and to get the most out of my time in graduate school. Dr. Georgy Manucharyan provided helpful insights as a member of my masters committee. I thank them all for their time, help, and support.

Shelly Carpenter and Dr. Zac Cooper welcomed me to the Deming ecosystem. Without Shelly's supervision in the lab, I would not have been able to learn the skills to perform the experiments or become an able microbiologist. Zac welcomed me to a city where I knew no one and showed me the ropes of being a graduate student when I needed it most. I'd like to extend my thanks to you both, and to the whole Deming ecosystem which in one way or another supported me and my work, with special thanks to Dr. Josephine Rapp and Dr. Max Showalter. Furthermore, I would like to thank Jackson Page-Roth and Audrey Moran, undergraduate students in the lab whose help and company was invaluable. Jackson's enthusiasm and perseverance allowed us to develop the Pioreactor method which generated high resolution optical density data. His ambition took us on a field expedition to Japan with Dr. Daiki Nomura, whom I thank for his hospitality.

I must also thank all those who have contributed to the science and to my training as a scientist. The faculty, graduate students, and staff of the School of Oceanography and the Astrobiology program who through talks, meetings, and workshops have created or contributed to opportunities for learning. I would specifically like to thank Dr. Ginger Armbrust and the members of the Center for Environmental Genomics for allowing me to sit-in on their lab meetings, for their statistical knowledge, and for their advice. I thank Dr. Deborah Kelley for the first scientific cruise I went on and showing me the beauty of hydrothermal vents. Thanks to the crew of the R/V *Thomas G. Thompson* for taking us there. The Astrobiology program was a unique opportunity to study our Universe. I am thankful for the experiences it has provided during the workshops and my research rotation,

especially our trip to New Mexico, and the time at the Apache Point Observatory which I hold very dearly in my heart. Thanks to Dr. Vikki Meadows for working to ensure the program's success and to secure funding for students and research rotations. The Astrobiology program is the reason I wanted to study at the University of Washington, and I am so glad it led me here.

Beyond the University of Washington, I am indebted to my collaborators at the University of Fairbanks, Dr. Go Iwahana and Dr. Hajo Eicken, and at Ames Research Center, Dr. Tori Hoehler, who made possible my work on bacterial energetics of cryopegs. Dr. Rika Anderson at Carleton College provided computer power for all the bioinformatics work and trusted me to lead one of her ROV dives at Axial seamount as a first-year graduate student. That experience was wonderful. Colleagues at the BEPSII Sea-Ice School gave me my first Arctic experience and taught me how to be a field sea-ice scientist. I will never forget coring my first ice core under the watchful eyes of Dr. CJ Mundy and Dr. Bruno Delille. Friends and colleagues at the University of Tromsø and the Norwegian Polar Institute continued that training during my first and second icebreaking cruises. For those opportunities, I thank Dr. Karley Campbell for inviting me aboard, and who as chief scientist trusted me to get the work done and in turn enabled me to do my work. I'd also like to thank Dr. Polona Itkin for her musings about snow and ice physics, Einar Eliasen for our games of chess, and the crew of the R/V *Kronprins Haakon*. I am also grateful for the wider sea-ice community which I have found to be an inviting and intellectually stimulating network. I am proud to be a part of it, and thankful for the collaborations and opportunities I've been provided. Thanks to Dr. Marc Neveu for his guidance and support during my astrobiology research rotation.

I've been fortunate to receive funding from the University of Washington Astrobiology Program, the College of the Environment, the School of Oceanography, the Gordon and Betty Moore Foundation, the Leo Maddox Foundation, and the National Aeronautics and Space Administration. Without their support none of this work would be possible.

Many educators have encouraged me through the years to pursue my passion for understanding how things work and why they exist the way they do. To all my teachers at the International College who saw in me a joy to learn, thank you. Special thanks to Nabih Fawaz and to Suheil Zarife, for an eternal love of math and biology. To the college professors who wrote letters of recommendation, introduced me to research, and cemented my love for science and engineering, thank you.

I would like to thank my friends and family for their support and love. My 2021 cohort of graduate students enriched my life at the university. My friends near and far have supported me as I undertake new hobbies, build my career, and "explore the intricacies of my strange mind" as Elaina said. Thank you to my friends in Seattle, Elaina, Mike, Kathy, Scott, Hannah, Kimberly, Jackson, Patrick, Ethan, Jess, and Ryan, who have listened, advised, scorned, imagined, and played with me. Thank you for tolerating all my lichen and tree facts. Thanks to my friends further away, Baby F, who through many hours of video games have gone through it all with me. Thank you to Daniel for making my posters more beautiful. Thanks to Fatou and GD for the voyage de la décennie.

Being away from my family has been the most challenging part of my graduate career. I was so privileged to meet a new cousin in Portland, and to get closer to an entire branch of my family that I did not know well. I am so thankful for you, the Passmans, Thropes, and Ghosseins — thank you for Thanksgiving, my favorite holiday. You brought family closer, especially you, Sadie, a train ride away. To the rest of my wonderfully large and close-knit cousins, great cousins, aunt, uncles, and grandparents, thank you for supporting me, I love you all.

A big hug to Kika, and the girls for showing me a different way to live, for the chance to teach, and for your love. To Yara for her culture, emotion, and purpose. To Pap for showing me how things work and answering my questions with thought and feeling. Thank you for coming to Seattle at the yearly lows. You've always nurtured my curiosity, helped me stay fit, and encouraged me to do what I love. À Mam pour ton amour inconditionnel, je t'aime.

Finally, thank you to the National Park Service for all those which it protects. The national parks have shown me the power of rivers, the reason for stress, the beauty of birds, the holiness of forests, and the awesomeness of bears. The Hoh rainforest in the Olympic National park has become one of my favorite places on our planet, and I appreciate its diversity and beauty. The coast has shown me the value of water. The wilderness has soothed my soul and inspires me to continue working to understand and conserve the wonders of our Universe.

DEDICATION

To all who have shaped me, be they people, pika, tree, or star.

INTRODUCTION

Memory is familiar to us all. We have intimate relationships with our memories which structure our beings. Often cherished, and sometimes dreaded, our memories elicit feeling and thought which is unique to our lived experiences, our life history. In response to an event or a stimulus, each of us may react differently in part due to past experiences which we recall, informing our actions in the present: due to memory. For example, should famous Lebanese singer Fairuz's 1970 hit song "Shady" start playing, I would fondly recall childhood memories of being driven to school in the morning, while someone else, having never heard it, would perhaps not react at all. The principle that memory alters an individual's response to a given stimulus structures many of the ideas motivating the work conducted in this thesis. Why do bacteria respond the way they do to certain environmental stressors?

Our relationship with the environment has become increasingly structured by memory. In fact, the study of memory between people and the environment has seen increased interest in the last decades (Teichler, 2024). Climate change forces us to contemplate the loss of environments and species which may persist exclusively in our memories (Craps et al., 2018; Jue, 2025). As the Arctic transforms four times faster than any other region on Earth (IPCC, 2022), memory in this ecosystem serves as a repository of information about a valuable past. Collectively, memory processes within the systems or organisms that compose an ecosystem could represent untapped potential to understand this environment past, present, and future.

As we observe the Arctic changing, with larger fluctuations becoming more frequent, additional interest in memory is warranted. Larger fluctuations in environmental conditions will select for organisms with well-suited acclimation mechanisms. Memory appears to be precisely such a mechanism (Lambert & Kussell, 2014; Mitchell et al., 2009). Environmental variability and uncertainty create conditions where organisms capable of encoding, storing, and recalling information about past conditions gain significant adaptive advantages. As sea ice and permafrost in the Arctic change rapidly and fundamentally, understanding the role that memory plays in structuring the ecosystem's response to these changes is urgent. Where better to look for memory than in some of the oldest and the most abundant organisms on Earth, the Bacteria?

At first glance, one might think it absurd that a single-celled organism is capable of memory, but the scientific literature suggests otherwise. Memory is so inherent to us that we could be forgiven to think it a purely human trait. Color vision is intrinsic to our experience, yet we know it is a trait shared with other animals (Gerl & Morris, 2008). I invite the reader to think of memory, or even consciousness, as simply another biological trait upon which evolution acts through natural selection.

The definition of memory is the subject of numerous philosophical essays tying into theory of mind and dividing memory into different, often field-specific, types (Bailey et al., 1996; Clark, 2005; Colaço, 2022; Littman & Singh, 2007; Malcolm, 1983; Mathis & Ackermann, 2017; Zemach, 1968; Zlotnik & Vansintjan, 2019). For my purposes, I define memory as a mechanism capable of encoding information, storing it intrinsically, and recalling it to influence present behavior and future outcomes. As this work addresses memory in the context of acclimation, I define acclimation as cellular processes resulting in a more fit response of the organism to the environment. I acknowledge that this definition of memory is broad; however, as Colaço (2022) argues, I believe a broad definition serves its purpose well in the context of posing hypotheses for testing, as is the case in this work. In other cases, literature cited herein may use the term "memory" but not adopt this definition. The environmental science literature adopts different definitions of memory yet repeatedly shows that memory plays an important role in understanding the functioning of life on our planet.

The concept of memory appears widely across the natural sciences. Atmospheric scientists refer to long-term feedback loops as memory (Colin & Sherwood, 2021; Li et al., 2025; Manucharyan et al., 2017; Vyushin & Kushner, 2009), showing how information encoded in the physical states of the atmosphere and ocean can influence longer term patterns in both. Li et al. (2025) demonstrate a coupling between sea surface temperature and atmospheric memory as defined mathematically. Similarly, the climate science field often refers to ocean memory as the "persistence of ocean conditions" (Shi et al., 2022), which has also been defined mathematically (Khatri et al., 2024; Woods, 1981). It is in biological systems that memory processes begin to fall into my working definition, and perhaps closer to an intuitive understanding of memory.

Animals have memory similar to ours; in fact, memory extends to insects as well (Collett et al., 2013; Crystal, 2010; Eichler et al., 2017; Hourcade et al., 2009; Lind et al., 2015; Mendl et al., 2001). Plants also have memory, as argued in the emphatically titled "Yes, plants do have memory" (Galviz et al., 2020) and in related literature showing memory-based adaptation strategies to drought, temperature, and osmotic stress (Abid et al., 2018; Abramson & Calvo, 2018; Amaral et al., 2020; Dobránszki et al., 2024; Friedrich et al., 2019; Hilker & Schmülling, 2019). Corals can remember stress experienced a decade ago (Hackerott et al., 2021). Algae have also shown evidence of memory. *Chlamydomonas reinhardtii* remembers nitrogen stress (Mikulski & Santos-Aberturas, 2022). *Nannochloropsis oceanica* possess a potentially ubiquitous short-term photoprotective memory system, advantageous when dealing with variable light levels (Short et al., 2023). Light related memory systems have also been shown in *Chlamydomonas reinhardtii* (Laroussi et al., 2024). In many microalgae, epigenetic mechanisms are suggested to play an important memory role (Bacova et al., 2020). It seems that wherever scientists have searched for it, systems recognizable as memory have been uncovered, from long-term feedback loops in physical systems to epigenetic memories of stress in unicellular alga. This ubiquity has motivated my pursuit of memory in Bacteria.

Indeed, memory extends to the Bacteria (Lyon, 2015; Mitchell et al., 2009). Memory in bacteria is a well-studied field (Riber & Hansen, 2021; C.-Y. Yang et al., 2020; J. Yang et al., 2025) that has produced specialized frameworks to quantify history-dependent behavior (Wolf et al., 2008) and different forms of memory (Mitchell & Pilpel, 2011; Tagkopoulos et al., 2008). One well-studied example involves persister cells. Persister cells are a subpopulation of cells that have temporarily acquired a certain phenotype, typically antibiotic resistance (Fisher et al., 2017; Kussell et al., 2005; Lewis, 2010; Miyaue et al., 2018). Miyaue et al. (2018) showed, across a wide diversity of bacteria, that the persister cell phenotype remains for many generations after exposure to the antibiotic, harboring genetic memory of the antibiotic stress; other types of antibiotic stress memory also exist (Mathis & Ackermann, 2017). Another well-studied example is chemotaxis, the ability of a bacterium to move along a chemical gradient, which requires memory. To determine the gradient's direction, the bacterium must be able to determine the difference between the concentrations at its current location and a previous location, thus requiring it to store information about the past (Gosztolai & Barahona, 2020; Lan & Tu, 2016; Mayo & Soto, 2025; Vladimirov & Sourjik, 2009).

Memory is also used by bacteria to better respond to stress, as in the cases of *Prochlorococcus* with light (Coe et al., 2021), *Bacillus subtilis* with heat (Runde et al., 2014), and *Escherichia coli* with a diversity of stresses including heat and antibiotics (Govers et al., 2018). Memory enables anticipation in *E. coli* (Mitchell et al., 2009), for example, by priming its carbohydrate metabolism (Tagkopoulos et al., 2008). Memory allows bacteria to follow environmental cues, such as tuning their circadian rhythms to different predictable, recurring environmental signals called zeitgebers (Eelderink-Chen et al., 2021). Cells can leverage information encoded in memory to make strategic decisions, such as adopting different phenotypes in response to the environment, or regulating re-integration of prophages (Bhattacharyya et al., 2023; Norman et al., 2013; Ronin et al., 2017; Vatareck et al., 2025; J. Yang et al., 2025).

Some bacterial memories can be inherited. The memory of a surface type has been shown to be inherited over multiple generation of bacteria, allowing cells to be primed to return to previously experienced surface types (Lee et al., 2018). Epigenetic mechanisms for memory inheritance vary; they include DNA methylation and cytoplasmic protein concentrations (Casadesús & D'Ari, 2002; Hu et al., 2018; Lambert & Kussell, 2014; J. Yang et al., 2025). Heritability can grant fitness benefits in fluctuating environments (Lambert & Kussell, 2014; Vermeersch et al., 2022), making memory particularly relevant when considering bacterial acclimation on multi-generational timescales.

Bacterial memory can exist at different scales, both in space and time. Bacterial biofilms encode spatial information through membrane potentials (C.-Y. Yang et al., 2020). Memory extends to spores, allowing them to respond to lower nutrient conditions (Wang et al., 2015). Bacterial communities retain a memory of ecological conditions (Letourneau et al., 2022) and, vice versa; they alter their environment's history, with the effects persisting and thus forming a memory of their passing and structuring the future (Gajrani et al., 2025; Steffen et al., 2018). Bacterial memory can act on timescales as short as a second (Jung et al., 2024) and as long as many months (Coe et al., 2021). Such long-term memory makes considering seasonal, and perhaps even yearly timescales, relevant.

Despite the diversity of functions, mechanisms, and timescales in bacterial memory, its ecological role remains obscure. The high seasonality that characterizes the Arctic provides us the opportunity to investigate the ecological role of memory. Furthermore, as the Arctic continues to change and physical fluctuations grow more extreme, climate change poses an urgent need to understand bacterial memory. Bacteria fundamentally structure their environment by driving large-scale biogeochemical cycles (Falkowski et al., 2008). This fundamental role remains true in sea ice where they alter nutrient cycling, contribute to the food web, and determine the habitability of their environment (Boetius et al., 2015; Krembs et al., 2011; Steffen et al., 2018). Understanding memory in Arctic bacteria is understanding the resilience or fragility of their communities in the face of change; it is understanding how the Arctic will change and what information will be lost.

Two ecosystems of the Arctic provide compelling environments to begin the study of ecological memory. Cryopegs are layers of relic marine sediments and seawater-derived brines which lie below the active layer of permafrost. Bacterial communities contained in cryopegs have been isolated from the surface environment for millennia (Iwahana et al., 2021). During that time, cryopegs have experienced few fluctuations in any physical parameter until the Anthropocene, during which they are beginning to experience less stable conditions as the permafrost thaws (Morgado et al., 2024). The change from stable conditions to variable conditions offers multiple opportunities. Have these communities retained a millennia-old memory of a fluctuating past? Will that memory allow them to acclimate to these new perturbations? If the community does not carry memory of its distant or closer past, how does that deficiency affect its capacity to acclimate?

My investigations are enriched by the existence of an ecosystem offering a natural counterpart to cryopegs. Sea ice is shorter-lived and fluctuates significantly more. Yet much like cryopeg, sea ice is also encased in ice, derived from seawater, and fundamentally structured by temperature. Unlike cryopeg, sea ice typically persists for less than a year, and during that time fluctuates in environmental parameters. With respect to variability and timescale, sea ice and cryopeg complement each other, offering a natural laboratory in which to study memory. Do bacteria in sea ice store memory of stress? How does a memory-capable versus memory-deficient community acclimate to variability in temperature and osmotic stress inherent to sea ice?

To begin addressing these questions, the nature of these environments, and the ways in which they do or do not contrast, need to be understood. While sea ice is well studied (Babin et al., 2025), interest in cryopeg is

relatively recent and studies more limited. However, recent comparative work between these environments has characterized the biodiversity and physiological adaptations of cryopeg communities (Cooper et al., 2019; Gilichinsky et al., 2003, 2005; Zhong et al., 2020). One area crucial to the study of memory and which remained unknown prior to this work was the microbiological history of the cryopeg. In Chapter 1, I address this knowledge gap by reconstructing a probable trajectory for bacterial cell densities and energetic requirements over time. To accomplish this goal, I developed a model that relates enzyme kinetics, energetic requirements, and available energy to cell density and organic carbon. By inputting information about model bacteria and physical conditions over time, one can estimate the heterotrophic community's history. The result of this work provides a foundational context for future studies of the possible memory mechanisms carried by these unique bacterial communities.

For immediately feasible memory investigations, the large body of work on sea-ice bacteria and their environment makes sea-ice communities better suited than cryopeg. In Chapter 2, I search for memory in a model sea-ice bacterium, *Colwellia psychrerythraea* strain 34H (Boetius et al., 2015), under alternating salinity conditions. Inspired by Coe et al. (2021) and others (Vermeersch et al., 2022), I designed this experiment to test for phenotypic evidence of memory in acclimation to salinity stress, examining changes in growth rate and lag time. DNA sequencing technologies were then used to determine whether DNA methylation might be an underlying mechanism for memory in this bacterium. Chapter 3 extends Chapter 2 to the environment. In this study, I compared the DNA methylation patterns between the thermally more variable top ice, strongly influenced by atmospheric fluctuations, and the more stable bottom ice at the ice-ocean interface. Using the same techniques applied to the whole bacterial community, I could then examine differences in DNA methylation across many organisms. While attributing observed patterns exclusively to memory was more difficult, this work underscores the role of a short-term acclimation mechanism and possible ecological functions of memory.

Much like memory, the origins of life and the ideas of habitability permeate the work presented in this thesis. Fundamentally, studying memory sums to understanding yet another strategy adopted by life to meet environmental challenges. In that sense, this work is closely tied to ideas of habitability. By understanding what allows bacteria to thrive in different subzero brines here on Earth, we push the boundaries for what can be considered an extraterrestrial habitable environment. Chapter 1 contributes to the growing body of work showing life's adaptations to the energetic edge (Hoehler & Jørgensen, 2013; Lever et al., 2015). This type of work reduces the energetic burden we place on an environment to classify it as habitable (Hoehler, 2007). Chapters 2 and 3 show how DNA methylation, an early-evolved mechanism (Blow et al., 2016; Iyer et al., 2011; Jurkowski & Jeltsch, 2011), may contribute to acclimation to stress, both generally and specifically under fluctuating conditions. For example, analogous conditions to the fluctuations in temperature and salinity experienced in sea-ice brine could take place as a volume of brine is convected within the ice sheet of an icy world. Understanding DNA methylation is thus relevant not only to the acclimation strategies of early life on Earth, but also to works exploring the origins of life and the habitability of other solar bodies. DNA methylation may have been preceded by RNA methylation (Rana & Ankri, 2016), which could have acted as an intermediary to the evolution of DNA (Poole et al., 2000). In the context of prebiotic chemistry, methylation is yet another chemical process for encoding prebiotic information, necessary for the formation of more complex life (Chatterjee & Yadav, 2019; Schneider et al., 2018). DNA methylation as it exists today is a complex process requiring sophisticated enzymes, cofactors, and equally complex substrate, unlikely to be present in its current form in a prebiotic world. However, insight into its ecological function and phylogeny allows us to better understand the evolutionary steps which led to its presence on early Earth and the ecology of ancient organisms.

REFERENCES

Abid, M., Hakeem, A., Shao, Y., Liu, Y., Zahoor, R., Fan, Y., Suyu, J., Ata-Ul-Karim, S. T., Tian, Z., Jiang, D., Snider, J. L., & Dai, T. (2018). Seed osmopriming invokes stress memory against post-germinative drought stress in wheat (Triticum aestivum L.). *Environmental and Experimental Botany*, *145*, 12–20. https://doi.org/10.1016/j.envexpbot.2017.10.002

Abramson, C. I., & Calvo, P. (2018). Memory and learning in plants. *Signaling and Communication in Plants*, 35–49. https://doi.org/10.1007/978-3-319-75596-0_3

Amaral, M. N. do, Arge, L. W. P., Auler, P. A., Rossatto, T., Milech, C., Magalhães, A. M. de, & Braga, E. J. B. (2020). Long-term transcriptional memory in rice plants submitted to salt shock. *Planta*, *251*(6), 111. https://doi.org/10.1007/s00425-020-03397-z

Babin, M., Deming, J. W., Maréchal, E., Rapp, J. Z., Rysgaard, S., & Vancoppenolle, M. (2025). Life in the frozen ocean. *Annual Review of Marine Science*. https://doi.org/10.1146/annurev-marine-032123-025316

Bacova, R., Kolackova, M., Klejdus, B., Adam, V., & Huska, D. (2020). Epigenetic mechanisms leading to genetic flexibility during abiotic stress responses in microalgae: A review. *Algal Research*, *50* (IntechOpen February 17th 2016), 101999. https://doi.org/10.1016/j.algal.2020.101999

Bailey, C. H., Bartsch, D., & Kandel, E. R. (1996). Toward a molecular definition of long-term memory storage. *Proceedings of the National Academy of Sciences*, *93*(24), 13445–13452. https://doi.org/10.1073/pnas.93.24.13445

Bhattacharyya, S., Bhattarai, N., Pfannenstiel, D. M., Wilkins, B., Singh, A., & Harshey, R. M. (2023). A heritable iron memory enables decision-making in Escherichia coli. *Proceedings of the National Academy of Sciences*, *120*(48), e2309082120. https://doi.org/10.1073/pnas.2309082120

Blow, M. J., Clark, T. A., Daum, C. G., Deutschbauer, A. M., Fomenkov, A., Fries, R., Froula, J., Kang, D. D., Malmstrom, R. R., Morgan, R. D., Posfai, J., Singh, K., Visel, A., Wetmore, K., Zhao, Z., Rubin, E. M., Korlach, J., Pennacchio, L. A., & Roberts, R. J. (2016). The Epigenomic Landscape of Prokaryotes. *PLoS Genetics*, *12*(2), e1005854. https://doi.org/10.1371/journal.pgen.1005854

Boetius, A., Anesio, A. M., Deming, J. W., Mikucki, J. A., & Rapp, J. Z. (2015). Microbial ecology of the cryosphere: sea ice and glacial habitats. *Nature Reviews Microbiology*, *13*(11), 677–690. https://doi.org/10.1038/nrmicro3522

Casadesús, J., & D'Ari, R. (2002). Memory in bacteria and phage. *BioEssays*, *24*(6), 512–518. https://doi.org/10.1002/bies.10102

Chatterjee, S., & Yadav, S. (2019). The origin of prebiotic information system in the peptide/RNA World: a simulation model of the evolution of translation and the genetic code. *Life*, *9*(1), 25. https://doi.org/10.3390/life9010025

Clark, A. (2005). Intrinsic content, active memory and the extended mind. *Analysis*, *65*(1), 1–11. https://doi.org/10.1093/analys/65.1.1

Coe, A., Biller, S. J., Thomas, E., Boulias, K., Bliem, C., Arellano, A., Dooley, K., Rasmussen, A. N., LeGault, K., O'Keefe, T. J., Stover, S., Greer, E. L., & Chisholm, S. W. (2021). Coping with darkness: The adaptive response of marine picocyanobacteria to repeated light energy deprivation. *Limnology and Oceanography*, *66*(9), 3300–3312. https://doi.org/10.1002/lno.11880

Colaço, D. (2022). What counts as a memory? Definitions, hypotheses, and "Kinding in progress." *Philosophy of Science*, *89*(1), 89–106. https://doi.org/10.1017/psa.2021.14

Colin, M., & Sherwood, S. C. (2021). Atmospheric convection as an unstable predator–prey process with memory. *Journal of the Atmospheric Sciences*, *78*(11), 3781–3797. https://doi.org/10.1175/jas-d-20-0337.1

Collett, M., Chittka, L., & Collett, T. S. (2013). Spatial memory in insect navigation. *Current Biology*, *23*(17), R789–R800. https://doi.org/10.1016/j.cub.2013.07.020

Cooper, Z. S., Rapp, J. Z., Carpenter, S. D., Iwahana, G., Eicken, H., & Deming, J. W. (2019). Distinctive microbial communities in subzero hypersaline brines from Arctic coastal sea ice and rarely sampled cryopegs. *FEMS Microbiology Ecology*, *95*(12), fiz166. https://doi.org/10.1093/femsec/fiz166

Craps, S., Crownshaw, R., Wenzel, J., Kennedy, R., Colebrook, C., & Nardizzi, V. (2018). Memory studies and the Anthropocene: A roundtable. *Memory Studies*, *11*(4), 498–515. https://doi.org/10.1177/1750698017731068

Crystal, J. D. (2010). Episodic-like memory in animals. *Behavioural Brain Research*, *215*(2), 235–243. https://doi.org/10.1016/j.bbr.2010.03.005

Dobránszki, J., Agius, D. R., Berger, M. M. J., Moschou, P. N., Gallusci, P., & Martinelli, F. (2024). Plant memory and communication of encounters. *Trends in Plant Science*, *30*(2), 199–212. https://doi.org/10.1016/j.tplants.2024.09.012

Eelderink-Chen, Z., Bosman, J., Sartor, F., Dodd, A. N., Kovács, Á. T., & Merrow, M. (2021). A circadian clock in a nonphotosynthetic prokaryote. *Science Advances*, *7*(2), eabe2086. https://doi.org/10.1126/sciadv.abe2086

Eichler, K., Li, F., Litwin-Kumar, A., Park, Y., Andrade, I., Schneider-Mizell, C. M., Saumweber, T., Huser, A., Eschbach, C., Gerber, B., Fetter, R. D., Truman, J. W., Priebe, C. E., Abbott, L. F., Thum, A. S., Zlatic, M., & Cardona, A. (2017). The complete connectome of a learning and memory centre in an insect brain. *Nature*, *548*(7666), 175–182. https://doi.org/10.1038/nature23455

Falkowski, P. G., Fenchel, T., & Delong, E. F. (2008). The microbial engines that drive Earth's biogeochemical cycles. *Science*, *320*(5879), 1034–1039. https://doi.org/10.1126/science.1153213

Fisher, R. A., Gollan, B., & Helaine, S. (2017). Persistent bacterial infections and persister cells. *Nature Reviews Microbiology*, *15*(8), 453–464. https://doi.org/10.1038/nrmicro.2017.42

Friedrich, T., Faivre, L., Bäurle, I., & Schubert, D. (2019). Chromatin-based mechanisms of temperature memory in plants. *Plant, Cell & Environment*, *42*(3), 762–770. https://doi.org/10.1111/pce.13373

Gajrani, S., Ye, X., & Ratzke, C. (2025). Environment-mediated interactions cause an externalized and collective memory in bacteria. *The ISME Journal*, *19*(1), wraf173. https://doi.org/10.1093/ismejo/wraf173

Galviz, Y. C. F., Ribeiro, R. V., & Souza, G. M. (2020). Yes, plants do have memory. *Theoretical and Experimental Plant Physiology*, *32*(3), 195–202. https://doi.org/10.1007/s40626-020-00181-y

Gerl, E. J., & Morris, M. R. (2008). The causes and consequences of color vision. *Evolution: Education and Outreach*, *1*(4), 476–486. https://doi.org/10.1007/s12052-008-0088-x

Gilichinsky, D., Rivkina, E., Bakermans, C., Shcherbakova, V., Petrovskaya, L., Ozerskaya, S., Ivanushkina, N., Kochkina, G., Laurinavichuis, K., Pecheritsina, S., Fattakhova, R., & Tiedje, J. M. (2005). Biodiversity of cryopegs in permafrost. *FEMS Microbiology Ecology*, *53*(1), 117–128. https://doi.org/10.1016/j.femsec.2005.02.003

Gilichinsky, D., Rivkina, E., Shcherbakova, V., Laurinavichuis, K., & Tiedje, J. (2003). Supercooled water brines within permafrost – an unknown ecological niche for microorganisms: a model for astrobiology. *Astrobiology*, *3*(2), 331–341. https://doi.org/10.1089/153110703769016424

Gosztolai, A., & Barahona, M. (2020). Cellular memory enhances bacterial chemotactic navigation in rugged environments. *Communications Physics*, *3*(1), 47. https://doi.org/10.1038/s42005-020-0312-8

Govers, S. K., Mortier, J., Adam, A., & Aertsen, A. (2018). Protein aggregates encode epigenetic memory of stressful encounters in individual Escherichia coli cells. *PLoS Biology*, *16*(8), e2003853. https://doi.org/10.1371/journal.pbio.2003853

Hackerott, S., Martell, H. A., & Eirin-Lopez, J. M. (2021). Coral environmental memory: causes, mechanisms, and consequences for future reefs. *Trends in Ecology & Evolution*, *36*(11), 1011–1023. https://doi.org/10.1016/j.tree.2021.06.014

Hilker, M., & Schmülling, T. (2019). Stress priming, memory, and signalling in plants. *Plant, Cell & Environment*, *42*(3), 753–761. https://doi.org/10.1111/pce.13526

Hoehler, T. M. (2007). An energy balance concept for habitability. *Astrobiology*, *7*(6), 824–838. https://doi.org/10.1089/ast.2006.0095

Hoehler, T. M., & Jørgensen, B. B. (2013). Microbial life under extreme energy limitation. *Nature Reviews Microbiology*, *11*(2), 83–94. https://doi.org/10.1038/nrmicro2939

Hourcade, B., Perisse, E., Devaud, J.-M., & Sandoz, J.-C. (2009). Long-term memory shapes the primary olfactory center of an insect brain. *Learning & Memory*, *16*(10), 607–615. https://doi.org/10.1101/lm.1445609

Hu, L., Xiao, P., Jiang, Y., Dong, M., Chen, Z., Li, H., Hu, Z., Lei, A., & Wang, J. (2018). Transgenerational epigenetic inheritance under environmental stress by genome-wide DNA methylation profiling in Cyanobacterium. *Frontiers in Microbiology*, *9*, 1479. https://doi.org/10.3389/fmicb.2018.01479

IPCC. (2022). *The Ocean and Cryosphere in a Changing Climate*. 447–588. https://doi.org/10.1017/9781009157964.013

Iwahana, G., Cooper, Z. S., Carpenter, S. D., Deming, J. W., & Eicken, H. (2021). Intra-ice and intra-sediment cryopeg brine occurrence in permafrost near Utqiaġvik (Barrow). *Permafrost and Periglacial Processes*, *32*(3), 427–446. https://doi.org/10.1002/ppp.2101

Iyer, L. M., Abhiman, S., & Aravind, L. (2011). Natural history of eukaryotic DNA methylation systems. *Progress in Molecular Biology and Translational Science*, *101*, 25–104. https://doi.org/10.1016/b978-0-12-387685-0.00002-0

Jue, M. (2025). Ocean memory in abalone stories of the Anthropocene. *Elem Sci Anth*, *13*(1). https://doi.org/10.1525/elementa.2025.00045

Jung, W., Chen, T.-Y., Santiago, A. G., & Chen, P. (2024). Memory effects of transcription regulator–DNA interactions in bacteria. *Proceedings of the National Academy of Sciences*, *121*(41), e2407647121. https://doi.org/10.1073/pnas.2407647121

Jurkowski, T. P., & Jeltsch, A. (2011). On the evolutionary origin of eukaryotic DNA methyltransferases and Dnmt2. *PLoS ONE*, *6*(11), e28104. https://doi.org/10.1371/journal.pone.0028104

Khatri, H., Williams, R. G., Woollings, T., & Smith, D. M. (2024). An ocean memory perspective: disentangling atmospheric control of decadal variability in the north Atlantic Ocean. *Geophysical Research Letters*, *51*(20). https://doi.org/10.1029/2024gl110333

Krembs, C., Eicken, H., & Deming, J. W. (2011). Exopolymer alteration of physical properties of sea ice and implications for ice habitability and biogeochemistry in a warmer Arctic. *Proceedings of the National Academy of Sciences*, *108*(9), 3653–3658. https://doi.org/10.1073/pnas.1100701108

Kussell, E., Kishony, R., Balaban, N. Q., & Leibler, S. (2005). Bacterial persistence. *Genetics*, *169*(4), 1807–1814. https://doi.org/10.1534/genetics.104.035352

Lambert, G., & Kussell, E. (2014). Memory and fitness optimization of bacteria under fluctuating environments. *PLoS Genetics*, *10*(9), e1004556. https://doi.org/10.1371/journal.pgen.1004556

Lan, G., & Tu, Y. (2016). Information processing in bacteria: memory, computation, and statistical physics: a key issues review. *Reports on Progress in Physics*, *79*(5), 052601. https://doi.org/10.1088/0034-4885/79/5/052601

Laroussi, T., Jarrahi, M., & Amselem, G. (2024). Short-term memory effects in the phototactic behavior of microalgae. *Soft Matter*, *20*(19), 3996–4006. https://doi.org/10.1039/d3sm01628e

Lee, C. K., Anda, J. de, Baker, A. E., Bennett, R. R., Luo, Y., Lee, E. Y., Keefe, J. A., Helali, J. S., Ma, J., Zhao, K., Golestanian, R., O'Toole, G. A., & Wong, G. C. L. (2018). Multigenerational memory and adaptive adhesion in early bacterial biofilm communities. *Proceedings of the National Academy of Sciences*, *115*(17), 4471–4476. https://doi.org/10.1073/pnas.1720071115

Letourneau, J., Holmes, Z. C., Dallow, E. P., Durand, H. K., Jiang, S., Carrion, V. M., Gupta, S. K., Mincey, A. C., Muehlbauer, M. J., Bain, J. R., & David, L. A. (2022). Ecological memory of prior nutrient exposure in the human gut microbiome. *The ISME Journal*, *16*(11), 2479–2490. https://doi.org/10.1038/s41396-022-01292-x

Lever, M. A., Rogers, K. L., Lloyd, K. G., Overmann, J., Schink, B., Thauer, R. K., Hoehler, T. M., & Jørgensen, B. B. (2015). Life under extreme energy limitation: a synthesis of laboratory- and field-based investigations. *FEMS Microbiology Reviews*, *39*(5), 688–728. https://doi.org/10.1093/femsre/fuv020

Lewis, K. (2010). Persister cells. *Microbiology*, *64*(1), 357–372. https://doi.org/10.1146/annurev.micro.112408.134306

Li, L., Lee, S., & Feldstein, S. B. (2025). Atmospheric memory and implications to sea surface temperature variability forced by the atmosphere. *Climate Dynamics*, *63*(10), 381. https://doi.org/10.1007/s00382-025-07884-5

Lind, J., Enquist, M., & Ghirlanda, S. (2015). Animal memory: A review of delayed matching-to-sample data. *Behavioural Processes*, *117*, 52–58. https://doi.org/10.1016/j.beproc.2014.11.019

Littman, D. R., & Singh, H. (2007). Asymmetry and immune memory. *Science*, *315*(5819), 1673–1674. https://doi.org/10.1126/science.1141184

Lyon, P. (2015). The cognitive cell: bacterial behavior reconsidered. *Frontiers in Microbiology*, *6*, 264. https://doi.org/10.3389/fmicb.2015.00264

Malcolm, N. (1983). *Causal Theories of Mind*. https://doi.org/10.1515/9783110843828.197

Manucharyan, G. E., Thompson, A. F., & Spall, M. A. (2017). Eddy memory mode of multidecadal variability in residual-mean ocean circulations with application to the Beaufort gyre. *Journal of Physical Oceanography*, *47*(4), 855–866. https://doi.org/10.1175/jpo-d-16-0194.1

Mathis, R., & Ackermann, M. (2017). Asymmetric cellular memory in bacteria exposed to antibiotics. *BMC Evolutionary Biology*, *17*(1), 73. https://doi.org/10.1186/s12862-017-0884-4

Mayo, M., & Soto, R. (2025). Bacterial chemotaxis considering memory effects. *Physical Review E*, *111*(5), L052402. https://doi.org/10.1103/physreve.111.l052402

Mendl, M., Burman, O., Laughlin, K., & Paul, E. (2001). Animal memory and animal welfare. *Animal Welfare*, *10*(S1), S141–S159. https://doi.org/10.1017/s0962728600023587

Mikulski, P., & Santos-Aberturas, J. (2022). *Chlamydomonas reinhardtii* exhibits stress memory in the accumulation of triacylglycerols induced by nitrogen deprivation. *Plant-Environment Interactions*, *3*(1), 10–15. https://doi.org/10.1002/pei3.10069

Mitchell, A., & Pilpel, Y. (2011). A mathematical model for adaptive prediction of environmental changes by microorganisms. *Proceedings of the National Academy of Sciences*, *108*(17), 7271–7276. https://doi.org/10.1073/pnas.1019754108

Mitchell, A., Romano, G. H., Groisman, B., Yona, A., Dekel, E., Kupiec, M., Dahan, O., & Pilpel, Y. (2009). Adaptive prediction of environmental changes by microorganisms. *Nature*, *460*(7252), 220–224. https://doi.org/10.1038/nature08112

Miyaue, S., Suzuki, E., Komiyama, Y., Kondo, Y., Morikawa, M., & Maeda, S. (2018). Bacterial memory of persisters: bacterial persister cells can retain their phenotype for days or weeks after withdrawal from colony–biofilm culture. *Frontiers in Microbiology*, *9*, 1396. https://doi.org/10.3389/fmicb.2018.01396

Morgado, A. M. O., Rocha, L. A. M., Cartwright, J. H. E., & Cardoso, S. S. S. (2024). Osmosis drives explosions and methane release in Siberian permafrost. *Geophysical Research Letters*, *51*(18). https://doi.org/10.1029/2024gl108987

Norman, T. M., Lord, N. D., Paulsson, J., & Losick, R. (2013). Memory and modularity in cell-fate decision making. *Nature*, *503*(7477), 481–486. https://doi.org/10.1038/nature12804

Poole, A., Penny, D., & Sjöberg, B.-M. (2000). Methyl-RNA: an evolutionary bridge between RNA and DNA? *Chemistry & Biology*, *7*(12), R207–R216. https://doi.org/10.1016/s1074-5521(00)00042-9

Rana, A. K., & Ankri, S. (2016). Reviving the RNA world: an insight into the appearance of RNA methyltransferases. *Frontiers in Genetics*, *7*, 99. https://doi.org/10.3389/fgene.2016.00099

Riber, L., & Hansen, L. H. (2021). Epigenetic memories: the hidden drivers of bacterial persistence? *Trends in Microbiology*, *29*(3), 190–194. https://doi.org/10.1016/j.tim.2020.12.005

Ronin, I., Katsowich, N., Rosenshine, I., & Balaban, N. Q. (2017). A long-term epigenetic memory switch controls bacterial virulence bimodality. *eLife*, *6*, e19599. https://doi.org/10.7554/elife.19599

Runde, S., Molière, N., Heinz, A., Maisonneuve, E., Janczikowski, A., Elsholz, A. K. W., Gerth, U., Hecker, M., & Turgay, K. (2014). Thiol oxidation in protein aggregate formation. *Molecular Microbiology*, *91*(5), 1036–1052. https://doi.org/10.1111/mmi.12521

Schneider, C., Becker, S., Okamura, H., Crisp, A., Amatov, T., Stadlmeier, M., & Carell, T. (2018). Noncanonical RNA nucleosides as molecular fossils of an early Earth—generation by prebiotic methylations and carbamoylations. *Angewandte Chemie International Edition*, *57*(20), 5943–5946. https://doi.org/10.1002/anie.201801919

Shi, H., Jin, F.-F., Wills, R. C. J., Jacox, M. G., Amaya, D. J., Black, B. A., Rykaczewski, R. R., Bograd, S. J., García-Reyes, M., & Sydeman, W. J. (2022). Global decline in ocean memory over the 21st century. *Science Advances*, *8*(18), eabm3468. https://doi.org/10.1126/sciadv.abm3468

Short, A., Fay, T. P., Crisanto, T., Mangal, R., Niyogi, K. K., Limmer, D. T., & Fleming, G. R. (2023). Kinetics of the xanthophyll cycle and its role in photoprotective memory and response. *Nature Communications*, *14*(1), 6621. https://doi.org/10.1038/s41467-023-42281-8

Steffen, K. R., Epshteyn, Y., Zhu, J., Bowler, M. J., Deming, J. W., & Golden, K. M. (2018). Network modeling of fluid transport through sea ice with entrained exopolymeric substances. *Multiscale Modeling & Simulation*, *16*(1), 106–124. https://doi.org/10.1137/17m1117513

Tagkopoulos, I., Liu, Y.-C., & Tavazoie, S. (2008). Predictive behavior within microbial genetic networks. *Science*, *320*(5881), 1313–1317. https://doi.org/10.1126/science.1154456

Teichler, H. (2024). Transoceanic Memory (Studies): Oceans as mode, method and material. *Memory Studies Review*, *1*(1), 76–92. https://doi.org/10.1163/29498902-20240006

Vatareck, E., Rick, T., Gomez, N. O., Bandyopadhyay, A., Kramer, J., Strunin, D., Erdmann, J., Hartmann, O., Alpers, K., Boedeker, C., Steffen, A., Sieben, C., Zhao, G., Tomasch, J., & Häussler, S. (2025). Epigenetic cellular memory in Pseudomonas aeruginosa generates phenotypic variation in response to host environments. *Proceedings of the National Academy of Sciences*, *122*(27), e2415345122. https://doi.org/10.1073/pnas.2415345122

Vermeersch, L., Cool, L., Gorkovskiy, A., Voordeckers, K., Wenseleers, T., & Verstrepen, K. J. (2022). Do microbes have a memory? History-dependent behavior in the adaptation to variable environments. *Frontiers in Microbiology*, *13*, 1004488. https://doi.org/10.3389/fmicb.2022.1004488

Vladimirov, N., & Sourjik, V. (2009). Chemotaxis: how bacteria use memory. *Bchm*, *390*(11), 1097–1104. https://doi.org/10.1515/bc.2009.130

Vyushin, D. I., & Kushner, P. J. (2009). Power-law and long-memory characteristics of the atmospheric general circulation. *Journal of Climate*, *22*(11), 2890–2904. https://doi.org/10.1175/2008jcli2528.1

Wang, S., Faeder, J. R., Setlow, P., & Li, Y. (2015). Memory of germinant stimuli in bacterial spores. *mBio*, *6*(6), 10.1128/mbio.01859-15. https://doi.org/10.1128/mbio.01859-15

Wolf, D. M., Fontaine-Bodin, L., Bischofs, I., Price, G., Keasling, J., & Arkin, A. P. (2008). Memory in microbes: quantifying history-dependent behavior in a bacterium. *PLoS ONE*, *3*(2), e1700. https://doi.org/10.1371/journal.pone.0001700

Woods, J. D. (1981). *Climatic Variations and Variability: Facts and Theories*. 63–83. https://doi.org/10.1007/978-94-009-8514-8_3

Yang, C.-Y., Bialecka-Fornal, M., Weatherwax, C., Larkin, J. W., Prindle, A., Liu, J., Garcia-Ojalvo, J., & Süel, G. M. (2020). Encoding membrane-potential-based memory within a microbial community. *Cell Systems*, *10*(5), 417-423.e3. https://doi.org/10.1016/j.cels.2020.04.002

Yang, J., Son, Y., Park, J., & Park, W. (2025). Dam-dependent epigenetic memory regulates prophage reintegration in Salmonella. *Nucleic Acids Research*, *53*(18), gkaf951. https://doi.org/10.1093/nar/gkaf951

Zemach, E. M. (1968). A definition of memory. *Mind*, *LXXVII*(308), 526–536. https://doi.org/10.1093/mind/lxxvii.308.526

Zhong, Z.-P., Rapp, J. Z., Wainaina, J. M., Solonenko, N. E., Maughan, H., Carpenter, S. D., Cooper, Z. S., Jang, H. B., Bolduc, B., Deming, J. W., & Sullivan, M. B. (2020). Viral ecogenomics of arctic cryopeg brine and sea ice. *mSystems*, *5*(3), e00246-20. https://doi.org/10.1128/msystems.00246-20

Zlotnik, G., & Vansintjan, A. (2019). Memory: An extended definition. *Frontiers in Psychology*, *10*, 2523. https://doi.org/10.3389/fpsyg.2019.02523

CHAPTER 1: MODELED ENERGETICS OF BACTERIAL COMMUNITIES IN ANCIENT SUBZERO BRINES

This chapter has been published:

Kanaan G, Hoehler TM, Iwahana G and Deming JW (2023) Modeled energetics of bacterial communities in ancient subzero brines. *Frontiers in Microbiology,* 14:1206641. doi: 10.3389/fmicb.2023.1206641

ABSTRACT

Cryopeg brines are isolated volumes of hypersaline water in subzero permafrost. The cryopeg system at Utqiaġvik, Alaska, is estimated to date back to 40 ka BP or earlier, a remnant of a late Pleistocene Ocean. Surprisingly, the cryopeg brines contain high concentrations of organic carbon, including extracellular polysaccharides, and high densities of bacteria. How can these physiologically extreme, old, and geologically isolated systems support such an ecosystem? This study addresses this question by examining the energetics of the Utqiaġvik cryopeg brine ecosystem. Using literature-derived assumptions and new measurements on archived borehole materials, we first estimated the quantity of organic carbon when the system formed. We then considered two bacterial growth trajectories to calculate the lower and upper bounds of the cell-specific metabolic rate of these communities. These bounds represent the first community estimates of metabolic rate in a subzero hypersaline environment. To assess the plausibility of the different growth trajectories, we developed a model of the organic carbon cycle and applied it to three borehole scenarios. We also used dissolved inorganic carbon and nitrogen measurements to independently estimate the metabolic rate. The model reconstructs the growth trajectory of the microbial community and predicts the present-day cell density and organic carbon content. Model input included measured rates of the in-situ enzymatic conversion of particulate to dissolved organic carbon under subzero brine conditions. A sensitivity analysis of model parameters was performed, revealing an interplay between growth rate, cell-specific metabolic rate, and extracellular enzyme activity. This approach allowed us to identify plausible growth trajectories consistent with the observed bacterial densities in the cryopeg brines. We found that the cell-specific metabolic rate in this system is relatively high compared to marine sediments. We attribute this finding to the need to invest energy in the production of extracellular enzymes, for generating bioavailable carbon from particulate organic carbon, and the production of extracellular polysaccharides for cryoprotection and osmoprotection. These results may be relevant to other isolated systems in the polar regions of Earth and to possible ice-bound brines on worlds such as Europa, Enceladus, and Mars.

INTRODUCTION

On Earth, bacteria often encounter energy-limited environments. Their prevalent physiological state is understood to be energy-limited (Lever et al., 2015). For example, the vast subsurface biosphere is energy-limited (Jørgensen & Boetius, 2007), yet sustains abundant microbial life (Jørgensen & Boetius, 2007; Teske, 2005). Understanding the strategies that allow bacteria to survive in such extreme environments prompts the question: what is their minimum metabolic requirement? Here we investigate the energetic needs over time of bacterial communities in cryopeg brine, a subzero hypersaline environment geologically isolated from surface inputs. We seek to answer the question posed by estimating the cell-specific metabolic rates of the bacterial communities residing in these extreme settings.

Cryopeg brines are considered extreme for various reasons, one of which is their assumed energetic isolation. These brines are volumes of hypersaline subzero liquid water found in permafrost well below the surface. The

Utqiaġvik system of cryopegs in the high Alaskan Arctic at approximately 8 m below surface has a temperature around −6°C and total salt concentration around 120 ppt (Cooper et al., 2019). Carbon-14 (^{14}C) measurements suggest the brines have been enclosed for approximately 40 ka BP (Iwahana et al., 2021). Two types of cryopeg brines exist within the permafrost here: those encased by a layer of frozen marine sediments and those encased by massive ice. Both types are thought to be isolated hydrologically (Iwahana et al., 2021). Together, these properties describe an environment that is not only energy-limited, but also energetically costly to inhabit due to challenging conditions. Despite these conditions, cell densities range from 10^5 to 10^8 cells mL^{-1} brine (Cooper et al., 2019), comparable to previously sampled cryopeg brines across the Arctic (Bakermans et al., 2006; Cooper et al., 2019; Gilichinsky et al., 2003, 2005). Metagenomic analyses show the presence of overwhelmingly heterotrophic bacterial communities dependent on organic carbon for their source of energy (Cooper et al., 2022; Rapp et al., 2021).

Investigations of cryopeg systems are relevant not only to our understanding of Earth-bound ecosystems but, excitingly, can inform our understanding of possible extraterrestrial life. Life within the icy mantles of Europa or Enceladus, and possibly the subsurface of Mars, could be inhabiting similarly extreme, energy-limited environments (Gomez-Buckley et al., 2022; Marion et al., 2003; Priscu & Hand, 2012; Sholes et al., 2019). To our knowledge, no estimate of cell-specific metabolic rate in subzero hypersaline environments is available. The objective of this study was to develop such estimates and contribute to our understanding of the habitability of subsurface subzero brines, be they Earth-bound or extraterrestrial.

We considered that the key to understanding the Utqiaġvik cryopeg system was to reconcile high cell densities with potential microbial kinetics and the available energy pool. We hypothesized that the minimum metabolic rate of the brine residents would be relatively high due to the extreme conditions and corresponding need to synthesize protective compounds, making the requirement for organic carbon correspondingly high to account for the observed cell densities. To test this hypothesis, we first made a series of simplifying assumptions to enable a first-order analysis of the system. The objective was to estimate the cell-specific metabolic rate of a resident community, assuming organic carbon as the sole energy source and considering two microbial growth trajectories to provide an upper and lower bound of this rate. This approach required us to measure the quantity of organic carbon in the sediments surrounding the brines. We then constructed a model of the organic carbon cycle within the brine, which allowed us to reconstruct microbial growth trajectories and relate them to available organic carbon. A sensitivity analysis of model parameters was performed to understand their relevance to model results and thus the limitations of our model. These parameters included the enzymatic conversion of particulate organic carbon (POC) to dissolved organic carbon (DOC) in the brine. POC represents the dominant form of organic carbon in surrounding permafrost yet is not available to bacteria until hydrolyzed to smaller molecular weight compounds (DOC).

Finally, we compared the model predictions to the available observations, which together allowed us to propose the system's microbial history under energetic isolation. We produced plausible simulations hinging on the precision of key parameters, and thus could identify research areas that would further advance understanding of bacterial energetics in extreme environments.

PHYSICAL AND BIOLOGICAL CONTEXT FOR THE MODEL

To provide context for our model we outline the relevant environmental characteristics of cryopeg brines in this section. The physical characteristics guided the development of the equations governing environmental interactions in the model. Microbial energetics of the bacteria found in the cryopeg brine constrained our analyses and provided an understanding of the biology that the model attempts to resolve. Together, the

physics and biology of the cryopeg brine underlie the design of our work, and the thoughts behind the analyses conducted.

PHYSICAL CHARACTERISTICS OF CRYOPEG BRINES

Cryopeg brines are volumes of hypersaline water that occur in cryopeg, a basal layer in permafrost of unfrozen sediment perennially at subzero temperatures (Everdingen, 2005). The brines studied herein were collected from below the Barrow Permafrost Tunnel at a depth of approximately 8 m below the surface, on the northernmost coast of Alaska. They are thought to have formed from saturated marine sediments in a lagoonal environment (Iwahana et al., 2021). As sea level fell during glaciation, these sediments would have been exposed to the atmosphere and become desiccated, causing previously dissolved solutes to concentrate and, following entrainment into permafrost, depress the freezing point of water to yield brine (Gilichinsky et al., 2003, 2005; Iwahana et al., 2021). This cryoconcentration effect leads to high salinities and possibly to concentrated organic matter. The marine origin of these brines is supported by ionic and microbiological evidence (Colangelo-Lillis et al., 2016; Iwahana et al., 2021). The temperature of these Alaskan brines perennially falls within a narrow range of −6 to −8°C and is thought to have remained within this range over their lifespan (Colangelo-Lillis et al., 2016; Cooper et al., 2019; Iwahana et al., 2021; Osman et al., 2021). The salinity of these brines ranges from 109 to 140‰ salt (Cooper et al., 2019). These brines are hydrologically isolated from each other as evidenced by the different pressure heads and equilibrium brine levels (Iwahana et al., 2021). Moreover, the combination of ice content plugging sediment pores and bacteria attached to surfaces is thought to preclude input of cells into the brine from the surrounding environment (Gilichinsky et al., 2005). However, possible input during partial melting at the brine/ice boundary cannot be excluded given slight seasonal temperature oscillations. They may be relevant to the observed microbiological similarities between proximate massive ice and sediment brines (Cooper et al., 2019).

The Utqiaġvik cryopeg system presents brines encased by marine sediments, as previously observed in other cryopegs, as well as those newly discovered to be encased by massive ice, respectively called intra-sediment and intra-ice brines (Iwahana et al., 2021). Intra-ice brines are thought to have migrated along the temperature gradient into the massive ice around 11 ka BP. This migration is suggested by the equal age of organic carbon in the brine and the massive ice surrounding it (Iwahana et al., 2021).

We considered brines sampled from three distinct cryopeg boreholes in the Barrow Permafrost Tunnel (Figure 1.1): two intra-sediment brines from boreholes CB1 and CB4, and one intra-ice brine from borehole CBIW. CBIW was sampled twice, in 2017 and 2018. All brines were sampled in May and were at −6°C when sampled, with salinities of 115, 121 and 140‰ salt, respectively (Cooper et al., 2019). No *in situ* oxygen measurements have been made in these or other tunnel boreholes, but anaerobic conditions are expected within the brines (Iwahana et al., 2021).

Cryopeg brines considered here featured POC concentrations of 2–12 mM and DOC concentrations of 30–102 mM, which are high when compared to the typical micromolar concentrations in seawater (Mathis et al., 2005; Goñi et al., 2021). The DOC concentrations are also high when compared to porewaters of nearby (unfrozen) marine sediments (e.g., < 7 mM on the Alaskan north slope; Coffin et al., 2017) and other Arctic marine sediments (1–6 mM, Arnosti and Jørgensen, 2006; < 1 mM, Rossel et al., 2020). Measured inorganic nutrients were also relatively high: nitrate, nitrite, and phosphate were present in micromolar concentrations, while ammonium concentrations were at millimolar levels (Cooper et al., 2019). Sulfate concentrations were similar to those in Chukchi Sea water, potentially drawn down in the brines from more concentrated values due to sulfate reduction or to mirabilite formation (Iwahana et al., 2021).

MICROBIAL ENERGETICS OF CRYOPEG BRINES

Across the Arctic, cryopeg brines have been found to harbor sizeable microbial communities, ranging between 10^5 and 10^8 cells mL^{-1} (Gilichinsky et al., 2003; 2005; Cooper et al., 2019). These brine communities are composed of a diverse set of organisms, which can include species of *Marinobacter*, *Psychrobacter*, *Gillisia*, *Frigoribacterium*, *Rhodococcus, Polaribacter*, and *Sulfurospirillum* (Bakermans et al., 2003, 2006; Bakermans & Nealson, 2004; Colangelo-Lillis et al., 2016; Cooper et al., 2019; Gilichinsky et al., 2005). Community composition appears to differ between Arctic regions, but the use of different methods across studies limits this assessment. The cryopeg brines below the Barrow Permafrost Tunnel, however, have been the subject of in-depth microbiological characterization.

The dominant bacterium in the brines from CB1 and CBIW, two of the brines we considered in this study, was a novel species of *Marinobacter*, recently brought into culture (Cooper et al., 2022). On average it comprised 49% of the total community (Cooper et al., 2019). In the brine from CB4, this *Marinobacter* sp. was abundant, but the dominant bacterium was *Psychrobacter* sp. at 54% of the total community (Cooper et al., 2019). Model parameters for microbial community kinetics were therefore based on the available data for these organisms. Regarding bacterial densities by epifluorescence microscopy, the brines from CB1, CB4 and CBIW (averaged over both sampling years) harbored 5.70 x 10^6, 1.14 x10^7 and 1.30 x10^8 cells mL^{-1}, respectively, with dividing cells observed in all three brines (Cooper et al., 2019). Dissolved extracellular polysaccharides (dEPS) made up between 19% and 28% of the DOC pool. Particulate extracellular polysaccharides (pEPS) made up between 2% and 13% of the POC pool (Colangelo-Lillis et al., 2016; Cooper et al., 2019).

Organisms reliant upon a range of metabolisms have been detected in cryopeg brines, including heterotrophs, sulfate reducers, acetogens and methanogens (Cooper et al., 2019; Gilichinsky et al., 2003, 2005). The genus *Marinobacter* features a highly versatile set of metabolisms, allowing its members to inhabit a wide diversity of environmental niches. Species of this genus, including from cryopeg brines, possess a complete tricarboxylic acid (TCA) cycle and glyoxylate shunt. The glyoxylate shunt bypasses the production of carbon dioxide and may play a role in oxidative stress response (Ahn et al., 2017). A genomic analysis of four strains of the dominant *Marinobacter sp*. isolated from Utqiaġvik cryopeg brines further reveals its metabolic potential (Cooper et al. 2022). This *Marinobacter sp.* possesses the genes required to derive energy from a wide range of organic compounds, including all 20 amino acids (with the possible exception of asparagine). As a substitute for glycolysis, it encodes the Entner–Doudoroff pathway, considered an adaptation for energy efficiency at low temperatures (Czajka et al., 2018). Its pathways for nitrogen cycling include nitrate oxidation and reduction, dissimilatory nitrate reduction, nitric oxide reduction, and nitrous oxide reduction. A C-P lyase system encoded in its genome may facilitate the scavenging of phosphate from organophosphates. The variety of nitrogen, sulfur and metal-based redox reactions encoded in its genome supports a facultative anaerobic lifestyle.

For a heterotrophic *Psychrobacter* sp. isolated from Siberian cryopeg, Bakermans et al. (2003) measured resazurin reduction rate (as a proxy for respiration) and growth rate across a temperature range of –10 to 22°C. From ratios of these rates, they concluded that cell metabolic requirements increase substantially at subzero temperatures. Such an increase is unexpected when considering that base energetic needs scale predominantly as a function of temperature, increasing with warming (Tijhuis et al., 1993; Price et al. 2004). Given the subzero temperature of cryopeg brines, a relatively low cell-specific metabolic rate would be reasonable to expect. However, multiple constraints may impose a higher energetic cost to life in this extreme brine system.

Constrained habitat volume and high cell density in cryopeg brines lead to higher rates of cell-to-cell (and virus-to-cell) contact than occur in seawater. Increased cell-to-cell contact rates exacerbate resource and space competition. An analysis of cryopeg brine metagenomes found high abundance of cells associated with the type VI secretion system and microcin C, both tools to lyse neighboring competitors (Rapp et al., 2021). This microbial weaponry can be understood within the framework of an energetic arms race. Such competition-associated costs could raise the energetic cost of living in this system.

Moreover, cryopeg brines host abundant viral communities of marine origin that appear to have mediated the exchange of genetic information (Colangelo-Lillis et al., 2016; Zhong et al., 2020). Viral interactions contribute to the rate of cell death by lysis, influencing the organic carbon cycle through release of cellular carbon content (Showalter, 2020). Thus, we can hypothesize a high turnover of cell biomass leading to increased energetic cost to maintain a steady-state population.

The required production of certain compounds may also increase the energetic cost of life in this system. Subzero brines are relatively viscous (Cox and Weeks, 1975), and must be especially viscous when they contain millimolar concentrations of EPS (Cooper et al., 2019), known for cryoprotection and osmoprotection (Deming and Young, 2017). Viscosity may lead to the creation of microscale environmental niches, for example, as cell lysis alters local biochemistry. Metagenomics on cryopeg brines revealed the abundance of genes encoding two-component signaling systems (Rapp et al., 2021). These systems would allow a bacterium to respond to a changing energetic landscape more rapidly to outcompete its immediate neighbors (Rapp et al., 2021). A microbial response to localized patches of high molecular weight organic matter may take the form of extracellular enzyme production. Extracellular enzyme activity (EEA) has been measured in cryopeg brines (Showalter, 2020), providing evidence of proactive management of substrate concentrations by the bacterial community. The production of extracellular compounds, from EPS to enzymes, is an additional energetic cost.

Although the current genomic data available provide promising insights into the metabolisms supported by cryopeg brines, they do not allow us to determine whether these brines have supported energetically isolated microbial communities for 40,000 years. To understand the energetics of the Utqiaġvik brines, their energetic histories need to be reconstructed. This effort necessarily involves the reconstruction of the microbial growth trajectory over the lifespan of the brine. Figure 1.2 illustrates several possible growth trajectories. The different fluctuations or constancy in cell densities over time in each case lead to different energetic requirements. Simplistically, a community that spent most of its history at 10^5 cells mL^{-1} will not require the same amount of energy as one at 10^8 cells mL^{-1}. More complex trajectories could also have occurred, such as when a microbial community declines due to insufficient energy, then recovers after an energy input (e.g., when intra-sediment brine is assumed to have migrated into massive ice).

MATERIALS AND METHODS

Here we indicate the methods used to quantify key variables, such as organic carbon, and show the equations developed to model the different processes involved in microbial energetics. Along with the mathematical outline of our model, we also present fundamental assumptions and limitations. All of the code used to describe and calculate the equations below and plot the results shown is available online on GitHub. The contents of this paper were generated from the most recent commit on the “paper” branch. Python v3.9 and Julia v1.8.2 (Bezanson et al., 2017) are used throughout, and plots were generated using Matplotlib v3.6.2 and Seaborn v0.12.1 (Hunter, 2007; Waskom, 2021).

ORGANIC CARBON AND NITROGEN IN SEDIMENT AND MASSIVE ICE

To determine the POC content of sediments surrounding the cryopeg brines, we used the method (Verardo et al., 1990). Duplicate samples of approximately 20 g of material were cleanly removed from previously collected sediments (Iwahana et al., 2021) that had been stored frozen (–20°C) until analysis. In each case, the sediment material was placed in a 50-cc polypropylene tube, weighed, dried in an oven at 60°C for at least 48 hours, and weighed again to obtain dry weight. Samples were then homogenized to a fine powder in a ceramic mortar and pestle and kept in the drying oven until further processing. In the Marine Chemistry Lab (School of Oceanography, University of Washington), 4–6 mg of each sample were weighed in duplicate in combusted silver "boats" after having been fumed in HCl for 24 hours to remove inorganic carbonates. Samples were dried again in the 60°C oven while acetanilide standards were prepared. Before analysis, the samples were cooled in a desiccator for at least 24 hours. The sediment organic carbon and nitrogen content was measured using a Model 440 CHN/O/S Elemental Analyzer and a combustion temperature of 1050°C. The organic carbon and nitrogen content of massive ice from this site was already available (Colangelo-Lillis et al, 2016).

To convert our sediment carbon measurements to in-situ concentrations we assumed a dry sediment density of 2.625 g mL^{-1}, the average of the density of kaolinite and sand. This assumption is guided by the fact that nearby sediment is composed of undefined clay minerals and sand (Iwahana et al., 2021). An expansion factor was needed to account for the fact that carbon quantification methods require thawing porewater, and that water density changes between its solid and liquid phases. We used a common expansion factor of 9.05% for permafrost porewater, and 8.042% for massive ice. Values for the volumetric ice content of permafrost, needed to determine the density of sediment *in situ*, were 73.1% in both CB1 and CBIW sediment, and 52.7% in CB4 sediment.

To determine DOC of porewater in the frozen sediment surrounding the cryopeg brines, subsamples of the sediment and ice were shaved off core sections with a sterile scalpel onto sterile aluminum foil. These subsamples were placed in 50-cc polypropylene tubes, weighed, and allowed to thaw at 4°C for 15 min before centrifuging for 10 min at 2000 rpm in a benchtop centrifuge (IEC, Model HN-SII IM201) at 2°C. The resulting supernatant was decanted and filtered into a clean EPA vial using a 0.2-µm syringe filter, then frozen until analyzed. The tube of leftover sediment was reweighed for porewater/sediment normalization. DOC was measured using a Shimadzu TOC-VCSH DOC analyzer according to standard protocols in the Marine Chemistry Lab (School of Oceanography, University of Washington). In the case of massive ice, we lacked suitable samples for DOC analysis, so measurements of dEPS (Colangelo-Lillis et al., 2016) were used as a proxy for DOC.

DISSOLVED INORGANIC CARBON

Dissolved inorganic carbon (DIC) was measured for a sample of CBIW brine taken in 2017 as an auxiliary to the ^{14}C dating procedure (Iwahana et al., 2021). Brine sample of approximately 200 mL was degassed under vacuum by pumping to the 10^{-4} Torr range. Dissolved carbon dioxide was liberated by the addition of anhydrous phosphoric acid. Purified carbon dioxide was isolated from other gases by gas distillation. DIC was then measured by the University of Arizona, Accelerator Mass Spectrometry Lab.

MODELING SCENARIOS

We considered three separate scenarios for modeling purposes. Each scenario is based on a unique occurrence of cryopeg brine below the permafrost tunnel. The scenarios are named after the borehole that yielded the brine they describe: CB1, CB4, and CBIW. The following variables define a scenario: brine cell

density, brine POC and DOC concentration, surrounding POC and DOC concentration, post-enclosure carbon addition, bacterial growth rate, and carbon content per cell.

The CB1 scenario was chosen to represent the multiple intra-sediment brines in the Utqiaġvik region of common geology and microbial composition. It was paired with organic carbon measurements made on regional permafrost from the nearby Barrow Environmental Observatory (BEO). As the dominant organism in this brine was the newly isolated *Marinobacter sp.,* its growth rate and a literature-informed approximation of its carbon content were used to represent the microbial community.

The CB4 scenario describes an intra-sediment brine that differs from the others in terms of its dominant organism, *Psychrobacter sp*. The published growth rate and carbon content for Arctic *Psychrobacter* sp. (Bakermans, 2003; 2006) were used to represent the microbial community. In this scenario we used our measurements of organic carbon in sediment immediately surrounding this brine.

The CBIW scenario represents cryopeg brine encased in massive ice instead of sediment. This brine is thought to have originated as intra-sediment brine, then migrated upwards into massive ice around 11,000 years BP to become surrounded by ice. This ^{14}C-dating provided evidence of a possible mechanism for addition of organic carbon from the ice into the brine (Iwahana et al., 2021). The CBIW scenario is therefore the only one for which we have modeled an addition of organic carbon past the initial stage of brine enclosure. We used a lower bound estimate of the amount of carbon added, based on the amount of carbon in the massive ice currently surrounding the brine (Colangelo-Lillis et al., 2016). As CBIW brine was dominated by the new *Marinobacter* sp., we used its traits to represent the microbial community.

Specific values for the variables we used to define a model scenario are provided in Table 1. For scenarios CB1 and CBIW, where *Marinobacter* sp. dominated the brine community, the cell carbon content, α_D, was taken from an average value for Arctic sea-ice bacteria from Nguyen and Maranger (2011), the closest relevant estimates for a subzero brine environment that we could find. For the CB4 scenario we took the average size for a proxy of its dominant bacterium, *Psychrobacter sp.*, as 0.365 μm^3 (Bakermans et al., 2006), using 148 fg C μm^{-3} as the carbon conversion factor (Kirchman et al., 2009). The maximum growth rate, μ_{max}, for scenarios CB1 and CBIW was derived from lab experiments with the *Marinobacter* sp. isolated from these cryopeg brines. The cultures were grown in nutrient-replete media under in-situ temperature and salinity (Cooper et al., 2021). For the CB4 scenario, we used the growth rate determined for a culture of *Psychrobacter sp.* grown in nutrient-replete media at –10°C (Bakermans et al., 2003). The model assumes these rates to be the in-situ growth rates, as they are the closest approximations available. We note that they were determined not only under nutrient-replete conditions but also under aerobic culture conditions, and therefore likely represent over-estimations of the in-situ growth rates given that cryopeg brine is assumed to be an anaerobic environment.

Cell-specific metabolic rate

A primary goal was to develop an equation to estimate the cell-specific metabolic rate of the microbial community, which is described below (Equation 1). The cell-specific metabolic rate term was inspired by Pirt (1982), who proposed a constant base maintenance energy term and a second growth-dependent term without distinguishing different types of metabolisms. In our model, we have abstracted the total organic carbon (TOC) consumed to a cell-specific metabolic rate term, as we do not have a good approximation of the growth-dependent term. Metabolic rate as a function of growth rate would be needed to more accurately approximate the growth-dependent term. We account for organic carbon usage for biomass production (growth) separately.

We assumed that the brine upon initial enclosure contained POC and DOC pools equivalent to those present in the continuously frozen material currently surrounding the brines. In the CBIW scenario, we considered the surroundings to have been equal in TOC content to regional frozen sediment at depth in the permafrost (sampled at BEO). We then took the difference between starting TOC and TOC measured in the brines. This calculation accounted for any carbon addition during the 40,000-year period by adding it to the starting TOC quantity. We subtracted from this difference the quantity of organic carbon diverted towards biomass.

To obtain bounds for our approximation we considered two cases of cell growth. The lower bound case requires the available quantity of organic carbon to be divided among as many cells as possible to minimize this per-cell quantity. This case corresponds to one in which no growth occurs (Pirt, 1982). The upper bound case minimizes the cell quantity to maximize the cell-specific metabolic rate. This approach is intuitive by realizing that biomass is the only sink of carbon in this equation. Therefore, the upper bound case is represented by the slowest possible rate of exponential growth.

To calculate the slowest possible rate of exponential growth, we determined the growth rate of a community over the simulation time of 40,000 years by fitting an exponential function between the starting cell density of 10^5 cells mL^{-1} and the observed ending cell density. The resulting rate is called the "minimum growth rate". This approach assumes that the microbial community was growing over the entire lifespan of the enclosed brine, and hence does not allow for death or dormancy. Inherent to Equation 1 is that our system is feasible under the minimum growth rate with either cell-specific metabolic rate bounds.

The cell-specific metabolic rate, m, is given in femtograms of carbon per cell per day by:

$$m = \frac{(S_0 + S_i) - S_f - \alpha_D(N_f - N_0)}{\int_0^f N(t)dt} \quad (1)$$

where α_D denotes the quantity of organic carbon content per cell in femtograms of carbon per cell; S, the concentration of TOC in femtograms of carbon per milliliter; N, the cell density in number of cells per milliliter, and 0 and f, the start and end times, respectively, in days. S_i is any organic carbon added at time i. Sympy v1.11.1 was used to calculate the integral (Meurer et al., 2017). We took N_f to be the observed cell density in the cryopeg brine of reference for each scenario (Table 1.1). We took N_0 to be 10^5 cells mL^{-1}, the order of magnitude of cell densities observed in coastal sea ice (Cooper et al., 2019). The use of a coastal sea ice value is based on physical similarities between the two environments, and the potential that coastal sea ice of 40,000 years ago, being a frozen, brine-containing surface environment, supported a microbiome resembling that of cryopeg brine when first formed.

Extracellular enzyme activity

Measurements of EEA in cryopeg brines are available (Showalter, 2020), but we sought to calculate EEA rate bounds to understand whether EEA might hint at the age and energetic requirements of the microbial community. These bounds were calculated similarly to those for the cell-specific metabolic rate, using Equation 2:

$$\gamma_{\text{cell}} = \frac{(P_0 + P_i) - P_f}{\int_0^f N(t)dt} \quad (2)$$

where cell-specific EEA rate, γ_{cell}, is given in femtograms of carbon per cell per day, and P denotes quantity of POC. We thus considered the difference in POC quantity between the brine and its surroundings, accounting for any additional POC input to the brine, with the resulting quantity divided by cell density over time. The

bounding growth trajectories were identical to those used to estimate the cell-specific metabolic rate. Using Equation 2, we could also predict the timespan of the system by replacing γ_{cell} with measured EEA rate and solving for t. We solved for the timespan using the growth case with the minimum calculated growth rate starting at 10^5 cells mL^{-1}.

Model description

To determine the plausibility of the calculated cell-specific metabolic rate value, and to understand the energetic requirements of the system, we developed a model of the organic carbon cycle in Utqiaġvik cryopeg brines. In this section we offer a non-mathematical description and schematic representation (Figure 1.3) of the model. The central assumptions are presented in the next section.

The model keeps track of four quantities: POC, DOC, DIC, and cell abundance. Five processes structure these quantities: respiration of DOC to DIC by bacteria, cell growth, cell death, hydrolysis of POC to DOC by extracellular enzymes, and organic carbon additions to the system.

Here the rate of respiration, as well as all other utilizations of organic carbon (e.g., cell growth, production and release of extracellular compounds), is encompassed in the cell-specific metabolic rate. Each unit of organic carbon respired is removed from the DOC pool and added to the DIC pool. The quantity of DIC in the model runs presented here are modified solely by this cellular respiration of DOC. Cells grow according to an equation relating their maximum growth rate to substrate concentration (Monod, 1949). As a cell grows, the quantity of DOC it contains is removed from the DOC pool. Conversely, cells release the DOC they contain upon death. Cell death is explicitly considered to occur when the quantity of available DOC is less than the cell-specific metabolic rate and thus is referred to as starvation death. Other death processes are abstracted by net growth rate. Extracellularly, the enzymatic conversion of POC to DOC contributes to the DOC pool.

As used in the CBIW scenario, the model allows for the addition of organic carbon to the system, beyond that available at time zero. A model feature not used here would allow consideration of a punctuated or a constant input of DIC through processes other than respiration, such as carbonate dissolution. Possible chemoautotrophy to remove DIC and generate new biomass (Rapp et al., 2021) would require modifications that are being considered for a future modeling effort.

Model assumptions and limitations

Due to the sparse data available on cryopeg brines, reconstructing their microbial history requires assumptions to obtain the first-order approximation of their energetics. These assumptions inherently introduce limitations to our results. We address the central assumptions here to contextualize our results.

A key assumption in our analyses is that the cryopeg brines started with an amount of organic carbon equivalent to the quantity observed in their contemporary surroundings. This assumption is required, as obtaining precise information on a cryopeg system at the time of its formation 40,000 years ago is not possible. The assumption is not unreasonable given the hydrological isolation of the brines and the near-constant temperatures that have kept their surroundings frozen throughout their lifetimes (Iwahana et al., 2021; Osman et al., 2021).

Our model does not account for diffusion of material throughout the brine, which neglects the likelihood of environmental niches (Rapp et al., 2021). Without *in situ* microscale observations of these remote systems, we cannot parameterize niches or differentiate the energetic requirements of inhabiting them. For the

purposes of conducting an overarching energetic analysis of the system, the lack of diffusivity may not be a critical limitation. The analysis is simply spread uniformly across the environment and the microbes.

We assumed that every cell in the system grows at the same rate. Of course, different subpopulations of cells express different phenotypes and levels of activity, including dormancy, at different times in their life histories. This assumption likely leads to an overestimation of the community growth rate and, in turn, an underestimation of the cell-specific metabolic rate. However, as will be seen in our results, the cell-specific metabolic rate compares reasonably well to existing estimations.

We also assumed that every cell in the system has the same carbon content throughout its lifetime. Of course, bacterial communities exhibit a range of cell sizes, with size and potentially content changing as a function of growth conditions, growth phase, starvation conditions, and dormancy. Until distribution data for cryopeg brines are obtained, the use of a uniform distribution of cell size and carbon content in our analyses leaves some uncertainty to our results. As will be seen, our model simulations are not overly sensitive to this parameter.

We have attributed cell death to starvation, but other processes can lead to cell death in these cryopeg brines. In particular, cell lysis following viral infection and "bacterial warfare" may contribute significantly (Rapp et al., 2021). Use of a net community growth rate includes such death processes implicitly. Our use of growth rates determined in cultures as net community growth rates likely represents an overestimation of the net rate. As a future research direction, this model could be modified to account explicitly for death mechanisms other than starvation.

We assumed that microbial community kinetics could be represented by those of the dominant bacterium. Many bacterial species exist within the cryopeg brine, each with presumably distinct kinetics. However, overall diversity was low and the dominant species was strongly dominant in each scenario considered, accounting for half or more of the community. Making this assumption allowed a first-order approximation despite the unknown complexities of community kinetics.

We assumed that all POC is inaccessible to the brine community until hydrolyzed enzymatically to DOC, and that all DOC is accessible and labile. An absence of data on the chemical composition and lability of either of these pools of organic carbon limits our analysis, as does the assumption that EEA rate is constant. Bacteria regulate their production of extracellular enzymes in response to environmental substrates, but we lack data to model this kinetic or enzyme lifetime. These assumptions could lead to biased results in EEA rate calculations and final carbon quantities (Figure A1).

Finally, we assumed that organic compounds are the only limiting source of carbon, nutrients and energy for cell respiration and growth. Sources of inorganic nutrients are plentiful in cryopeg brines (Cooper et al., 2019), but are not included explicitly in our model. While data on the existence of other sources of chemical energy in the system are limited, the levels of POC and DOC in the brines indicate this assumption to be reasonable. The microbial communities in the brines examined were dominated overwhelmingly by organoheterotrophs, further supporting the assumption.

MODEL EQUATIONS

The model was solved using the DifferentialEquations.jl package v7.6.0 (Rackauckas & Nie, 2016) using a Rosenbrock23 solver (Shampine & Reichelt, 1997) set up to solve an initial-value problem.

The growth term, G, is solved with a straightforward Monod equation (Monod, 1949) that relates the maximum net growth rate, μ_{max}, to substrate concentration, D, using a half-velocity term, K_D, where the substrate is DOC (Equation 3):

$$G = \mu_{max} * \frac{D}{K_D + D} * N * \left(1 - \frac{N}{N_{max}}\right) \quad (3)$$

A logistic growth term has been added to cap the growth as the cell density, N, approaches carrying capacity, N_{max}. If cell density declined to zero at the time of a carbon addition (e.g., in the CBIW scenario), we set $N = 1$ to simulate a viable cell able to respond to the addition.

The death term, Δ, corresponds to deaths by starvation (Equation 4):

$$\Delta = \frac{max(mN - D, 0)}{m} \quad (4)$$

This term accounts for the assumption that cells will lyse if they do not have enough substrate to maintain their integrity, i.e., cannot satisfy their metabolic need (m). Other death-inducing processes such as viral infection or bacterial warfare are included implicitly in net growth rate (Equation 3). The net change in cell density is the difference between growth and death by starvation (Equation 5):

$$\frac{dN}{dt} = G - \Delta \quad (5)$$

While the cell-specific EEA rate remains constant throughout our simulations, the absolute EEA rate, γ, must be lower or equal to the available quantity of substrate, P. To satisfy this constraint, we used a minimum function (Equation 6):

$$\gamma = min(\gamma_{cell} * N,\ P) \quad (6)$$

where P is the quantity of POC, which is given by the sum of two terms. The first term, $P_{in,}$ represents any addition of POC into the system. The second term is the absolute EEA rate, γ, subtracted to remove the quantity of POC hydrolyzed to DOC.

$$\frac{dP}{dt} = P_{in} - \gamma \quad (7)$$

The quantity of DOC in the system is the sum of five terms (Equation 8):

$$\frac{dD}{dt} = D_{in} + \alpha_D(\Delta - G) - m(N - \Delta) + \gamma + min(I_{xr}, I) \quad (8)$$

The first term is any addition of organic carbon into the system, D_{in}, which allows the simulation of single or repeated carbon additions from the surrounding environment into the cryopeg brine. The second term is DOC sequestered or released by biomass, equal to the change in cell abundance multiplied by the quantity of organic carbon per cell, α_D. The third term accounts for the metabolism of the remaining population. The fourth term, γ, is the quantity of POC converted to DOC by EEA. The final term simulates autotrophy in the system by taking a DIC fixation rate, I_{xr}, which removes carbon from the DIC pool and adds to the DOC pool. This rate cannot be smaller than the quantity of DIC. In this work, we have set this term to zero, for lack of measurements of I_{xr} in cryopeg brines and expecting the rate to be minor based on metagenomic information (Rapp et al., 2021). If such rates become available for future simulations, the model would need modification to accommodate the flow of DIC into new cell biomass instead of directly into DOC (Section 3.7).

The equation for change in DIC is constructed similarly, though the EEA term is absent as it need not be considered (Equation 9):

$$\frac{dI}{dt} = I_{in} + \alpha_I(\Delta - G) + m(N - \Delta) - min(I_{xr}, I) \quad (9)$$

In this equation, α_I is the quantity of DIC per cell. While α_I and I_{xr} are set to zero here, they could be used in a future study to model autotrophy in this system.

Model inputs and simulations

In addition to the variables defined for each cryopeg brine scenario (Table 1.1), a set of constants were input to the model (Table 1.2). For each constant, we used the most accurate estimate we could find. In some cases, the chosen value was less relevant to our unique environment than we had hoped. However, given that we are striving for order of magnitude estimations, we expect these to be adequate, especially when considering the results of our sensitivity analysis (Sections 3.10 and 4.4).

K_D was derived by taking an average of the values for amino acid uptake rates measured at –1°C in Arctic seawater by Yager and Deming (1999), then taking the dissolved combined amino acids to be 41% carbon (as in Rowe and Deming, 1985). No adjustment was made for temperature, as the original data, determined across a range of temperatures, showed no conventional Q10 effect (Yager and Deming, 1999).

We ran simulations to obtain growth trajectories (changes in cell density over time) for each of the three cryopeg scenarios under different boundary conditions. Each simulation represents one of 8 unique combinations of the lower or upper bound of three variables: m, μ_{max}, and γ_{cell}. Simulations thus address minimum and maximum growth rate, lower and upper bound cell-specific metabolic rate, and calculated and measured extracellular enzyme activity. They also track POC and DOC during the 40,000-year time span of the resulting growth trajectories.

Sensitivity analysis

To understand how the accuracy of our estimates affects model results, we conducted a sensitivity analysis of model parameters. Using GlobalSensitivity.jl package v2.1.2 (Ma et al., 2021) we executed a global sensitivity analysis using a variation of the Sobol variance decomposition method and estimator (Sobol 2001; Sobol et al., 2007). The analysis was allowed to converge to obtain a satisfactory confidence interval at a confidence level of at least 95%.

Briefly, this variance decomposition method varies each parameter within given bounds and measures the corresponding variance of the output. The resulting first-order Sobol index of a parameter is a measure of how much variance in the output can be attributed to that parameter. The total-effect Sobol index encompasses interactions between the variance of that parameter and the others in the analysis. The bounds passed for each parameter aim to encompass the range of microbiologically plausible values; these can be found in Table 3.

The sensitivity analysis was executed on the CB1 scenario, excluding environmental parameters. This choice was made to understand the influence of bacterial parameters, such as carbon content per cell and growth rate, on our results. Furthermore, these constitute the few parameters that future lab work may attempt to quantify, whereas more accurate environmental data is elusive.

Results

Here we provide the results of the different measurements made to fill gaps and complement the datasets available in the literature and thus enable our model simulations. These measurements include sediment carbon and nitrogen content of cryopeg and regional sediments and brine DIC for one borehole sample. Estimates of cell-specific metabolic rate and extracellular enzyme rate are shown for the three different scenarios examined. Finally, a sensitivity analysis of model parameters and the model predictions are presented.

Sediment carbon and nitrogen measurements

To improve the accuracy of our model, we measured the quantity of organic carbon in sediment permafrost previously sampled at two locations in the BEO. The average value for POC was 0.0232 ± 0.0006 μg C μg sediment^{-1} at a depth of 367–383 cm (n = 4). The porewater salt concentration was 6‰. The concentration of DOC in this porewater was 51.2 μg C mL^{-1}. The nitrogen content of the sediment was 0.0016 ± 0.00005 μg N μg sediment^{-1}.

We also measured the concentration of organic carbon in sediment surrounding the CB4 cryopeg brine. For POC, the average value in this sediment layer was 0.0136 ± 0.0012 μg C μg sediment^{-1} (n = 3). The porewater salt concentration ranged between 22‰ and 30‰. The concentration of DOC in this porewater at 187-cm depth was 1286 μg C mL^{-1}. The nitrogen content of the sediment was 0.0010 ± 0.00015 μg N μg sediment^{-1}. CB4 sediment thus had a C:N ratio of 15.8 mol C mol N^{-1}.

Brine dissolved inorganic carbon

The dissolved inorganic carbon content of CBIW (2017) brine was measured as 6.93 x 10^{10} fg C mL^{-1}. The dissolved inorganic carbon content of frozen sediment from CBIW (2018) was 4.9 x 10 x 10^{10} fg C mL^{-1}. We do not have DIC measurements for other brines.

Estimates of cell-specific metabolic rate

The lower and upper bounds of the cell-specific metabolic rate that we estimated for each of the three cryopeg brine scenarios ranged from 0.008 to 0.743 fg C cell^{-1} day^{-1} (Table 1.4). As expected, due to the input of organic carbon, the lowest of these rates was obtained for the CBIW scenario. The calculated minimum growth rate ranged between 2.77 x 10^{-7} and 4.95 x 10^{-7} day^{-1}. These extremely low growth rates, which correspond to doubling times on the order of 10^3 years, are due to the significant age of the system and rely upon our assumption of a starting cell population of 10^5 cells mL^{-1}.

Extracellular enzyme activity rate estimates and predicted timespan

We calculated the EEA rate required to hydrolyze the difference between surrounding sediment POC and brine POC. In the case of the CB1 scenario, the bounds of estimated EEA rates were 0.195 and 0.802 fg C cell^{-1} day^{-1}. At the measured EEA rate of 0.012 fg C cell^{-1} day^{-1}, the time required to hydrolyze the POC difference in this scenario would have been 81,200 years. In the CB4 scenario, the estimated bounds of EEA rates were 0.101 and 0.483 fg C cell^{-1} day^{-1}, with a predicted timespan of 71,000 years. Finally, in the CBIW scenario (that received organic input), the estimated bounds of EEA rates were 0.806 and 0.584, with a predicted timespan of 48,700 years, much closer to the observed age of the cryopeg system. In all cases, this independent estimation of the system's timespan is near to or less than double the measured timespan, well within the goal of obtaining order of magnitude estimates.

Model sensitivity analysis

A sensitivity analysis of model parameters revealed the importance of the three parameters at the heart of the Monod growth term (Figure 1.4): growth rate, cell-specific metabolic rate, and half-velocity constant. These

are the only parameters with notable first-order indices. They have a measurable direct impact on model output, whereas cell carbon content and initial cell density do not. The total-effect indices offer more nuance. These indices reflect the added importance of carrying capacity. As a whole, this sensitivity analysis offers insight into which parameters account for much of the variability in the model results.

Model predictions

In two of the eight sets of conditions used for model simulations, our model fully or partially succeeds in explaining the cell densities observed at 40,000 years. With conditions of minimum growth rate paired with low cell-specific metabolic rate and calculated EEA, all three cryopeg brine scenarios reach their observed cell densities (Figure 1.5A). With measured EEA (Figure 1.5B), the observed cell density is reached only for the CBIW scenario; CB1 and CB4 scenarios fall short of their densities (Figure 1.5B). The CBIW scenario succeeds in reaching the observed cell density because it includes an addition of DOC, while the other two depend upon the hydrolysis of existing POC to generate DOC for bacterial growth. Insufficient POC is hydrolyzed towards the end of the trajectory (Figure A1) to support these other two communities.

By Equation 1, minimum growth rate paired with the upper bound cell-specific metabolic rate should yield the observed cell densities. However, this is not the case. Common to all the minimum growth rate simulations (Figures 1.5A–D) is a long plateau for the first few thousand years. In those simulations where minimum growth rate and upper bound cell-specific metabolic rate are paired, the populations subsequently grow weakly before declining (Figure 1.5C and D). Given that abundant POC remains in the system in all cases (Figure A1), these results are explained by an EEA rate inferior to the cell-specific metabolic rate requirements. The CBIW population does start to recover due to addition of DOC at 29,000 years, but the growth rate is too low to allow recovery to the observed cell densities before the simulation ends (Figure 1.5C and D).

When the maximum growth rate is used, the microbial populations rapidly reach the system carrying capacity (Figure 1.5E–H). Once they consume all available DOC, the populations decline. The time elapsed before the decline is governed by the demand for DOC driven by the cell-specific metabolic rate. Because CBIW sees a punctual addition of DOC at 29,000 years, the high growth rate allows the population to recover for a short time before declining again (Figure 1.5E-H). However, not enough carbon has been added to sustain the population to the end of this simulation.

Discussion

Our overall approach can be considered a bulk energetic analysis. We have made the fundamental assumption that the total energy use of the system corresponds to the difference in organic carbon between the permafrost and the cryopeg brine, assuming these started with equal amounts. This approach mitigates the lack of a secondary metabolic state (i.e., dormancy) in our model. In this way, our cell-specific metabolic rate calculations provide bounds on the average energy requirement of a bacterium in this setting.

Multiple analyses increase our confidence in the mentioned assumption and our model predictions. Using the measured rate of EEA and following our assumption on total energy use in this system, we calculated an expected timespan of the system equal or less than double the measured timespan. We also used the measured C:N ratio of CB4 sediment and the previously measured quantity of ammonia in the brine from Cooper et al. (2019) to estimate the amount of organic carbon consumed. We obtained a value of 8.59×10^{11} fg C mL^{-1}, two orders of magnitude below the quantity produced by our assumption. This calculation is expected to produce a lower bound quantity given that it does not consider nitrogen cycling or the concentration of other nitrogen species in the brine. Thus, this quantity does not contradict our assumption or

prediction. Similarly, the DIC value measured is three orders of magnitude below our expectations based on DOC consumed in CBIW. This analysis indicates that we may be overestimating DIC in the model by not accounting for the complexities of the inorganic carbon system in a subzero brine (Marion et al., 1999), supported by the measured DIC in surrounding frozen sediment. Together these results confirm the plausibility of our assumptions, while providing crucial context for our results. Future work could focus on modelling the DIC sinks of these brines in order to increase the fidelity of this model and understand the potential role for autotrophy in this extreme microbial community.

To understand the biological plausibility of our metabolic rate estimates we sought to compare them to existing measurements and estimates of metabolic rates in other remote and energy-limited environments. Assuming an energetic yield of 30 kJ mol C^{-1} our cell-specific metabolic rate values range on the order of 10^{-17} to 10^{-19} W $cell^{-1}$. This range overlaps at the high end of the range for estimated energy turnover from cold anoxic subsurface marine sediments, the closest analog we can find, on the order of 10^{-19} W $cell^{-1}$ and 10^{-20} W $cell^{-1}$ (Hoehler & Jørgensen, 2013; Lever et al., 2015). For deep crustal fluids, another energy-limited but open and oxygenated environment, sample incubations amended with ^{13}C-substrates at 4°C yielded potential anabolic rates that range from 10^{-3} to 30 fg C $cell^{-1}$ day^{-1} (Trembath-Reichert et al. 2021). Our metabolic rates, which represent net anabolic and catabolic activities at –6°C, fall at the low end of this range (order of 10^{-3} to 10^{-1} fg C $cell^{-1}$ day^{-1}; Table 4), as expected given the significant differences between these environments.

Thus, the cell-specific metabolic rate values we obtained, being framed by other existing rates, are biologically plausible. Our calculation of the cell-specific metabolic rate implicitly includes every cellular process but growth, including membrane, protein and other adaptations to low temperature and high salinity. The relatively high cell-specific metabolic rate of bacteria in the cryopeg brine system, compared to deep subsurface marine sediments, can be accounted for at least partly by the production of extracellular compounds. Moreover, cell carbon mass in these environments may be larger than cells in deep sediments, which could also account for some of the difference in cell-specific metabolic rate between cryopeg brines and cold (unfrozen) marine sediments.

Extracellular enzyme activity has been documented in cryopeg brines (Showalter, 2020). Producing extracellular enzymes is a costly endeavor, with the price reflected in higher cell-specific metabolic rate requirements (Lever et al., 2015; Vetter et al., 1998). Extracellular polysaccharides are also present in high concentrations in cryopeg brines (Cooper et al., 2019). These polysaccharides take on many critical functions, offering cell protection against the effects of both subzero temperatures and hypersaline conditions (Carillo et al., 2015; Deming & Young, 2008; Krembs et al., 2002). While extracellular polysaccharides appear to be fundamental in allowing a cryopeg microbial community to exist, their chemical nature and high concentration in cryopeg brines implies a significant energetic cost, again implicitly built into our cell-specific metabolic rate calculation.

We calculated the minimum growth rate of bacteria in this system, making an important assumption on the starting cell concentration of these brines. While we have made an informed assumption in using cell density in sea ice, the value remains at best an educated guess. We have no data on the actual starting cell concentration of these cryopeg brines. Nevertheless, our sensitivity analysis suggests little influence of this parameter on model output. Assuming a starting cell concentration of 10^5 cells mL^{-1}, we obtain maximum doubling times on the order of 10^3 years. This result is microbiologically feasible, based on similarly long doubling times (20–2,500 years) calculated for other, related energy-limited environments, particularly marine and deep subsurface sediments (Hoehler & Jørgensen, 2013; Lever et al., 2015). As we discuss below, very slow doubling times are not necessary in all cases to explain our observations.

The sensitivity analysis reflects the importance of the parameters we chose to manipulate in our simulations. Growth rate, cell-specific metabolic rate, and Monod half-velocity constant each have high first-order and total-effect Sobol indices. These high indices reflect an important interplay between the parameters in determining the outcome of the model. The EEA rate also presents a high total-effect index in its role of determining the quantity of DOC in the system. Surprisingly, EEA rate does not exhibit a high first-order index, despite other data suggesting this variable is key to cryopeg brine energetics. In fact, EEA does have a high Sobol index when only considering the end concentration of POC in the system (not shown).

In all but two (of 8) sets of conditions for simulations, the model fails to reconstruct a cell growth trajectory that yields the observed cell densities. In these cases, cell density collapses to zero due to the lack of available DOC to meet community energetic requirements. However, in most cases, plenty of POC, a potential source of energy, remains (Figure A1). The extinction of available DOC in these simulations (Figure A1) is caused by the cell-specific metabolic rate being higher than the cell-specific EEA rate. In other words, individual cells are consuming DOC faster than their enzymes can convert POC to DOC.

While the half-velocity constant presents high Sobol indices, this result must be nuanced. First, the chosen value is orders of magnitude lower that the quantity of DOC present in the system. Thus, the impact of this term at the beginning of the simulation is low, and growth proceeds unimpeded. A higher value might slow growth, but the timespan here is long enough that the effect would be negligible. When the quantity of DOC in the system is closer to or below the value chosen, the community is typically on a trajectory towards extinction in the model. Hence, the half-velocity constant, while important because it modulates growth, does not alone explain why the model is limited in explaining our observations.

Simulations based on the CBIW scenario provide some insight on model success versus failure in predicting the observations. In this scenario, the lower bound cell-specific metabolic rate is lower than the extracellular enzyme activity rate used, whether the calculated or measured value (Table 1.4, Section 4.3). Thus, with abundant DOC available, the model can reproduce the observed cell density using the minimum growth rate (Figure 1.5A and B). Observed cell densities are also obtained for the CB1 and CB4 scenarios if the calculated EEA rate is used (Figure 1.5A). In contrast, using the maximum growth rate in conjunction with the calculated EEA rate leads to the depletion of the POC pool, unless carrying capacity is reduced by one order of magnitude (not shown).

Clearly, the EEA rate has the potential to make bioavailable a significant energy source in the system: POC. We note that the observed cell-specific rate of EEA used in the simulations is the average of activities measured on only three substrates in CBIW brine. This rate is kept constant throughout every simulation. This simplification does not accurately reflect the number and specificity of enzymes produced in a cryopeg brine, their complex kinetics, the regulation of their production, or their lifetimes under subzero brine conditions. The cell-specific EEA rate surely fluctuated over the lifespan of the brine as a function of cell density, DOC concentration, and extracellular enzyme turnover time. We were thus led to calculate the range of EEA rates that would allow for enough POC to be hydrolyzed to sustain the microbial community. For the CB1 and CB4 scenarios, these calculated rates are an order of magnitude higher than the measured rate used. Conversely, we calculated the amount of time needed for the chosen EEA rate to hydrolyze the required amount of POC. The results point to a longer lifespan for the cryopeg brines than the measured 40,000 years (by carbon dating), as high as 81,200 years in one case. This discrepancy, based on the chosen EEA rates being too low, provides one explanation as to why our model fails in many cases to explain the observed cell densities. A lack of data to account for cell size differences between *in vitro* and *in situ* measurements may represent another. Future research on extracellular enzyme production and kinetics at subzero temperatures and high salinities,

coupled with cell-size measurements, could allow for an improved understanding of bacterial energetics in cryopeg brines.

Despite being detected (Colangelo-Lillis et al., 2016; Cooper et al., 2019), hydrogen sulfide is not considered here as a potential source of chemical energy in these cryopeg brines. Most members of the bacterial communities as revealed by metagenomics are not known to utilize it (Rapp et al., 2021), bacterial kinetics for those that do are not available under in-situ conditions, and hydrogen sulfide concentrations are not known. However, the presence of sulfur-oxidizing and sulfur-reducing bacteria was recorded in these brines (Cooper et al., 2019). Therefore, a large enough endogenous source of hydrogen sulfide in the cryopeg brines could change the energetic balance of these communities. We also note that sulfur concentration may be impacted by abiotic processes such as mirabilite precipitation (Marion et al., 1999). Armed with the relevant kinetics, a future study could establish an upper bound on the possible energetic contribution of hydrogen sulfide to this system. A more detailed analysis could account for metabolically different bacterial populations and different metabolic states.

Conclusion

Here we have produced a first estimation of cell-specific metabolic rate in cryopeg brines, ancient, geologically isolated, subzero hypersaline liquids in Arctic permafrost. Comparing our estimates to the few other estimates available on natural microbial systems is difficult, given the use of different approaches and reporting units. Our estimates suggest that cell-specific metabolic rate in a cryopeg system is much higher than in subsurface marine sediments (Hoehler and Jørgensen, 2013), the closest parallel we can find. Although both are sediment-based systems, the differences between them are marked: subsurface marine sediments are neither subzero nor hypersaline and they lack the energy resources that surround a cryopeg system. However, our estimates of cell-specific metabolic rate may be high primarily because we define cell-specific metabolic rate to include every cellular process but growth. The energetically costly production of extracellular enzymes and extracellular polysaccharides may best explain our result of high cell-specific metabolic rate.

To further understand the energetics of the cryopeg system, we developed a model of a simplified organic carbon cycle in subzero cryopeg brines. The results of a selective sensitivity analysis of this model suggest that growth rate, cell-specific metabolic rate and EEA rate are key parameters in determining the fate of the microbial community. Running simulations representative of different energetic bounds for each cryopeg brine improved our understanding of the history of a cryopeg microbial community. In most cases, the energetic requirement is too high and the microbial community collapses. A higher EEA rate would allow the community to take advantage of the energy locked within the high amounts of POC in the system. Where we modeled a punctual addition of DOC into the system, the population was either too slow growing to achieve the observed cell density, or the quantity of DOC was insufficient to sustain it. In cases where the lower bound cell-specific metabolic rate was inferior to the EEA rate, the model was successful in reproducing the observed cell densities after 40,000 years. In calculating the required EEA rate to satisfy the energetic requirements in each of the cryopeg brine scenarios considered, we concluded that the 40,000-year timespan could be reconciled with the measured EEA rate if the energetic requirements of the bacterial community are low enough. The calculated EEA based on our assumption on starting DOC and POC conditions yields an expected system timespan within a factor of two of the measured timespans. This result increases our confidence in the assumptions underlying our energetic analyses.

Although our model unavoidably relies on numerous assumptions, it has produced testable hypotheses for the continued study of cryopeg brines. It also leads us to conclude that the microbial densities observed today

in cryopeg brines could well have been reached in energetic isolation over an estimated system lifespan of 40,000 years. In general, the success of these communities would have required a lower growth rate than that observed under in-situ conditions in the lab and higher average rate of EEA. The calculated cell-specific metabolic rate of bacteria in these systems can be met by the assumed available quantity of POC and DOC in the system and appears to be biologically plausible, particularly for bacteria functioning under the extreme conditions of subzero temperature and hypersalinity. Finally, this model could be tuned in its parameters to describe theoretical astrobiologically relevant environments within the icy crusts of Europa or Enceladus.

ACKNOWLEDGEMENTS

We thank the many people who provided helpful discussions, data, and encouragement to develop the model and associated calculations: Shelly Carpenter for help in the lab and with the sediment carbon measurements; Dr. Hajo Eicken for providing important input that stimulated this effort; Dr. Zac Cooper and Dr. Josephine Rapp for helpful discussions about brine genomics; Dr. Max Showalter for the critical EEA data and helpful modeling discussions; and Dr. Jodi Young and Kaitlin Harrison for discussion regarding the potential for chemoautotrophy in cryopeg brines. GK would also like to thank the organizers of the Microenergy Conference 2022 for the opportunity to present and discuss an early version of this work, Scott Martin for helpful mathematical discussion, and Mario Nohra for reviewing and auditing the project's codebase.

CONFLICT OF INTEREST

The authors declare that the research was conducted in the absence of any commercial or financial relationships that could be construed as a potential conflict of interest.

AUTHOR CONTRIBUTIONS

GK developed the carbon model, estimated the cell-specific metabolic rate values, performed all calculations, model runs, and lab work, and drafted the manuscript. TH provided the methodological ideas required to estimate cell-specific metabolic rate, crucial feedback on the model, including the suggestion to conduct a sensitivity analysis, and critical revisions to the manuscript. GI provided organic and inorganic carbon data, expansion factors for ice, interpretation of dating measurements, and edits to the manuscript. JD supervised all work, advised GK, administered the grant, provided lab facilities, and revised and edited the manuscript. All authors approved this submission.

FUNDING

This work was initially supported by the Gordon and Betty Moore Foundation (grant number GBMF5488). GK also received support from a private sponsorship and the Karl M. Banse professorship to JWD.

DATA AVAILABILITY STATEMENT

The datasets used in this study are published as cited. The code to reproduce the analyses in this study can be found in the GitHub repository of this project at https://github.com/Ge0rges/Cryopeg-Carbon-Model.

REFERENCES

Ahn, S., Jung, J., Jang, I.-A., Madsen, E. L., & Park, W. (2017). Role of glyoxylate shunt in oxidative stress response. *Journal of Biological Chemistry*, *291*(22), 11928–11938. https://doi.org/10.1074/jbc.m115.708149

Bakermans, C., Ayala-del-Río, H. L., Ponder, M. A., Vishnivetskaya, T., Gilichinsky, D., Thomashow, M. F., & Tiedje, J. M. (2006). Psychrobacter cryohalolentis sp. nov. and Psychrobacter arcticus sp. nov., isolated from Siberian permafrost. *International Journal of Systematic and Evolutionary Microbiology*, *56*(6), 1285–1291. https://doi.org/10.1099/ijs.0.64043-0

Bakermans, C., & Nealson, K. H. (2004). Relationship of critical temperature to macromolecular synthesis and growth yield in *Psychrobacter cryopegella*. *Journal of Bacteriology*, *186*(8), 2340–2345. https://doi.org/10.1128/jb.186.8.2340-2345.2004

Bakermans, C., Tsapin, A. I., Souza-Egipsy, V., Gilichinsky, D. A., & Nealson, K. H. (2003). Reproduction and metabolism at − 10°C of bacteria isolated from Siberian permafrost. *Environmental Microbiology*, *5*(4), 321–326. https://doi.org/10.1046/j.1462-2920.2003.00419.x

Bezanson, J., Edelman, A., Karpinski, S., & Shah, V. B. (2017). Julia: a fresh approach to numerical computing. *SIAM Review*, *59*(1), 65–98. https://doi.org/10.1137/141000671

Carillo, S., Casillo, A., Pieretti, G., Parrilli, E., Sannino, F., Bayer-Giraldi, M., Cosconati, S., Novellino, E., Ewert, M., Deming, J. W., Lanzetta, R., Marino, G., Parrilli, M., Randazzo, A., Tutino, M. L., & Corsaro, M. M. (2015). A unique capsular polysaccharide structure from the psychrophilic marine bacterium *Colwellia psychrerythraea* 34H that mimics antifreeze (glyco)proteins. *Journal of the American Chemical Society*, *137*(1), 179–189. https://doi.org/10.1021/ja5075954

Colangelo-Lillis, J., Eicken, H., Carpenter, S. D., & Deming, J. W. (2016). Evidence for marine origin and microbial-viral habitability of sub-zero hypersaline aqueous inclusions within permafrost near Barrow, Alaska. *FEMS Microbiology Ecology*, *92*(5), fiw053. https://doi.org/10.1093/femsec/fiw053

Cooper, Z. S. (2021). Microbial evolution and ecology in subzero hypersaline environments. *University of Washington*. http://hdl.handle.net/1773/48545

Cooper, Z. S., Rapp, J. Z., Carpenter, S. D., Iwahana, G., Eicken, H., & Deming, J. W. (2019). Distinctive microbial communities in subzero hypersaline brines from Arctic coastal sea ice and rarely sampled cryopegs. *FEMS Microbiology Ecology*, *95*(12), fiz166. https://doi.org/10.1093/femsec/fiz166

Cooper, Z. S., Rapp, J. Z., Shoemaker, A. M. D., Anderson, R. E., Zhong, Z.-P., & Deming, J. W. (2022). Evolutionary divergence of *Marinobacter* strains in cryopeg brines as revealed by pangenomics. *Frontiers in Microbiology*, *13*, 879116. https://doi.org/10.3389/fmicb.2022.879116

Czajka, J. J., Abernathy, M. H., Benites, V. T., Baidoo, E. E. K., Deming, J. W., & Tang, Y. J. (2018). Model metabolic strategy for heterotrophic bacteria in the cold ocean based on Colwellia psychrerythraea 34H. *Proceedings of the National Academy of Sciences*, *115*(49), 12507–12512. https://doi.org/10.1073/pnas.1807804115

Deming, J. W., & Young, J. N. (2008). The role of exopolysaccharides in microbial adaptation to cold habitats. In R. Margesin (Ed.), *Psychrophiles: From Biodiversity to Biotechnology* (pp. 247–264). Springer. https://doi.org/10.1007/978-3-319-57057-0_12

Everdingen, R. van. (2005). Multi-language glossary of permafrost and related ground-ice terms. *Boulder, CO: National Snow and Ice Data Center/World Data Center for Glaciology*. http://nsidc.org/fgdc/glossary

Gilichinsky, D., Rivkina, E., Bakermans, C., Shcherbakova, V., Petrovskaya, L., Ozerskaya, S., Ivanushkina, N., Kochkina, G., Laurinavichuis, K., Pecheritsina, S., Fattakhova, R., & Tiedje, J. M. (2005). Biodiversity of cryopegs in permafrost. *FEMS Microbiology Ecology*, *53*(1), 117–128. https://doi.org/10.1016/j.femsec.2005.02.003

Gilichinsky, D., Rivkina, E., Shcherbakova, V., Laurinavichuis, K., & Tiedje, J. (2003). Supercooled water brines within permafrost: an unknown ecological niche for microorganisms: a model for astrobiology. *Astrobiology*, *3*(2), 331–341. https://doi.org/10.1089/153110703769016424

Gomez-Buckley, A. C., Showalter, G. M., & Wong, M. L. (2022). Modeling virus and bacteria populations in Europa's subsurface ocean. *Life*, *12*(5), 620. https://doi.org/10.3390/life12050620

Hoehler, T. M., & Jørgensen, B. B. (2013). Microbial life under extreme energy limitation. *Nature Reviews Microbiology*, *11*(2), 83–94. https://doi.org/10.1038/nrmicro2939

Hunter, J. D. (2007). Matplotlib: A 2D graphics environment. *Computing in Science & Engineering*, *9*(3), 90–95. https://doi.org/10.1109/mcse.2007.55

Iwahana, G., Cooper, Z. S., Carpenter, S. D., Deming, J. W., & Eicken, H. (2021). Intra-ice and intra-sediment cryopeg brine occurrence in permafrost near Utqiaġvik (Barrow). *Permafrost and Periglacial Processes*, *32*(3), 427–446. https://doi.org/10.1002/ppp.2101

Jørgensen, B. B., & Boetius, A. (2007). Feast and famine — microbial life in the deep-sea bed. *Nature Reviews Microbiology*, *5*(10), 770–781. https://doi.org/10.1038/nrmicro1745

Kirchman, D. L., Hill, V., Cottrell, M. T., Gradinger, R., Malmstrom, R. R., & Parker, A. (2009). Standing stocks, production, and respiration of phytoplankton and heterotrophic bacteria in the western Arctic Ocean. *Deep Sea Research Part II: Topical Studies in Oceanography*, *56*(17), 1237–1248. https://doi.org/10.1016/j.dsr2.2008.10.018

Krembs, C., Eicken, H., Junge, K., & Deming, J. W. (2002). High concentrations of exopolymeric substances in Arctic winter sea ice: implications for the polar ocean carbon cycle and cryoprotection of diatoms. *Deep Sea Research Part I: Oceanographic Research Papers*, *49*(12), 2163–2181. https://doi.org/10.1016/s0967-0637(02)00122-x

Lever, M. A., Rogers, K. L., Lloyd, K. G., Overmann, J., Schink, B., Thauer, R. K., Hoehler, T. M., & Jørgensen, B. B. (2015). Life under extreme energy limitation: a synthesis of laboratory- and field-based investigations. *FEMS Microbiology Reviews*, *39*(5), 688–728. https://doi.org/10.1093/femsre/fuv020

Ma, Y., Dixit, V., Innes, M. J., Guo, X., & Rackauckas, C. (2021). A comparison of automatic differentiation and continuous sensitivity analysis for derivatives of differential equation solutions. *2021 IEEE High Performance Extreme Computing Conference (HPEC)*, *00*, 1–9. https://doi.org/10.1109/hpec49654.2021.9622796

Marion, G. M., Fritsen, C. H., Eicken, H., & Payne, M. C. (2003). The search for life on Europa: limiting environmental factors, potential habitats, and Earth analogues. *Astrobiology*, *3*(4), 785–811. https://doi.org/10.1089/153110703322736105

Meurer, A., Smith, C. P., Paprocki, M., Čertík, O., Kirpichev, S. B., Rocklin, M., Kumar, Am., Ivanov, S., Moore, J. K., Singh, S., Rathnayake, T., Vig, S., Granger, B. E., Muller, R. P., Bonazzi, F., Gupta, H., Vats, S., Johansson, F., Pedregosa, F., … Scopatz, A. (2017). SymPy: symbolic computing in Python. *PeerJ Computer Science*, *3*, e103. https://doi.org/10.7717/peerj-cs.103

Meyer, H., Schirrmeister, L., Andreev, A., Wagner, D., Hubberten, H.-W., Yoshikawa, K., Bobrov, A., Wetterich, S., Opel, T., Kandiano, E., & Brown, J. (2010). Lateglacial and Holocene isotopic and environmental history of northern coastal Alaska – Results from a buried ice-wedge system at Barrow. *Quaternary Science Reviews*, *29*(27–28), 3720–3735. https://doi.org/10.1016/j.quascirev.2010.08.005

Monod, J. (1949). The growth of bacterial cultures. *Annual Reviews in Microbiology*. https://doi.org/10.1146/annurev.mi.03.100149.002103

Nguyen, D., & Maranger, R. (2011). Respiration and bacterial carbon dynamics in Arctic sea ice. *Polar Biology*, *34*(12), 1843–1855. https://doi.org/10.1007/s00300-011-1040-z

Osman, M. B., Tierney, J. E., Zhu, J., Tardif, R., Hakim, G. J., King, J., & Poulsen, C. J. (2021). Globally resolved surface temperatures since the Last Glacial Maximum. *Nature*, *599*(7884), 239–244. https://doi.org/10.1038/s41586-021-03984-4

Pirt, S. J. (1982). Maintenance energy: a general model for energy-limited and energy-sufficient growth. *Archives of Microbiology*, *133*(4), 300–302. https://doi.org/10.1007/bf00521294

Priscu, J. C., & Hand, K. P. (2012). Microbial habitability of icy worlds. *Microbe Magazine*, *7*(4), 167–172. https://doi.org/10.1128/microbe.7.167.1

Rackauckas, C., & Nie, Q. (2016). DifferentialEquations.jl – A performant and feature-rich ecosystem for solving differential equations in Julia. *Journal of Open Research Software*, *5*(1), 15. https://doi.org/10.5334/jors.151

Rapp, J. Z., Sullivan, M. B., & Deming, J. W. (2021). Divergent genomic adaptations in the microbiomes of arctic subzero sea-ice and cryopeg brines. *Frontiers in Microbiology*, *12*, 701186. https://doi.org/10.3389/fmicb.2021.701186

Rowe, G. T., & Deming, J. W. (1985). The role of bacteria in the turnover of organic carbon in deep-sea sediments. *Journal of Marine Research*, *43*(4), 925–950. https://doi.org/10.1357/002224085788453877

Shampine, L. F., & Reichelt, M. W. (1997). The MATLAB ODE Suite. *SIAM Journal on Scientific Computing*, *18*(1), 1–22. https://doi.org/10.1137/s1064827594276424

Sholes, S. F., Krissansen-Totton, J., & Catling, D. C. (2019). A maximum subsurface biomass on Mars from untapped free energy: CO and H2 as potential antibiosignatures. *Astrobiology*, *19*(5), 655–668. https://doi.org/10.1089/ast.2018.1835

Showalter, G. M. (2020). Acquisition, degradation, and cycling of organic matter within sea - ice brines by bacteria and their viruses. *University of Washington*.

Teske, A. P. (2005). The deep subsurface biosphere is alive and well. *Trends in Microbiology*, *13*(9), 402–404. https://doi.org/10.1016/j.tim.2005.07.004

Verardo, D. J., Froelich, P. N., & McIntyre, A. (1990). Determination of organic carbon and nitrogen in marine sediments using the Carlo Erba NA-1500 analyzer. *Deep Sea Research Part A. Oceanographic Research Papers*, *37*(1), 157–165. https://doi.org/10.1016/0198-0149(90)90034-s

Vetter, Y. A., Deming, J. W., Jumars, P. A., & Krieger-Brockett, B. B. (1998). A predictive model of bacterial foraging by means of freely released extracellular enzymes. *Microbial Ecology*, *36*(1), 75–92. https://doi.org/10.1007/s002489900095

Waskom, M. (2021). seaborn: statistical data visualization. *Journal of Open Source Software*, *6*(60), 3021. https://doi.org/10.21105/joss.03021

Yager, P. L., & Deming, J. W. (1999). Pelagic microbial activity in an arctic polynya: Testing for temperature and substrate interactions using a kinetic approach. *Limnology and Oceanography*, *44*(8), 1882–1893. https://doi.org/10.4319/lo.1999.44.8.1882

Zhong, Z.-P., Rapp, J. Z., Wainaina, J. M., Solonenko, N. E., Maughan, H., Carpenter, S. D., Cooper, Z. S., Jang, H. B., Bolduc, B., Deming, J. W., & Sullivan, M. B. (2020). Viral ecogenomics of arctic cryopeg brine and sea ice. *mSystems*, *5*(3), e00246-20. https://doi.org/10.1128/msystems.00246-20

FIGURES

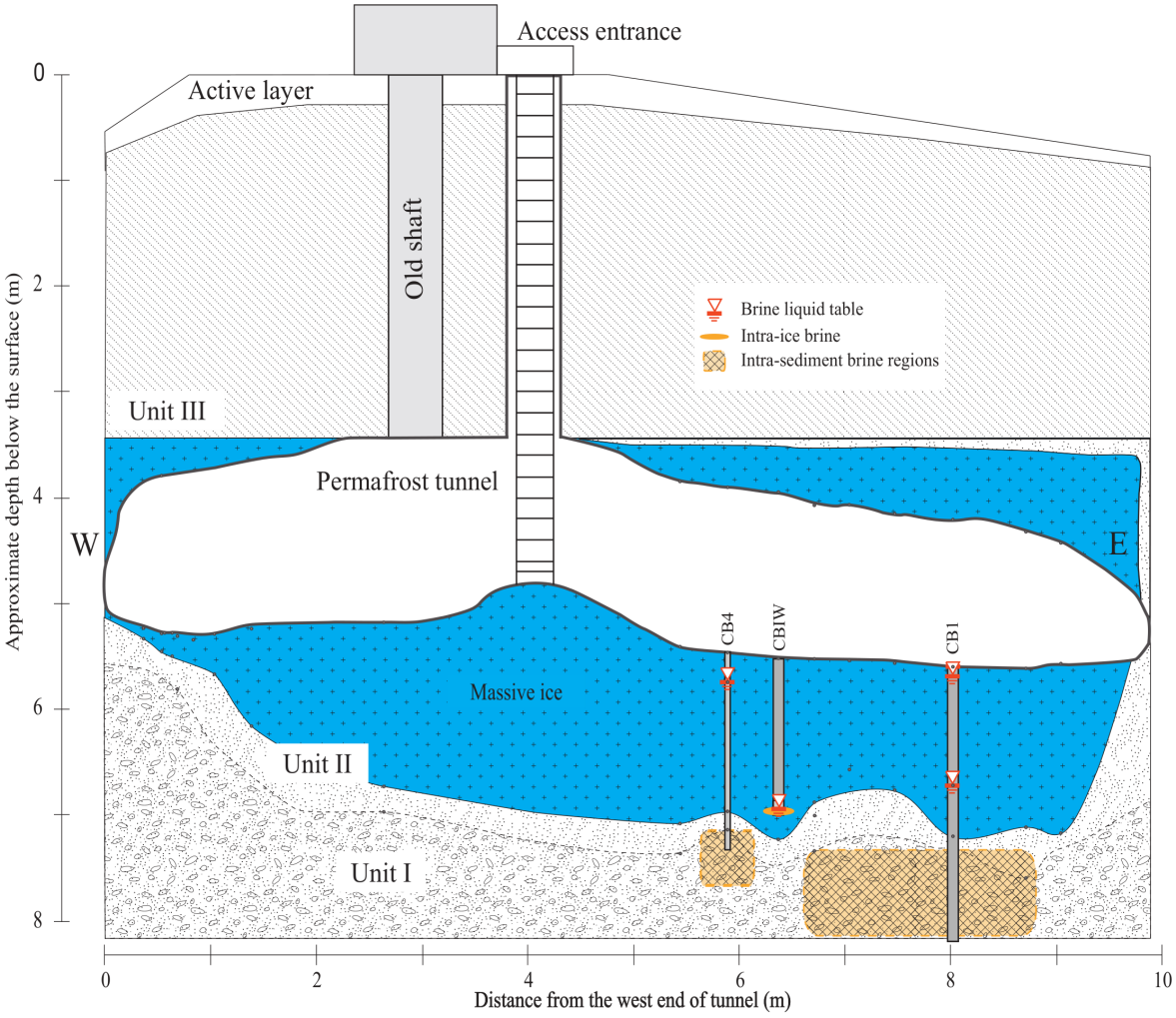

Figure 1.1. NNW-facing cross-sectional diagram of the Barrow Permafrost Tunnel providing access to cryopeg brines near Utqiaġvik, Alaska. Depicted are the cryopeg boreholes CB1, CBIW and CB4 considered in this study. CB1 and CB4 accessed intra-sediment brines 7–8 m below the massive ice; CBIW accessed intra-ice brine thought to have migrated upwards into the massive ice 11,000 years BP (Iwahana et al., 2021). Units I-III refer to permafrost regions (Meyer et al., 2010). Figure adapted from Iwahana et al. (2021).

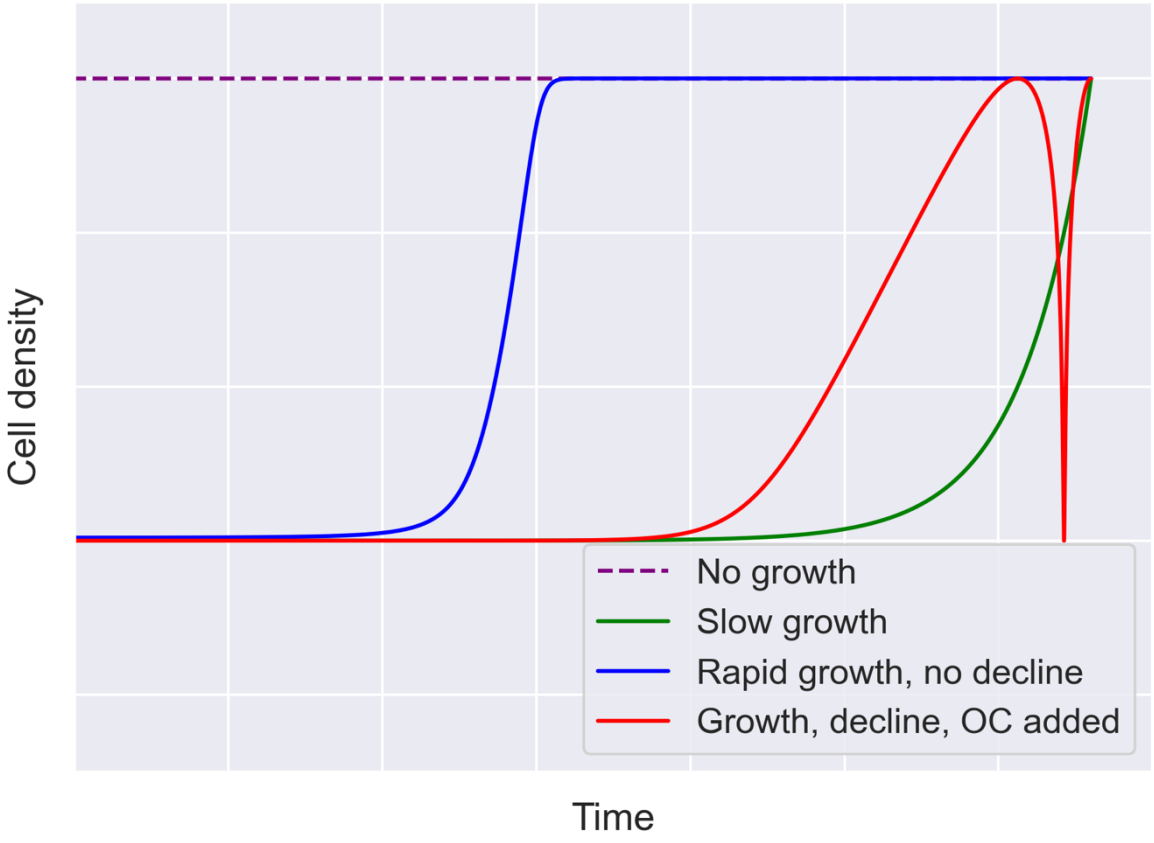

Figure 1.2. Hypothetical growth trajectories to account for a given endpoint cell density. Four possible cases for growth are illustrated here to describe why endpoint measurements leave open many possible trajectories. The case for rapid initial growth followed by stasis is presented in blue. The case for slow growth leading to the observed cell density is presented in green. In red, an intermediate growth rate, followed by decline due to insufficient energy and then an input of organic carbon (OC), depicts recovery of the community to the given endpoint. The no growth scenario, requiring the starting community to be as dense as the endpoint, is indicated by the dashed purple line. Growth lines are intended to be logarithmic, but all lines are conceptual (not drawn to scale).

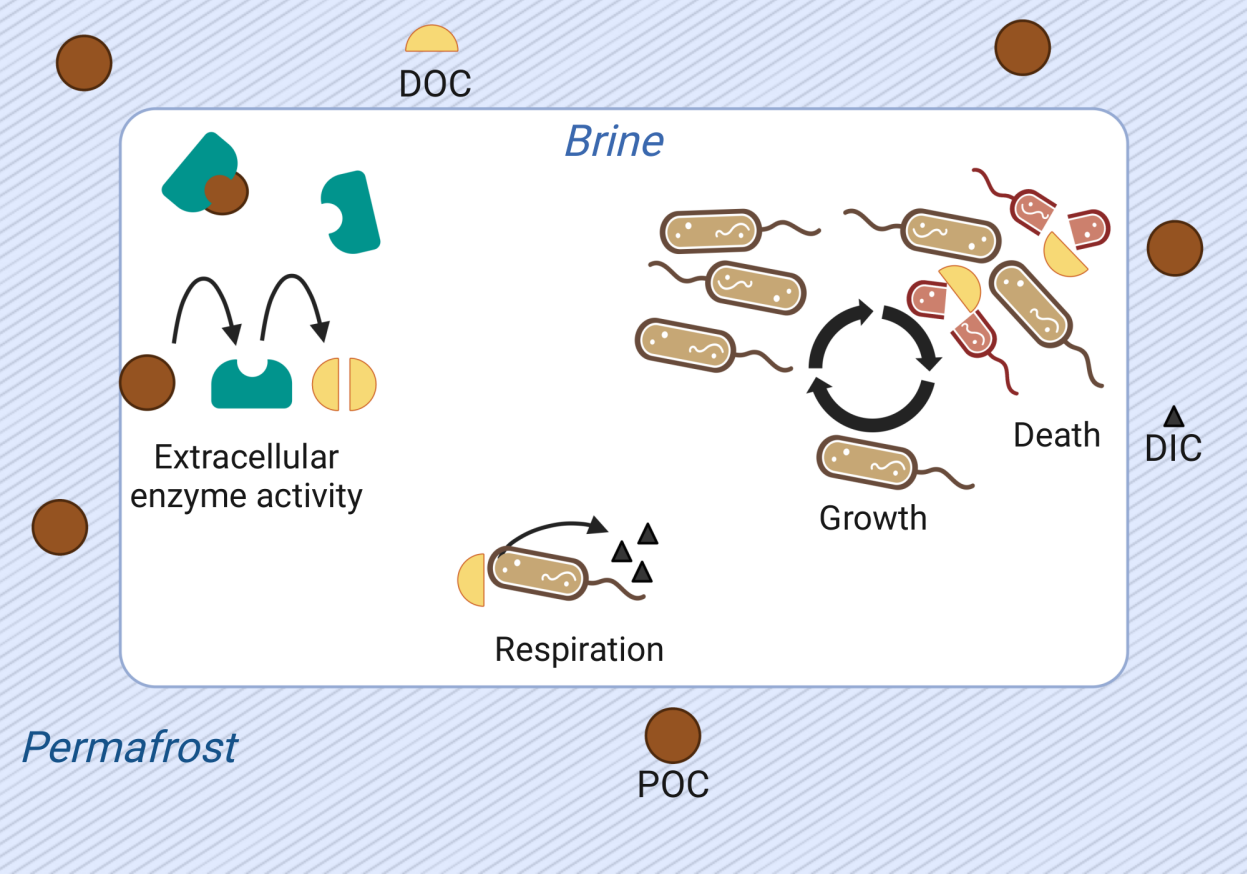

Figure 1.3. Graphical representation of processes and quantities modeled for permafrost-enclosed cryopeg brine. Particulate organic carbon (POC) is shown as dark brown circles; dissolved organic carbon (DOC), as yellow semi-circles; and dissolved inorganic carbon (DIC), as black triangles. Extracellular enzymes (teal-colored shapes) produced and released by bacteria hydrolyze POC to DOC. Bacteria take up DOC, respiring it to dissolved DIC or assimilating it into biomass to grow and reproduce. They release DOC back to the brine upon death, attributed explicitly to starvation in the model.

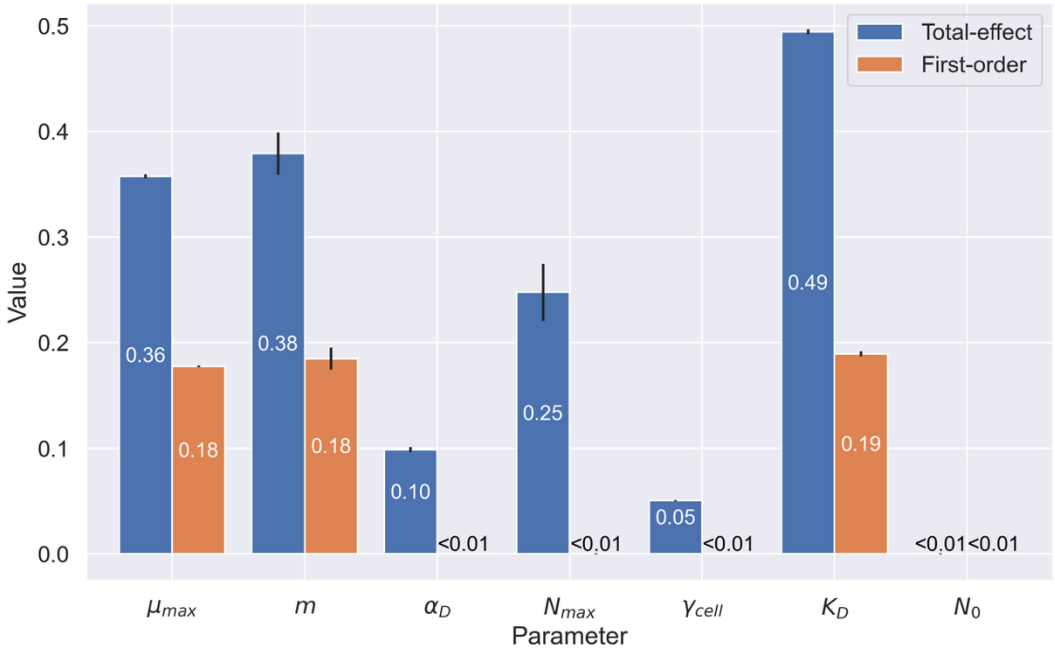

Figure 1.4. Sensitivity analysis of microbial parameters used in the organic carbon model. Numerical values represent the first-order (in orange) and total-effect (in blue) Sobol indices of the selected parameters: maximum growth rate (μ_{max}), cell-specific metabolic rate (m), cell carbon content (α_D), carrying capacity (N_{max}), cell specific extracellular enzyme activity (γ_{cell}), half-velocity constant for carbon uptake (K_D), and starting cell density (N_0). First-order indices show the sensitivity of the model when varying only the parameter in question. Total-effect indices show the sensitivity of the model when varying the selected parameter in conjunction with the other parameters selected in this analysis. Values shown are rounded at 10^{-2}.

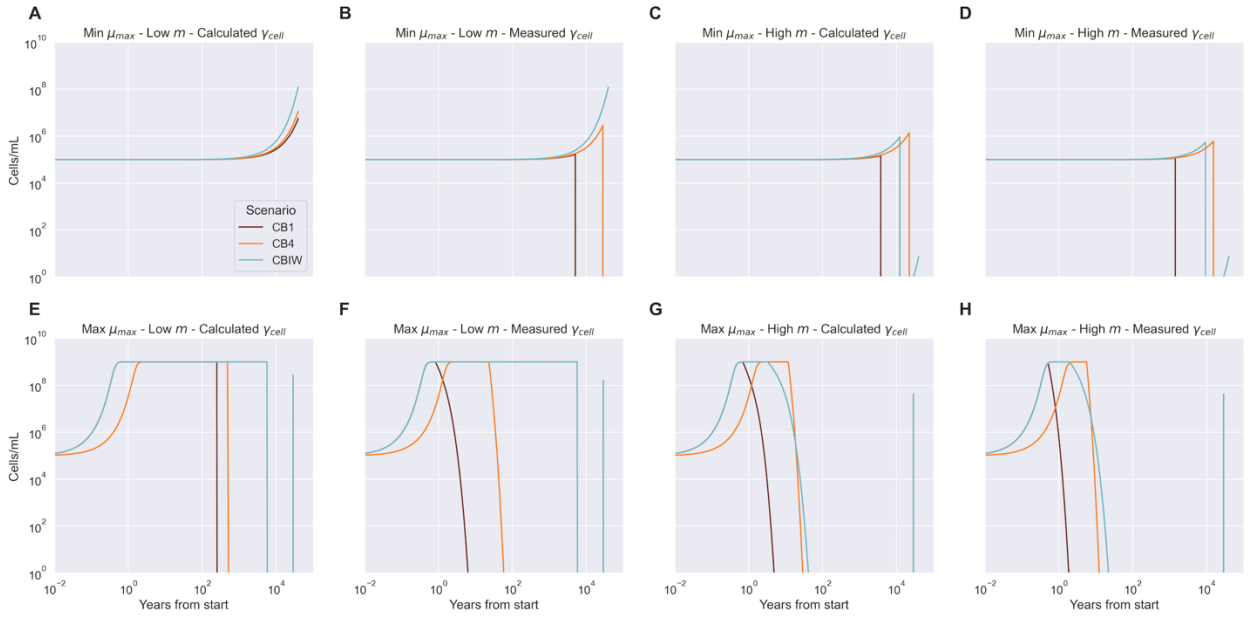

Figure 1.5. Model predictions of cell density over the lifetime of the system for each cryopeg brine scenario. Measured cell densities at 40,000 years are recreated by the model only under conditions shown in panel A: lower bound net growth rate (μ_{max}), lower bound cell-specific metabolic rate (m), and the calculated cell-specific extracellular enzyme activity (γ_{cell}); and for CBIW in panel B: lower bound net growth rate (μ_{max}), lower bound cell-specific metabolic rate (m), and the measured cell-specific extracellular enzyme activity (γ_{cell}). Panels C through H depict cases where the predicted end cell density did not match the observed cell density, regardless of the combination of bounds applied.

Table 1.1. Variables and values used to define each of three cryopeg brine scenarios.

Variable	Symbol (units)	CB1 scenario (source[a])	CB4 scenario (source[a])	CBIW scenario (source[a])
Cell density	N_f (cells mL^{-1})	5.70 x 10^6 (CB1; Colangelo-Lillis et al., 2016)	1.14 x 10^7 (CB4; Cooper et al., 2019)	1.39 x 10^8 (CBIW; Cooper et al., 2019)
Sediment POC	P_0 (fg C cm^{-3})	1.64 x 10^{13} (BEO; this study)	1.75 x 10^{13} (CB4; this study)	1.64 x 10^{13} (BEO; this study)
Sediment DOC	D_0 (fg C cm^{-3})	3.41 x 10^{10} (BEO; this study)	6.17 x 10^{11} (CB4; this study)	3.41 x 10^{10} (BEO; this study)
Brine POC	P_f (fg C mL^{-1})	1.49 x 10^{11} (CB1; Cooper et al., 2019)	4.97 x 10^{10} (CB4; Cooper et al., 2019)	2.38 x 10^{10} (CBIW; Cooper et al., 2019)
Brine DOC	D_f (fg C mL^{-1})	1.23 x 10^{12} (CB1; Cooper et al., 2019)	1.02 x 10^{12} (CB4; Cooper et al., 2019)	3.60 x 10^{11} (CBIW; Cooper et al., 2019)
Added DOC[b]	D_{in} (fg C mL^{-1})	0	0	3.88 x 10^{10} (massive ice; Colangelo-Lillis et al., 2016)
Added POC[b]	P_{in} (fg C mL^{-1})	0	0	1.86 x 10^{10} (massive ice; Colangelo-Lillis et al., 2016)
Cell carbon content	α_D (fg C cell^{-1})	15.7 (Nguyen & Maranger, 2011)	54.04 (Bakermans et al., 2006; Kirchman et al., 2009)	15.7 (Nguyen & Maranger, 2011)
Net growth rate[c]	μ_{max} (day^{-1})	0.06 (Cooper, 2021)	0.016 (Bakermans et al., 2003)	0.06 (Cooper, 2021)

[a] CB1, CB4, and CBIW indicate boreholes; BEO indicates Barrow Environmental Observatory. CB1 and CBIW were dominated by *Marinobacter* sp.; CB4, by *Psychrobacter* sp.

[b] Single addition at 29,000 years (11,000 years BP) into the 40,000-year trajectory.

[c] Net (community) growth rate was set to the maximum growth rate of the dominant bacterium (see Section 3.7)

Table 1.2. Constants used to model cryopeg brine scenarios

Constant	Symbol (unit)	Value	Reference
Carrying capacity	N_{max} (cells mL^{-1})	10^9	Assumed, based on Schmidt et al. (1998)
Monod half-velocity constant	K_D (fg C mL^{-1})	8.82 x 10^5	(Rowe & Deming, 1985; Yager & Deming, 1999)
Cell density at t_0	N_0 (cells mL^{-1})	10^5	Assumed, based on density in coastal sea ice (Cooper et al., 2019)
Extracellular enzyme activity rate	γ_{max} (fg C cell^{-1} day^{-1})	1.22 x 10^{-2}	Measured in CBIW (Showalter, 2020)
Simulation timespan	t_f (years)[a]	40,000	(Iwahana et al., 2021)

[a] Converted to days for all calculations.

Table 1.3. Parameter bounds of the sensitivity analysis

Parameter (units)	Lower bound	Upper bound
Growth rate (day^{-1})	1 x 10^{-6}	1 x 10^2
Cell-specific metabolic rate (fg C cell^{-1} day^{-1})	1 x 10^{-5}	5 x 10^2
Cell carbon content (fg C cell^{-1})	1 x 10^2	5 x 10^2
EEA rate (fg C cell^{-1} day^{-1})	0	1 x 10^2
Monod half-velocity constant (fg C)	1 x 10^3	1 x10^8
Carrying capacity (cells mL^{-1})	1 x 10^8	1 x 10^9
Starting cell density (cells mL^{-1})	1	1 x 10^8

Table 1.4. Cell-specific metabolic rate bounds and calculated maximum doubling time and minimum growth rate for each cryopeg brine scenario.

Parameter (units)	CB1 scenario	CB4 scenario	CBIW scenario
Cell-specific metabolic rate (fg C cell^{-1} day^{-1})	0.181–0.743	0.099–0.474	0.008–0.057
Maximum doubling time (years)	6,860	5,850	3,870
Minimum growth rate (day^{-1})	2.77 x 10^{-7}	3.24 x 10^{-7}	4.95 x 10^{-7}

CHAPTER 2: ACCLIMATION TO OSMOTIC STRESS AND POSSIBLE MEMORY MECHANISM IN *COLWELLIA PSYCHRERYTHRAEA* 34H

ABSTRACT

Bacterial memory systems enable organisms to anticipate and prepare for recurring environmental stresses, enhancing fitness in temporally variable habitats. Sea-ice bacteria experience osmotic stress driven by temperature-dependent salinity fluctuations ranging from below seawater levels during melting to over 200 ppt in winter. We investigated whether the model sea-ice bacterium *Colwellia psychrerythraea* strain 34H exhibits physiological and epigenetic memory of osmotic stress exposure. Using near-continuous optical density monitoring via replicate Pioreactor systems, we subcultured 34H repeatedly (up to 24 times), alternating between optimal (33 ppt) and stressful (55 ppt) salinity conditions, with constant-salinity controls. Growth rates decreased and lag times shortened under stressful salinity in the alternating treatments, mirroring trends observed in the high-salinity control, suggesting that memory of recent stress was maintained despite intermittent recovery periods under optimal salinity. Nanopore sequencing with nucleotide methylation-calling revealed dynamic remodeling of the DNA methylome in response to salinity transitions, with an average difference of 3% (a high Wasserstein distance metric) in methylation patterns between optimal and stressful. The GATC motif, recognized by a Dam methyltransferase, was depleted in promoter regions and prophage yet occurred in over 600 promoters, suggesting a regulatory role on a functionally diverse subset of genes. Differential methylation was identified in promoters of key osmotic stress response genes, including *GbsR* (compatible solute synthesis regulator), *FldA* (stress-tolerant replacement of ferrodoxin), and *AcrR* (efflux pump regulator). Over successive alternating subculturing steps, methylation patterns diverged from controls, with the methylome under alternating conditions retaining signatures most similar to recent stress history. These findings indicate that DNA methylation participates in the osmotic stress response in a psychrophilic bacterium and may encode information about past stressful exposures.

INTRODUCTION

The study of Bacteria has revealed the existence of information-encoding systems, or memory systems, granting some organisms a key advantage to acclimate or adapt to their environment. For example, *Bacillus subtilis* synchronizes its gene expression to predictable recurring environmental signals such as light (Eelderink-Chen et al., 2021). In *Escherichia coli* an asymmetrical anticipatory regulatory network of lactose and maltose genes was identified (Mitchell et al., 2009): when the bacteria encounter lactose, they upregulate maltose operon activity in anticipation of subsequent maltose availability, reflecting the sequential order of these sugars in the mammalian gut.

Memory also enables organisms to anticipate and prepare for recurrent stress. *Bacillus subtilis* shows improved recovery rates to heat shock when first exposed to mild heat (primed to mild heat; Runde et al., 2014). In this case, a gene associated with quality control of proteins under oxidative stress was determined to play a role in the stress response. The abundant marine bacterium *Prochlorococcus* demonstrates memory and acclimation to periods of light stress (Coe et al., 2021). By monitoring *Prochlorococcus* growth during alternating optimal and stressful light conditions, Coe et al. (2021) found that growth rates decreased initially before increasing after just two stress exposures, evidence of acclimation to the stressful condition. The memory of this stressful condition persisted for over 6 months of repeated subculturing under optimal conditions.

The body of work on bacterial memory, particularly studies demonstrating the role of memory in stress acclimation, motivated us to search for memory in sea-ice bacteria. Sea ice is a temporally recurrent environment subject to seasonality; its microbial communities experience annual fall entrainment and summer release cycles.

A bacterial system that anticipates fluctuations in osmotic stress may enhance organism fitness (Lambert & Kussell, 2014). Within the network of sea-ice brines, salinity is dependent on temperature. At very cold winter temperatures, brine salinity can exceed 220 ppt (–28°C; Collins et al., 2008), many times greater than seawater salinity. Due to this temperature dependence, variations of just a few degrees, as occur frequently in upper sea ice (Collins et al., 2008; Cox & Weeks, 1983; Ewert & Deming, 2013), will expose the microbial community to osmotic stress (Firth et al., 2016; Junge et al., 2001). Strong temperature gradients exist within ice: proximity to the ocean raises the temperature and reduces its variability, while the inverse occurs near the atmosphere. As temperatures fluctuate in the ice, fresher then saltier periods occur in the brines, potentially favoring bacteria that remain primed for osmotic stress following recent exposure. Sea-ice communities show better survival rates to osmotic stress than seawater communities (Collins et al., 2010; Kaartokallio et al., 2005), evidence of acclimation mechanisms. Work on sea-ice algae shows that they are primed for the return of spring light (Lewis et al., 2019). Together, these findings validate the relevance of searching for memory in bacteria from this environment.

We investigated memory in the osmotic stress response of *Colwellia psychrerythraea* strain 34H (hereafter "34H"), a model sea-ice bacterium (Boetius et al., 2015; Huston, 2003; Methé et al., 2005). Various osmotic stress responses of 34H have been characterized, including the production of extracellular polysaccharides and use of compatible solutes such as choline (Carillo et al., 2015; Ewert & Deming, 2014; Firth et al., 2016; Junge et al., 2006; Marx et al., 2009). Inspired by Coe et al. (2021), we designed a novel experiment to obtain high resolution optical density curves of 34H grown under alternating optimal and stressful salinities. We anticipated that 34H would exhibit initially slower growth rates under osmotic stress than in optimal salinity, which would increase following repeated growth under stress. This increase over time would reflect acclimation to the stressful condition. Furthermore, we predicted that acclimation to stress would persist despite intermittent growth periods under optimal conditions. Our hypothesis was that the bacterium maintains a memory of prior osmotic stress that primes it for subsequent growth under this same stress.

Incubation conditions were chosen to allow measurable growth of 34H to densities that would allow confident measurement of optical density and subsequent analysis. We used Pioreactors (pioreactor.com), small, cost-effective culture systems, each with integrated optical density sensor, stir bar, and temperature control. These systems provided near-continuous OD measurements and generated high-definition growth curves under controlled conditions. To identify mechanisms underlying expected growth rate changes, we collected samples near the end of each period of logarithmic growth for genomic and epigenomic analysis. By coupling physiological monitoring with molecular analysis, we aimed to connect observable growth phenotypes with their underlying epigenetic regulatory mechanisms.

DNA methylation is a good candidate for a memory mechanism for several reasons. It encodes information on environmentally relevant timescales (Collier et al., 2007; Ghosh et al., 2019; Gopalan-Nair et al., 2024; Rambo et al., 2019); the information is inheritable and already suggested to underlie memory (Casadesús & D'Ari, 2002; Hu et al., 2018; Riber & Hansen, 2021; Yang et al., 2025); and it plays regulatory roles in stress responses (Hu et al., 2018; Yano et al., 2020), including cold stress in a psychrophile (Bu et al., 2025). Moreover, it has been linked to memory of phage integration (Yang et al., 2025). Therefore, we hypothesized that a methyltransferase in 34H would methylate portions of promoter regions for genes involved in osmotic stress

response, regulating their expression during growth under salinity stress. We further hypothesized that subsets of these methylation patterns would persist through periods of favorable conditions, retaining encoded information about past stresses and underlying memory systems. If confirmed, such a memory system would represent a fundamental acclimation strategy for microorganisms in temporally variable environments, with implications for understanding microbial resilience in polar ecosystems.

MATERIALS AND METHODS

CULTURING

Two batches of half-strength marine broth 2216 (Difco) were prepared: one at a salinity of 33 ppt, an optimal growth salinity for 34H (Huston, 2003); and the other at a salinity of 55 ppt. The stressful salinity was determined by subtracting a margin from the maximum growth salinity for 34H (approximately 60 ppt at its optimal growth temperature of 8°C; Huston, 2003; Huston et al., 2004). The broth was prepared following the manufacturer's protocol to dissolve the powder, then filter through a glass fiber filter (Whatman). The filtered broth was diluted with an equal volume of artificial seawater (ASW: 0.4 M NaCl, 9 mM KCl, 26 mM $MgCl_2$, 28 mM $MgSO_4$, and 5 mM TAPSO buffer), yielding a final salinity of 33 ppt ("33 ppt medium"). The higher salinity batch was supplemented with additional NaCl to bring the salinity to 55 ppt ("55 ppt medium"). Finally, the media were autoclaved, and salinity confirmed by refractometer after autoclaving.

Glycerol-protected stocks of 34H were reconstituted from –70°C freezer storage in 33 ppt medium. The stock was checked for contamination by 16S rRNA amplicon sequencing. The stock was then subcultured into 200 mL of 33 ppt medium at 8°C to obtain the seed culture for the experiment. To begin the experiment, 100 µL of the seed culture were inoculated into each vial of the experimental set-up. The vials were 20 mL capacity glass Pioreactor vials, first cleaned with soap and water, thoroughly rinsed with distilled water then autoclaved.

EXPERIMENTAL SET-UP

For the experimental set-up, we used four Pioreactor systems, small modular culturing systems, each with built-in OD600 sensor, stir bar, and temperature control (pioreactor.com). The units were tested in advance for long-term performance in the cold and proved reliable. Four units were used: Unit 1 for the alternating treatment; Unit 2 for the replicate alternating treatment; Unit 3 for the control at optimal salinity; and Unit 4 for the control at stressful salinity. All Pioreactors and cultures were housed in a cold room set to 8°C (± 1.5°C). For the alternating treatments, 34H was first grown in 33 ppt medium, then subcultured in 55 ppt medium, then subcultured in 33 ppt medium, etc., for a total of 14 complete growth cycles. We call each complete cycle (or subculture) a step. The optimal control, always subcultured into 33 ppt medium, had 24 steps in the same time frame, while the stressful control, always subcultured in 55 ppt medium, had 13 steps.

In all cases, 100 µL of culture from the previous vial was used to inoculate the next vial. All vials contained 15 mL of media and were stirred continuously with a stir bar at 800 rpm. Growth in the cultures was monitored using the built-in OD600 sensors of the Pioreactors, which measured OD600 every 5 seconds, adjusted later in the experiment to every 30 seconds. The Pioreactors also controlled the stir bar and monitored the temperature (which remained well within the cold room's setting) To control for inoculum growth phase, we aimed to subculture during mid-exponential phase. Preliminary tests of 34H growth in the Pioreactors under optimal control conditions revealed that an empirically set threshold of OD600 at 0.24 defined this growth phase accurately. To that end, we subcultured at the earliest possible time once an OD600 value of 0.24 was recorded.

Growth curves

Optical density data were quality-controlled before analysis. For each step, the first 2 minutes of optical density data were discarded to remove potential artifacts caused by vial manipulation. Optical density measurements were corrected using the Pioreactor's calibration to account for blank media and the intrinsic variance of each sensor. Other artifacts caused by misaligned vials or accidental vial movement during regular checks were also filtered out. The data were then aggregated into 10-minute bins, and the mean optical density was taken to minimize variance from noise. The natural logarithm of each value was then plotted over time, providing curves from which growth rate and lag time could be calculated.

Growth rates were determined following an established method (Hall et al., 2014) implemented by custom code (https://github.com/Ge0rges/pio-bacterial-memory). Briefly, we first calculated the rolling slope along a window of 10 points (representing 100 minutes) using a linear regression in scikit-learn v1.5.1 (Pedregosa et al., 2011). The maximum slope was identified, and then every set of points with a slope greater or equal to 95% of the maximum slope were grouped together, on which a final linear regression was performed to obtain the maximum growth rate ($hour^{-1}$; Figure 2.1). The lag time was calculated conventionally, by identifying the intersection of the line fitting this group of points and the line fitting the first 30 minutes of data for each step (Figure 2.1).

Trends in growth rate and lag time were determined by performing a robust linear regression using statsmodels v0.14.4 (Seabold & Perktold, 2010) on the group of points of interest for each of the four experimental conditions. The reported *P* value tests the hypothesis that the slope is non-zero, and shaded areas on a plot represent the 95% confidence interval. Equality comparisons between regressions were performed using statsmodels to fit an ordinary least squares model on the group of points with a group interaction term. A *P* value of the interaction term less then 0.05 was taken to mean that trends in each group were different.

Sequencing

At the end of each step, a 1 mL aliquot of culture was removed and placed immediately in a metal block at –70°C. DNA was extracted using a Masterpure Complete DNA & RNA Purification Kit following the manufacturer's protocol, with an added lysozyme step prior to protocol start. DNA sequencing was performed by the University of Washington's Nanopore Sequencing Core on PromethION flow cells using a rapid barcode library preparation. Reads were basecalled using dorado SUP model, with 4mC, 5mC, and 6mA modifications using the latest models available in August 2025.

Bioinformatic analysis

All reads with a quality score below Q10 or length below 100 were discarded. Reads were mapped from each sample onto the 34H reference genome using minimap 2 -ayx map-ont v2.28 (Li, 2021). To determine the isogenicity of the cultures medaka v2.0.1 was used with the medaka_variant tool which identifies haploid variants. Reads were then piled up at the location to determine the proportion of the population with each allele. Two populations were determined to be isogenic using a binomial test (background error rate of 5%) with minimum effect size of 10%.

Using modkit v0.5.0, the reads were piled up, and motifs were identified *de novo* with a confidence threshold of 0.95 and minimum coverage of 30. The resulting methylation data were analyzed using custom code available on GitHub (https://github.com/Ge0rges/Methylation-analysis) commit #309b49b. Only positions with at least 30x coverage in every sample were considered further. We obtained a normalized methylation fraction for each position by a weighted mean by coverage.

The differences in the entire methylome between treatment pairs were determined using a bootstrapped Wasserstein distance test with $P < 0.05$ taken as the threshold for significance. We also performed a Kolmogorov–Smirnov test, an Epps-Singleton test, and an energy distance test (Epps & Singleton, 1986; Goerg & Kaiser, 2009; Virtanen et al., 2020; Zwillinger & Kokoska, 1999). The test results and significance were highly correlated (Pearson correlation >0.98; and >0.66 for Epps-Singleton). To assess the significance of differences in frequency of motif occurrence in different areas of the genome, we used a chi-squared test. The same test was used to determine the significance of differences in methylation frequency between a pair of treatments at any motif instance. Multiple test correction was applied throughout using two-stage Benjamin/Hochberg (Seabold & Perktold, 2010). When determining the significance of difference in methylation frequency using the chi-square test, we handled the presence or absence of replicates as follows. When a replicate was present, we first tested replicates against each other: if the test was insignificant (i.e., the replicates were consistent with each other), then the replicate frequencies were pooled together and a chi-square test was performed between the treatments; if they were inconsistent, the test was rejected. Finally, an additional effect size threshold was imposed on motif instance comparisons: in addition to the *P* value being significant, the difference in methylation fraction between treatments had to be greater or equal to the mean standard deviation of methylation fraction for each motif instance multiplied by two, an empirically conservative threshold.

We employed an ensemble feature selection approach integrating multiple statistical methods to identify biologically relevant variables. Partial least squares (PLS) regression and complementary principal component analysis (PCA) with two components were used to identify features with loadings in the top 10%. Additionally, we performed chi-squared, ANOVA, and mutual information on each feature against time, salinity condition, and experimental group (control versus treatment) to assess feature relevance comprehensively across multiple analytical frameworks. Each test was performed on the set of features with variance above 0.000625 (approximately one standard deviation), and the resulting features were selected by significance of the *P* value after Benjamini-Hochberg correction in the case of ANOVA and chi-squared tests; for the mutual information test, the top 10% of scores were kept.

To understand the effects of DNA methylation on previously identified candidate prophage in 34H (Wells, 2006), we sought to identify prophage *de novo* with modern tools. To that end, geNomad v1.11.0 (Camargo et al., 2024) and CheckV 1.0.3 (Nayfach et al., 2021) were used.

Plots were generated using python v3.10.14, matplotlib v3.10.3, seaborn v0.13.2, pandas v2.2.3, and polars v1.27.1. Statistics were executed using scipy v1.13.1 and statsmodels v0.14.4 (Hunter, 2007; Pedregosa et al., 2011; Seabold & Perktold, 2010; Waskom, 2021).

RESULTS AND DISCUSSION

GROWTH PHENOTYPE

High resolution growth curves of 34H under optimal and stressful conditions over time were generated (Figure 2.2). Growth rates of 34H under optimal salinity conditions (33 ppt) ranged from 0.12 $hour^{-1}$ to 0.17 $hour^{-1}$, corresponding to a mean doubling time of approximately 5 hours. This growth rate is consistent with the known growth characteristics of strain 34H at this temperature (Czajka et al., 2018; Huston, 2003). Under salinity stress (55 ppt), growth rates were reduced substantially to a range of 0.031 to 0.087 $hour^{-1}$, representing an approximate 2.5-fold decrease compared to optimal conditions. Stressed cultures also exhibited greater variability in growth rates, with mean standard deviation 1.3-fold greater than under optimal conditions (0.017 $hour^{-1}$ versus 0.013 $hour^{-1}$) and even greater variability in lag times, with mean standard deviation 3.2-fold

greater than under optimal conditions (5.6 hours versus 1.7 hours). Lag times had a range of 15.1–24.5 hours under optimal conditions, and a range of 15.3–42.6 hours under stressful conditions.

To investigate whether 34H acclimated to salinity stress over time through a memory mechanism, we analyzed trends in growth rates and lag times under each experimental condition (Figure 2.2). Stressful conditions led to a decrease in growth rate and lag time, with some linear trends reaching statistical significance (Figures 2.3 and 2.4).

Contrary to expectations, growth rates continued to decline under stress in all cases, with a significant decrease in the high salinity control ($P < 0.001$) and a nearly significant decrease in the stress steps in one replicate (Unit 1; $P = 0.076$). The similarity in trends under stress between this replicate and the control is supported by the interaction analysis ($P > 0.10$), indicating no significant difference in their slopes. Growth rates in the steps under optimal conditions showed no trend in this replicate or in the optimal salinity control ($P > 0.20$). Once more the similarity is supported by the interaction analysis ($P > 0.10$), and this similarity extended to the second replicate (Unit 2). Therefore, we can confidently say that trends in growth rates across stressful conditions were similar to each other (and likely decreasing) while trends in growth rates under optimal conditions were similar and constant. Moreover, interaction analysis confirmed that trends between stress and optimal controls were different ($P < 0.01$) and that replicate 1 (Unit 1) under a given condition differs from the control of the opposite condition ($P < 0.03$).

Similar patterns were identified in the lag times (Figure 2.4). Lag times generally showed acclimation to stress over time by shortening, while under optimal conditions they remained constant. Trends between the controls differed ($P < 0.02$), while trends between replicate conditions and their opposite control also differed. In replicate 1, trends under optimal conditions differed from its own trend under stress ($P < 0.03$), while in both replicates the trends under stress differed from the trend in the optimal control ($P < 0.04$).

Methylation

To address the hypothesis that a methyltransferase in 34H regulates the expression of genes responsive to osmotic stress, we considered methyltransferases that have lost their associated restriction enzyme: orphan methyltransferases. These enzymes can serve in regulatory roles rather than immune defense (see Chapter 3). The 34H genome encodes two known orphan methyltransferases, one of which recognizes the G**A**TC motif and methylates the adenine nucleotide (Roberts et al., 2022). We identified this motif *de novo* in our dataset as well, though we could not identify the motif recognized by the second methyltransferase. The methyltransferase with unknown recognition sequence may recognize a sequence close to GATC, making its detection challenging. Here we analyzed the methylome and genetic characteristics of the G**A**TC motif to determine the role of its associated methyltransferase. The methyltransferase recognizing the G**A**TC is associated with the dam methyltransferase (as annotated by the NCBI and REBASE) first identified in *E. coli* (Løbner-Olesen et al., 2005). This dam methyltransferase is involved in the DNA mismatch repair process but also plays multiple regulatory roles including memory of phage incorporation (Barbeyron et al., 1984; Boye & Løbner-Olesen, 1990; Løbner-Olesen et al., 2005; Schlagman et al., 1986; Yang et al., 2025).

Genetic analysis

Across the experiment, the cultures were determined to be isogenic ($P < 0.0001$). Therefore, variability in methylation patterns and growth phenotype cannot be attributed to the selection of different genetic subpopulations in the culture.

To begin to understand the role of the GATC motif, we first sought to determine whether it is enriched in any areas of the genome. Given the GC content of the 34H genome (38%), the expected frequency of encountering the GATC motif, all else being equal, is every 288 bp. We found that the distribution of GATC motifs around the origin of replication was similar to the genomic average (232 bp) at windows of 1000 bp (166 bp, $P > 0.05$), 2500 bp (208 bp, $P > 0.05$), and 5000 bp (227 bp, $P > 0.05$) flanking the origin with respect to the remaining genome. The lack of significant enrichment in a wide area around the origin indicates that the methyltransferase does not play a cell cycle regulatory role (Collier et al., 2007). Moreover, the motif is not present within 100 bp of the transcription start site of the SeqA protein, which plays a key role in the initiation of DNA replication.

The motif occurs less frequently in genic areas (338.6 bp, $P < 0.0001$) and in promoter areas. The latter was confirmed by testing expanding sizes of promoter areas and comparing them with the remaining intergenic areas. For a promoter size of 35 bp, the frequency was 357.6 bp ($P < 0.0001$) and the intergenic frequency was 77.1 bp ($P < 0.0001$). As the promoter size was expanded to 60 bp and 100 bp, the frequency within the promoter areas decreased to 292.0 bp and 225.6 bp, respectively, remaining significantly depleted compared to intergenic regions ($P < 0.0001$). With a promoter size of 300 bp, the frequency in the promoter regions (72.7 bp) increased to a level comparable to that of intergenic regions (94.8 bp). This distribution is evidence that the motif's depletion is localized to the immediate upstream region of genes. In light of these results, we defined promoter regions conservatively as the 60 bp upstream of the transcription start site for later analyses.

The general depletion in both genic and promoter areas disqualifies a broad regulatory role for this motif. However, it still occurs 338 times in promoter areas within 35 bp of the transcription start sites, 634 times within 60 bp of the transcription start sites, and 1116 times within 100 bp of the transcription start sites. To determine whether specific functions might be targeted by this regulatory mechanism, we performed a chi-squared test comparing functional frequencies between genes with and without the motif in their promoters. We detected no statistical evidence for functional enrichment, suggesting that while the motif's presence in many promoters supports a regulatory capacity, its lack of functional bias indicates that any such regulation operates across diverse cellular functions rather than targeting specific pathways. Therefore, the GATC motif distribution in 34H is consistent with a regulatory role for DNA methylation on a limited but functionally diverse subset of genes. This conclusion is supported by existing literature on Dam methyltransferase function (Løbner-Olesen et al., 2005).

Recent work shows a connection between phage integration memory and the Dam methyltransferase via methylation of the *intA* promoter (Yang et al., 2025). While 34H lacks *intA*, it does show evidence of methylation interaction with a prophage. The 34H genome contains evidence of prophage (Wells, 2006). We identified *de novo* one prophage using geNomad (78% virus score) which was confirmed by CheckV (high-quality). This prophage presents lower frequencies (422 bp, $P = 0.0011$) of the GATC motif, perhaps enabling the prophage to avoid regulatory interference. The decrease in motif occurrences in the prophage is not in response to a restriction-modification system exerting selective pressure because the bacterium does not present a restriction enzyme recognizing the G**A**TC motif.

Furthermore, a database of known and predicted protein-protein interactions (String-DB) suggests that the dam methyltransferase in 34H plays a mismatch repair role via mutH (high confidence) and may play a role in regulating the methionine regulon (medium confidence; Szklarczyk et al., 2022). The methionine regulation role is further supported by the fact that a methionine biosynthesis gene has GATC in its promoter.

Methylome

The 34H methylome presents a flat trend in methylation fraction over the promoters and across the whole genome during exponential growth (Figures 2.5 and B1). In *Caulobacter crescentus* the cell cycle regulatory role played by DNA methylation has been associated with a whole methylome pattern showing a global low in methylation fraction near *ori,* and a global high near *ter* (Collier et al., 2007). Therefore, the 34H methylome supports the earlier conclusion that the Dam methyltransferase does not play a cell cycle regulatory role.

To determine the effect of continuous salinity stress and alternating stressful conditions on the methylome of 34H, we first considered the whole methylome. We assessed the differences in the methylome between the endpoints of every treatment and found significant differences throughout the experiment (Figure 2.6). When considering only motifs occurring within the defined promoter region (a window 60 bp upstream of a transcription start site), the trends were similar to those of the whole methylome (Figure B2, B3, B4). The trend also held when considering only motifs occurring outside the promoters (not shown). In all cases, the Pearson correlation of the Wasserstein distance between groups was over 0.99 ($P < 0.001$). Given that our goal is to understand the regulatory role of DNA methylation, we have focused on the promoter group.

Considering the optimal salinity controls, the differences in methylation patterns within this group show a significant change after the first subculturing step, with an effect size above one standard deviation, and only slight changes over time thereafter. The larger change in comparisons involving optimal control S24 is likely due to significantly lower coverage of that sample (Figure B5). The high salinity controls are statistically similar ($P > 0.05$).

When considering the alternating treatments, the differences between them are overall more pronounced than within the controls, reaching 4.5% by the Wasserstein metric. There is significant variation over time between subcultures of different salinities, with an average difference between salinities of 3% which is over one standard deviation (2.5%). Subcultures of the same salinity are relatively similar to each other with a distance of less than 2%. These findings indicate marked differences between optimal and stressful salinity conditions, with smaller variations over time for a given salinity, with the methylome under optimal conditions remaining more consistent (1.23%) than under stressful conditions (1.68%).

Finally, comparing the alternating treatments to the controls also reveals differences (Figure 2.6). The first alternating step is identical to the first control step, which is expected as they are the same condition inoculated from the same source at the same time. The first high salinity step is similar to its salinity controls, which is also expected given that the controls do not change in salinity over time. However, there are significant differences between the last optimal alternating subculture and the remaining optimal controls, indicating a drift in the methylome over time from the controls. The last optimal subculture is most similar to the beginning of the 33 ppt control (Wasserstein distance metric of 1.25%). Similarly, the last high salinity subculture is most similar to the 55 ppt control closest in time to it (1.38%). Together these data suggest that under alternating growth conditions the methylome diverges from the controls, remaining closest to the initial state under optimal conditions, and closest to the last state under stressful conditions.

We sought to understand what specific changes in the methylome can explain these differences. To begin, we identified all the motif instances that may be under regulation by DNA methylation, considering only motifs within a window 60 bp upstream of the transcription start site (promoters). Then, to be highly conservative, we considered the list of sites with a standard deviation over the experiment at least three times higher than the rest of the dataset, or with a value above or below three times the standard deviation plus the mean in any given treatment (Table S1).

Next, to narrow the list of candidates to the set of motifs responding to the salinity changes imposed in this experiment, we adopted two approaches. The first approach was to use unsupervised methods to identify the most informative features. The second approach was to use the chi-square test to identify sites with a methylation fraction that had changed significantly between any pair of treatments and then use that information to identify genes that varied differently between treatment and controls, over time, or between salinity conditions (Table S3).

Overlapping the results from these different analyses, we identified numerous motif instances of interest. Among a total of 107 motif instances supported by at least one set of tests, 33 were supported by three different metrics, and 8 by four or five (Table 2.1). We retained those supported by at least three different metrics. Many are known to have direct roles in the osmotic response; the most relevant functions are noted here. The most relevant motif instance may be at position 4,001,064, in the promoter of the gene *GbsR*. Its methylation fraction varied significantly over time in the alternating treatment under stress (Figure B3). *GbsR* is known to be involved in the synthesis of compatible solutes, which are crucial compounds in the osmotic stress response in general (Nau-Wagner et al., 2012; Ronzheimer et al., 2018; Warmbold et al., 2020), and specifically in experimental work with sea ice (Firth et al., 2016).

Additional motif instances were identified in promoters of genes that encode multidrug efflux pump components, including *AcrA* at position 1,266,992. Efflux pumps play established roles in bacterial adaptation to osmotic stress, functioning not only in antimicrobial resistance but also in the extrusion of toxic compounds that accumulate during environmental stress conditions. The AcrAB efflux system is known to be upregulated under osmotic shock and other stress conditions. Moreover, at positions 4,174,147 and at 5,027,643 (not shown), motifs in the promoter of two *AcrR* genes also showed evidence of regulation. *AcrR* is also involved in the regulation of an efflux pump, part of the osmotic stress response (Deng et al., 2013; Harmon & Ruiz, 2022; Su et al., 2007; Subhadra et al., 2020).

At position 3,970,228, a motif instance in the promoter of the *Asd* gene was identified as relevant. *Asd* codes for aspartate-semialdehyde dehydrogenase, an enzyme that produces a key precursor for the biosynthesis of ectoine and hydroxyectoine, compatible solutes widely used by bacteria for osmoadaptation (Stöveken et al., 2011). This specialized metabolic pathway for compatible solute synthesis is typically upregulated under osmotic stress conditions.

At position 5,367,866, we identified a motif instance in the promoter for *FldA*, which encodes flavodoxin. Flavodoxin offers superior resistance to oxidative stress than its functional counterpart ferrodoxin and has been shown to be upregulated during osmotic stress (Godard et al., 2020). Moreover, this gene had three other instances of the motif in its promoter region with varying levels of supporting evidence. With four motifs in its promoter region, DNA methylation very likely plays a role in its regulation.

At positions 1,376,940 and 1,156,35, we found motif instances in the promoter of genes for DnaJ-class molecular chaperones and a DnaJ domain-containing protein. DnaJ proteins function as stress sensors and are induced by multiple stressors including heat, cold, and osmotic shock, playing critical roles in maintaining protein homeostasis under stress conditions (Bui et al., 2012; Ngoc et al., 2023; Tripathy et al., 2014; Zhang et al., 2014).

Several motif instances were detected in the promoters of periplasmic proteases and protein quality-control systems known to be involved in stress responses (Gottesman et al., 1997). At positions 4,903,080 and 4,580,548, we identified notable methylation patterns in the promoters of genes for PtrB (Protease II) and DegQ, a periplasmic serine protease. DegQ is a protease that maintains protein homeostasis in the bacterial

cell envelope and functions as a first-response protease under environmental stress, with existing work highlighting it as an essential gene in osmotic stress tolerance (Flannagan et al., 2007; Leandro et al., 2021; Lipinska et al., 1990; Sawa et al., 2011).

Motif instances in the promoter of flagellar biosynthesis genes were identified at position 1,512,639 (*FlgP*). Flagellar gene expression is known to be modulated by osmotic stress in 34H (Ewert et al., 2025; Junge et al., 2003; Nunn et al., 2015; Showalter & Deming, 2017).

At position 4,352,570, we found a motif instance in the promoter of MutS, a DNA mismatch repair protein. Known for maintaining replication fidelity, MutS and related mismatch repair proteins have also been implicated in stress responses and the activation of stress-protective pathways. Its function is intimately linked with the Dam methyltransferase (Schlagman et al., 1986), and this link is suggested by String-DB via MutH, an enzyme in the same system, by String-DB (Szklarczyk et al., 2022). These converging lines of evidence support the methods applied to identify genes of interest in this study (Schlagman et al., 1986).

We did not find a motif instance in a promoter that differed significantly between the first and last step of the alternating treatments, likely due to inconsistencies between the replicates. However, when considering all possible motif instances (beyond promoters), one instance was significantly different. At position 3,716,877, motif instance 970 bp upstream of a *CheC* gene was generally very lowly methylated (<20%) yet showed large variations between beginning and end of the alternating treatment (16%; Figure B7). The *CheC* gene encodes a protein involved in chemotaxis. Chemotaxis, halotaxis, and chemohalotaxis are known behaviors of 34H in subzero brines (Showalter & Deming, 2017). Upon experiencing changing salinity after subculturing, 34H may be triggered to move, providing a reason for this motif to be differentially methylated.

Synthesis

The results of our growth experiment and analyses clearly show acclimation to salinity stress. The much longer lag time under stress relative to optimal conditions early in the experiment indicates delayed entry into exponential growth under hypersaline stress, yet convergence to a similar lag time between conditions by the end of the experiment is clear evidence of acclimation to stress (Figure 2.4). Contrary to expectation, growth rates decreased over the repeated subculturing steps, which together with the shortening of lag times suggests that, while 34H is primed to respond to stress, its response is to grow more slowly rather than expend resources to improve its growth rate. This strategy may be a way of minimizing energy costs: enact an efficient and rapid, energy-requiring response to stress (shortened lag), but a conservative expenditure on growth while the stress lasts (see Chapter 1).

The growth results and analysis are also suggestive of memory. The decline in growth rate under stress in alternating conditions follows the same trend as the stressful control. If no memory mechanism were present, responses to stress or optimal conditions under the alternating conditions would be the same for every exposure, regardless of the previous conditions: we would expect to see a trend in the alternating treatments under stress (no change) that differed from the stressful control (a decline). That is not the case. Instead, the growth data suggest that 34H retains a memory of stressful episodes under alternating conditions, as the trend in those stressed groups mirrors that of the control. Lag time patterns have also been used to quantify memory in similar systems (Vermeersch et al., 2022), and our results demonstrate a similar principle. The variability in both growth rate and lag time trends that we observed between the alternating replicates could be due to inherent stochasticity in the gene network as part of a bet-hedging strategy (Groot et al., 2023). Additional replicates and more steps in a longer-term experiment would allow for clearer identification of trends and different phenotypes that may occur in different replicates under the same conditions.

The genetic and methylome analyses provide important insights for the observed epigenomic patterns. The G**A**TC motif recognized by the Dam methyltransferase of 34H showed significant depletion in promoter regions yet still occurred 338 times within these regulatory windows. This distributional pattern suggests that the Dam methyltransferase regulates a subset of genes. This suggestion agrees with known functions of Dam in other organisms where it is known to regulate gene expression and be involved in memory (Løbner-Olesen et al., 2005; Yang et al., 2025) .

The reduced G**A**TC frequency in the 34H prophage (422 bp, $P = 0.0011$) is particularly intriguing. In the absence of a cognate restriction enzyme, this depletion likely reflects evolutionary selection against regulatory interference by host methylation machinery. Recent work has shown that Dam-mediated methylation can regulate prophage excision and reintegration, with regions of lower methylation showing increased prophage activity (Yang et al., 2025). The 34H prophage may represent an integration whose regulatory independence from host methylation systems facilitated long-term stable integration.

The DNA methylation results are suggestive of memory but may not be the mechanism for it. The persistence of distinct methylation patterns through multiple cycling events suggests that these modifications encode information about past osmotic exposures. In the alternating treatment, the last optimal salinity step showed greatest similarity to the beginning of the optimal control, while the last high salinity step remained closest to the last stressful control. This pattern indicates that the methylome under alternating conditions diverges from non-alternating controls over time, reflecting recent stress history rather than converging to a control state. Though we could not identify a specific motif instance carrying memory information, such behavior may be consistent with an epigenetic memory system that retains information about the most recent environmental state while remaining poised to respond to the next transition. It may also be the case that a different mechanism in 34H underlies the observed phenotypic memory and affects the methylome causing the observed patterns. To identify the underlying memory mechanism, future work could investigate the role of other epigenetic systems such as RNA modifications, small non-coding RNAs, or intracellular protein concentrations, as was done by others searching to explain a memory phenotype (Coe et al., 2021). No specific demethylase enzyme is known in bacteria. However, demethylation in bacteria with *Dam* occurs at replication due to competition between the methyltransferase and proteins seeking to bind to the same area (Anton & Roberts, 2021). Given this role of proteins in regulating the methylation fraction, studying protein concentrations over time should be prioritized.

Our results show that DNA methylation participates in the osmotic shock response though differential methylation of gene promoters. The data demonstrate that 34H maintains significantly different methylation states between saline conditions. The average methylome difference was above one standard deviation (approximately 3% by the Wasserstein distance metric) between optimal (33 ppt) and stressful (55 ppt) salinity conditions under alternating treatments. Thus, the methylome responds to stress under alternating conditions. The *GbsR* transcriptional regulator, which controls compatible solute synthesis, showed differential methylation in its promoter. Compatible solutes are crucial for osmotic stress tolerance, and their regulation via DNA methylation would represent an elegant mechanism for maintaining preparedness for recurrent stress. Similarly, differential methylation was detected broadly in the *FldA* (flavodoxin) promoter, and in multiple genes involved in the AcrAB response (*AcrA* and *AcrR*). Flavodoxin confers superior oxidative stress resistance compared to ferredoxin, and osmotic stress generates secondary oxidative stress in bacteria. *AcrR* regulates efflux pumps as part of the osmotic stress response. The co-regulation of osmotic and oxidative stress responses via methylation would be adaptive given the coupled nature of these stresses. Evidence of broader regulation of known stress responses in 34H, such as a motility gene or other well-known

stress response genes such as two DnaJ-involved genes, suggests a broad regulatory role of DNA methylation in the osmotic shock response of 34H.

Conclusion

Application of an original experimental design yielded evidence of acclimation under salinity stress in *Colwellia psychrerythraea* 34H. Growth rates and lag times both decreased under continuous conditions of stress. These trends persisted despite intermittent periods of growth in optimal conditions in the alternating salinity treatment. Strain 34H appears to acclimate to and remember periods of salinity stress.

The experimental design and subsequent DNA analyses also enabled detection of dynamic DNA methylation changes in 34H under osmotic stress. The promoters of key osmotic and oxidative stress response genes were differentially methylated. These methylation patterns appear to persist through environmental transitions and diverge from controls over time, consistent with a memory response. However, despite the larger methylome trend, no specific motif instance provided evidence of memory, although the chemotaxis gene, *CheC,* presented an exception worth pursuing. Future investigations of memory systems in 34H could benefit from a focus on intracellular protein concentrations.

These findings suggest that epigenetic mechanisms and memory may contribute significantly to the resilience of polar bacterial communities facing large environmental fluctuations. The timescales of epigenetic memory (hours to days, potentially persisting for generations) align well with the temporal dynamics of sea-ice formation and melt, providing a mechanistic basis for the superior stress adaptation previously observed in ice-derived versus open-water bacterial communities (Collins et al., 2010; Kaartokallio et al., 2005).

REFERENCES

Barbeyron, T., Kean, K., & Forterre, P. (1984). DNA adenine methylation of GATC sequences appeared recently in the *Escherichia coli* lineage. *Journal of Bacteriology*, *160*(2), 586–590. https://doi.org/10.1128/jb.160.2.586-590.1984

Boetius, A., Anesio, A. M., Deming, J. W., Mikucki, J. A., & Rapp, J. Z. (2015). Microbial ecology of the cryosphere: sea ice and glacial habitats. *Nature Reviews Microbiology*, *13*(11), 677–690. https://doi.org/10.1038/nrmicro3522

Boye, E., & Løbner-Olesen, A. (1990). The role of dam methyltransferase in the control of DNA replication in *E. coli*. *Cell*, *62*(5), 981–989. https://doi.org/10.1016/0092-8674(90)90272-g

Bu, X., Dou, X., Chen, Z., Liu, L., Mei, Y., & Ren, M. (2025). DNA methylation confers epigenetic changes in cold-adapted microorganisms in response to cold stress. *Extremophiles*, *29*(1), 16. https://doi.org/10.1007/s00792-025-01381-7

Bui, X. T., Qvortrup, K., Wolff, A., Bang, D. D., & Creuzenet, C. (2012). Effect of environmental stress factors on the uptake and survival of *Campylobacter jejuni* in *Acanthamoeba castellanii*. *BMC Microbiology*, *12*(1), 232. https://doi.org/10.1186/1471-2180-12-232

Camargo, A. P., Roux, S., Schulz, F., Babinski, M., Xu, Y., Hu, B., Chain, P. S. G., Nayfach, S., & Kyrpides, N. C. (2024). Identification of mobile genetic elements with geNomad. *Nature Biotechnology*, *42*(8), 1303–1312. https://doi.org/10.1038/s41587-023-01953-y

Carillo, S., Casillo, A., Pieretti, G., Parrilli, E., Sannino, F., Bayer-Giraldi, M., Cosconati, S., Novellino, E., Ewert, M., Deming, J. W., Lanzetta, R., Marino, G., Parrilli, M., Randazzo, A., Tutino, M. L., & Corsaro, M. M. (2015). A unique capsular polysaccharide structure from the psychrophilic marine bacterium *Colwellia psychrerythraea* 34H that mimics antifreeze (glyco)proteins. *Journal of the American Chemical Society*, *137*(1), 179–189. https://doi.org/10.1021/ja5075954

Casadesús, J., & D'Ari, R. (2002). Memory in bacteria and phage. *BioEssays*, *24*(6), 512–518. https://doi.org/10.1002/bies.10102

Coe, A., Biller, S. J., Thomas, E., Boulias, K., Bliem, C., Arellano, A., Dooley, K., Rasmussen, A. N., LeGault, K., O'Keefe, T. J., Stover, S., Greer, E. L., & Chisholm, S. W. (2021). Coping with darkness: The adaptive response of marine picocyanobacteria to repeated light energy deprivation. *Limnology and Oceanography*, *66*(9), 3300–3312. https://doi.org/10.1002/lno.11880

Collier, J., McAdams, H. H., & Shapiro, L. (2007). A DNA methylation ratchet governs progression through a bacterial cell cycle. *Proceedings of the National Academy of Sciences*, *104*(43), 17111–17116. https://doi.org/10.1073/pnas.0708112104

Collins, R. E., Carpenter, S. D., & Deming, J. W. (2008). Spatial heterogeneity and temporal dynamics of particles, bacteria, and pEPS in Arctic winter sea ice. *Journal of Marine Systems*, *74*(3–4), 902–917. https://doi.org/10.1016/j.jmarsys.2007.09.005

Collins, R. E., Rocap, G., & Deming, J. W. (2010). Persistence of bacterial and archaeal communities in sea ice through an Arctic winter. *Environmental Microbiology*, *12*(7), 1828–1841. https://doi.org/10.1111/j.1462-2920.2010.02179.x

Cox, G. F. N., & Weeks, W. F. (1983). Equations for determining the gas and brine volumes in sea-ice samples. *Journal of Glaciology*, *29*(102), 306–316. https://doi.org/10.1017/s0022143000008364

Czajka, J. J., Abernathy, M. H., Benites, V. T., Baidoo, E. E. K., Deming, J. W., & Tang, Y. J. (2018). Model metabolic strategy for heterotrophic bacteria in the cold ocean based on *Colwellia psychrerythraea* 34H. *Proceedings of the National Academy of Sciences*, *115*(49), 12507–12512. https://doi.org/10.1073/pnas.1807804115

Deng, W., Li, C., & Xie, J. (2013). The underling mechanism of bacterial TetR/AcrR family transcriptional repressors. *Cellular Signalling*, *25*(7), 1608–1613. https://doi.org/10.1016/j.cellsig.2013.04.003

Eelderink-Chen, Z., Bosman, J., Sartor, F., Dodd, A. N., Kovács, Á. T., & Merrow, M. (2021). A circadian clock in a nonphotosynthetic prokaryote. *Science Advances*, *7*(2), eabe2086. https://doi.org/10.1126/sciadv.abe2086

Epps, T. W., & Singleton, K. J. (1986). An omnibus test for the two-sample problem using the empirical characteristic function. *Journal of Statistical Computation and Simulation*, *26*(3–4), 177–203. https://doi.org/10.1080/00949658608810963

Ewert, M., & Deming, J. W. (2013). Sea ice microorganisms: environmental constraints and extracellular responses. *Biology*, *2*(2), 603–628. https://doi.org/10.3390/biology2020603

Ewert, M., & Deming, J. W. (2014). Bacterial responses to fluctuations and extremes in temperature and brine salinity at the surface of Arctic winter sea ice. *FEMS Microbiology Ecology*, *89*(2), 476–489. https://doi.org/10.1111/1574-6941.12363

Ewert, M., Nunn, B. L., Firth, E., & Junge, K. (2025). Metabolic responses, cell recoverability, and protein signatures of three extremophiles: sustained life during long-term subzero incubations. *Microorganisms*, *13*(2), 251. https://doi.org/10.3390/microorganisms13020251

Firth, E., Carpenter, S. D., Sørensen, H. L., Collins, R. E., & Deming, J. W. (2016). Bacterial use of choline to tolerate salinity shifts in sea-ice brines. *Elementa*, *4*, 000120. https://doi.org/10.12952/journal.elementa.000120

Flannagan, R. S., Aubert, D., Kooi, C., Sokol, P. A., & Valvano, M. A. (2007). *Burkholderia cenocepacia* requires a periplasmic HtrA protease for growth under thermal and osmotic stress and for survival in vivo. *Infection and Immunity*, *75*(4), 1679–1689. https://doi.org/10.1128/iai.01581-06

Ghosh, D., Veeraraghavan, B., Elangovan, R., & Vivekanandan, P. (2019). Antibiotic resistance and epigenetics: more to it than meets the eye. *Antimicrobial Agents and Chemotherapy*, *64*(2), 10.1128/aac.02225-19. https://doi.org/10.1128/aac.02225-19

Godard, T., Zühlke, D., Richter, G., Wall, M., Rohde, M., Riedel, K., Poblete-Castro, I., Krull, R., & Biedendieck, R. (2020). Metabolic rearrangements causing elevated proline and polyhydroxybutyrate accumulation during the osmotic adaptation response of *Bacillus megaterium*. *Frontiers in Bioengineering and Biotechnology*, *8*, 47. https://doi.org/10.3389/fbioe.2020.00047

Goerg, S. J., & Kaiser, J. (2009). Nonparametric testing of distributions—the Epps–Singleton two-sample test using the empirical characteristic function. *The Stata Journal*, *9*(3), 454–465. https://doi.org/10.1177/1536867x0900900307

Gopalan-Nair, R., Coissac, A., Legrand, L., Lopez-Roques, C., Pécrix, Y., Vandecasteele, C., Bouchez, O., Barlet, X., Lanois, A., Givaudan, A., Brillard, J., Genin, S., & Guidot, A. (2024). Changes in DNA methylation contribute to rapid adaptation in bacterial plant pathogen evolution. *PLOS Biology*, *22*(9), e3002792. https://doi.org/10.1371/journal.pbio.3002792

Gottesman, S., Wickner, S., & Maurizi, M. R. (1997). Protein quality control: triage by chaperones and proteases. *Genes & Development*, *11*(7), 815–823. https://doi.org/10.1101/gad.11.7.815

Groot, D. H. de, Tjalma, A. J., Bruggeman, F. J., & Nimwegen, E. van. (2023). Effective bet-hedging through growth rate dependent stability. *Proceedings of the National Academy of Sciences*, *120*(8), e2211091120. https://doi.org/10.1073/pnas.2211091120

Hall, B. G., Acar, H., Nandipati, A., & Barlow, M. (2014). Growth rates made easy. *Molecular Biology and Evolution*, *31*(1), 232–238. https://doi.org/10.1093/molbev/mst187

Harmon, D. E., & Ruiz, C. (2022). The multidrug efflux regulator AcrR of *Escherichia coli* responds to exogenous and endogenous ligands to regulate efflux and detoxification. *mSphere*, *7*(6), e00474-22. https://doi.org/10.1128/msphere.00474-22

Hu, L., Xiao, P., Jiang, Y., Dong, M., Chen, Z., Li, H., Hu, Z., Lei, A., & Wang, J. (2018). Transgenerational epigenetic inheritance under environmental stress by genome-wide DNA methylation profiling in cyanobacterium. *Frontiers in Microbiology*, *9*, 1479. https://doi.org/10.3389/fmicb.2018.01479

Hunter, J. D. (2007). Matplotlib: A 2D graphics environment. *Computing in Science & Engineering*, *9*(3), 90–95. https://doi.org/10.1109/mcse.2007.55

Huston, A. L. (2003). *Bacterial adaptation to the cold: in situ activities of extracellular enzymes in the North Water Polynya and characterization of a cold-active aminopeptidase from Colwellia psychrerythraea strain 34H*. University of Washington.

Huston, A. L., Methe, B., & Deming, J. W. (2004). Purification, characterization, and sequencing of an extracellular cold-active aminopeptidase produced by marine psychrophile *Colwellia psychrerythraea* strain 34H. *Applied and Environmental Microbiology*, *70*(6), 3321–3328.

Junge, K., Eicken, H., & Deming, J. W. (2003). Motility of *Colwellia psychrerythraea* strain 34H at subzero temperatures. *Applied and Environmental Microbiology*, *69*(7), 4282–4284. https://doi.org/10.1128/aem.69.7.4282-4284.2003

Junge, K., Eicken, H., Swanson, B. D., & Deming, J. W. (2006). Bacterial incorporation of leucine into protein down to −20°C with evidence for potential activity in sub-eutectic saline ice formations. *Cryobiology*, *52*(3), 417–429. https://doi.org/10.1016/j.cryobiol.2006.03.002

Junge, K., Krembs, C., Deming, J., Stierle, A., & Eicken, H. (2001). A microscopic approach to investigate bacteria under in situ conditions in sea-ice samples. *Annals of Glaciology*, *33*, 304–310. https://doi.org/10.3189/172756401781818275

Kaartokallio, H., Laamanen, M., & Sivonen, K. (2005). Responses of Baltic Sea ice and open-water natural bacterial communities to salinity change. *Applied and Environmental Microbiology*, *71*(8), 4364–4371. https://doi.org/10.1128/aem.71.8.4364-4371.2005

Lambert, G., & Kussell, E. (2014). Memory and fitness optimization of bacteria under fluctuating environments. *PLoS Genetics*, *10*(9), e1004556. https://doi.org/10.1371/journal.pgen.1004556

Leandro, M. R., Vespoli, L. de S., Andrade, L. F., Soares, F. S., Boechat, A. L., Pimentel, V. R., Moreira, J. R., Passamani, L. Z., Silveira, V., & Filho, G. A. de S. (2021). DegP protease is essential for tolerance to salt stress in the plant growth-promoting bacterium *Gluconacetobacter diazotrophicus* PAL5. *Microbiological Research*, *243*, 126654. https://doi.org/10.1016/j.micres.2020.126654

Lewis, K. M., Arntsen, A. E., Coupel, P., Joy-Warren, H., Lowry, K. E., Matsuoka, A., Mills, M. M., Dijken, G. L., Selz, V., & Arrigo, K. R. (2019). Photoacclimation of Arctic Ocean phytoplankton to shifting light and nutrient limitation. *Limnology and Oceanography*, *64*(1), 284–301. https://doi.org/10.1002/lno.11039

Li, H. (2021). New strategies to improve minimap2 alignment accuracy. *Bioinformatics*, *37*(23), 4572–4574. https://doi.org/10.1093/bioinformatics/btab705

Lipinska, B., Zylicz, M., & Georgopoulos, C. (1990). The HtrA (DegP) protein, essential for *Escherichia coli* survival at high temperatures, is an endopeptidase. *Journal of Bacteriology*, *172*(4), 1791–1797. https://doi.org/10.1128/jb.172.4.1791-1797.1990

Løbner-Olesen, A., Skovgaard, O., & Marinus, M. G. (2005). Dam methylation: coordinating cellular processes. *Current Opinion in Microbiology*, *8*(2), 154–160. https://doi.org/10.1016/j.mib.2005.02.009

Marx, J. G., Carpenter, S. D., & Deming, J. W. (2009). Production of cryoprotectant extracellular polysaccharide substances (EPS) by the marine psychrophilic bacterium *Colwellia psychrerythraea* strain 34H under extreme conditions. *Canadian Journal of Microbiology*, *55*(1), 63–72. https://doi.org/10.1139/w08-130

Methé, B. A., Nelson, K. E., Deming, J. W., Momen, B., Melamud, E., Zhang, X., Moult, J., Madupu, R., Nelson, W. C., Dodson, R. J., Brinkac, L. M., Daugherty, S. C., Durkin, A. S., DeBoy, R. T., Kolonay, J. F., Sullivan, S. A., Zhou, L., Davidsen, T. M., Wu, M., … Fraser, C. M. (2005). The psychrophilic lifestyle as revealed by the genome sequence of *Colwellia psychrerythraea* 34H through genomic and proteomic analyses. *Proceedings of the National Academy of Sciences*, *102*(31), 10913–10918. https://doi.org/10.1073/pnas.0504766102

Mitchell, A., Romano, G. H., Groisman, B., Yona, A., Dekel, E., Kupiec, M., Dahan, O., & Pilpel, Y. (2009). Adaptive prediction of environmental changes by microorganisms. *Nature*, *460*(7252), 220–224. https://doi.org/10.1038/nature08112

Nayfach, S., Camargo, A. P., Schulz, F., Eloe-Fadrosh, E., Roux, S., & Kyrpides, N. C. (2021). CheckV assesses the quality and completeness of metagenome-assembled viral genomes. *Nature Biotechnology*, *39*(5), 578–585. https://doi.org/10.1038/s41587-020-00774-7

Ngoc, A. T. T., Van, K. N., & Lee, Y. H. (2023). DnaJ, a heat shock protein 40 family member, is essential for the survival and virulence of plant pathogenic *Pseudomonas cichorii* JBC1. *Research in Microbiology*, *174*(7), 104094. https://doi.org/10.1016/j.resmic.2023.104094

Nunn, B. L., Slattery, K. V., Cameron, K. A., Timmins-Schiffman, E., & Junge, K. (2015). Proteomics of *Colwellia psychrerythraea* at subzero temperatures – a life with limited movement, flexible membranes and vital DNA repair. *Environmental Microbiology*, *17*(7), 2319–2335. https://doi.org/10.1111/1462-2920.12691

Pedregosa, F., Varoquaux, G., Gramfort, A., Michel, V., Thirion, B., Grisel, O., Blondel, M., Prettenhofer, P., Weiss, R., Dubourg, V., Vanderplas, J., Passos, A., Cournapeau, D., Brucher, M., Perrot, M., & Duchesnay, É. (2011). Scikit-learn: machine learning in Python. *Journal of Machine Learning Research*, *12*(85), 2825–2830. http://jmlr.org/papers/v12/pedregosa11a.html

Rambo, I. M., Marsh, A., & Biddle, J. F. (2019). Cytosine methylation within marine sediment microbial communities: potential epigenetic adaptation to the environment. *Frontiers in Microbiology*, *10*, 1291. https://doi.org/10.3389/fmicb.2019.01291

Riber, L., & Hansen, L. H. (2021). Epigenetic memories: the hidden drivers of bacterial persistence? *Trends in Microbiology*, *29*(3), 190–194. https://doi.org/10.1016/j.tim.2020.12.005

Roberts, R. J., Vincze, T., Posfai, J., & Macelis, D. (2022). REBASE: a database for DNA restriction and modification: enzymes, genes and genomes. *Nucleic Acids Research*, *51*(D1), D629–D630. https://doi.org/10.1093/nar/gkac975

Sawa, J., Malet, H., Krojer, T., Canellas, F., Ehrmann, M., & Clausen, T. (2011). Molecular adaptation of the DegQ protease to exert protein quality control in the bacterial cell envelope. *Journal of Biological Chemistry*, *286*(35), 30680–30690. https://doi.org/10.1074/jbc.m111.243832

Schlagman, S. L., Hattman, S., & Marinus, M. G. (1986). Direct role of the *Escherichia coli* Dam DNA methyltransferase in methylation-directed mismatch repair. *Journal of Bacteriology*, *165*(3), 896–900. https://doi.org/10.1128/jb.165.3.896-900.1986

Seabold, S., & Perktold, J. (2010). Statsmodels: econometric and statistical modeling with Python. *Proceedings of the 9th Python in Science Conference*, 92–96. https://doi.org/10.25080/majora-92bf1922-011

Showalter, G. M., & Deming, J. W. (2017). Low-temperature chemotaxis, halotaxis and chemohalotaxis by the psychrophilic marine bacterium *Colwellia psychrerythraea* 34H. *Environmental Microbiology Reports*, *10*(1), 92–101. https://doi.org/10.1111/1758-2229.12610

Stöveken, N., Pittelkow, M., Sinner, T., Jensen, R. A., Heider, J., & Bremer, E. (2011). A specialized aspartokinase enhances the biosynthesis of the osmoprotectants ectoine and hydroxyectoine in *Pseudomonas stutzeri* A1501. *Journal of Bacteriology*, *193*(17), 4456–4468. https://doi.org/10.1128/jb.00345-11

Su, C.-C., Rutherford, D. J., & Yu, E. W. (2007). Characterization of the multidrug efflux regulator AcrR from *Escherichia coli*. *Biochemical and Biophysical Research Communications*, *361*(1), 85–90. https://doi.org/10.1016/j.bbrc.2007.06.175

Subhadra, B., Surendran, S., Lim, B. R., Yim, J. S., Kim, D. H., Woo, K., Kim, H.-J., Oh, M. H., & Choi, C. H. (2020). Regulation of the AcrAB efflux system by the quorum-sensing regulator AnoR in *Acinetobacter nosocomialis*. *Journal of Microbiology (Seoul, Korea)*, *58*(6), 507–518. https://doi.org/10.1007/s12275-020-0185-2

Tripathy, S., Sen, R., Padhi, S. K., Sahu, D. K., Nandi, S., Mohanty, S., & Maiti, N. K. (2014). Survey of the transcriptome of *Brevibacillus borstelensis* exposed to low temperature shock. *Gene*, *550*(2), 207–213. https://doi.org/10.1016/j.gene.2014.08.030

Vermeersch, L., Cool, L., Gorkovskiy, A., Voordeckers, K., Wenseleers, T., & Verstrepen, K. J. (2022). Do microbes have a memory? History-dependent behavior in the adaptation to variable environments. *Frontiers in Microbiology*, *13*, 1004488. https://doi.org/10.3389/fmicb.2022.1004488

Virtanen, P., Gommers, R., Oliphant, T. E., Haberland, M., Reddy, T., Cournapeau, D., Burovski, E., Peterson, P., Weckesser, W., Bright, J., Walt, S. J. van der, Brett, M., Wilson, J., Millman, K. J., Mayorov, N., Nelson, A. R. J., Jones, E., Kern, R., Larson, E., … Vázquez-Baeza, Y. (2020). SciPy 1.0: fundamental algorithms for scientific computing in Python. *Nature Methods*, *17*(3), 261–272. https://doi.org/10.1038/s41592-019-0686-2

Waskom, M. (2021). seaborn: statistical data visualization. *Journal of Open Source Software*, *6*(60), 3021. https://doi.org/10.21105/joss.03021

Wells, L. (2006). *Viral adaptations to life in the cold*. University of Washington.

Yang, J., Son, Y., Park, J., & Park, W. (2025). Dam-dependent epigenetic memory regulates prophage reintegration in *Salmonella*. *Nucleic Acids Research*, *53*(18), gkaf951. https://doi.org/10.1093/nar/gkaf951

Yano, H., Alam, Md. Z., Rimbara, E., Shibata, T. F., Fukuyo, M., Furuta, Y., Nishiyama, T., Shigenobu, S., Hasebe, M., Toyoda, A., Suzuki, Y., Sugano, S., Shibayama, K., & Kobayashi, I. (2020). Networking and specificity-changing DNA methyltransferases in *Helicobacter pylori*. *Frontiers in Microbiology*, *11*, 1628. https://doi.org/10.3389/fmicb.2020.01628

Zhang, X., Jiang, X., Yang, L., Fang, L., Shen, H., Lu, X., & Fang, W. (2014). DnaJ of *Streptococcus suis* type 2 contributes to cell adhesion and thermotolerance. *Journal of Microbiology and Biotechnology*, *25*(6), 771–781. https://doi.org/10.4014/jmb.1408.08085

Zwillinger, D., & Kokoska, S. (1999). *CRC Standard Probability and Statistics Tables and Formulae*. CRC Press: Boca Raton. https://doi.org/10.1201/9780367802417

FIGURES

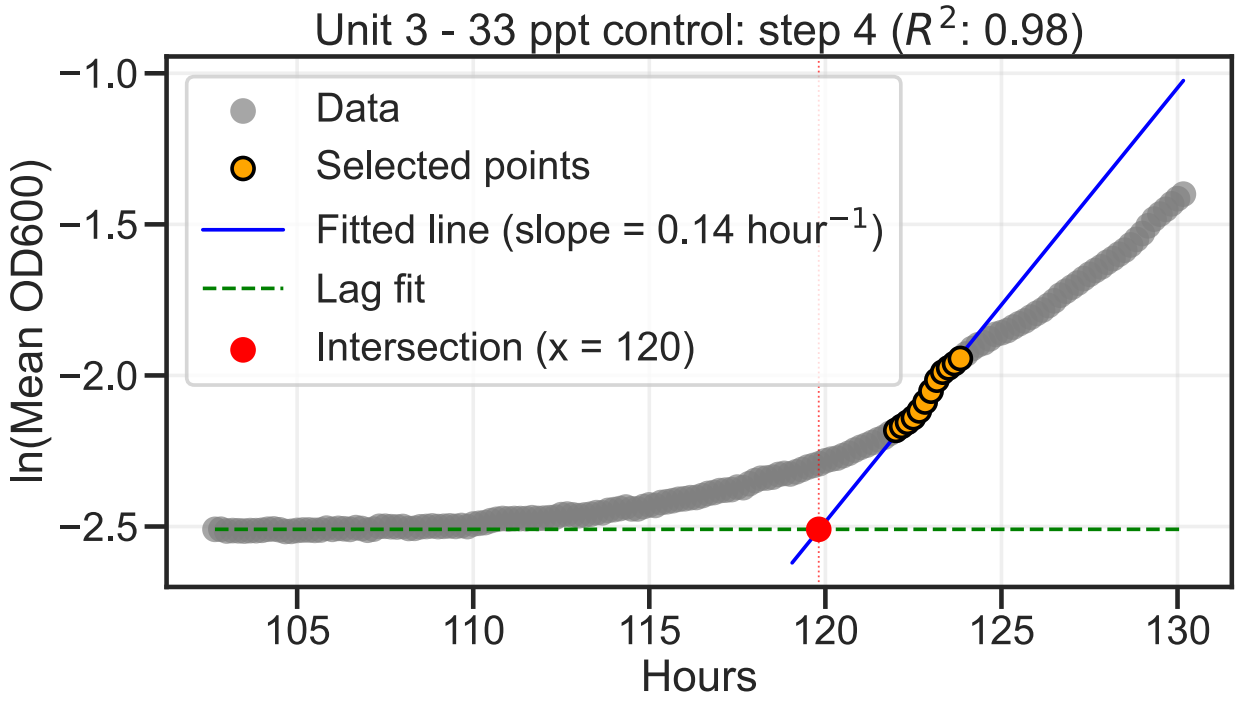

Figure 2.1. The procedure to identify the growth rate and lag time. This random example illustrates the obtained fit on step 4 of the optimal salinity control (33 ppt). The group of points in orange are those where linear regression in rolling groups of 10 produced a slope within 95% of the maximum slope across the curve (R^2 = 0.98 in this case). The maximum growth rate is the slope of the line fitting these points. The lag time is the value of the X coordinate of the point at the intersection between the line fitting the selected points, and a line fitting the first 30 minutes of data.

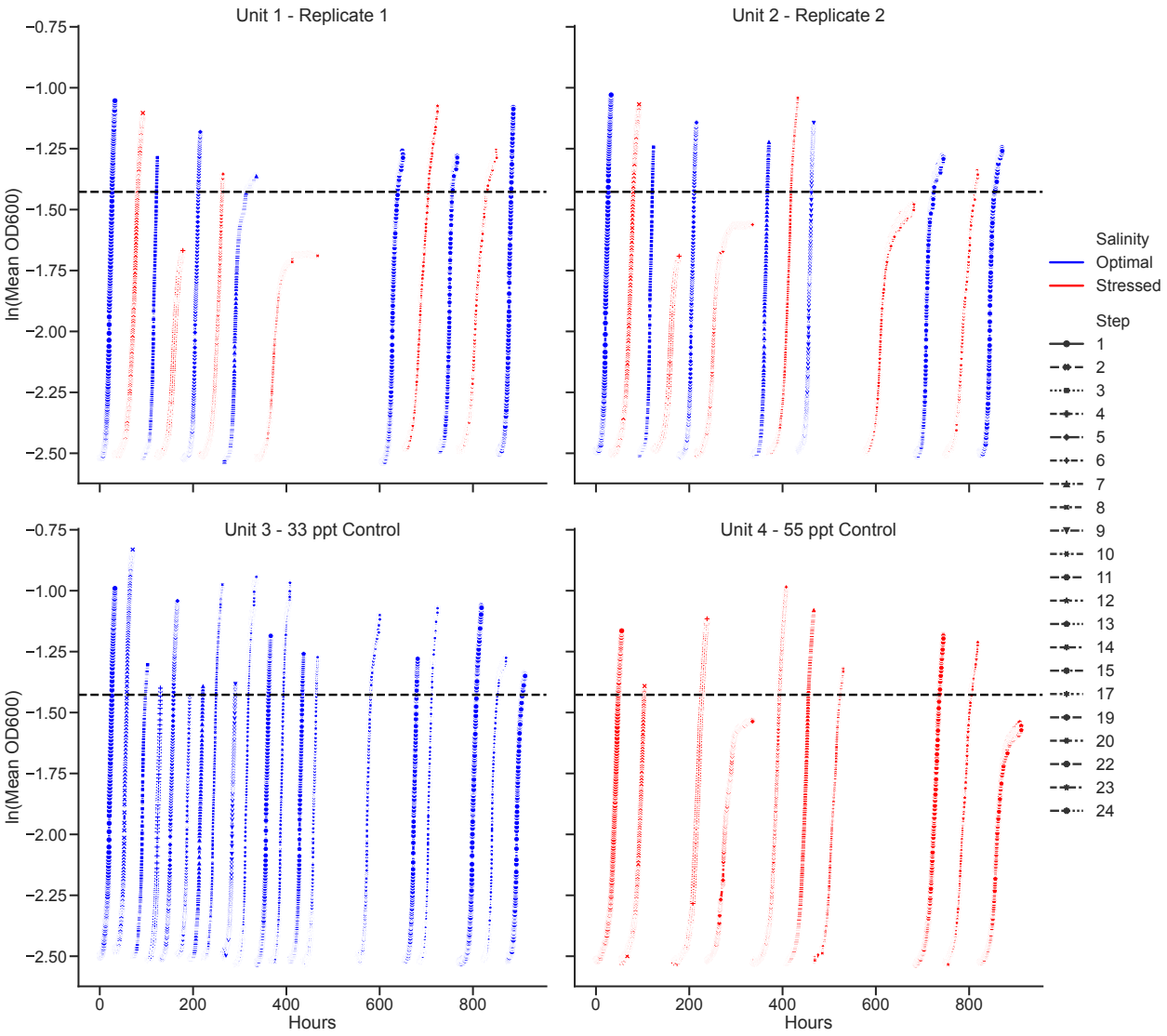

Figure 2.2. The growth curves from the experiment. Each panel corresponds to a Pioreactor unit: the upper panels are the alternating treatments (replicates 1 and 2); the bottom left is the optimal salinity control (33 ppt); and the bottom right is the stressful control (55 ppt). Blue indicates a step (complete growth cycle) under optimal salinity; red indicates a step under stressful salinity. The natural logarithm of the 10-minute mean of OD600 is plotted over hours since first inoculation with stock culture in 33 ppt media. The black dashed horizontal line is the subculture threshold. Some steps did not attain the threshold before entering late exponential phase and were subcultured below the threshold to avoid bias from stationary phase. Missing steps are due to quality-control procedures.

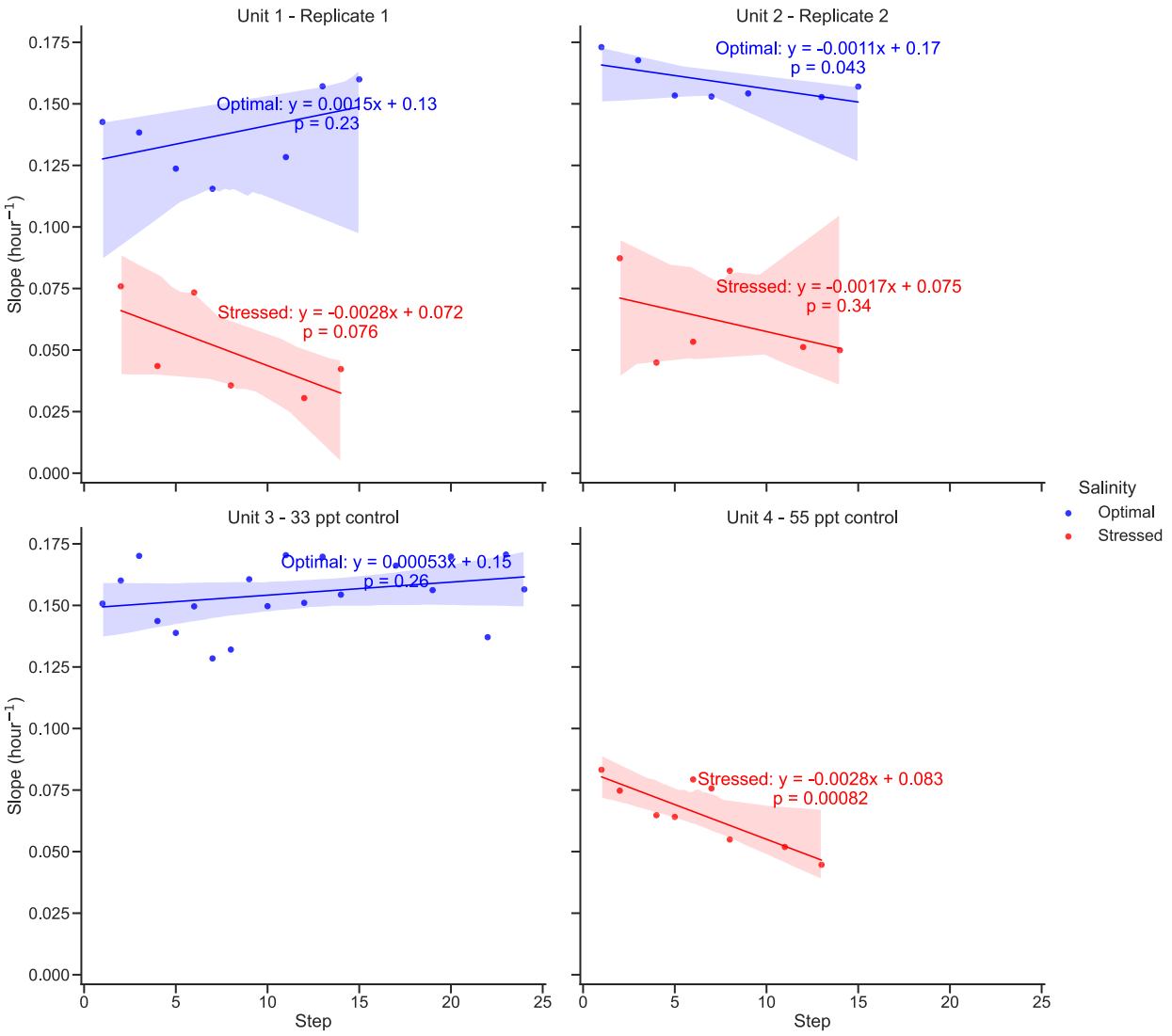

Figure 2.3. Trends in growth rates throughout the experiment. Analysis of growth rate response across the time course of complete growth cycles (steps) under optimal (blue) and stressful (red) salinity conditions. Four units are shown: Unit 1 (Replicate 1), Unit 2 (Replicate 2), Unit 3 (35 ppt Control), and Unit 4 (55 ppt Control). Robust linear regression analysis reveals contrasting dynamics, with nearly flat trends under optimal conditions and negative slopes under stressed conditions. Statistical significance varies across units, with notable significance in Unit 2 under optimal conditions (P = 0.043) and Unit 4 under stressed conditions (P = 0.00082). Confidence intervals (shaded regions) indicate uncertainty bounds for each regression line. These patterns suggest that growth rate decreases under stress and remains relatively unchanged under optimal conditions. Keeping statistical significance in mind, the decrease in growth rate under stress in the alternating conditions (Units 1 and 2) is evidence of memory of stress.

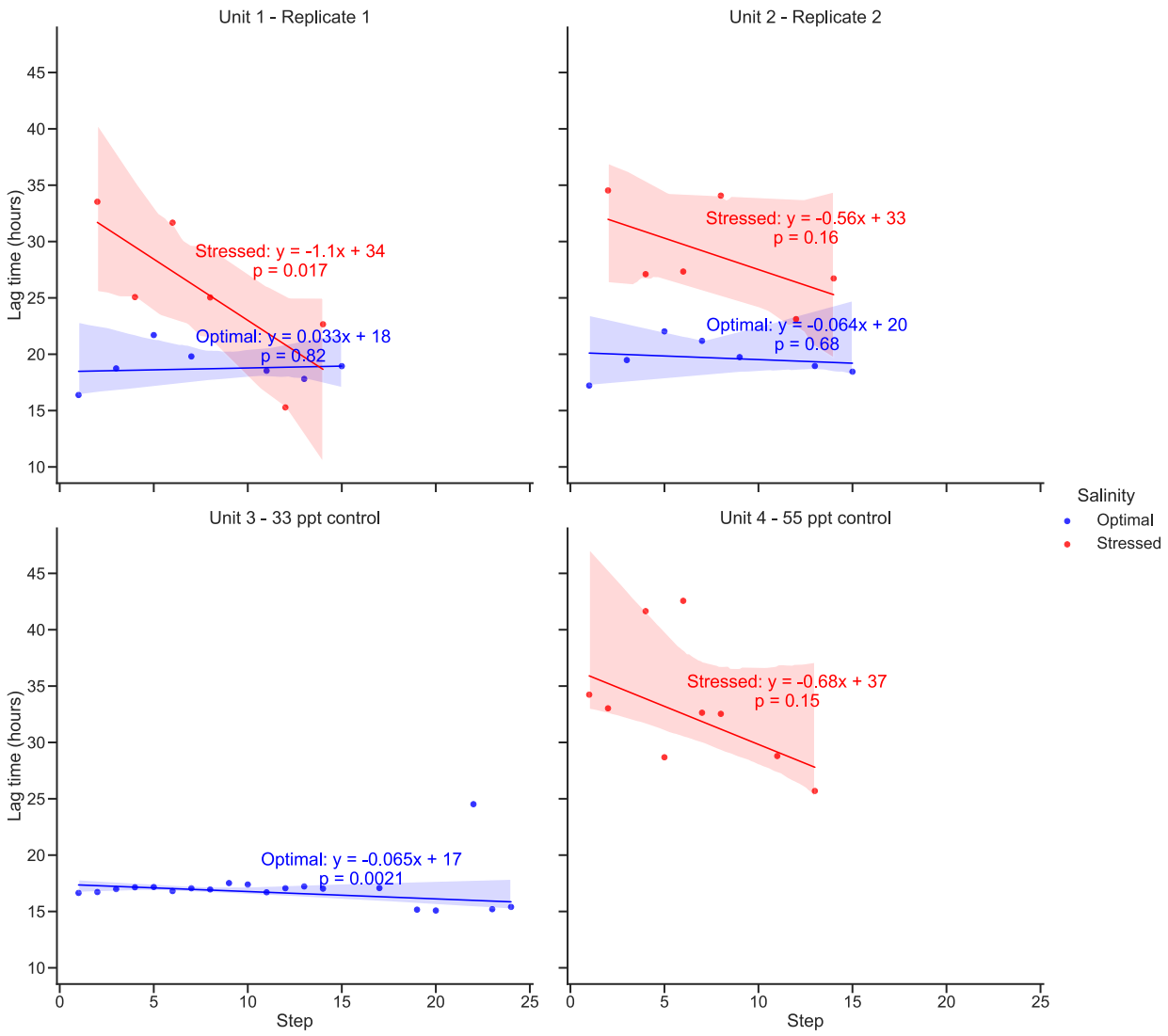

Figure 2.4. Trends in lag times throughout the experiment. Analysis of lag time response across the time course of complete growth cycles (steps) under optimal (blue) and stressful (red) salinity conditions. Four units are shown: Unit 1 (Replicate 1), Unit 2 (Replicate 2), Unit 3 (35 ppt Control), and Unit 4 (55 ppt Control). Robust linear regression analysis reveals contrasting dynamics, with flat trends under optimal conditions and negative slopes under stressed conditions. Statistical significance varies across units, with notable significance in Unit 1 stressed conditions ($P = 0.017$). Confidence intervals (shaded regions) indicate uncertainty bounds for each regression line. These patterns suggest that lag time decreases under stress and remains unchanged under optimal conditions. Keeping statistical significance in mind, the decrease in lag time under stress in the alternating conditions (Units 1 and 2) is evidence of memory of stress.

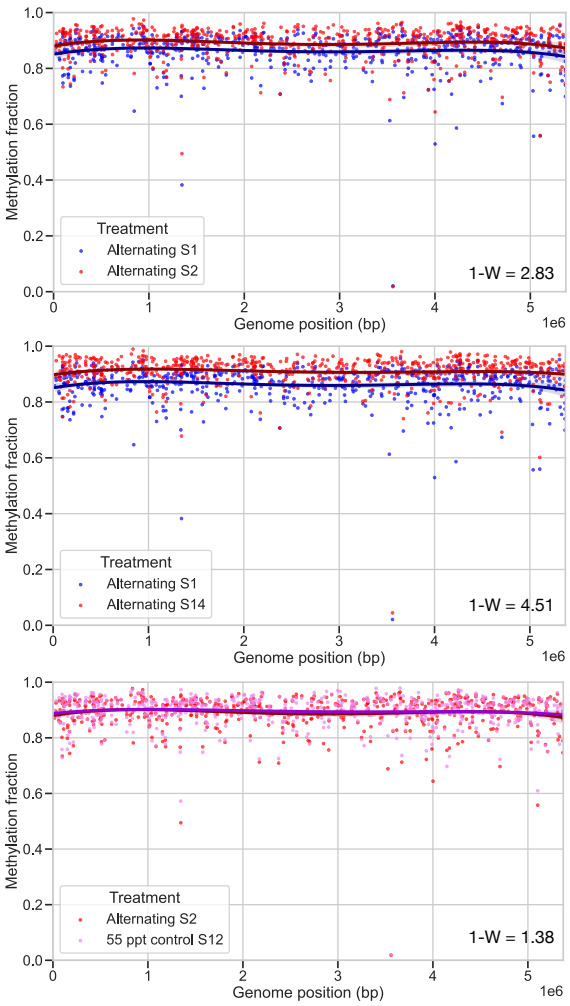

Figure 2.5. Examples of statistically significant differences and similarity in methylation distributions between treatments. Individual G**A**TC methylation fractions of promoters genome-wide are plotted against genomic position for three pairwise comparisons of growth treatments (Figure 2.2): alternating steps 1 and 2 (S1, S2) in the upper panel, alternating steps 1 and 14 (S1, S14) in the middle panel, and alternating step 2 and 55 ppt control step 12 (S2, S12) in the bottom panel. In each panel, the fractions from the two treatments are overlaid with a quadratic fit, revealing the significant differences in the upper and middle panels ($P < 0.001$) and similarity in the bottom panel. The 1-Wasserstein metric (1–W) displayed in each panel quantifies the overall methylation distance between the compared steps, with values of 2.83, 4.51, and 1.38 in the upper, middle and bottom panels, respectively. The colors represent the salinity of the sample: blue for optimal salinity (33 ppt); red or pink for stressful salinity (55 ppt).

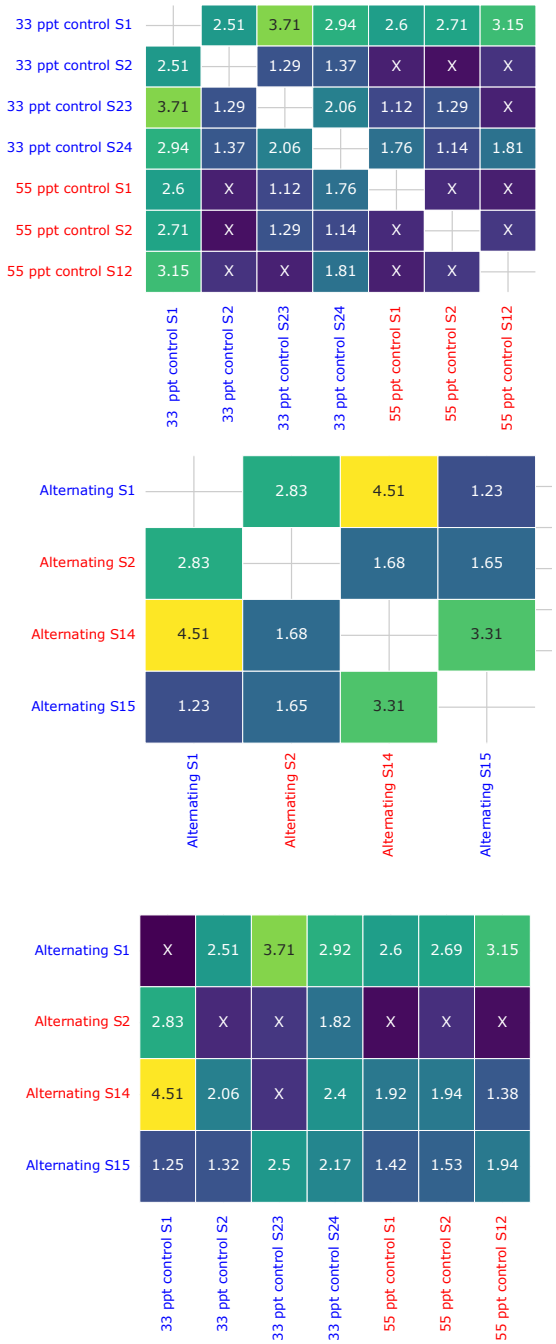

Figure 2.6. Wasserstein distance metric for motifs in promoters between steps. Cultures grown under optimal salinity (33 ppt, shown in blue) and stressful salinity (55 ppt, shown in red) conditions across different steps (S1, S2, etc.; see Figure 2.2). The left panel shows within-control comparisons, the middle panel shows within-alternating treatment comparisons, and the right panel contrasts alternating against control treatments. Higher Wasserstein distances (yellow) indicate greater dissimilarity between distributions, with the most pronounced differences occurring between steps at different salinities (e.g., 33 ppt versus 55 ppt), while X marks statistically insignificant ($P > 0.05$) comparisons.

Table 2.1. Motif instances with statistically supported methylation patterns of interest.

Position	Supporting evidence[a]	COG20 Function
1266992r	MI (Salinity), MI (Group), PCA, PLS, Constant in high salinity, changes in low salinity	Multidrug efflux pump subunit *AcrA* (membrane-fusion protein) (*AcrA*)
1155518f	MI (Salinity), MI (Group), PCA, PLS, Constant in high salinity, changes in low salinity	Fe-S cluster assembly scaffold protein IscU, NifU family (*IscU*)
5207393r	PCA, PLS, outlier, Constant in controls, changes in experimental/Constant within low salinity but different from high salinity	Metal-dependent amidase/aminoacylase/carboxypeptidase (*AbgB*)
4174147r	MI (Step), PCA, PLS, Constant in high salinity, changes in low salinity	Sulfate permease or related transporter, MFS superfamily (*SUL1*)
388582f	MI (Step), PCA, PLS, Constant in high salinity, changes in low salinity	Acyl-CoA reductase or other NAD-dependent aldehyde dehydrogenase (*AdhE*)
2739211r	MI (Step), PCA, PLS, Constant in high salinity, changes in low salinity	Permease of the drug/metabolite transporter (DMT) superfamily (*RhaT*)
1038953f	MI (Step), PCA, PLS, Constant within low salinity but different from high salinity/Constant in controls, changes in experimental	Regulator of RNase E activity RraB (*RraB*)
5367866r	MI (Step), PCA, PLS	Flavodoxin (*FldA*)
511021r	MI (Group), PCA, Constant in high salinity, changes in low salinity	Pantothenate kinase-related protein Tda10 (topoisomerase I damage affected protein) (*Tda10*)
5027643r	MI (Salinity), MI (Group), PCA	DNA-binding protein, AcrR family, includes nucleoid occlusion protein SlmA (*AcrR*)
4903080f	PCA, PLS, Constant in high salinity, changes in low salinity	Protease II (*PtrB*)
4580548f	PCA, PLS, Constant in high salinity, changes in low salinity	Periplasmic serine protease, S1-C subfamily, contain C-terminal PDZ domain (*DegQ*)
436984r	MI (Step), PCA, Constant in high salinity, changes in low salinity	WD40 repeat (*WD40*)
4352570f	PCA, PLS, Constant in high salinity, changes in low salinity	DNA mismatch repair ATPase MutS (*MutS*)
4244324f	PCA, PLS, Constant in high salinity, changes in low salinity	Formyltetrahydrofolate hydrolase (*PurU*)
4001064f	PCA, PLS, High variance/outlier	DNA-binding transcriptional regulator GbsR, MarR family (*GbsR*)
3970228r	MI (Step), PCA, Constant in controls, changes in experimental/Constant within low salinity but different from high salinity	Aspartate-semialdehyde dehydrogenase (*Asd*)
3760629r	MI (Salinity), PLS, Constant in high salinity, changes in low salinity	Signal transduction protein containing GAF and PtsI domains
3718834f	PCA, PLS, Constant in high salinity, changes in low salinity	2-polyprenyl-6-methoxyphenol hydroxylase and related FAD-dependent oxidoreductases (*UbiH*)

3711689f	MI (Group), PLS, Constant in high salinity, changes in low salinity/Changes in controls, constant in experimental	ssRNA-specific RNase YbeY, 16S rRNA maturation enzyme (*YbeY*) (PDB:1XM5)
343271f	MI (Salinity), PLS, Constant within low salinity but different from high salinity/Constant in controls, changes in experimental	Malic enzyme (*SfcA*)
3328199f	PCA, PLS, Constant in high salinity, changes in low salinity/Constant in controls, changes in experimental	Folate-dependent phosphoribosylglycinamide formyltransferase PurN (*PurN*) (PDB:1C2T)
32522f	PCA, PLS, Constant in high salinity, changes in low salinity	Shikimate 5-dehydrogenase (*AroE*)
3249330r	MI (Group), PCA, Changes in controls, constant in experimental/Constant in high salinity, changes in low salinity	Transposase and inactivated derivatives, IS30 family (*Tra8*)
3193876r	MI (Salinity), PCA, Constant in high salinity, changes in low salinity	Catechol 2,3-dioxygenase or related enzyme, vicinal oxygen chelate (VOC) family (*GloA*)
3061753f	MI (Group), PCA, PLS	Formylglycine-generating enzyme, required for sulfatase activity, contains SUMF1/FGE domain (*YfmG*)
3035359f	PCA, PLS, Constant in controls, changes in experimental/Constant in high salinity, changes in low salinity	Regulator of phage lambda lysogenization HflD, binds to CII and stimulates its degradation (*HflD*)
3033593f	MI (Group), PCA, PLS	ADP-ribose pyrophosphatase YjhB, NUDIX family (*YjhB*)
2716802f	MI (Group), PCA, Constant in low salinity, changes in high salinity/Constant within low salinity but different from high salinity/Constant in controls, changes in experimental	6-pyruvoyl-tetrahydropterin synthase (*QueD*)
1512639f	PCA, PLS, Constant within low salinity but different from high salinity	Flagellar basal body lipoprotein FlgP, LPP20 family (*FlgP*)
1376940f	MI (Salinity), PCA, PLS	DnaJ-class molecular chaperone with C-terminal Zn finger domain (*DnaJ*)
1156351f	PCA, PLS, Constant in high salinity, changes in low salinity	DnaJ domain-containing protein (*DjlA*)
1059134r	MI (Group), PCA, Constant in high salinity, changes in low salinity	ABC-type transport system involved in cytochrome c biogenesis, permease component (*CcmB*)
1030022f	PCA, PLS, Constant within low salinity but different from high salinity	HD-like signal output (HDOD) domain, no enzymatic activity (*HDOD*)

[a]Principal component analysis (PCA), mutual information (MI), partial least squares (PLS)

CHAPTER 3: MULTIPLE ROLES OF DNA METHYLATION IN SEA-ICE BACTERIAL COMMUNITIES AND ASSOCIATED VIRUSES

This chapter has been published:

Kanaan G and Deming JW (2025) Multiple roles of DNA methylation in sea-ice bacterial communities and associated viruses, *The ISME Journal*, wraf198. doi: 10.1093/ismejo/wraf198

ABSTRACT

Despite growing evidence for the role of DNA methylation in bacterial acclimation to environmental stress, this epigenetic mechanism remains unexplored in sea-ice microbial communities known to tolerate multiple stressors. This study presents a first analysis of DNA methylation patterns in bacterial communities and associated viruses across the vertical thickness of sea ice. Using a novel stepped-sackhole method, we collected sea-ice brines from distinct horizons of an Arctic ice floe, capturing microbial communities that had been exposed to different environmental conditions. Through Oxford Nanopore sequencing, we characterized methylation patterns in bacterial and associated viral DNA, analysing for methylation motifs and differences between ice horizons. We identified 22 unique bacterial methylation motifs and 27 viral motifs across three nucleotide methylation types (5mC, 6mA, and 4mC), with evidence of differential methylation between upper and lower ice. Analysis of metagenome-assembled genomes revealed the regulatory potential of methylation in both ice-adapted (*Psychromonas* and *Polaribacter*) and non-adapted bacteria (*Pelagibacter*); e.g., in *Pelagibacter*, differential methylation of the GANTC motif between upper and lower ice affected genes involved in core cellular processes. Viral methylation patterns showed evidence of recent infection. We also identified orphan methyltransferases in sea-ice phages, suggesting a mechanism for bypassing host restriction-modification systems and regulating host genes. Our findings reveal that DNA methylation serves functions in sea ice beyond traditional restriction-modification systems that protect against foreign DNA, opening new avenues for research on the role of epigenetic mechanisms not only in acclimation to the cryosphere but also more generally in microbial ecology and evolution.

INTRODUCTION

The dynamic environment of sea ice represents one of Earth's most extreme habitats, characterized seasonally by steep gradients of temperature, salinity, light, and space availability across relatively short distances [1]. Despite harsh conditions, sea ice harbours diverse microbial communities, members of which are known to have evolved sophisticated adaptive mechanisms to survive and thrive within its challenging microenvironments (Deming & Collins, 2017). Although numerous studies have examined the taxonomic composition, metabolic functions, and ecological interactions of sea-ice microbiomes (Boetius et al., 2015; Bowman, 2015), the epigenetic mechanisms underlying microbial survival and acclimation in this extreme environment remain unexplored.

DNA methylation, the addition of methyl groups to specific nucleotide positions within the genome, represents one of the most fundamental epigenetic mechanisms across all domains of life (Blow et al., 2016; Casadesús & Low, 2006). In prokaryotes, DNA methylation has been associated traditionally with restriction-modification systems that protect against foreign DNA (Vasu & Nagaraja, 2013). Four types of restriction-modification systems exist, classified based on their structure and function. Type I systems are multisubunit complexes (R, M, S proteins) requiring ATP to cleave DNA at variable distances from bipartite recognition sites. Type II systems employ restriction endonucleases and methyltransferases that act independently, cleaving at or near unmethylated recognition sequences. Type III systems combine R and M proteins into a heterodimer, methylating one DNA strand and cutting nearby, leading to incomplete digestion. Type IV systems lack methylase activity and exclusively target previously modified DNA (e.g., methylated or hydroxymethylated sequences) (Roberts et al., 2003; Sánchez-Romero et al., 2015). Restriction-modification systems that have lost the R protein may leave behind an orphan methyltransferase, often from a Type II system. Orphan methyltransferases, common in bacteria (Anton & Roberts, 2021) allow DNA methylation to play roles beyond defence, including regulation of gene expression, timing of DNA replication, and DNA repair (Adhikari & Curtis, 2016; Sánchez-Romero et al., 2015; Seong et al., 2021). These regulatory functions are particularly relevant in habitats where environmental conditions vary, requiring organisms to modulate their physiology in response (Beaulaurier et al., 2019; Reisenauer et al., 1999).

Sea ice presents a promising natural system for studying these various roles of DNA methylation in the acclimation and adaptation of microbes to a dynamic environment. The vertical structure of sea ice creates natural gradients in environmental conditions, with upper horizons experiencing greater fluctuations in temperature and brine salinity than less extreme and more stable bottom layers near the seawater interface (Ewert & Deming, 2013). The brines within sea ice also host prokaryotic and viral communities in higher concentrations than in seawater, enabling investigation of methylation patterns across an environment where high cell-to-cell and cell-to-virus contact rates may accentuate interactions (Collins & Deming, 2011; Luhtanen et al., 2014; Wells & Deming, 2006). Sea-ice brines have long been hypothesized as sites for host-viral interactions due to the concentrating effects of the freezing process (Deming, 2007), which may give DNA methylation an outsized ecological role in this community.

The study of DNA methylation in environmental microbiomes has been revolutionized by recent advances in long-read sequencing technologies, particularly Oxford Nanopore sequencing, which can detect various forms of DNA modification directly during the sequencing process. This capability allows for characterization of methylation patterns at single-nucleotide resolution across entire genomes without the need for chemical treatment or enrichment steps and their associated biases. Despite these technological advances, our ecological understanding of DNA methylation at the community level, and how it may contribute to microbial acclimation to extreme conditions, remains limited. Previous studies have investigated methylation patterns

in marine pelagic bacterial communities (Hiraoka et al., 2019; Seong et al., 2022), a freshwater bacterium (Gärtner et al., 2019; Hu et al., 2018), a plant pathogen (Gopalan-Nair et al., 2024), model and pathogenic bacteria (Løbner-Olesen et al., 2005; Mattei et al., 2022; Vandenbussche et al., 2020; Yano et al., 2020), and recently in a cultured psychrophile (Bu et al., 2025), but neither the methylome of a sea-ice community nor a community from any other extreme environment has been characterized, to our knowledge. This knowledge gap is notable given the unique environmental gradients and seasonal fluctuations presented by sea ice and its importance as a model system for studying microbial adaptation to extreme conditions and analogous extraterrestrial environments (Gomez-Buckley et al., 2022; Vance et al., 2021).

Here we present a multi-faceted analysis of DNA methylation patterns across bacterial communities and associated viruses in sea-ice brines, the inhabited portion of sea ice [27], focusing on methylation signatures in ice horizons across the environmental gradients inherent to sea ice. Our objective was to collect brines from distinct horizons, using a stepped-sackhole method, to capture microbial communities with different environmental histories. All methods for sampling sea-ice microbes have limitations (Chamberlain et al., 2022) but collecting brines directly in situ avoids biases due to osmotic shock and contaminants introduced by the traditional approach of melting ice into a melting solution. Using Oxford Nanopore sequencing and bioinformatic analyses, we aimed to characterize the methylation patterns of the recovered bacterial DNA, identify methylation motifs, and examine differences in methylation between ice horizons.

We hypothesized that bacterial methylation patterns would differ between upper and lower ice, as bacteria would use DNA methylation differently in response to more extreme and dynamic conditions (upper) versus more moderate and stable conditions (lower) in their distinctive horizons. Initially we focused on methylation as a regulatory mechanism in the bacterial communities and metagenome-assembled genomes (MAGs) obtained, documenting methylation motifs and differential methylation patterns between upper and lower ice. As we also obtained associated viral genomes, we followed with analyses of their methylated motifs and corresponding bacterial signatures, seeking evidence for host-viral interactions. We again found differential methylation across the ice and, unexpectedly, that methylated motifs in viruses may reveal infection histories. Additional roles for DNA methylation were suggested by the presence of phage-encoded methyltransferases. By elucidating the methylation landscape of sea-ice microbial communities and associated viruses, this study provides insights into epigenetic mechanisms underlying responses to an extreme environment and opens new avenues for research on the role of DNA methylation in microbial ecology and evolution.

MATERIALS AND METHODS

Here we provide a brief description of materials and methods. Complete details for each section are available in Supplemental File S3 (ISME).

ICE FLOE DRIFT

The ice floe's drift path was reconstructed using sidrift commit #05075ca (Dr. Polona Itkin, https://github.com/loniitkina/sidrift). Environmental data (surface air temperature, sea-ice age/thickness, snow thickness, seawater salinity/temperature) were sourced from Copernicus Marine's Arctic Ocean Physics Analysis and Forecast dataset cmems_mod_arc_phy_anfc_6km_detided_P1D-m (Melsom et al., 2012; Sakov et al., 2012).

ICE SAMPLING

Samples were collected during the BREATHE expedition (BR7008) on R/V *Kronsprins Haakon*, drifting for 10 days over the Yermak Plateau, Arctic Ocean, 17–27 May 2023. Sackhole brines (Junge et al., 2001) were

sampled at 81°2'55.94''N, 10°28'41.90''E on 21 May (Figures 3.1, C1). A stepped-sackhole method was used: holes were drilled to pre-determined depths, brine was drained for at least 1.5 hours per horizon, collected, and the process repeated until no further drainage. Depth horizons were defined by bulk salinity profiles: 0–40 cm (“top”), 40–70 cm (“middle”), 70–160 cm (“bottom”). Four sackholes (1 m apart) were cored as environmental replicates (Table C1); due to sample loss, three were analysed. Brines were collected with a Masterflex peristaltic pump into acid-washed, Milli-Q rinsed Cubitainers. Adjacent ice cores sampled two days later, using a Kovacs Mark II system, were sectioned into corresponding horizons, and isohaline-melted to limit osmotic shock (Table C2) (Chamberlain et al., 2022).

Shipboard processing

A blank control was filtered before samples. Brines were filtered at 1°C within 4 hours onto 0.22 µm Sterivex® filters, flash-frozen in liquid nitrogen, and stored at –80°C. Brine salinity was measured on filtrate. Samples were labelled SX-Y by sackhole and horizon (Table C1).

DNA extraction and sequencing

DNA was extracted using the Masterpure kit with modifications: Sterivex filters were cracked open, lysozyme digestion was added, and DNA pellet recovery used 14,000 x g centrifugation. DNA was quality-checked (NanoDrop), cleaned (Zymo MagBead Kit), and quantified (Qubit for later runs). Libraries were prepared with Oxford Nanopore kits and sequenced on a PromethION flow cell. Suboptimal yields were attributed to free adapter, polysaccharides, and low DNA input.

Assembly, metagenomics, and bin curation

Reads <100 bp or Phred <Q10 were removed (Chopper (Coster & Rademakers, 2023)). Contaminant reads were filtered (SingleM (Woodcroft et al., 2024), see Text S1). Quality-controlled reads were co-assembled (Flye (Kolmogorov et al., 2020)), discarding contigs <1000 bp. Adapter/oligo contamination was removed (NCBI FCS tool (Astashyn et al., 2024)). Annotation and binning used Anvi'o, KEGG KoFams, COGs, pyrodigal, CONCOCT, METABAT2, and manual curation [41-48]. MAGs were assessed for redundancy/completeness (Anvi'o, CheckM2 (Aroney et al., 2025)); coverage was determined with CoverM. MAGs with >10% redundancy were discarded; only MAGs >30% complete were considered further. Viral contigs/plasmids were identified (geNomad (Camargo et al., 2024), CheckV (Nayfach et al., 2021)). Taxonomy was assigned to bacterial MAGs using gtdb-tk (Chaumeil et al., 2022), to contigs for community composition using Diamond (Buchfink et al., 2015) and MEGAN6-LR (database NCBI_nr 2025-01-05) (Huson et al., 2018), to contigs for methylation analysis using Kaiju (database refseq_nr 2024-08-13) (Menzel et al., 2016).

Methylation analysis

Reads were mapped (minimap2 (Li, 2021)), and methylation was called per nucleotide (modkit, confidence ≥95%). De novo motif identification and differential methylation were performed with modkit. The nucleotide in a motif known to be the methylation site is bolded, e.g. [5m**C**]G. Only sites with sufficient coverage (≥5x) and statistical significance (modkit, $P < 0.05$) were considered. Genes for restriction-modification systems were identified using MicrobeMod (Crits-Christoph et al., 2023). Contigs were reordered for *Pelagibacter* MAG analysis of origin (*ore*) and terminus (*ter*) (Mauve (Darling et al., 2004), gc_skew (Brown et al., 2016)). Methylation fractions were normalized by coverage, with methylation levels categorized as low (<33%), medium (33–66%), or high (>66%). Motif enrichment was tested (chi-squared), and differences between horizons were assessed (Kolmogorov-Smirnov with Benjamini/Hochberg correction, $\alpha = 0.01$) (Seabold & Perktold, 2010).

Software stack

Figures were generated with seaborn v0.13.2 (Waskom, 2021), cartopy v0.23.0 (MET Office, 2010), and matplotlib v3.8.4 (Hunter, 2007). Python v3.10.14 was used throughout. Data processing relied on polars v1.9.0 (Gelderen, 2025) and pandas v2.2.2 (McKinney, 2010). Virtual environments were managed with conda v24.1.2 and mamba v2.0.5. Workflows used snakemake v7.32.4 (Mölder et al., 2021).

Results and discussion

After providing the environmental and sampling context of the study, we describe sequencing and assembly outcomes, including limitations and quality controls. We then present a brief overview of the dominant members of the sampled communities revealed by metagenomic analyses, before focusing on DNA methylation patterns observed in bacterial and viral contigs. We highlight key findings regarding methylation motifs, restriction-modification systems, and evidence for regulatory and unexpected roles, supported by case studies of MAGs and prophages.

Sampling and environmental history

The ice floe we sampled was 209 cm thick, with a snow cover of 2–11 cm across our sampling site and air temperatures that stayed close to –1°C, ranging between 0°C and –5°C (Table C1). The salinity of sackhole brine samples confirmed them to be sea-ice brines with no seawater infiltration (see freeboard in Table C2). The floe was identified as first-year sea ice, with a thin layer of second-year ice in some places (Figures C1, C2). To understand the environmental history of the sampled microbial communities, we mapped sea-ice related variables and atmospheric temperature along the floe's drift path (Figure C2). Atmospheric temperature drives temperature and salinity changes in the upper portions of sea ice, while bottom ice remains relatively stable due to proximity to the ocean which remains at or above the freezing point. Mapping atmospheric temperature to the path travelled by the sampled ice floe since its formation (Figure 3.1) confirmed that upper ice horizons experienced more variable and extreme conditions compared to the bottom ice as the temperature varied significantly over time. This contrast forms the basis of our hypothesis that different methylation profiles will be found across the ice as a response to different environmental conditions.

Sequencing, assembly, and curation

To assess patterns in brine communities across the ice, we performed a co-assembly using long-read data from corresponding ice-core samples, which improved assembly accuracy (e.g. we were able to recover MAGs with low coverage in brine samples; Figure C6) and yielded 101,882 contigs totalling 2.31 Gb. Read counts were generally lower than anticipated and varied between brine samples, but the control sample indicated little environmental or cross contamination during processing (Figure C3). Sequencing difficulty was likely due to polysaccharide contamination in the extracted DNA, disrupting availability to the sensitive nanopores, and suboptimal DNA quantity. Future Nanopore sequencing efforts might benefit from additional DNA purification steps. Although useful for co-assembly, the ice-core data were excluded from analyses of methylated DNA as the melting procedure may artificially affect the community methylome.

Relative abundances should be interpreted cautiously given the uneven read counts between samples, despite being assessed conservatively for dominant organisms (Figure C4). The MEGAN6 analysis, however, showed consensus in community composition across the sackhole brines, with ice-adapted genera *Polarella* and *Polaribacter* and seawater-adapted *Pelagibacter* abundantly present, as previously observed in Arctic sea-ice communities (Boetius et al., 2015; Collins et al., 2010; Cooper et al., 2019; Montresor et al., 2003).

We recovered eukaryotic, bacterial, archaeal, and viral contigs from the assembly, but focus here on bacterial and viral contigs. From 19,915 bacterial contigs we recovered 37 MAGs (File S1 (ISME)), 6 of which were >90% complete (Figure C5), considered to be high-quality as defined by the MiXS standard (Yilmaz et al., 2011): *Lentimonas*, *Psychroflexus*, *Paraglaciecola*, *ASP10-02a* (Oceanospirillaceae), *Psychromonas*, and *Polaribacter*. Only the *Pelagibacter* MAG had sufficient coverage in both top and bottom samples (Figure C6) for differential methylation analysis between horizons. For viral analyses, the 4,896 contigs with a geNomad virus score above 90% yielded 8 classified as complete, and 285 as high quality by CheckV.

THE BACTERIAL METHYLATION LANDSCAPE

To assess the distributions of methylation motifs in bacterial contigs from sea-ice brines, we identified through homology analysis genes for restriction-modification enzymes recognizing 47 distinct methylation motifs. The most prevalent of these motifs were GANTC, GATC, and GGCC (File S2 (ISME)), with 6mA as the most abundant nucleotide methylation type (63%). De novo identification yielded 22 unique methylation motifs across 1,592 (8%) contigs; most (65%) had no detectable motif, whereas the remaining (27%) had insufficient data for identification. Most of these motifs were 5mC-based (97%), predominantly featuring [5m**C**]G. This methylation landscape thus shows striking differences between genetic potential and epigenomic observation: the encoded restriction modification enzymes mediate primarily 6mA methylation, whereas de novo motifs were overwhelmingly 5mC-based. These proportions differ sharply from a pelagic metamethylome, where the most abundant methylation type was m6A (57–63%), with only 15–20% being 5mC (Hiraoka et al., 2022), and 20 of the 22 motifs were not previously identified in a marine pelagic community (Seong et al., 2022). Although perhaps unsurprising, given differences in community composition and sequencing approach and the conserved nature of selected motifs across taxa (Barbeyron et al., 1984; Fullmer et al., 2019; Harris & Goldman, 2020; Hiraoka et al., 2022; Wion & Casadesús, 2006), this contrast suggests that sea-ice bacterial communities harbour methyltransferases and restriction enzymes with previously unidentified recognition motifs.

To estimate the balance between defence and regulatory (or other) roles of DNA methylation in the sampled brine communities, we estimated the number of orphan methyltransferases in bacterial contigs. We found a surplus of orphan methyltransferases (Z scores of 5.51 for Type I, and 8.86 for Type II, equivalent to $P < 0.01$) (Figure 3.2). Their abundance suggests that many bacteria were using DNA methylation for regulatory roles rather than defence.

To investigate DNA methylation as a mechanism for gene regulation under different environmental conditions, we compared methylation fractions between top and bottom ice of motifs occurring on the 8 bacterial contigs with sufficient coverage. We found that all had statistically significant differences in methylation fractions between ice horizons (Figure 3.3). Some showed differences in promoter-only regions between ice horizons, suggesting that gene expression was differentially regulated. Of the 182 instances of differentially methylated motifs across these contigs, none was contained in, or flanked by, genes with known functional annotation. Although we cannot indicate what function DNA methylation may have been regulating, these findings provide significant evidence for a regulatory role of DNA methylation in the bacterial community response to environmental differences across the ice. We can hypothesize that logical targets for this regulatory role would be genes related to acclimation to sea-ice conditions, such as extracellular polysaccharide production, osmolyte regulation, and extracellular enzyme production (Ewert & Deming, 2014; Firth et al., 2016; Huston, 2003; Mykytczuk et al., 2013).

MAGs allow for understanding the genetic context of DNA methylation and interrogating its role in specific taxa. Of the 37 MAGs recovered from the sea-ice brines (File S1 (ISME)), we focused on the four with de novo methylation motifs (Table 3.1). *Psychromonas* and *Pelagibacter* are characterized later, as more information was available; *Polaribacter* and *Paraglaciecola* could be examined for defense versus regulatory roles.

In the *Polaribacter* MAG, we found 5 restriction modification operons, each with a methyltransferase and restriction enzyme system of type I (1), type II (3), or type III (1). The motifs were recognized separately by methyltransferases in separate operons of type II and type III, GGCC and AAGACC, respectively, though the latter had only 58% shared identity with the REBASE reference. Three putative orphan restriction enzymes of type I (2) and type II (1) were also identified with no known recognition motif. The lack of orphan methyltransferases, however, meant that DNA methylation was unlikely to be playing a role beyond defence in this MAG.

The *Paraglaciecola* MAG has 2 type II orphan methyltransferases, one of which recognizes GATC motif, also identified de novo. It also has 2 restriction enzymes, one type I (with no known REBASE homolog) and one type IV. Given that type IV restriction enzymes cleave methylated DNA, we can hypothesize that it plays an immune defence role. The genetic identification of an orphan methyltransferase recognizing the GATC motif, however, supports the hypothesis that *Paraglaciecola* also uses DNA methylation to regulate its DNA. With very little data in the top ice for this MAG (29 sites out of 22,094), conducting a differential methylation analysis between ice horizons for *Paraglaciecola* was not possible.

THE VIRAL METHYLATION LANDSCAPE

By surveying methylation motifs across thousands of viral genomes, we gained new insights into the molecular strategies that may shape virus-host interactions in extreme environments. Of the 4,593 viral contigs analysed, 26% (1,224) did not have sufficient data for de novo motif identification and 70% (3,257) showed no detectable methylation motif. The remaining 2% (112) of contigs together showed 36 unique motifs, the most common being **C** and **C**C. The methylation type distribution in de novo motifs was 70% for 5mC, 24% for 4mC, and 5% for 6mA. By homology of genes to REBASE, we identified 29 motifs, the most common being G**A**TC, CCCGGG, and G**C**. At least one restriction-modification gene was detected on each of 359 contigs.

The genetic analysis revealed 49 viral contigs which coded for at least one restriction enzyme. Among the higher quality contigs, all but one belonged to class *Caudoviricetes,* with the remaining one belonging to *Megaviricetes*. *Megaviricetes* infect eukaryotes and are known to encode restriction enzymes (Jeudy et al., 2020; Oliveira et al., 2021), whereas *Caudoviricetes*, which infect both Bacteria and Archaea, including halophilic archaea, encode complete restriction modification systems (Liu et al., 2021). These systems are thought to have many functions: preventing superinfection, deteriorating specific mobile genetic elements, or regulating DNA replication timing (Kobayashi, 2001; Liu et al., 2021; Murphy et al., 2013a).

Our viral contigs had a surplus of methyltransferases, suggesting broad presence of orphan methyltransferases in sea-ice phages (Z-score of 21.8 for Type II, equivalent to $P < 0.01$) (Figure 3.2). Orphan methyltransferases can be advantageous to phage for many reasons, but primarily by allowing them to bypass host restriction-modification systems (Murphy et al., 2013a). As viruses cannot express their own genes, methylation of the viral genome occurs via methyltransferases during infection, when the host is expressing either virally or host-coded enzymes. During viral DNA replication, methyltransferases can modify recognized motifs before the DNA is packaged into the viral capsid, where the methylated DNA persists for the lifetime of

the phage (Hill et al., 1991; Murphy et al., 2013b, 2014; Sun et al., 2023). This modification grants resistance to restriction-modification systems targeting those motifs in subsequent infection cycles.

In essence, the presence and methylation fraction of specific motifs act as a memory of phage infection history, offering clues about its passage through different hosts. This capacity to reconstruct infection histories could be particularly valuable in assessing the impacts of a dynamically stressful sea-ice environment, where hypothetically viruses could be pushed to broaden their host range (Huang et al., 2024). By pairing motif profiles between phages and potential hosts, hypothesizing candidate infection histories becomes possible, especially in scenarios where hosts target distinct methylation motifs (Takahashi et al., 2025). Such analyses demand comprehensive genomic data for both hosts and phages, including information on methyltransferase presence and motif recognition sites.

A comprehensive analysis of infection histories cannot be conducted with our dataset, but the data do show some evidence of different methylation states within the ice (Figure 3.4). Many motifs would be expected to have similar methylation fractions across horizons, as these motifs are required for phage to bypass the RM systems of their hosts. Nevertheless, we identified eight motifs de novo in common to both bacteria and viruses, with evidence of differential methylation in viruses between ice horizons. Most striking is viral contig c_000000093169 (belonging to *Caudoviricetes*), with its AC**A**Y motif highly methylated in bottom ice. We identified a Type I restriction enzyme that recognizes ACAYNNNNNRTT on contig c_000000079259 and determined its taxonomy as *Polaribacter*. This taxonomic assignment is further supported by the fact that the homologous enzyme was found in *Polaribacter* sp. BM10, matching the results of a BLAST alignment search (Roberts et al., 2022). Given that type I enzymes are combination restriction-and-modification enzymes, this finding may suggest a recent infection of *Polaribacter* by this phage. No tRNA could be identified on c_000000093169 using tRNA-Scan (Zou et al., 2015) or matching CRISPR spacers on c_000000079259 using CRASS (Skennerton et al., 2013).

Turning to prophages, we found 39 in our dataset, most belonging to classes *Caudoviricetes* and *Prasinovirus*. Among these, five encoded restriction-modification genes, all of which were methyltransferases. Three of the methyltransferases were homologous to enzymes with known motifs: two to GATC and one to GGATG. Two MAGs (s__scgc-aaa076-p13_sp905182885__bin_0_21_12-contigs, and g__psychromonas__bin.102; Table 1) were each found to contain a prophage, neither of which coded for a methyltransferase. As the former had no restriction modification genes and no methylation motif, we did not analyse it further. Case studies of the *Psychromonas* methylome and its prophage, as well as a prophage identified in a *Pelagibacter* contig, appear below.

A high-quality prophage with an orphan methyltransferase was identified on contig c_000000073417 classified as *Polaribacter* sp. This contig is 45,419 bp long, including the prophage which is 36,496 bp long. The prophage was annotated as belonging to *Caudoviricetes*. An orphan type II methyltransferase was identified on this prophage as a homolog of *M.Uph13359ORFH1P* which recognizes the GATC motif. GATC was found 180 times on the prophage, and 32 times on the rest of the contig. The motif occurred 1.4x more frequently in the host than in the phage ($P = 0.11$). Without a complete MAG associated with this contig, we can only hypothesize the role of this methyltransferase. *Polaribacter* species are known to have multiple restriction modification systems, though none have a restriction enzyme recognizing this motif (Roberts et al., 2022). The frequent occurrence of GATC within the prophage suggests it is not under selective pressure from host restriction enzymes. Intriguingly, GATC is often linked to regulatory functions in bacteria, hinting at a possible regulatory role for this motif in both the phage and its host, potentially contributing to adaptation in the sea-ice environment. No functional annotations were available to further clarify the regulatory influence of this motif.

CASE STUDY: *PSYCHROMONAS* METHYLOME

The *Psychromonas* methylome reveals a dynamic interplay between prophage and host methylation patterns, offering clues about host-phage regulatory relationships in sea-ice ecosystems. A prophage belonging to *Caudoviricetes* was identified on contig c_000000087963, binned as part of our *Psychromonas* MAG. We refined the taxonomic assignment of this contig by blasting it against the NCBI core nucleotide database; the best hit was *Psychromonas ingrahamii*. A previous in-depth genomic analysis of this bacterium did not identify a prophage, though integration sites were found (Riley et al., 2008). Of the five genomes available for *Psychromonas* on REBASE, two coded for a methyltransferase with GATC as a known recognition motif, one of which was *Psychromonas ingrahamii* (Roberts et al., 2022). This finding aligns with our de novo detection of a G**A**TC motif in the *Psychromonas* MAG, as well as the identification of a methyltransferase on contig c_000000028297 that is highly homologous to M.Pin37DamP from *Psychromonas ingrahamii*.

With the taxonomic context established, we next quantified the distribution of the GATC motif across the host and prophage genomes. In our *Psychromonas* MAG, the GATC motif occurs 35,280 times over 4,938,485 nucleotides (excluding prophage). In the prophage, the GATC motif occurs 144 times over 32,300 nucleotides. Although no known restriction enzyme recognizing GATC was found in our MAG, restriction enzymes without a clear corresponding methyltransferase were identified. Theoretically, these enzymes could recognize the GATC motif, which would apply a selective pressure on this virus to reduce the number of GATC sites. However, given that the putative orphan methyltransferase recognizing GATC in *Psychromonas* is homologous to a *Dam*-like methyltransferase, methylation of the GATC motif is more likely to play a regulatory or DNA mismatch repair role (Boye & Løbner-Olesen, 1990; Løbner-Olesen et al., 2005; Schlagman et al., 1986; Wion & Casadesús, 2006). Thus, the disparity in GATC motifs, 1.6x higher in the host compared to the prophage ($P < 0.0001$), suggests evolutionary pressure on the phage to minimize regulatory interference. While the functional annotations of flanking genes did not provide additional insight, the absence of GATC-associated restriction enzymes coupled with the Dam-like methyltransferase homology reinforces the hypothesis that methylation here serves a purpose beyond defence.

CASE STUDY: *PELAGIBACTER* METHYLOME

In the hypersaline, subzero sea-ice environment, the *Pelagibacter* methylome revealed unexpected strategies for surviving extreme conditions, including methylation-mediated regulation and prophage-host interplay. We identified one de novo methylation motif in our *Pelagibacter* MAG: G**A**NTC. This finding is consistent with the identified methylation-related genes found in the MAG. We found one methyltransferase from a restriction modification type II system, with 99.44% homolog identity to M.PgiNP1I which has a known cognate motif of G**A**NTC previously identified in *Pelagibacter* genomes and MAGs (Roberts et al., 2022; Seong et al., 2022). This motif has been identified consistently in other marine Alphaproteobacteria (Hiraoka et al., 2022). Of 1,923 instances of this motif in our MAG, sufficient data for 84% (1,623) were present in our dataset. The identified motif and corresponding methyltransferase were suggested previously to play a cell cycle regulator role in *Pelagibacter* (Seong et al., 2022). This claim is supported by a variation of the mean methylation fraction across the genome between the *ori* and *ter* and based on the functioning of the *CcrM* gene in *Caulobacter crescentus*. Although we cannot definitively identify *ori* and *ter* in our MAG, the pattern of across-genome variation in methylation fraction closely resembles that reported by Seong et al. from the North Pacific [70] (Figure 3.5). While they attributed this variation to exponential growth, the environmental conditions of sea ice cast doubt on a relationship between the observed pattern and exponential growth occurring *in situ*, as *Pelagibacter* is not

known to grow at subzero temperature and hypersalinity (Morris et al., 2020). However, we also identified 46 motif instances that were significantly differentially methylated in *Pelagibacter* MAG between top and bottom ice (Table 3.2), suggesting that methylation acts as a dynamic regulatory tool in response to environmental conditions. In three instances, the motifs were within the transcription start site of a flanking gene (taken to be 60 nucleotides upstream from the start codon). The functional diversity of these genes (Table 3.2) suggests a broad regulatory role for DNA methylation, consistent with the identified methyltransferase acting as a cell cycle regulator. In the case of *Pelagibacter* entrained into sea-ice brine, this regulator function may be to conserve energy to survive.

A prophage was identified on contig c_000000080048 belonging to *Pelagibacter* sp. but not the binned MAG. A BLAST search against the NCBI core nucleotide database revealed the closest match to *Pelagibacter* sp. UISW137, a strain isolated from under-ice seawater at our sampling site (by M Sadler of the same sampling team). Although no prophage was identified in the isolate, additional checks of our contig with VirSorter2 (Guo et al., 2021) and identification of multiple reads spanning the start of the prophage and the host genome confidently support this *Pelagibacter* prophage belonging to *Caudoviricetes*. The contig was 88,007 bp long, including the prophage which was 63,960 bp long. A type II methyltransferase was detected on the prophage which was homologous to *M.Pgl14TORF343P* which recognizes the GGATG motif. This motif was found 97 times on the prophage and 23 times in the rest of the contig. In the isolate, this motif occurs 1,302 times on a genome of length 1,403,101 bp. Thus, we find that this motif occurs approximately every 1,045 bp in the host part of the contig, every 659 bp in the prophage, and every 1,078 bp in the complete genome of the isolate and putative host. The prophage thus has a higher frequency of this motif than the contig ($P < 0.0001$ contig) or the isolate ($P < 0.0001$), suggesting a potential regulatory rather than defensive role, because selective pressure on the phage would reduce, not increase, the frequency of a motif being targeted defensively by an endonuclease. This finding aligns with the absence of cognate restriction enzymes in the *Pelagibacter* isolate, which retains only an orphan methyltransferase for G**A**TC. The methyltransferase of the prophage we detected thus likely influences gene expression by its host. The UISW 137 genome contains 34 instances of the G**A**TC motif within 70 bp of a gene transcription start site (Table C3). The function of these genes varies and includes a wide range of central metabolic functions. This range includes functions we identified as regulated by methylation in the *Pelagibacter* MAG (Table C3), which suggests that the impact of this prophage on UISW 137 would be consequential (e.g. regulation of anti-sigma factor). This relationship underscores the dual role of DNA methylation in sea-ice systems: a tool for viral persistence and a mediator of host adaptation under extreme conditions.

CONCLUSIONS

Our study, in providing this characterization of DNA methylation patterns in sea-ice bacterial communities and associated viruses, has revealed that methylation serves additional functions beyond defence against foreign DNA, as traditionally mediated by restriction-modification systems (Labrie et al., 2010). Through nanopore sequencing of stepped-sackhole brines from different ice horizons, we uncovered distinct methylation signatures between the top and bottom ice, suggesting epigenetic responses to the differing environmental conditions across the ice. The methylation landscape of the sea-ice bacterial community featured 5mC methylation (97%) and many orphan methyltransferases, known for their regulatory rather than defence functions. The differential methylation patterns by ice horizon, particularly in the G**A**NTC motif in *Pelagibacter*, also point to a regulatory role for methylation, likely in response to the more extreme environmental conditions over time in the upper ice than encountered in bottom ice. Our results suggest that DNA methylation in this pelagic bacterium may facilitate survival, possibly even growth, in the challenging sea-ice environment by

regulating core metabolic functions. However, further studies are needed to directly link the observed methylation patterns to a specific modulation of metabolic activity or growth.

In the viral component, we also obtained evidence of differential methylation, which we hypothesize reflects varying infection histories between ice horizons. The identification of orphan methyltransferases in sea-ice phages suggests that these phages use this known strategy to bypass host restriction-modification systems (Murphy et al., 2013a). The discovery of prophages encoding methyltransferases, including in a *Pelagibacter* strain isolated from under-ice seawater at our sampling site, provides new insights into phage-host interactions in sea ice. These prophages may influence host metabolism through methylation-based regulation, representing a previously uncharacterized mechanism of viral influence on sea-ice microbial communities similar to the influence of auxiliary metabolic genes.

Overall, our findings demonstrate that DNA methylation represents an important, previously overlooked mechanism for responding to the dynamically stressful sea-ice environment. The identification of numerous methylation motifs, many without known associated enzymes in reference databases, suggests that sea-ice communities are using unique methylation systems that warrant further investigation. Future studies with greater sequencing depth and broader sampling could further elucidate how DNA methylation contributes to microbial survival and evolution in this extreme ecosystem, potentially revealing adaptative strategies relevant to other challenging environments and extraterrestrial analogues.

Acknowledgments

The authors thank Dr. Karley Campbell for inviting GK on the BREATHE 2023 cruise and the R/V *Kronprins Haakon* crew for safe passage. We acknowledge Michael Sadler for help in the field, sequencing guidance, and insightful discussion, Einar Eliassen for ice safety, Dr. Tom Delmont for MAG binning assistance, and Dr. Murat Eren for Anvi'o support. Thanks to Arthur Rand (Nanopore) for incorporating feedback into modkit, Dr. Stephen Blaskowski and Kathy Qi for statistical discussions, and the Centre for Environmental Genomics (UW) for their insights. We also appreciate the UW Nanopore Sequence Core for troubleshooting support, and are grateful to Dr. Rika Anderson for computing resources.

Funding

This work was funded by a Benjamin Hall Conservation Genetics award to G.K. and the Karl M. Banse professorship to J.D. Fieldwork and sample collection was partially supported by the Research Council of Norway BREATHE project (no. 325405).

Data availability

All demultiplexed reads were uploaded to NCBI SRA as part of BioProject PRJNA1227241. Assembled contigs used in this study are also published within this BioProject. This study has been conducted using E.U. Copernicus Marine Service Information; https://doi.org/10.48670/moi-00001.

Conflict of interest

The authors have no conflict of interest to declare.

REFERENCES

Adhikari, S., & Curtis, P. D. (2016). DNA methyltransferases and epigenetic regulation in bacteria. *FEMS Microbiology Reviews*, *40*(5), 575–591. https://doi.org/10.1093/femsre/fuw023

Anton, B. P., & Roberts, R. J. (2021). Beyond restriction modification: epigenomic roles of DNA methylation in prokaryotes. *Annual Review of Microbiology*, *75*(1), 1–21. https://doi.org/10.1146/annurev-micro-040521-035040

Aroney, S. T. N., Newell, R. J. P., Nissen, J. N., Camargo, A. P., Tyson, G. W., & Woodcroft, B. J. (2025). CoverM: read alignment statistics for metagenomics. *arXiv*. https://doi.org/10.48550/arxiv.2501.11217

Astashyn, A., Tvedte, E. S., Sweeney, D., Sapojnikov, V., Bouk, N., Joukov, V., Mozes, E., Strope, P. K., Sylla, P. M., Wagner, L., Bidwell, S. L., Brown, L. C., Clark, K., Davis, E. W., Smith-White, B., Hlavina, W., Pruitt, K. D., Schneider, V. A., & Murphy, T. D. (2024). Rapid and sensitive detection of genome contamination at scale with FCS-GX. *Genome Biology*, *25*(1), 60. https://doi.org/10.1186/s13059-024-03198-7

Barbeyron, T., Kean, K., & Forterre, P. (1984). DNA adenine methylation of GATC sequences appeared recently in the Escherichia coli lineage. *Journal of Bacteriology*, *160*(2), 586–590. https://doi.org/10.1128/jb.160.2.586-590.1984

Beaulaurier, J., Schadt, E. E., & Fang, G. (2019). Deciphering bacterial epigenomes using modern sequencing technologies. *Nature Reviews Genetics*, *20*(3), 157–172. https://doi.org/10.1038/s41576-018-0081-3

Blow, M. J., Clark, T. A., Daum, C. G., Deutschbauer, A. M., Fomenkov, A., Fries, R., Froula, J., Kang, D. D., Malmstrom, R. R., Morgan, R. D., Posfai, J., Singh, K., Visel, A., Wetmore, K., Zhao, Z., Rubin, E. M., Korlach, J., Pennacchio, L. A., & Roberts, R. J. (2016). The epigenomic landscape of prokaryotes. *PLoS Genetics*, *12*(2), e1005854. https://doi.org/10.1371/journal.pgen.1005854

Boetius, A., Anesio, A. M., Deming, J. W., Mikucki, J. A., & Rapp, J. Z. (2015). Microbial ecology of the cryosphere: sea ice and glacial habitats. *Nature Reviews Microbiology*, *13*(11), 677–690. https://doi.org/10.1038/nrmicro3522

Bowman, J. S. (2015). The relationship between sea ice bacterial community structure and biogeochemistry: A synthesis of current knowledge and known unknowns. *Elementa*, *3*, 000072. https://doi.org/10.12952/journal.elementa.000072

Boye, E., & Løbner-Olesen, A. (1990). The role of dam methyltransferase in the control of DNA replication in E. coli. *Cell*, *62*(5), 981–989. https://doi.org/10.1016/0092-8674(90)90272-g

Brown, C. T., Olm, M. R., Thomas, B. C., & Banfield, J. F. (2016). Measurement of bacterial replication rates in microbial communities. *Nature Biotechnology*, *34*(12), 1256–1263. https://doi.org/10.1038/nbt.3704

Bu, X., Dou, X., Chen, Z., Liu, L., Mei, Y., & Ren, M. (2025). DNA methylation confers epigenetic changes in cold-adapted microorganisms in response to cold stress. *Extremophiles*, *29*(1), 16. https://doi.org/10.1007/s00792-025-01381-7

Buchfink, B., Xie, C., & Huson, D. H. (2015). Fast and sensitive protein alignment using DIAMOND. *Nature Methods*, *12*(1), 59–60. https://doi.org/10.1038/nmeth.3176

Camargo, A. P., Roux, S., Schulz, F., Babinski, M., Xu, Y., Hu, B., Chain, P. S. G., Nayfach, S., & Kyrpides, N. C. (2024). Identification of mobile genetic elements with geNomad. *Nature Biotechnology*, *42*(8), 1303–1312. https://doi.org/10.1038/s41587-023-01953-y

Casadesús, J., & Low, D. (2006). Epigenetic gene regulation in the bacterial world. *Microbiology and Molecular Biology Reviews*, *70*(3), 830–856. https://doi.org/10.1128/mmbr.00016-06

Chamberlain, E. J., Balmonte, J. P., Torstensson, A., Fong, A. A., Snoeijs-Leijonmalm, P., & Bowman, J. S. (2022). Impacts of sea ice melting procedures on measurements of microbial community structure. *Elementa: Science of the Anthropocene*, *10*(1). https://doi.org/10.1525/elementa.2022.00017

Chaumeil, P.-A., Mussig, A. J., Hugenholtz, P., & Parks, D. H. (2022). GTDB-Tk v2: memory friendly classification with the genome taxonomy database. *Bioinformatics*, *38*(23), 5315–5316. https://doi.org/10.1093/bioinformatics/btac672

Collins, R. E., & Deming, J. W. (2011). Abundant dissolved genetic material in Arctic sea ice Part II: Viral dynamics during autumn freeze-up. *Polar Biology*, *34*(12), 1831–1841. https://doi.org/10.1007/s00300-011-1008-z

Collins, R. E., Rocap, G., & Deming, J. W. (2010). Persistence of bacterial and archaeal communities in sea ice through an Arctic winter. *Environmental Microbiology*, *12*(7), 1828–1841. https://doi.org/10.1111/j.1462-2920.2010.02179.x

Cooper, Z. S., Rapp, J. Z., Carpenter, S. D., Iwahana, G., Eicken, H., & Deming, J. W. (2019). Distinctive microbial communities in subzero hypersaline brines from Arctic coastal sea ice and rarely sampled cryopegs. *FEMS Microbiology Ecology*, *95*(12), fiz166. https://doi.org/10.1093/femsec/fiz166

Coster, W. D., & Rademakers, R. (2023). NanoPack2: population-scale evaluation of long-read sequencing data. *Bioinformatics*, *39*(5), btad311. https://doi.org/10.1093/bioinformatics/btad311

Crits-Christoph, A., Kang, S. C., Lee, H. H., & Ostrov, N. (2023). MicrobeMod: A computational toolkit for identifying prokaryotic methylation and restriction-modification with nanopore sequencing. *bioRxiv*, 2023.11.13.566931. https://doi.org/10.1101/2023.11.13.566931

Darling, A. C. E., Mau, B., Blattner, F. R., & Perna, N. T. (2004). Mauve: multiple alignment of conserved genomic sequence with rearrangements. *Genome Research*, *14*(7), 1394–1403. https://doi.org/10.1101/gr.2289704

Deming, J. W. (2007). Extreme high-pressure marine environments. *Manual of Environmental Microbiology*. 575–590. https://doi.org/10.1128/9781555815882.ch46

Deming, J. W., & Collins, R. E. (2017). Sea ice as a habitat for Bacteria, Archaea and viruses. In D. N. Thomas (Ed.), *Sea Ice* (pp. 326–351). https://doi.org/10.1002/9781118778371.ch13

Ewert, M., & Deming, J. W. (2013). Sea ice microorganisms: environmental constraints and extracellular responses. *Biology*, *2*(2), 603–628. https://doi.org/10.3390/biology2020603

Ewert, M., & Deming, J. W. (2014). Bacterial responses to fluctuations and extremes in temperature and brine salinity at the surface of Arctic winter sea ice. *FEMS Microbiology Ecology*, *89*(2), 476–489. https://doi.org/10.1111/1574-6941.12363

Firth, E., Carpenter, S. D., Sørensen, H. L., Collins, R. E., & Deming, J. W. (2016). Bacterial use of choline to tolerate salinity shifts in sea-ice brines. *Elementa*, *4*, 000120. https://doi.org/10.12952/journal.elementa.000120

Fullmer, M. S., Ouellette, M., Louyakis, A. S., Papke, R. T., & Gogarten, J. P. (2019). The patchy distribution of restriction–modification system genes and the conservation of orphan methyltransferases in *Halobacteria*. *Genes*, *10*(3), 233. https://doi.org/10.3390/genes10030233

Gärtner, K., Klähn, S., Watanabe, S., Mikkat, S., Scholz, I., Hess, W. R., & Hagemann, M. (2019). Cytosine N4-Methylation via M.Ssp6803II Is Involved in the Regulation of Transcription, Fine- Tuning of DNA Replication and DNA Repair in the Cyanobacterium Synechocystis sp. PCC 6803. *Frontiers in Microbiology*, *10*, 1233. https://doi.org/10.3389/fmicb.2019.01233

Vink, R., de Gooijer, S., Beedie, A., Gorelli, M. E., Peters, O., Burghoorn, G., Guo, W., van Zundert, J., Hulselmans, G., Marshall, Grinstead, C., Manley, L., chielP, Turner-Trauring, I., Mitchell, L., Santamaria, M., Harbeck, H., Heres, D., … van Gelderen, M.. (2025). *pola-rs/polars: Python Polars 1.26.0*. https://doi.org/10.5281/zenodo.15071487

Gomez-Buckley, A. C., Showalter, G. M., & Wong, M. L. (2022). Modeling Virus and Bacteria Populations in Europa's Subsurface Ocean. *Life*, *12*(5), 620. https://doi.org/10.3390/life12050620

Gopalan-Nair, R., Coissac, A., Legrand, L., Lopez-Roques, C., Pécrix, Y., Vandecasteele, C., Bouchez, O., Barlet, X., Lanois, A., Givaudan, A., Brillard, J., Genin, S., & Guidot, A. (2024). Changes in DNA methylation contribute to rapid adaptation in bacterial plant pathogen evolution. *PLOS Biology*, *22*(9), e3002792. https://doi.org/10.1371/journal.pbio.3002792

Guo, J., Bolduc, B., Zayed, A. A., Varsani, A., Dominguez-Huerta, G., Delmont, T. O., Pratama, A. A., Gazitúa, M. C., Vik, D., Sullivan, M. B., & Roux, S. (2021). VirSorter2: a multi-classifier, expert-guided approach to detect diverse DNA and RNA viruses. *Microbiome*, *9*(1), 37. https://doi.org/10.1186/s40168-020-00990-y

Harris, A., & Goldman, A. D. (2020). The complex phylogenetic relationships of a 4mC/6mA DNA methyltransferase in prokaryotes. *Molecular Phylogenetics and Evolution*, *149*, 106837. https://doi.org/10.1016/j.ympev.2020.106837

Hill, C., Miller, L. A., & Klaenhammer, T. R. (1991). In vivo genetic exchange of a functional domain from a type II A methylase between lactococcal plasmid pTR2030 and a virulent bacteriophage. *Journal of Bacteriology*, *173*(14), 4363–4370. https://doi.org/10.1128/jb.173.14.4363-4370.1991

Hiraoka, S., Okazaki, Y., Anda, M., Toyoda, A., Nakano, S., & Iwasaki, W. (2019). Metaepigenomic analysis reveals the unexplored diversity of DNA methylation in an environmental prokaryotic community. *Nature Communications*, *10*(1), 159. https://doi.org/10.1038/s41467-018-08103-y

Hiraoka, S., Sumida, T., Hirai, M., Toyoda, A., Kawagucci, S., Yokokawa, T., & Nunoura, T. (2022). Diverse DNA modification in marine prokaryotic and viral communities. *Nucleic Acids Research*, *50*(3), 1531–1550. https://doi.org/10.1093/nar/gkab1292

Hu, L., Xiao, P., Jiang, Y., Dong, M., Chen, Z., Li, H., Hu, Z., Lei, A., & Wang, J. (2018). Transgenerational epigenetic inheritance under environmental stress by genome-wide DNA methylation profiling in Cyanobacterium. *Frontiers in Microbiology*, *9*, 1479. https://doi.org/10.3389/fmicb.2018.01479

Huang, D., Xia, R., Chen, C., Liao, J., Chen, L., Wang, D., Alvarez, P. J. J., & Yu, P. (2024). Adaptive strategies and ecological roles of phages in habitats under physicochemical stress. *Trends in Microbiology*, *32*(9), 902–916. https://doi.org/10.1016/j.tim.2024.02.002

Hunter, J. D. (2007). Matplotlib: A 2D graphics environment. *Computing in Science & Engineering*, *9*(3), 90–95. https://doi.org/10.1109/mcse.2007.55

Huson, D. H., Albrecht, B., Bağcı, C., Bessarab, I., Górska, A., Jolic, D., & Williams, R. B. H. (2018). MEGAN-LR: new algorithms allow accurate binning and easy interactive exploration of metagenomic long reads and contigs. *Biology Direct*, *13*(1), 6. https://doi.org/10.1186/s13062-018-0208-7

Huston, A. L. (2003). Bacterial adaptation to the cold: in situ activities of extracellular enzymes in the North Water Polynya and characterization of a cold-active aminopeptidase from Colwellia psychrerythraea strain 34H. *University of Washington*.

Jeudy, S., Rigou, S., Alempic, J.-M., Claverie, J.-M., Abergel, C., & Legendre, M. (2020). The DNA methylation landscape of giant viruses. *Nature Communications*, *11*(1), 2657. https://doi.org/10.1038/s41467-020-16414-2

Junge, K., Krembs, C., Deming, J., Stierle, A., & Eicken, H. (2001). A microscopic approach to investigate bacteria under in situ conditions in sea-ice samples. *Annals of Glaciology*, *33*, 304–310. https://doi.org/10.3189/172756401781818275

Kobayashi, I. (2001). Behavior of restriction–modification systems as selfish mobile elements and their impact on genome evolution. *Nucleic Acids Research*, *29*(18), 3742–3756. https://doi.org/10.1093/nar/29.18.3742

Kolmogorov, M., Bickhart, D. M., Behsaz, B., Gurevich, A., Rayko, M., Shin, S. B., Kuhn, K., Yuan, J., Polevikov, E., Smith, T. P. L., & Pevzner, P. A. (2020). metaFlye: scalable long-read metagenome assembly using repeat graphs. *Nature Methods*, *17*(11), 1103–1110. https://doi.org/10.1038/s41592-020-00971-x

Labrie, S. J., Samson, J. E., & Moineau, S. (2010). Bacteriophage resistance mechanisms. *Nature Reviews Microbiology*, *8*(5), 317–327. https://doi.org/10.1038/nrmicro2315

Li, H. (2021). New strategies to improve minimap2 alignment accuracy. *Bioinformatics*, *37*(23), 4572–4574. https://doi.org/10.1093/bioinformatics/btab705

Liu, Y., Demina, T. A., Roux, S., Aiewsakun, P., Kazlauskas, D., Simmonds, P., Prangishvili, D., Oksanen, H. M., & Krupovic, M. (2021). Diversity, taxonomy, and evolution of archaeal viruses of the class Caudoviricetes. *PLoS Biology*, *19*(11), e3001442. https://doi.org/10.1371/journal.pbio.3001442

Løbner-Olesen, A., Skovgaard, O., & Marinus, M. G. (2005). Dam methylation: coordinating cellular processes. *Current Opinion in Microbiology*, *8*(2), 154–160. https://doi.org/10.1016/j.mib.2005.02.009

Luhtanen, A.-M., Eronen-Rasimus, E., Kaartokallio, H., Rintala, J.-M., Autio, R., & Roine, E. (2014). Isolation and characterization of phage–host systems from the Baltic Sea ice. *Extremophiles*, *18*(1), 121–130. https://doi.org/10.1007/s00792-013-0604-y

Mattei, A. L., Bailly, N., & Meissner, A. (2022). DNA methylation: a historical perspective. *Trends in Genetics*, *38*(7), 676–707. https://doi.org/10.1016/j.tig.2022.03.010

McKinney, W. (2010). Data structures for statistical computing in Python. *SciPy Proceedings*. 56–61. https://doi.org/10.25080/majora-92bf1922-00a

Melsom, A., Counillon, F., LaCasce, J. H., & Bertino, L. (2012). Forecasting search areas using ensemble ocean circulation modeling. *Ocean Dynamics*, *62*(8), 1245–1257. https://doi.org/10.1007/s10236-012-0561-5

Menzel, P., Ng, K. L., & Krogh, A. (2016). Fast and sensitive taxonomic classification for metagenomics with Kaiju. *Nature Communications*, *7*(1), 11257. https://doi.org/10.1038/ncomms11257

Mölder, F., Jablonski, K., Letcher, B., Hall, M., Tomkins-Tinch, C., Sochat, V., Forster, J., Lee, S., Twardziok, S., Kanitz, A., Wilm, A., Holtgrewe, M., Rahmann, S., Nahnsen, S., & Köster, J. (2021). Sustainable data analysis with Snakemake [version 1; peer review: 1 approved, 1 approved with reservations]. *F1000Research*, *10*(33). https://doi.org/10.12688/f1000research.29032.1

Montresor, M., Lovejoy, C., Orsini, L., Procaccini, G., & Roy, S. (2003). Bipolar distribution of the cyst-forming dinoflagellate Polarella glacialis. *Polar Biology*, *26*(3), 186–194. https://doi.org/10.1007/s00300-002-0473-9

Morris, R. M., Cain, K. R., Hvorecny, K. L., & Kollman, J. M. (2020). Lysogenic host–virus interactions in SAR11 marine bacteria. *Nature Microbiology*, *5*(8), 1011–1015. https://doi.org/10.1038/s41564-020-0725-x

Murphy, J., Klumpp, J., Mahony, J., O'Connell-Motherway, M., Nauta, A., & Sinderen, D. van. (2014). Methyltransferases acquired by lactococcal 936-type phage provide protection against restriction endonuclease activity. *BMC Genomics*, *15*(1), 831. https://doi.org/10.1186/1471-2164-15-831

Murphy, J., Mahony, J., Ainsworth, S., Nauta, A., & Sinderen, D. van. (2013a). Bacteriophage orphan DNA methyltransferases: insights from their bacterial origin, function, and occurrence. *Applied and Environmental Microbiology*, *79*(24), 7547–7555. https://doi.org/10.1128/aem.02229-13

Murphy, J., Mahony, J., Ainsworth, S., Nauta, A., & Sinderen, D. van. (2013b). Bacteriophage orphan DNA methyltransferases: insights from their bacterial origin, function, and occurrence. *Applied and Environmental Microbiology*, *79*(24), 7547–7555. https://doi.org/10.1128/aem.02229-13

Mykytczuk, N. C. S., Foote, S. J., Omelon, C. R., Southam, G., Greer, C. W., & Whyte, L. G. (2013). Bacterial growth at −15 °C; molecular insights from the permafrost bacterium *Planococcus halocryophilus* Or1. *The ISME Journal*, *7*(6), 1211–1226. https://doi.org/10.1038/ismej.2013.8

Nayfach, S., Camargo, A. P., Schulz, F., Eloe-Fadrosh, E., Roux, S., & Kyrpides, N. C. (2021). CheckV assesses the quality and completeness of metagenome-assembled viral genomes. *Nature Biotechnology*, *39*(5), 578–585. https://doi.org/10.1038/s41587-020-00774-7

Office, M. (2010). *Cartopy: a cartographic python library with a Matplotlib interface*. https://scitools.org.uk/cartopy

Oliveira, J. dos S., Lavell, A. A., Essus, V. A., Souza, G., Nunes, G. H. P., Benício, E., Guimarães, A. J., Parent, K. N., & Cortines, J. R. (2021). Structure and physiology of giant DNA viruses. *Current Opinion in Virology*, *49*, 58–67. https://doi.org/10.1016/j.coviro.2021.04.012

Reisenauer, A., Kahng, L. S., McCollum, S., & Shapiro, L. (1999). Bacterial DNA methylation: a cell cycle regulator? *Journal of Bacteriology*, *181*(17), 5135–5139. https://doi.org/10.1128/jb.181.17.5135-5139.1999

Riley, M., Staley, J. T., Danchin, A., Wang, T. Z., Brettin, T. S., Hauser, L. J., Land, M. L., & Thompson, L. S. (2008). Genomics of an extreme psychrophile, Psychromonas ingrahamii. *BMC Genomics*, *9*(1), 210. https://doi.org/10.1186/1471-2164-9-210

Roberts, R. J., Belfort, M., Bestor, T., Bhagwat, A. S., Bickle, T. A., Bitinaite, J., Blumenthal, R. M., Degtyarev, S. Kh., Dryden, D. T. F., Dybvig, K., Firman, K., Gromova, E. S., Gumport, R. I., Halford, S. E., Hattman, S., Heitman, J., Hornby, D. P., Janulaitis, A., Jeltsch, A., … Xu, S. (2003). A nomenclature for restriction enzymes, DNA methyltransferases, homing endonucleases and their genes. *Nucleic Acids Research*, *31*(7), 1805–1812. https://doi.org/10.1093/nar/gkg274

Roberts, R. J., Vincze, T., Posfai, J., & Macelis, D. (2022). REBASE: a database for DNA restriction and modification: enzymes, genes and genomes. *Nucleic Acids Research*, *51*(D1), D629–D630. https://doi.org/10.1093/nar/gkac975

Sakov, P., Counillon, F., Bertino, L., Lisæter, K. A., Oke, P. R., & Korablev, A. (2012). TOPAZ4: an ocean-sea ice data assimilation system for the North Atlantic and Arctic. *Ocean Science*, *8*(4), 633–656. https://doi.org/10.5194/os-8-633-2012

Sánchez-Romero, M. A., Cota, I., & Casadesús, J. (2015). DNA methylation in bacteria: from the methyl group to the methylome. *Current Opinion in Microbiology*, *25*, 9–16. https://doi.org/10.1016/j.mib.2015.03.004

Schlagman, S. L., Hattman, S., & Marinus, M. G. (1986). Direct role of the *Escherichia coli* Dam DNA methyltransferase in methylation-directed mismatch repair. *Journal of Bacteriology*, *165*(3), 896–900. https://doi.org/10.1128/jb.165.3.896-900.1986

Seabold, S., & Perktold, J. (2010). Statsmodels: econometric and statistical modeling with Python. *Proceedings of the 9th Python in Science Conference*, 92–96. https://doi.org/10.25080/majora-92bf1922-011

Seong, H. J., Han, S.-W., & Sul, W. J. (2021). Prokaryotic DNA methylation and its functional roles. *Journal of Microbiology*, *59*(3), 242–248. https://doi.org/10.1007/s12275-021-0674-y

Seong, H. J., Roux, S., Hwang, C. Y., & Sul, W. J. (2022). Marine DNA methylation patterns are associated with microbial community composition and inform virus-host dynamics. *Microbiome*, *10*(1), 157. https://doi.org/10.1186/s40168-022-01340-w

Skennerton, C. T., Imelfort, M., & Tyson, G. W. (2013). Crass: identification and reconstruction of CRISPR from unassembled metagenomic data. *Nucleic Acids Research*, *41*(10), e105. https://doi.org/10.1093/nar/gkt183

Sun, C., Chen, J., Jin, M., Zhao, X., Li, Y., Dong, Y., Gao, N., Liu, Z., Bork, P., Zhao, X., & Chen, W. (2023). Long-read sequencing reveals extensive DNA methylations in human gut phagenome contributed by prevalently phage-encodedmethyltransferases. *Advanced Science*, *10*(25), 2302159. https://doi.org/10.1002/advs.202302159

Takahashi, M., Hiraoka, S., Matsumoto, Y., Shibagaki, R., Ujihara, T., Maeda, H., Seo, S., Nagasaki, K., Takeuchi, H., & Matsuzaki, S. (2025). Host-encoded DNA methyltransferases modify the epigenome and host tropism of invading phages. *iScience*, *28*(4), 112264. https://doi.org/10.1016/j.isci.2025.112264

Vance, S. D., Journaux, B., Hesse, M., & Steinbrügge, G. (2021). The salty secrets of icy ocean worlds. *Journal of Geophysical Research: Planets*, *126*(1). https://doi.org/10.1029/2020je006736

Vandenbussche, I., Sass, A., Pinto-Carbó, M., Mannweiler, O., Eberl, L., & Coenye, T. (2020). DNA methylation epigenetically regulates gene expression in *Burkholderia cenocepacia* and controls biofilm formation, cell eggregation, and motility. *mSphere*, *5*(4), 10.1128/msphere.00455-20. https://doi.org/10.1128/msphere.00455-20

Vasu, K., & Nagaraja, V. (2013). Diverse functions of restriction-modification systems in addition to cellular defense. *Microbiology and Molecular Biology Reviews*, *77*(1), 53–72. https://doi.org/10.1128/mmbr.00044-12

Waskom, M. (2021). seaborn: statistical data visualization. *Journal of Open Source Software*, *6*(60), 3021. https://doi.org/10.21105/joss.03021

Wells, L. E., & Deming, J. W. (2006). Modelled and measured dynamics of viruses in Arctic winter sea-ice brines. *Environmental Microbiology*, *8*(6), 1115–1121. https://doi.org/10.1111/j.1462-2920.2006.00984.x

Wion, D., & Casadesús, J. (2006). N6-methyl-adenine: an epigenetic signal for DNA–protein interactions. *Nature Reviews Microbiology*, *4*(3), 183–192. https://doi.org/10.1038/nrmicro1350

Woodcroft, B. J., Aroney, S. T. N., Zhao, R., Cunningham, M., Mitchell, J. A. M., Blackall, L., & Tyson, G. W. (2024). SingleM and Sandpiper: Robust microbial taxonomic profiles from metagenomic data. *bioRxiv*, 2024.01.30.578060. https://doi.org/10.1101/2024.01.30.578060

Yano, H., Alam, Md. Z., Rimbara, E., Shibata, T. F., Fukuyo, M., Furuta, Y., Nishiyama, T., Shigenobu, S., Hasebe, M., Toyoda, A., Suzuki, Y., Sugano, S., Shibayama, K., & Kobayashi, I. (2020). Networking and specificity-changing DNA methyltransferases in *Helicobacter pylori*. *Frontiers in Microbiology*, *11*, 1628. https://doi.org/10.3389/fmicb.2020.01628

Yilmaz, P., Gilbert, J. A., Knight, R., Amaral-Zettler, L., Karsch-Mizrachi, I., Cochrane, G., Nakamura, Y., Sansone, S.-A., Glöckner, F. O., & Field, D. (2011). The genomic standards consortium: bringing standards to life for microbial ecology. *The ISME Journal*, *5*(10), 1565–1567. https://doi.org/10.1038/ismej.2011.39

Zou, Q., Guo, J., Ju, Y., Wu, M., Zeng, X., & Hong, Z. (2015). Improving tRNAscan-SE annotation results via ensemble classifiers. *Molecular Informatics*, *34*(11-12), 761–770. https://doi.org/10.1002/minf.201500031

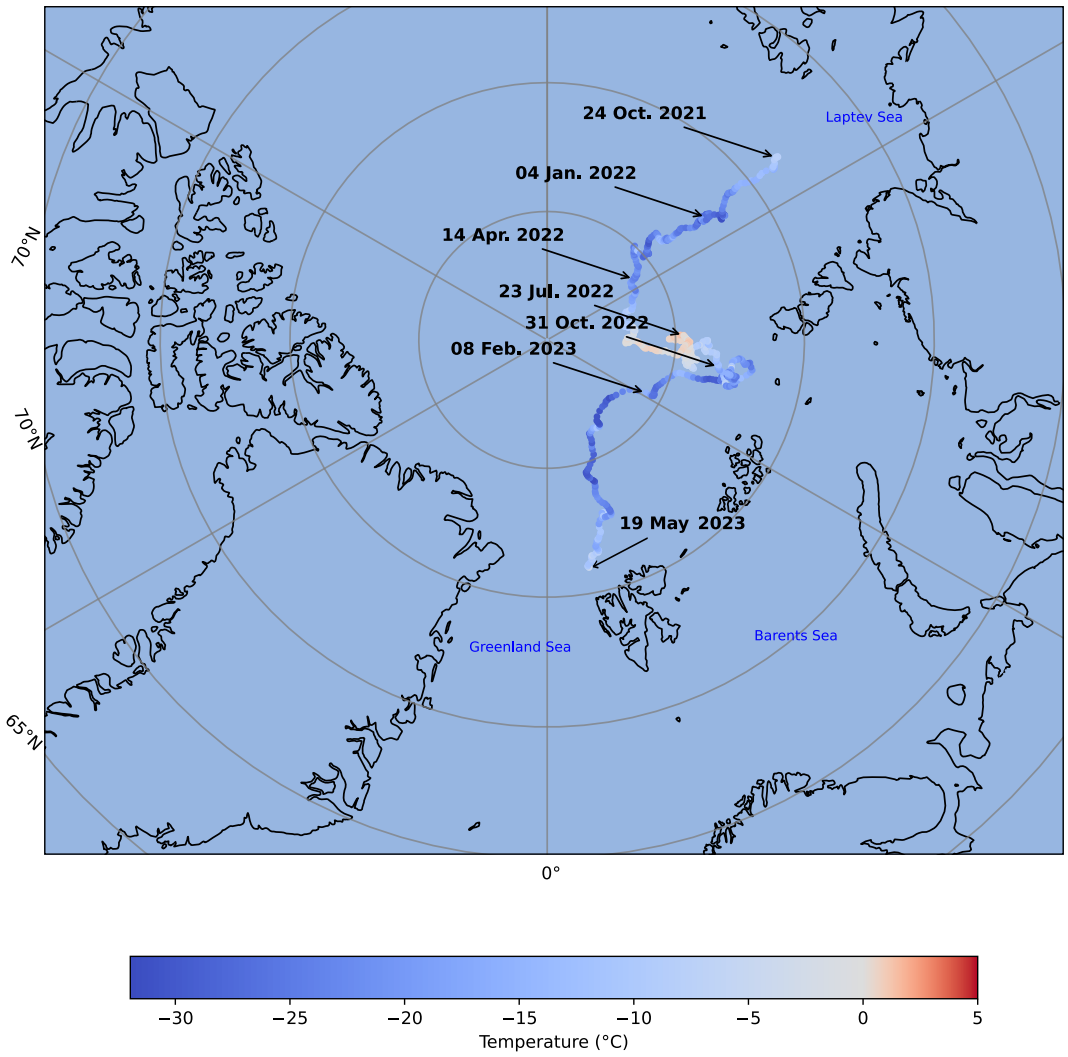

Figure 1. Atmospheric temperature along the floe drift path. Atmospheric temperature from October 2021 to May 2023, along the estimated drift path of the floe sampled in this study. Warm temperatures in summer 2022 and cold yet dynamic temperature variations throughout the ensuing year indicate that by sampling time in May 2023 the top of the sea ice had experienced more extreme and greater variability in environmental conditions than bottom ice influenced by the relatively stable conditions of underlying seawater (Figure S1).

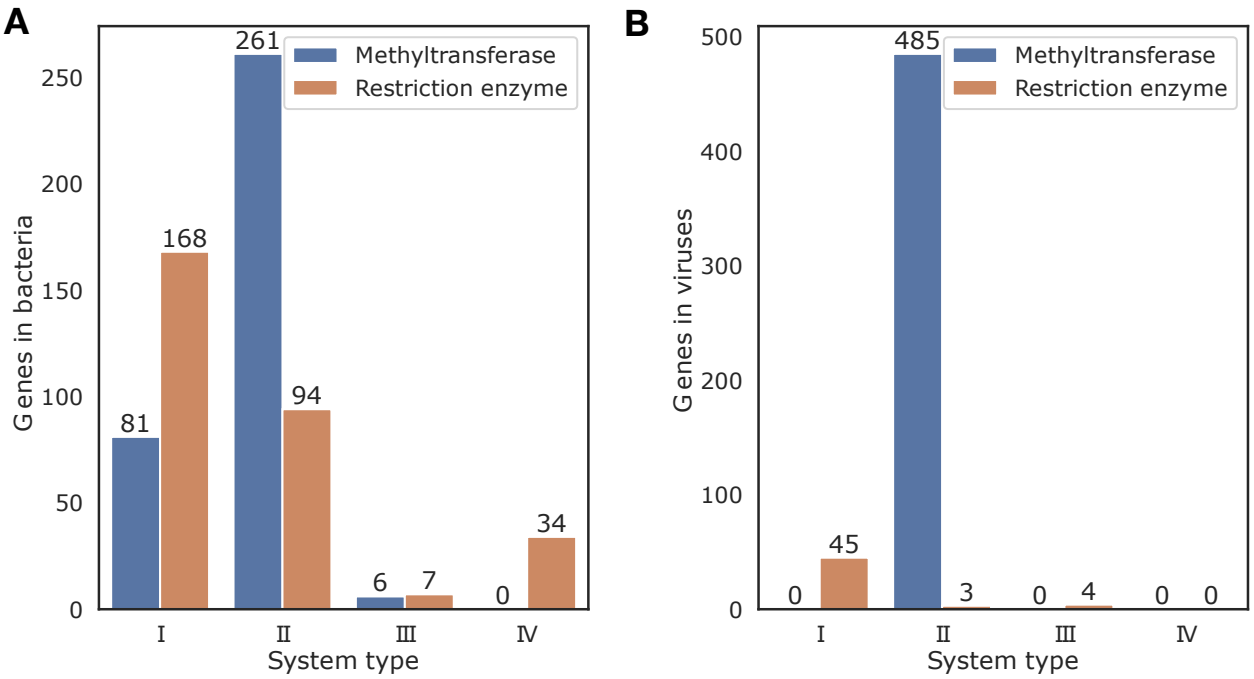

Figure 2. Number of genes involved in known restriction-modification systems in the sea-ice bacterial metagenome and the viruses. A) Gene counts of the four known types of restriction-modification systems in the sea-ice bacterial metagenome. A surplus of methyltransferases (blue) of over restriction enzymes (orange) suggests a high number of orphan methyltransferases, known to perform functions other than defence against foreign DNA, such as gene regulation and DNA repair. B) Gene counts in the viruses associated with the sea-ice community. Only three types of restriction-modification systems were detected, but the surplus of Type II methyltransferases (>10x the restriction enzymes) again suggests orphan methyltransferases with regulatory or DNA repair functions. The surplus holds when considering only *Caudoviricetes* (376 methyltransferases versus 48 restriction enzymes). A complete list with E-value and homology information, quantifying the accuracy of these results, can be found in File S2 (ISME).

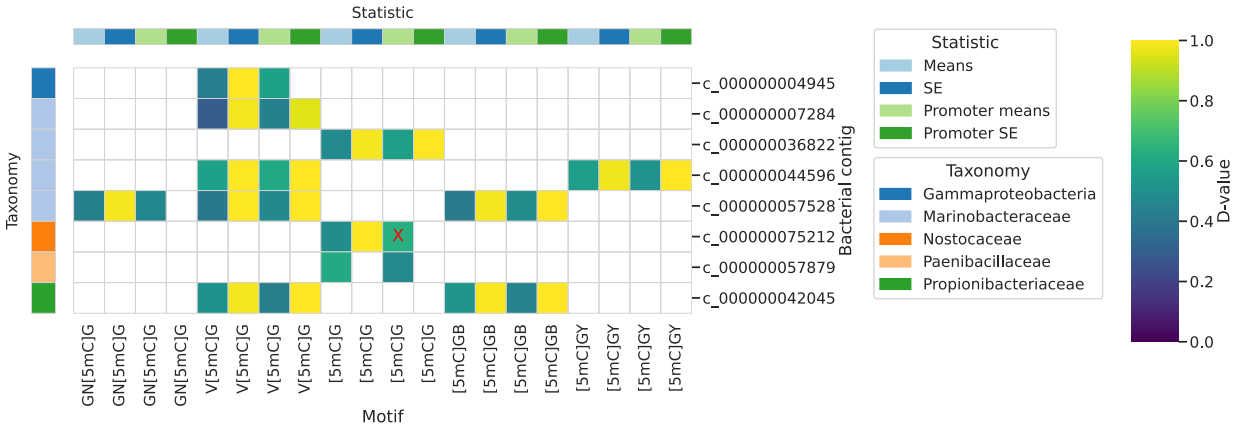

Figure 3. Significance of differential methylation in bacterial contigs between top and bottom ice. The d-value of the Kolmogorov-Smirnov similarity test is shown for each of the 8 bacterial contigs with sufficient data. Red "X" signifies that the statistical test result is insignificant (p >= 0.05), and thus the methylation distribution for this contig can be considered the same between horizons. D-value of 1 indicates largest difference in distribution, 0 indicates no difference. Most contigs show significant differences in the distribution of per-nucleotide mean methylation fraction, when considering all motif instances and only those within promoter regions. Significant differences in standard error of the distributions suggest possible differences within the population.

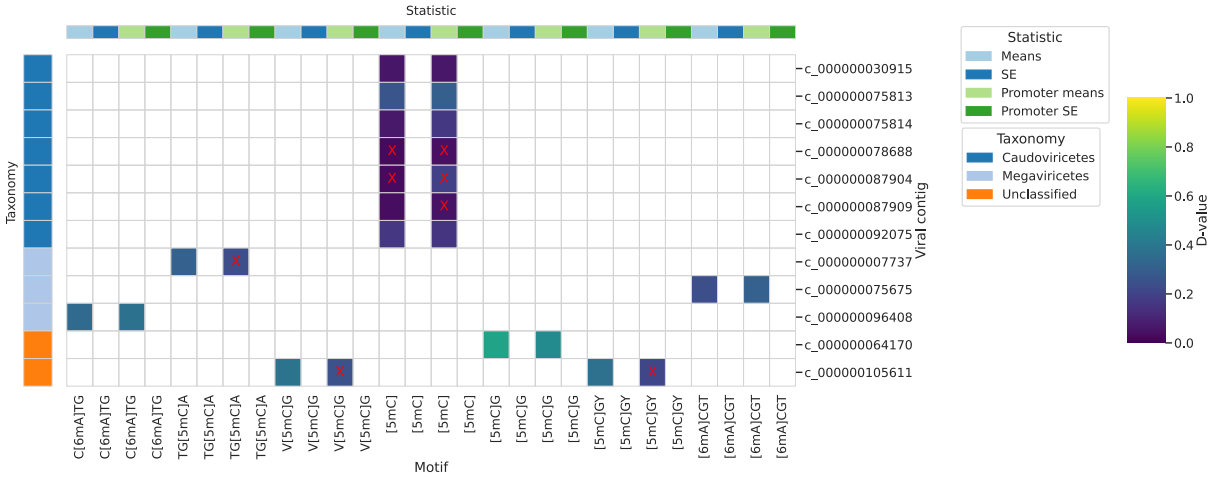

Figure 4. Significance of differential methylation in viral contigs between top and bottom ice. The d-value of the Kolmogorov-Smirnov similarity test is shown for each of the 12 viral contigs with sufficient data. Red "X" signifies that the statistical test result is insignificant ($p >= 0.05$), and thus the methylation distribution for this contig can be considered the same between horizons. D-value of 1 indicates largest difference in distribution, 0 indicates no difference. Many contigs show significant differences in the distribution of per-nucleotide mean methylation fraction, when considering all motif instances and only those within promoter regions. As all contigs had insufficient replicate data to calculate standard error, a population characterization cannot be made.

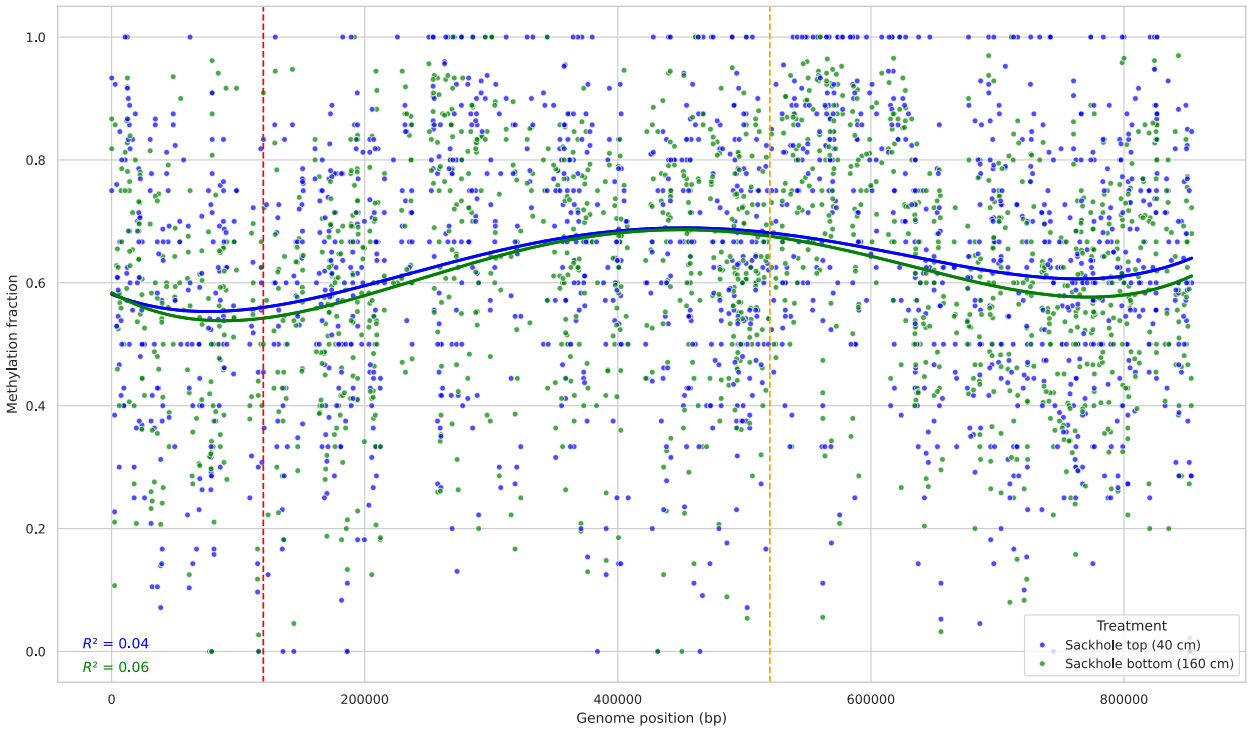

Figure 5. The methylome of a binned *Pelagibacter* MAG. In this MAG, the only identified methylation motif was G**A**NTC, consistent with previous studies [21, 72]. Here we plot the methylation fraction for each instance of the 6mA-methylated motif across the MAG for both the top and bottom ice horizons. The solid lines are a quartic fit for each treatment. The dashed vertical lines mark the terminus (red) and origin (orange) of replication. Similar variation in methylation over a genome was previously suggested to be evidence of cell cycle regulation (Seong et al., 2022).

CONCLUSION

This thesis began by asking, what is the ecological role of bacterial memory, specifically in allowing bacteria to acclimate to subzero brines? Through investigations of two Arctic ecosystems, cryopeg brines and sea ice, I have laid foundational work to allow this question to be addressed more extensively in the environment and obtained evidence of memory in a model sea-ice bacterium.

In Chapter 1, I reconstructed the environmental history of heterotrophic bacterial communities in cryopeg brines. By determining a probable trajectory of cell density and energetic needs over the system's lifespan, I estimated that cell-specific metabolic rates in cryopegs are higher than those in marine sediments despite the lower temperatures. This finding challenges the expectation that colder temperatures alone dictate lower metabolic rates. Instead, the high energy cost suggests substantial investment in producing extracellular enzymes to liberate organic carbon and in synthesizing protective compounds such as extracellular polysaccharides for cryoprotection and osmoprotection. These results provide important context for considering memory in cryopeg communities, raising new questions: if these bacteria possess memory of a more variable past, does that memory remain after 40,000 years of environmental stability? In either case, what are the implications for their capacity to acclimate as permafrost thaws and conditions become increasingly variable?

In Chapter 2, I set out in search of bacterial memory in *Colwellia psychrerythraea* strain 34H, a model sea-ice bacterium. An experimental approach culturing 34H successively in alternating salinity conditions showed acclimation to the repeated stress evidenced by changes in growth rates and lag times. This phenotypic evidence of acclimation was consistent with bacterial memory. An effort to determine the mechanistic basis for this memory focused on the DNA methylation pattern of 34H. DNA methylation was confirmed as regulating gene expression in response to osmotic stress. However, DNA methylation did not emerge clearly as the mechanism for memory in 34H; the underlying memory mechanism remains to be determined. To identify the underlying memory mechanism, future work could investigate the role of RNA modifications, small non-coding RNAs, or intracellular protein concentrations. The finding that 34H may be capable of osmotic stress memory informs our understanding of memory's ecological role in sea ice. Its role is particularly relevant at a time when fluctuations in the Arctic atmosphere, impacting sea-ice conditions, are increasing in both magnitude and frequency, allowing us to understand the resiliency of sea-ice communities.

Chapter 3 extended the work of Chapter 2 to the environment by studying DNA methylation patterns of sea-ice bacterial communities *in situ*. By comparing the thermally variable top ice with the more stable bottom ice, I found differential methylation across temperature and salinity gradients in various members of the community. This study revealed that DNA methylation in sea-ice communities serves multiple roles: it functions classically in defense through restriction-modification systems, clearly in gene regulation as evidenced by differential methylation between ice horizons, and unexpectedly in prophage-host interactions. The abundance of orphan methyltransferases, enzymes without corresponding restriction partners, suggests that much of this methylation serves purposes beyond immune defense. Along with Chapter 2, this study motivates a wider search for memory in bacterial communities through DNA methylation studies over time.

Together, these three chapters contribute to our understanding of acclimation in subzero brines. Cryopeg communities must have been energetically efficient to reach the high cell densities observed today. A sea-ice bacterium shows evidence of osmotic stress memory. DNA methylation is used by many sea-ice bacteria to regulate gene expression across environmental gradients. This body of work lays a foundation for a deeper understanding of memory in its ecological setting. The contrast between cryopeg and sea ice offers an

opportunity to understand how environmental variability shapes the deployment of memory: in stable cryopegs, long-term memory may become relevant as permafrost warms, while in sea ice fluctuating on the short term, rapid methylation-based regulation could be essential to responding to current environmental changes.

The implications of this work extend beyond Arctic microbiology to fundamental questions about habitability and the origins of life. By estimating the energetic requirements for bacteria to thrive in subzero hypersaline brines this dissertation helps define the environments we consider habitable. The cryopeg system serves as a terrestrial analog for ice-bound brines that may exist in the subsurface of Mars or within the icy shells of Europa and Enceladus. As DNA methylation is an ancient mechanism, its role in acclimation is relevant not only to modern extremophiles but also to the origins and early evolution of life on Earth.

As the Arctic transforms at an unprecedented pace, with sea-ice extent declining and permafrost thawing, the bacterial communities studied here face accelerating environmental change. Understanding memory in these communities is understanding their resilience or fragility. Sea-ice bacteria, already adapted to fluctuating conditions and equipped with dynamic methylation-based regulatory systems, may be better prepared for increased variability than cryopeg communities, which have experienced millennia of stability. The potential loss of cryopeg habitats represents not only the loss of unique microbial ecosystems but also the erasure of biological information encoded in their genomes and epigenomes, information that has persisted since the late Pleistocene. This work underscores the urgency of studying these systems before they disappear.

Future research could address several key questions that remain. Do cryopeg bacterial communities retain memory of the fluctuating conditions they experienced at formation, or has 40,000 years of isolation rendered such memory lost? This question could be addressed by exposing these microbial communities to a diverse set of variable conditions and probing their response for history-dependent behavior (Wolf et al., 2008). How do energetic constraints interact with memory? Perhaps the energetic cost of maintaining a form of memory defines a timespan after which the advantages of memory in responding to future stress are outweighed. What is the underlying mechanism of memory in 34H? How widespread is osmotic stress memory in the environment? By executing a longer running experiment with additional replicates using 34H and other marine bacteria, additional analyses investigating intracellular protein concentrations, small RNAs, and other epigenetic systems could be conducted to gain a mechanistic understanding of memory. Thereafter, a time-series study of sea ice over the course of seasons could target the identified memory mechanisms to more precisely ascertain the role of memory in the environment. The typically destructive nature of sea-ice sampling will require innovative sampling design and robust lab-based results.

This dissertation contributes to the growing body of evidence that bacterial memory and DNA methylation play significant ecological roles; it provides a framework of ecosystems in which to contrast memory's role in the face of multiple environmental stressors. My hope is that this work sparks curiosity about bacterial memory and serves as a foundation for further ecological investigations. At a time when drastic environmental change can be recorded by one's own memory, how will the bacteria use theirs to continue driving our planet's biogeochemical cycles?

APPENDIX A. SUPPLEMENTARY INFORMATION FOR MODELED ENERGETICS OF BACTERIAL COMMUNITIES IN ANCIENT SUBZERO BRINES

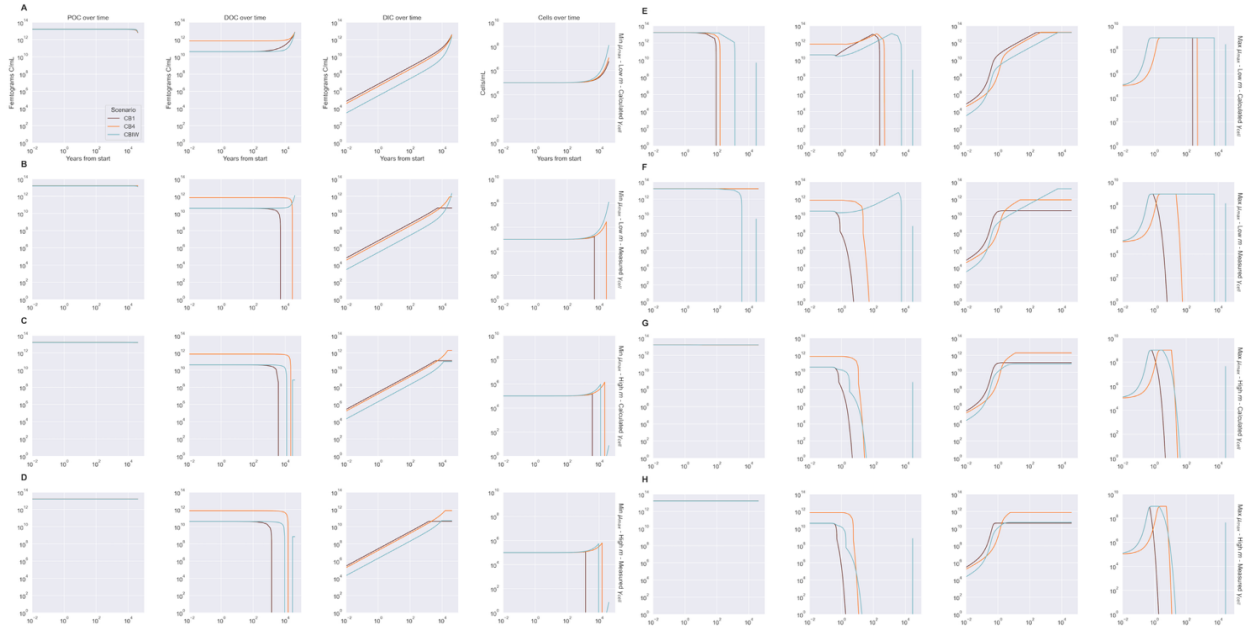

Figure A1. Model predictions of particulate (POC) and dissolved organic carbon (DOC), dissolved inorganic carbon (DIC), and cell density over the lifetime of the system for each cryopeg brine scenario (CB1, CB4, CBIW). Each row (A–H) depicts simulations based on a unique combination of conditions: minimum or maximum growth rate (μ_{max}), low or high cell-specific metabolic rate (m), and measured or calculated cell-specific extracellular enzyme activity (EEA) rate (α_{cell}). The resulting variations show the importance of EEA, which dictates the quantity of available DOC to the system. When EEA is high enough to allow the community to use all available POC, as in row E, the energetic demand posed by the fast-growing community depletes the available organic system in the system before simulation end. In other cases, such as in row G, significant quantities of POC remain due to an EEA bottleneck.

APPENDIX B. SUPPLEMENTARY INFORMATION FOR ACCLIMATION TO OSMOTIC STRESS AND POSSIBLE MEMORY MECHANISM IN *COLWELLIA PSYCHRERYTHRAEA* 34H

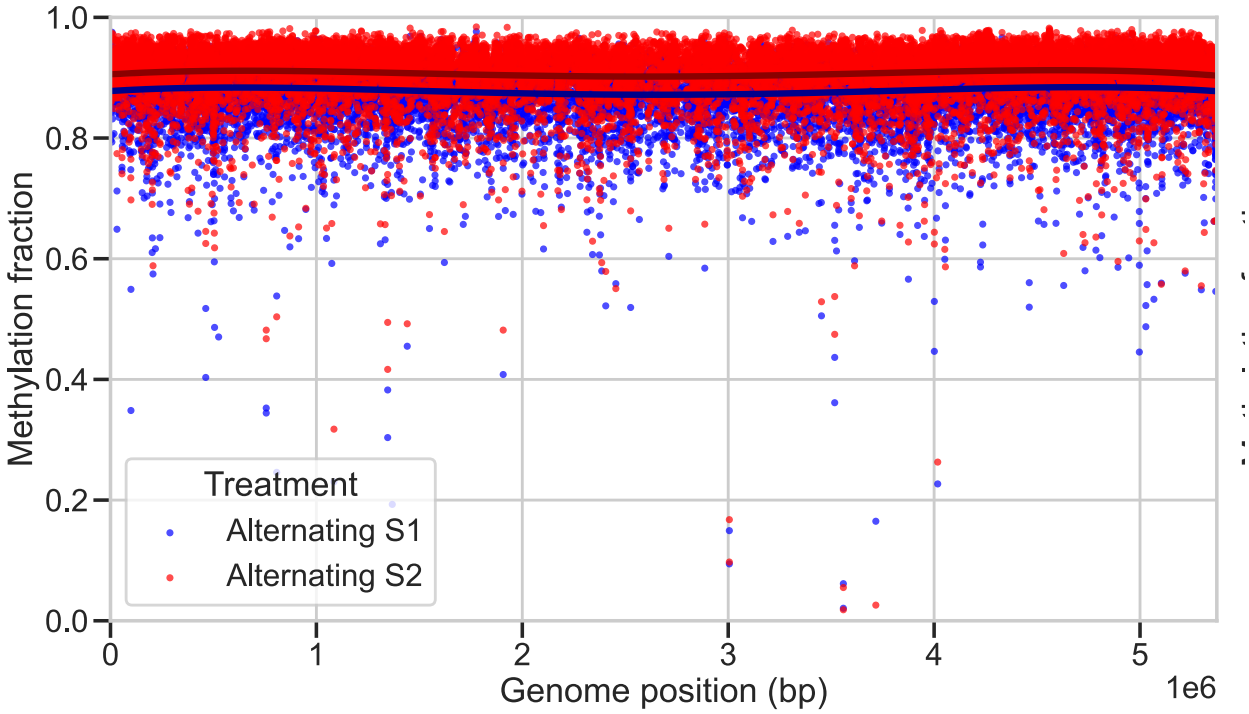

Figure B1. Example of whole genome methylation distributions in two treatments. Individual G**A**TC methylation fractions of promoters genome-wide are plotted against genomic position for two growth treatments: alternating steps 1 and 2 (S1, S2). The fractions from the two treatments are overlaid with a quadratic fit, revealing the flat trend in mean methylation fraction across the genome. The colors represent the salinity of the sample: blue for optimal salinity (33 ppt); red for stressful salinity (55 ppt).

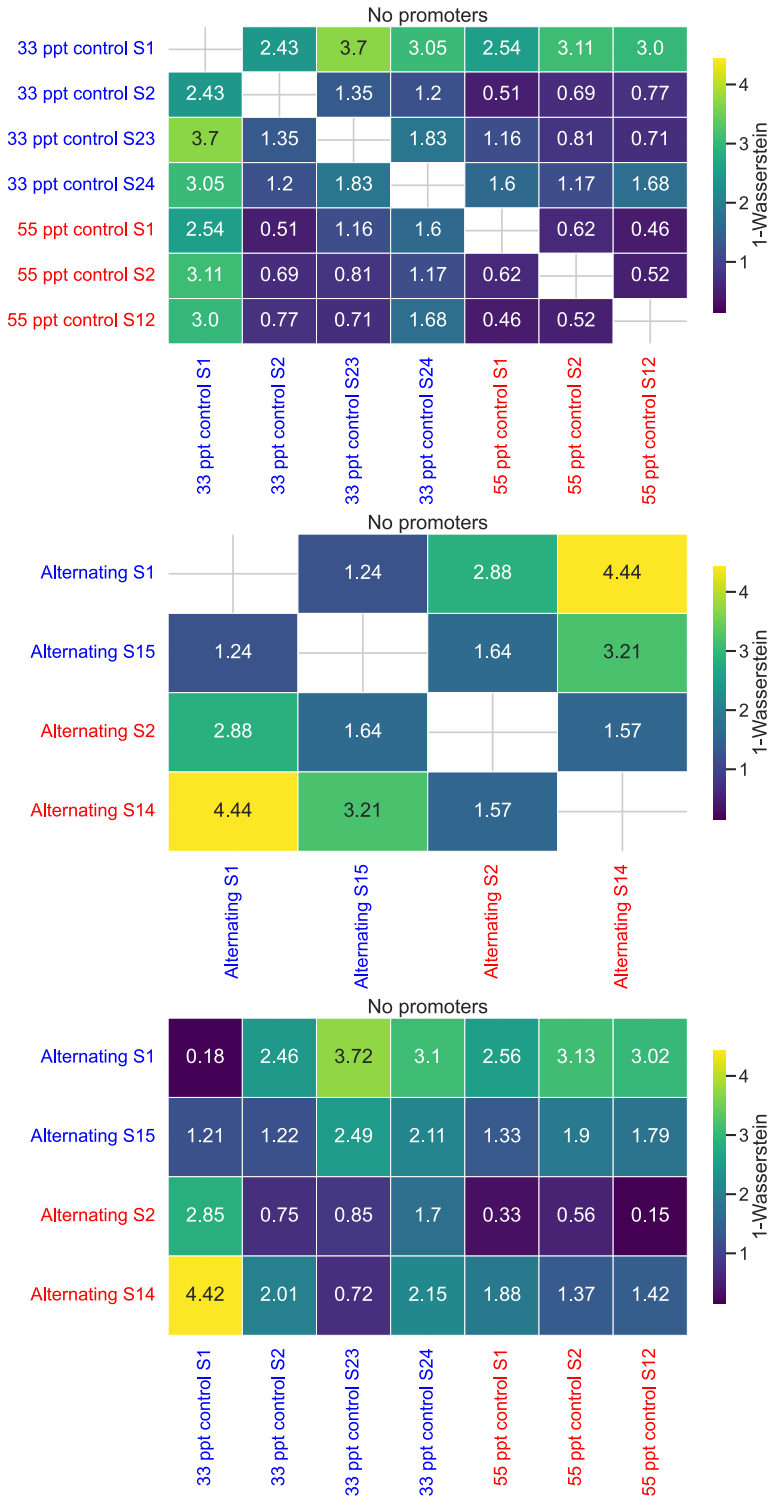

Figure B2. Wasserstein distance metrics for the methylome, excluding promoters, between treatments. Each heatmap shows the Wasserstein distance metric between the treatment on the Y and X axes. We considered motif instances outside promoters (60 bp upstream of a transcription start site). An X indicates no statistically significant difference. Blue font indicates a complete growth cycle (step, S) in optimal salinity (33 ppt); red font, in stressful salinity (55 ppt).

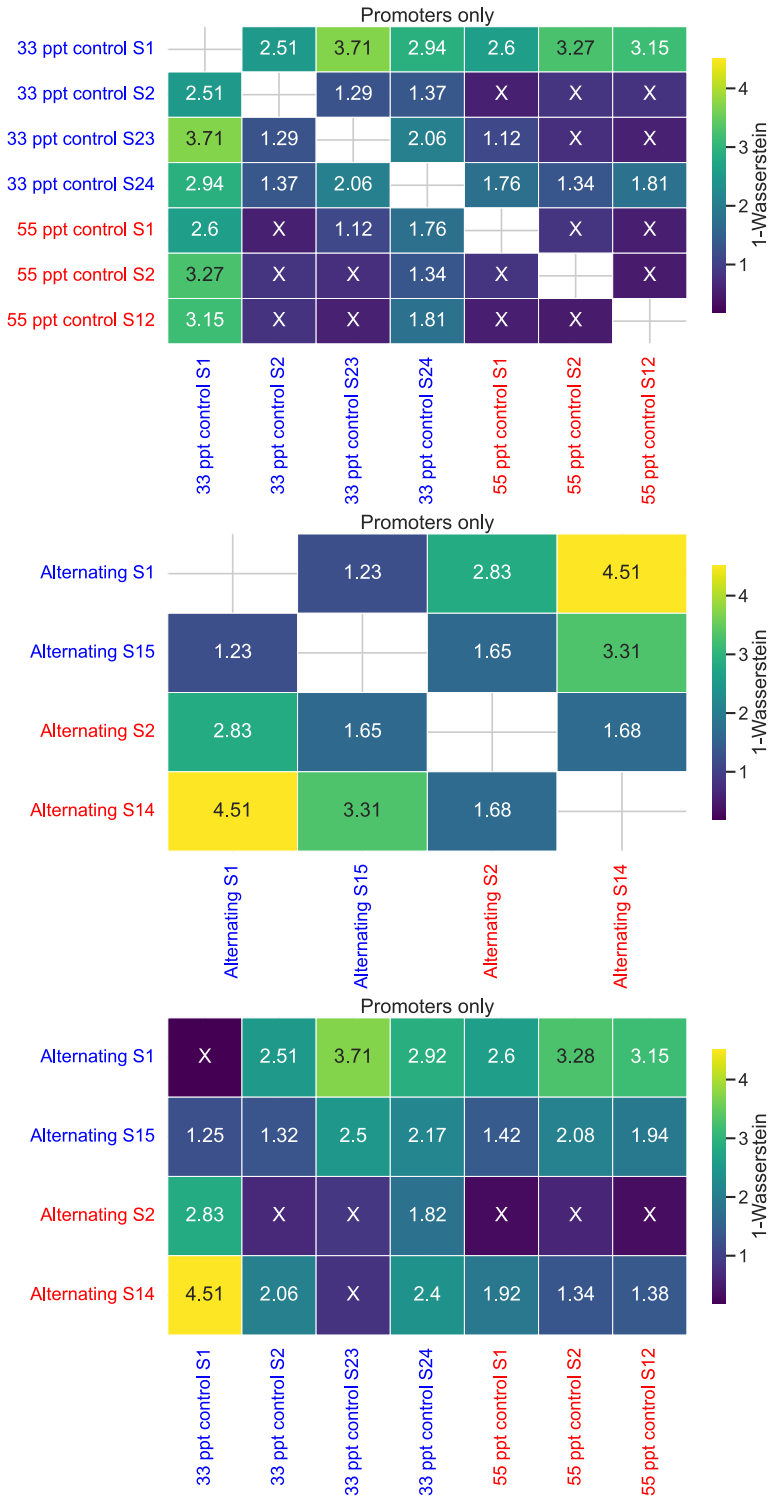

Figure B3. Wasserstein distance metrics for the promoter methylome between treatments. Each heatmap shows the Wasserstein distance metric between the treatment on the Y and X axes. We considered motif instances inside promoter (60 bp upstream of a transcription start site). An X indicates no statistically significant difference. Blue font indicates a complete growth cycle (step, S) in optimal salinity (33 ppt); red font, in stressful salinity (55 ppt).

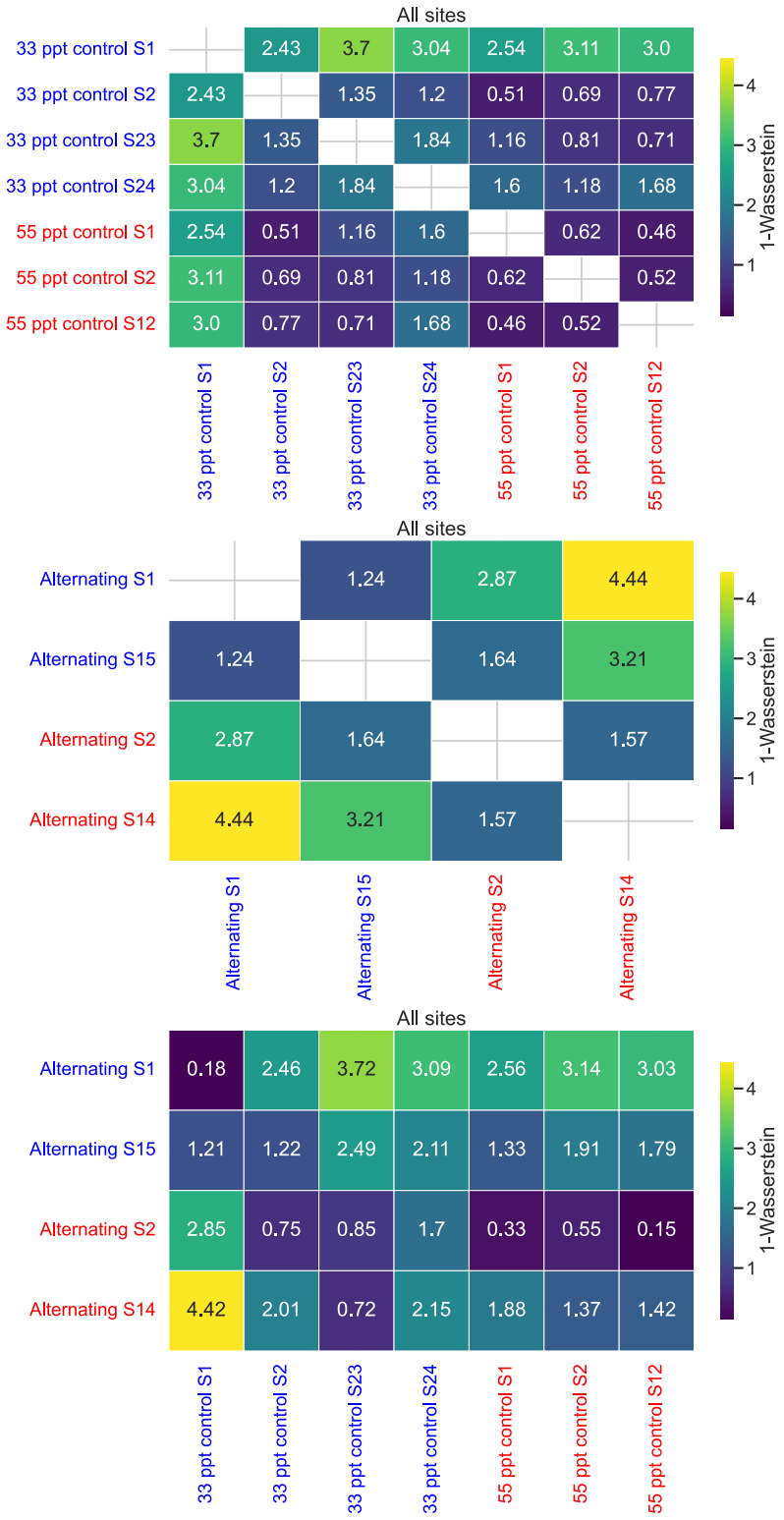

Figure B4. Wasserstein distance metrics for the entire methylome between treatments. Each heatmap shows the Wasserstein distance metric between the treatment on the Y and X axes. We considered all motif instances. An X indicates no statistically significant difference. Blue font indicates a complete growth cycle (step, S) in optimal salinity (33 ppt); red font, in stressful salinity (55 ppt).

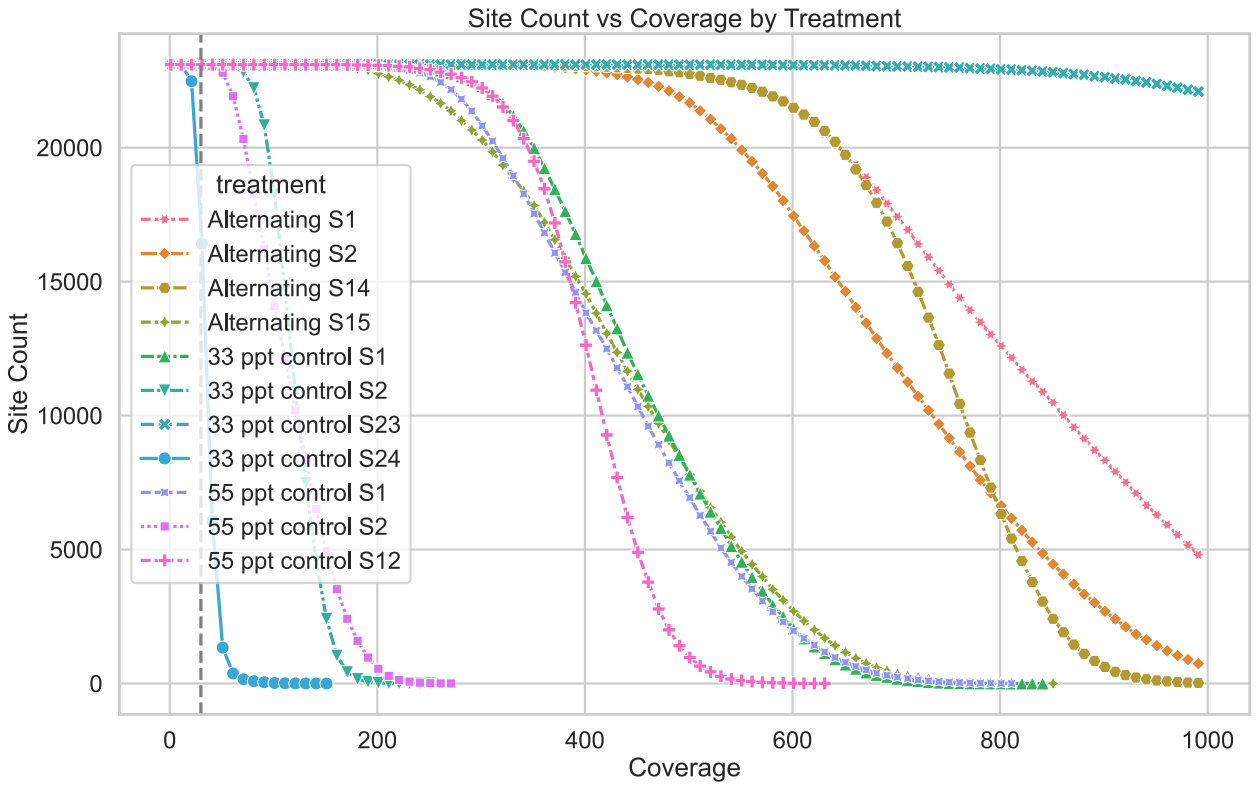

Figure B5. Coverage of methylation data in each sample. The number of motif instances with valid methylation data after all quality controls is on the Y-axis, and the coverage is on the X-axis. Differently colored and shaped lines indicate different samples. Replicate alternating treatments were pooled. The black vertical dashed line is the minimum coverage threshold (30), where only one sample drops off significantly below that threshold: 33 ppt control S24.

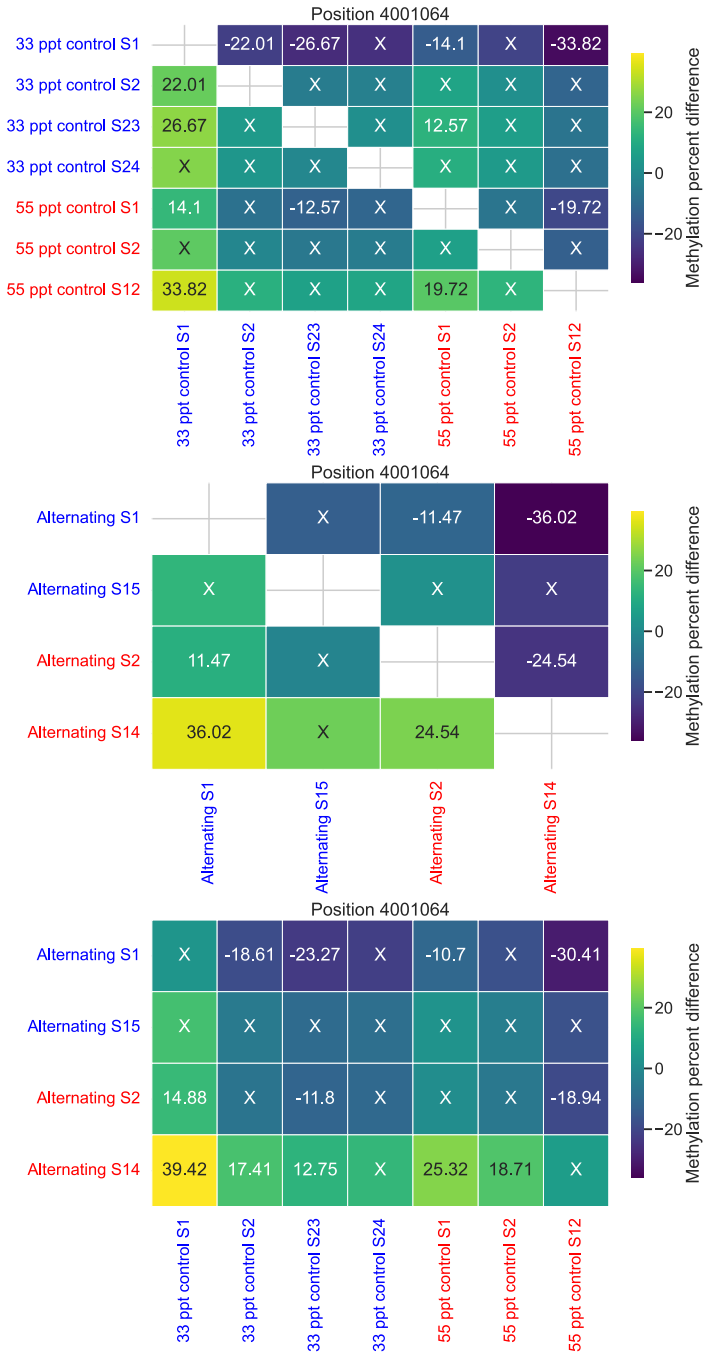

Figure B6. The variation of position 4,001,064 between treatments. This position inside the promoter of *GbsR*, a gene involved in compatible solute synthesis regulation, varied between 85% and 90%. Here the change between treatments is shown with an X designating no statistically significant difference according to the chi-squared test. The fraction shown is the difference between the fraction in the treatment on the Y axis and the treatment on the X axis. Thus, a negative value means more methylation in the treatment on the X axis. Blue font indicates a complete growth cycle (step, S) in optimal salinity (33 ppt); red font, in stressful salinity (55 ppt).

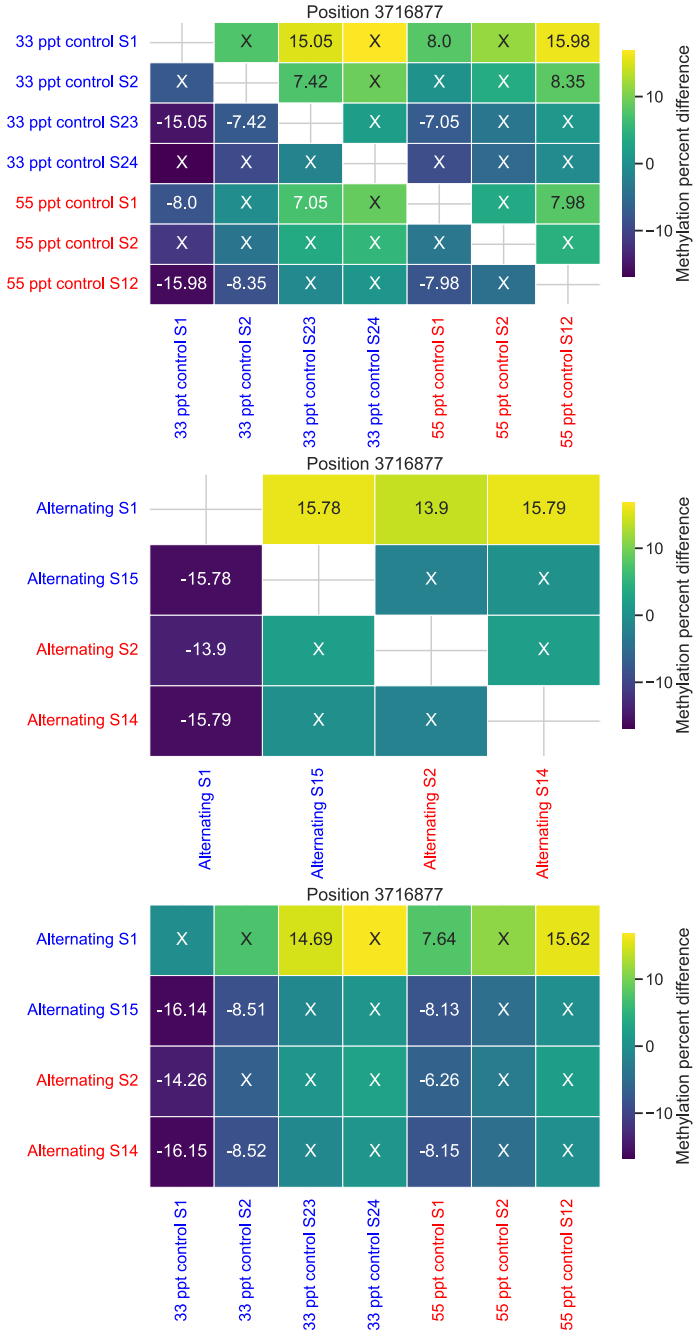

Figure B7. The variation of position 3,716,877 between treatments. This position 970 bp upstream of *CheC*, a gene involved in chemotaxis, was low in methylation in absolute terms (<20%). Here the change between treatments is shown with an X designating no statistically significant difference according to the chi-squared test. The fraction shown is the difference between the fraction in the treatment on the Y axis and the treatment on the X axis. Thus, a negative value means more methylation in the treatment on the X axis. Blue font indicates a complete growth cycle (step, S) in optimal salinity (33 ppt); red font, in stressful salinity (55 ppt).

APPENDIX C. SUPPLEMENTARY INFORMATION FOR MULTIPLE ROLES OF DNA METHYLATION IN SEA-ICE BACTERIAL COMMUNITIES AND ASSOCIATED VIRUSES

SAMPLING AND ENVIRONMENTAL HISTORY

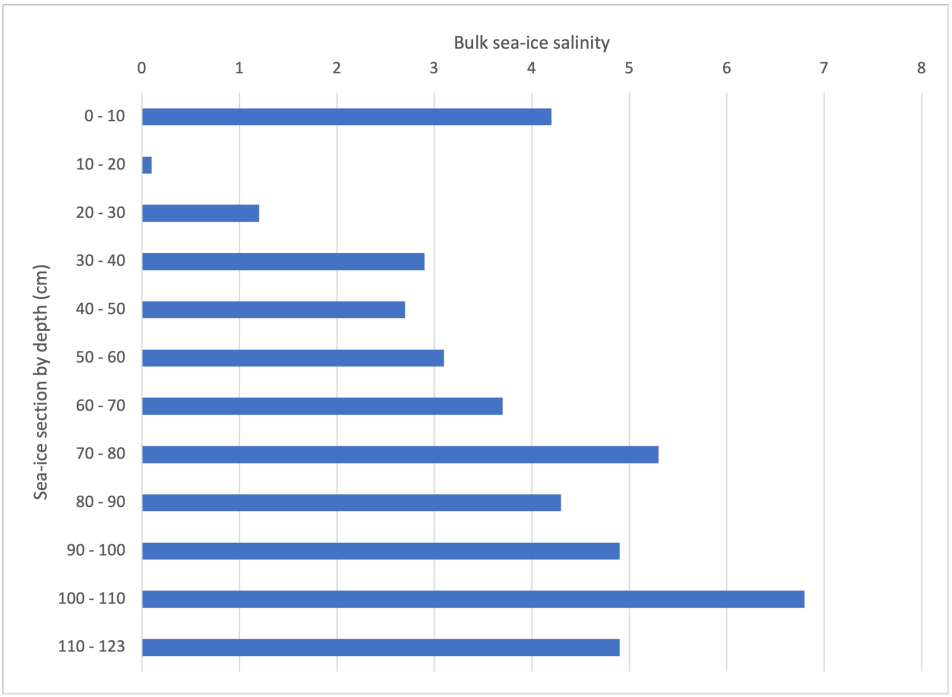

Figure C1. Bulk salinity of a sea-ice core taken near the sackhole sampling site. Bulk salinity was measured on 10 cm sea-ice sections, melted directly, and used to determine stepped-sackhole depths. A fresh (low salinity) section of ice at 10–20 cm is evidence of past melting, suggesting a thin patch of second year ice overlaying this predominantly first-year ice floe. No brine was possible to collect via drainage between 0 and 10 cm. Additional ice physical parameters can be found at https://doi.org/10.21334/NPOLAR.2025.44A880E0.

Table C1. Sackhole brine environmental parameters.

Sample[a]	Horizon (cm)[b]	Brine salinity	Volume filtered (mL)	Snow cover (cm)
S2-1	0–40	108	1750	11
S2-2	40–75	99	5550	11
S2-3	75–160	90	3510	11
S3-1	0–40	105	620	2
S3-2	40–70	99	3900	2
S3-3	70–158	90	3050	2
S4-1	0–40	96	150	5
S4-2	40–70	114	4770	5
S4-3	70–161	N/A	4650	5

[a]Sample notation is SX-Y, where X indicates a stepped sackhole, and Y indicates the step number; four stepped sackholes were sampled from the same sampling site, but processed samples from the first sackhole (S1) were compromised during transit to the home laboratory.

[b]0 cm is the top of the ice; total ice thickness was 209 cm.

Table C2. Ice-core environmental parameters and melt solution information.

Ice core	Sample[a]	Horizon (cm)[b]	Freeboard (cm)	Melt solution	
				Volume added (mL)	Salinity
3	IC3-1	0–30	18	1128	115.2–97.2
3	IC3-4	30–70	18	1003	108
3	IC3-2	70–160	18	2220	91.8
3	IC3-3	160–207	18	1347	103.8
4	IC3-1	0–30	17	1128	160.8–109.2
4	IC3-4	30–70	17	1003	104.4
4	IC3-2	70–160	17	2220	77.4
4	IC3-3	160–205	17	1347	89.4
5	IC3-1	0–30	16	1128	190.2–97.2
5	IC3-4	30–70	16	1003	109.8
5	IC3-2	70–160	16	2220	83.4
5	IC3-3	160–205	16	1347	117

[a]Sample notation is IC3-Y, where Y indicates the horizon number; three ice-core horizons were pooled (after being melted separately) to get sufficient biomass for DNA extraction.

[b]0 cm is the top of the ice; snow cover was 8 cm.

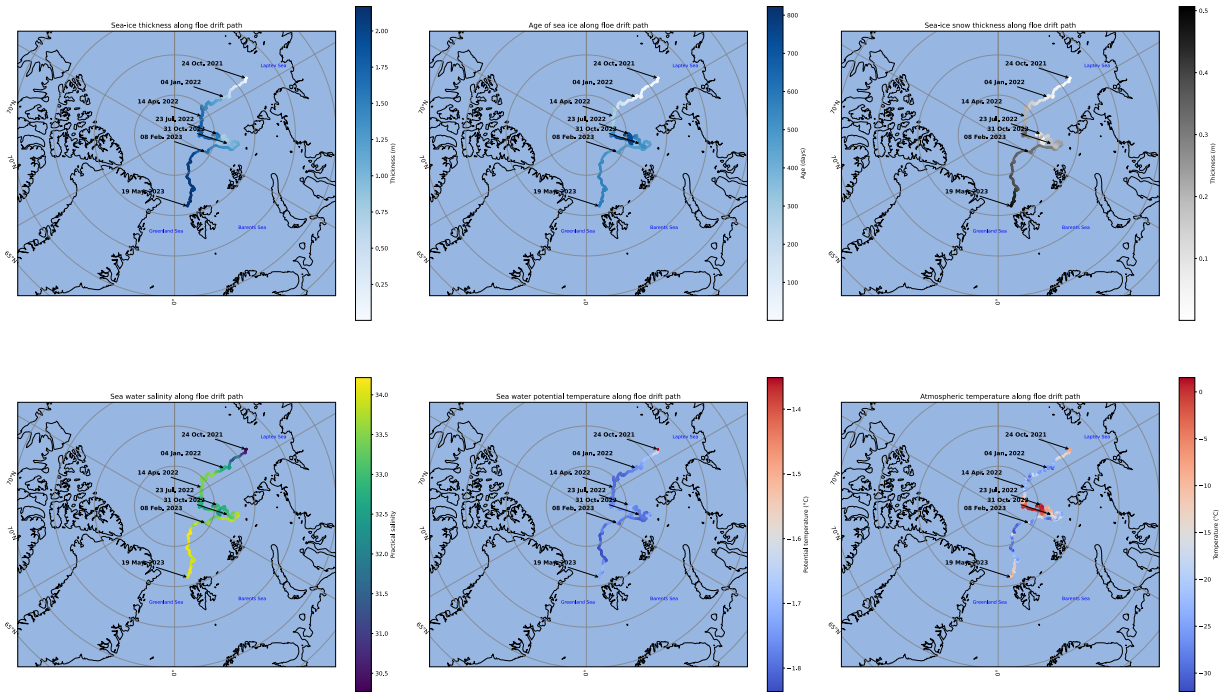

Figure C2. Environmental data along the floe drift track. Over the year preceding sampling, the floe had experienced changing environmental conditions: ice thickness (upper left), ice age (upper middle), snow thickness (upper right), seawater salinity (lower left), seawater temperature (lower middle), and atmospheric temperature (lower right). Hence the bacterial community encased in the top sea-ice horizon had been subjected to larger and more extreme variations in temperature and salinity than the community near the bottom of the ice where the temperature remains near the freezing point. Note the difference in colour-bar scales for seawater temperature and atmospheric temperature.

ASSEMBLY, METAGENOMICS AND BIN CURATION

- List of contaminants removed during read quality control, NCBI identifier: 7711, 90964, 1300, 1912216, 32207, 2093 32008, 544, 579, 547, 620, 590, 1330547, 158483, 34064, 1747, and the human genome GRCh38.

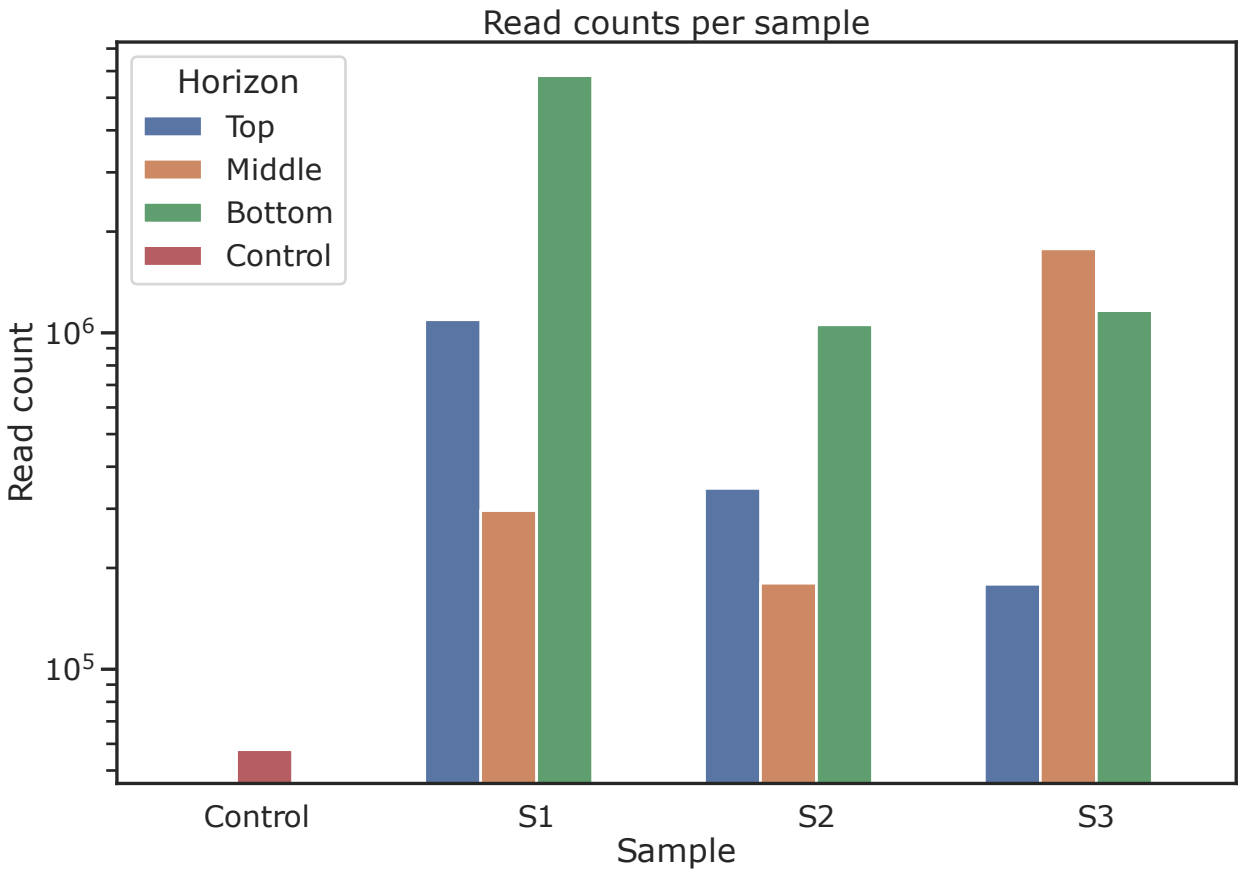

Figure C3. Read counts per sea-ice brine sample recovered from the three separate stepped sackholes (S1–S3). Coverage was uneven between different ice horizons (top, middle, bottom); processing control yielded a minimal read count.

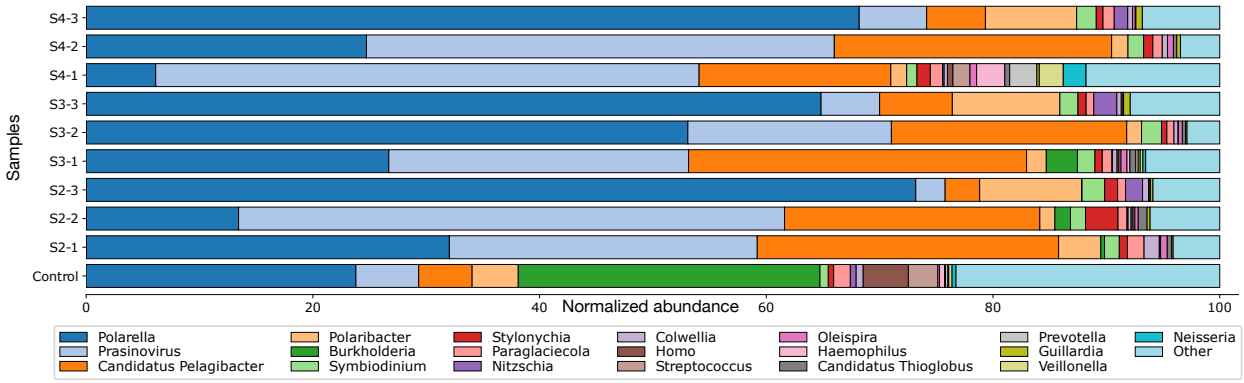

Figure C4. Community composition and normalized abundance in sea-ice brine samples as determined by MEGAN6-LR. Eukaryotes (e.g. *Polarella)* have an outsized role in community composition as our sampling strategy did not include size fractionation. *Pelagibacter* (dark orange) and *Polaribacter* (like orange) were the most abundant prokaryotes; Archaea were rare. Note that the total read count for the control was only a fraction of the sample counts (Figure C3).

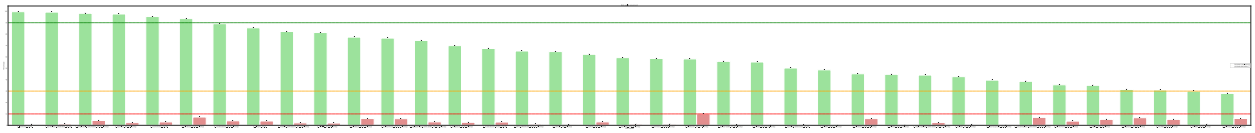

Figure C5. Completeness (%, green) and redundancy (%, red) of the 37 curated metagenome-assembled genomes. MAGs are identified on the x-axis. We recovered 6 MAGs with high quality completeness (≥ 90%). We did not include in our methylation analyses any MAG that was either less than 30% complete or more than 10% redundant, as determined by CheckM2.

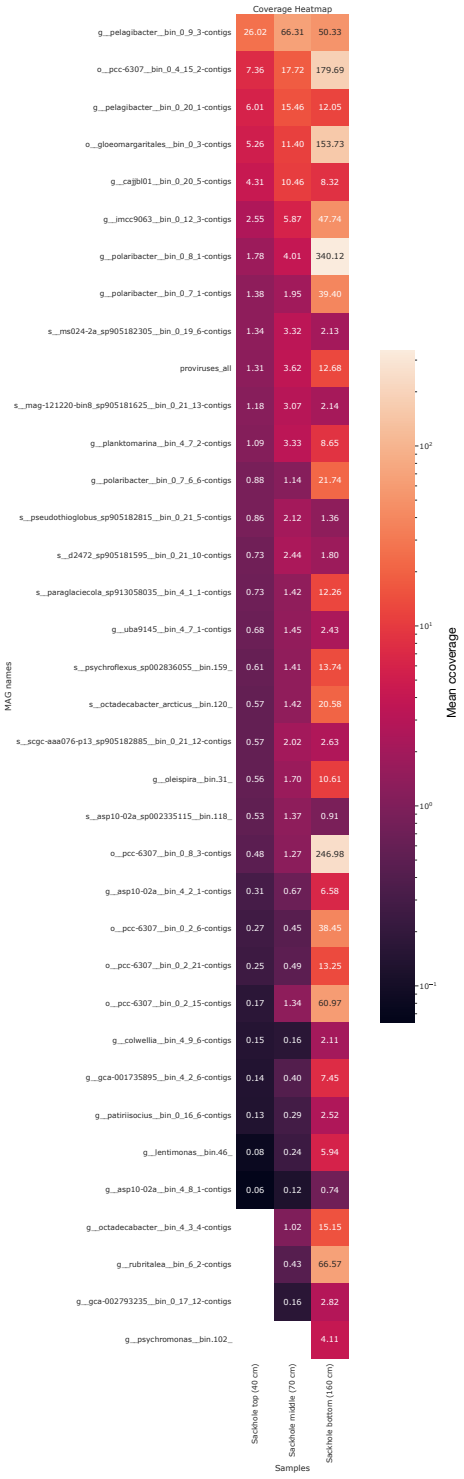

Figure C6. Coverage of the 37 curated metagenome-assembled genomes from the sackhole brine samples and the control sample. Note that only *Pelagibacter* (top row) had sufficient coverage in both top and bottom ice horizons for a cross-horizon comparison. MAGs with insufficient coverage in the brines were assembled thanks to the inclusion of ice-core reads in the co-assembly.

Table C3. Functions of genes with a GGATG motif within 70 bp of their start codon in the putative UISW 137 prophage. This putative prophage may impact the regulation of these genes due to the presence of the recognized motif within or near their promoter region, thus potentially down-regulating central metabolic functions.

Distance from gene start	KEGG annotation
0	putative tricarboxylic transport membrane protein
–10	DNA repair protein RecO (recombination protein O)
–10	branched-chain amino acid transport system ATP-binding protein
–14	F-type H+-transporting ATPase subunit delta
–15	tRNA-uridine 2-sulfurtransferase [EC:2.8.1.13]
–19	single-strand DNA-binding protein
–25	diaminopimelate epimerase [EC:5.1.1.7]
–25	multiple antibiotic resistance protein
–26	sarcosine oxidase, subunit gamma [EC:1.5.3.24 1.5.3.1]
–26	sarcosine oxidase, subunit gamma [EC:1.5.3.24 1.5.3.1]
–26	enoyl-[acyl-carrier protein] reductase I [EC:1.3.1.9 1.3.1.10]
–28	isocitrate dehydrogenase [EC:1.1.1.42]
–29	UDP-N-acetylmuramate--alanine ligase [EC:6.3.2.8]
–30	methylglutamate dehydrogenase subunit B [EC:1.5.99.5]
–30	sarcosine oxidase, subunit delta [EC:1.5.3.24 1.5.3.1]
–38	glyceraldehyde 3-phosphate dehydrogenase (phosphorylating) [EC:1.2.1.12]
–38	metalloendopeptidase OMA1, mitochondrial [EC:3.4.24.-]
–42	renalase [EC:1.6.3.5]
–44	ubiquinol-cytochrome c reductase cytochrome b subunit

–46	uncharacterized protein
–49	branched-chain amino acid transport system ATP-binding protein
–51	beta-alanine--pyruvate transaminase [EC:2.6.1.18]
–52	S-adenosylmethionine uptake transporter
–54	protoporphyrinogen IX oxidase [EC:1.3.99.-]
–55	O-antigen biosynthesis protein WbqP
–60	bile acid:Na+ symporter, BASS family
–61	acetylornithine deacetylase [EC:3.5.1.16]
–61	enoyl-CoA hydratase [EC:4.2.1.17]
–64	phosphoribosyl-ATP pyrophosphohydrolase [EC:3.6.1.31]
–67	biopolymer transport protein TolR
–67	maleate isomerase [EC:5.2.1.1]
–67	anti-sigma B factor antagonist
–68	uncharacterized protein
–70	Fe-S cluster assembly protein SufD

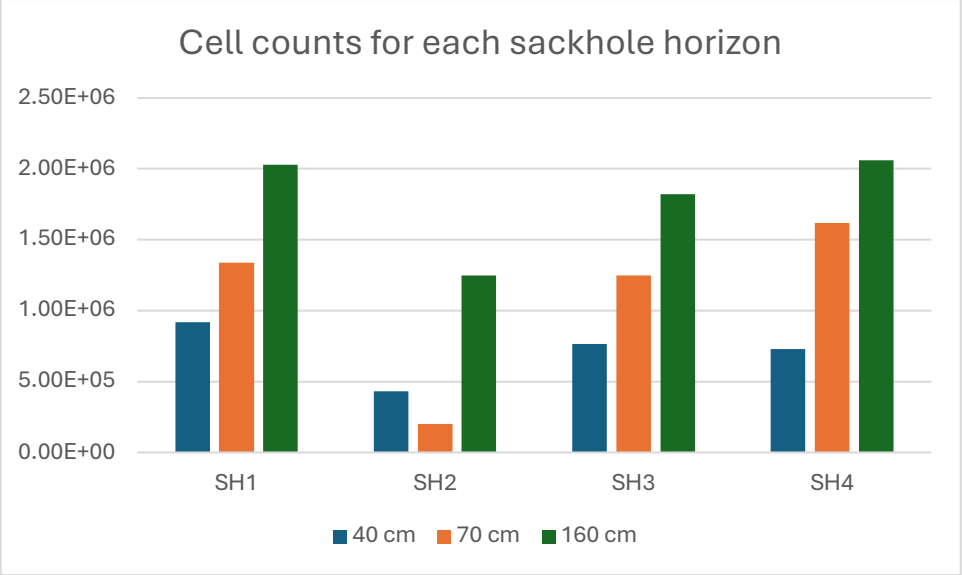

Figure C7. Cell counts from the sackhole samples. Epifluorescence cell counts by DAPI and acridine orange were taken for each horizon (in blue 0–40 cm; in orange 40–70 cm; in green 70–160 cm) from the stepped sackhole.

APPENDIX D. BRIEF REPORT ON THE EMULSIFICATION POTENTIAL OF EXTRACELLULAR COMPOUNDS FROM SELECTED ARCTIC BACTERIA

The research I outline below and the subsequent scientific impacts, were made possible by the Leo Maddox Foundation. This work was conducted with the help of Shelly Carpenter, and undergraduate students Aditya Sai and Jackson Page-Roth. This grant had the goal of honoring Leo's memory by funding projects that tackle ocean pollution. I proposed to investigate the capacity of psychrophilic Arctic bacteria to produce extracellular compounds capable of acting as emulsifiers. Emulsifiers allow water and oil to mix by modifying surface tension and binding to each molecule, acting as a "bridge" between oil and water (De et al., 2015). For that reason, emulsifiers are an important tool in treating marine oil spills. By adding an emulsifier to an oil spill, oil becomes mixed in the water and can then be degraded by marine bacteria already present in seawater. However, evidence suggests that commercial emulsifiers currently used for this purpose, such as Corexit, are toxic to the environment (Kleindienst et al., 2015). Thus, the goal of this project was to find a suitable non-toxic alternative produced by bacteria. The reason we focused on Arctic bacteria was to ensure that the resulting emulsifier we might find would work under Arctic conditions. The Arctic is a particularly vulnerable environment which, due to climate change, will see increased ship traffic and resource exploitation, raising the risk of an oil spill.

To test for emulsifiers produced by Arctic bacteria, we first grew a set of these microorganisms in the lab at 8°C, their typical optimal growth temperature for (Bonilla et al., 2005; Bowman et al., 1998; Huston, 2003). We selected promising strains from our culture collection based on their production rate of other extracellular products, particularly sugar-based compounds that they use for cryoprotection (Krembs et al., 2011; Marx et al., 2009). The bacteria were grown in their preferred medium, a liquid broth (Difco Marine Broth 2216, MB2216); we had to recover the candidate emulsifiers separately from the bacterial cells. To do so we centrifuged (30 min at 12000 x g) the broth culture and then filtered it (0.45 µm pore size), obtaining a cell-free supernatant. To test for emulsification, we then added 2 mL of this supernatant to 2 mL of kerosene (a "clean" lab proxy for crude oil), mixed them together using a vortex, and waited 24 hours for an emulsification layer to develop and stabilize at room temperature (Bonilla et al., 2005). After that time, we measured the height of the different layers to obtain a standard emulsification index, reported as the percentage of the total height of the sample occupied by the emulsification layer. At this point we had several strains that showed promising results (Figure D1). We then tested for emulsification of Prudhoe Bay crude oil using a similar assay in which concentrated supernatant was added to a solution containing artificial seawater and small amounts of crude oil (Venosa et al., 2002). We did not find any clear crude-oil emulsifiers among our candidate compounds, short-circuiting the possible pursuit of the effects of such compounds on disaggregating microplastics. However, we did observe an unanticipated and intriguing effect.

When certain supernatants were frozen for storage, they showed stronger signals of kerosene emulsification after being frozen than they had prior to freezing. We hypothesize that freezing (as when sea ice forms) modifies the structure of these compounds, enhancing their emulsifier traits. We froze supernatants obtained from these organisms at –20°C and –60°C for a period of 4 weeks, testing the kerosene emulsification potential at 1-week intervals. The results suggest that *Colwellia demingiae* strain ACAM459 may produce compounds with emulsification traits that increase after prolonged freezing, though further work is needed to confirm this hypothesis, understand the underlying mechanism, and rule out an effect of the medium (Figures D2–D5).

We also tested the supernatants of a variety of algal cultures obtained from Dr. Jodi Young's lab. An axenic *Fragilariopsis cylindrus* strain produced the highest kerosene emulsification index at 45%. See bacterial indices in Figure D1 for comparative purposes.

REFERENCES

Bonilla, M., Olivaro, C., Corona, M., Vazquez, A., & Soubes, M. (2005). Production and characterization of a new bioemulsifier from *Pseudomonas putida* ML2. *Journal of Applied Microbiology*, *98*(2), 456–463. https://doi.org/10.1111/j.1365-2672.2004.02480.x

Bowman, J. P., GOSINK, J. J., McCAMMON, S. A., LEWIS, T. E., NICHOLS, D. S., NICHOLS, P. D., SKERRATT, J. H., STALEY, J. T., & McMeekin, T. A. (1998). *Colwellia demingiae* sp. nov., *Colwellia hornerae* sp. nov., *Colwellia rossensis* sp. nov. and *Colwellia psychrotropica* sp. nov.: psychrophilic Antarctic species with the ability to synthesize docosahexaenoic acid (22:ω63). *International Journal of Systematic and Evolutionary Microbiology*, *48*(4), 1171–1180. https://doi.org/10.1099/00207713-48-4-1171

Cooper, Z. S., Rapp, J. Z., Shoemaker, A. M. D., Anderson, R. E., Zhong, Z.-P., & Deming, J. W. (2022). Evolutionary divergence of *Marinobacter* strains in cryopeg brines as revealed by pangenomics. *Frontiers in Microbiology*, *13*, 879116. https://doi.org/10.3389/fmicb.2022.879116

De, S., Malik, S., Ghosh, A., Saha, R., & Saha, B. (2015). A review on natural surfactants. *RSC Advances*, *5*(81), 65757–65767. https://doi.org/10.1039/c5ra11101c

Huston, A. L. (2003). Bacterial adaptation to the cold: in situ activities of extracellular enzymes in the North Water Polynya and characterization of a cold-active aminopeptidase from *Colwellia psychrerythraea* strain 34H. *University of Washington*.

Kleindienst, S., Seidel, M., Ziervogel, K., Grim, S., Loftis, K., Harrison, S., Malkin, S. Y., Perkins, M. J., Field, J., Sogin, M. L., Dittmar, T., Passow, U., Medeiros, P. M., & Joye, S. B. (2015). Chemical dispersants can suppress the activity of natural oil-degrading microorganisms. *Proceedings of the National Academy of Sciences*, *112*(48), 14900–14905. https://doi.org/10.1073/pnas.1507380112

Krembs, C., Eicken, H., & Deming, J. W. (2011). Exopolymer alteration of physical properties of sea ice and implications for ice habitability and biogeochemistry in a warmer Arctic. *Proceedings of the National Academy of Sciences*, *108*(9), 3653–3658. https://doi.org/10.1073/pnas.1100701108

Marx, J. G., Carpenter, S. D., & Deming, J. W. (2009). Production of cryoprotectant extracellular polysaccharide substances (EPS) by the marine psychrophilic bacterium *Colwellia psychrerythraea* strain 34H under extreme conditions. *Canadian Journal of Microbiology*, *55*(1), 63–72. https://doi.org/10.1139/w08-130

Venosa, A. D., King, D. W., & Sorial, G. A. (2002). The baffled flask test for dispersant effectiveness: a round robin evaluation of reproducibility and repeatability. *Spill Science & Technology Bulletin*, *7*(5–6), 299–308. https://doi.org/10.1016/s1353-2561(02)00072-5

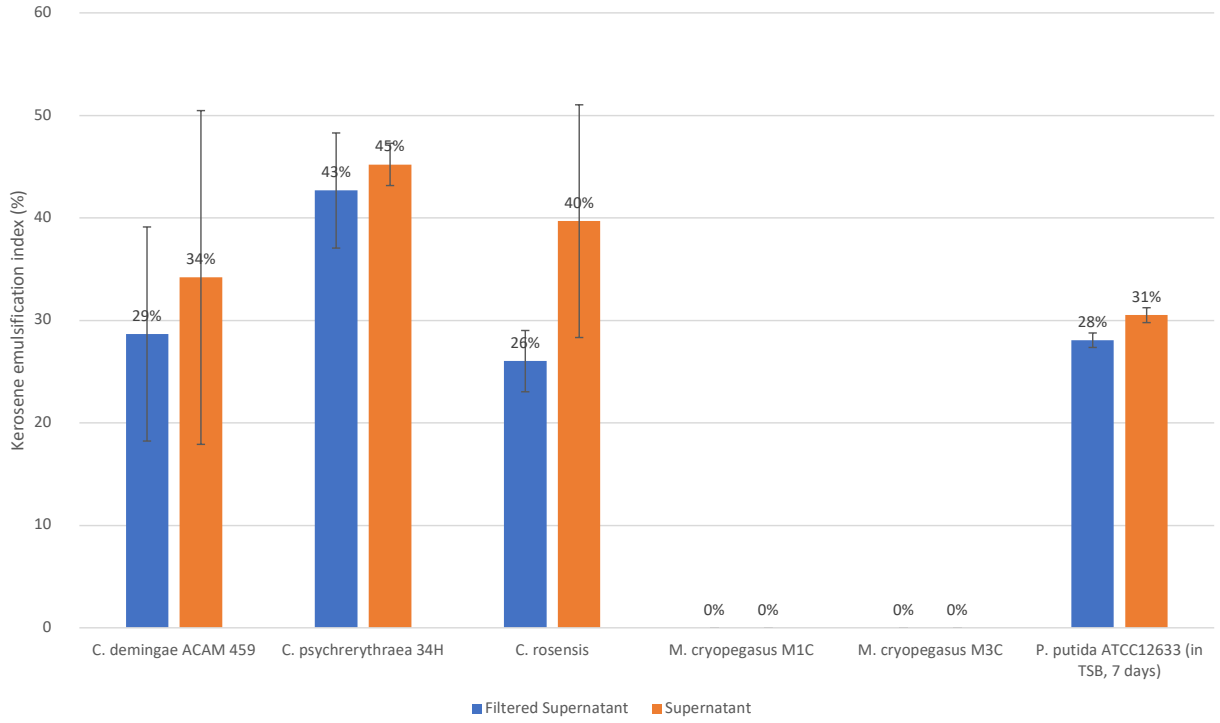

Figure D1. Mean kerosene emulsification index of selected psychrophiles. The kerosene emulsification index of filtered (0.45 µm) and unfiltered supernatant from 30-day-old cultures of five psychrophiles is shown here: three *Colwellia* species (*demingiae, psychrerythraea,* and *rossensis*), and two *Marinobacter cryopegasus* strains (M1C and M3C; Cooper et al., 2022). *Pseudomonas putida* was selected as a control bacterium, as it is known to produce kerosene emulsifiers. The psychrophiles were grown in Marine Broth 2216 at 8°C, whereas *P. putida* was grown in its ATCC-recommended medium at room temperature. Kerosene emulsification index was measured 24 h after mixing to assess long-term emulsification potential. Error bars indicate standard deviation, n = 3.

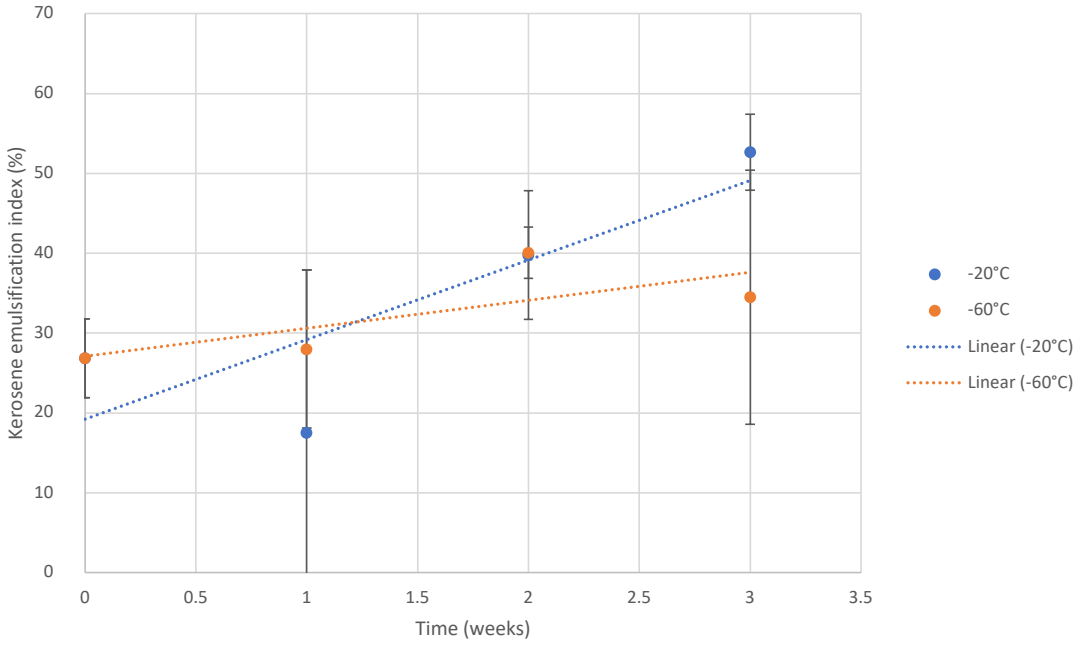

Figure D2. Mean kerosene emulsification index after 24 h for supernatant from *Colwellia demingiae* strain ACAM459 frozen for different periods of time (weeks). Dotted lines are linear regressions for incubations at –20°C (blue) and –60°C (orange). Error bars indicate standard deviation, n = 3.

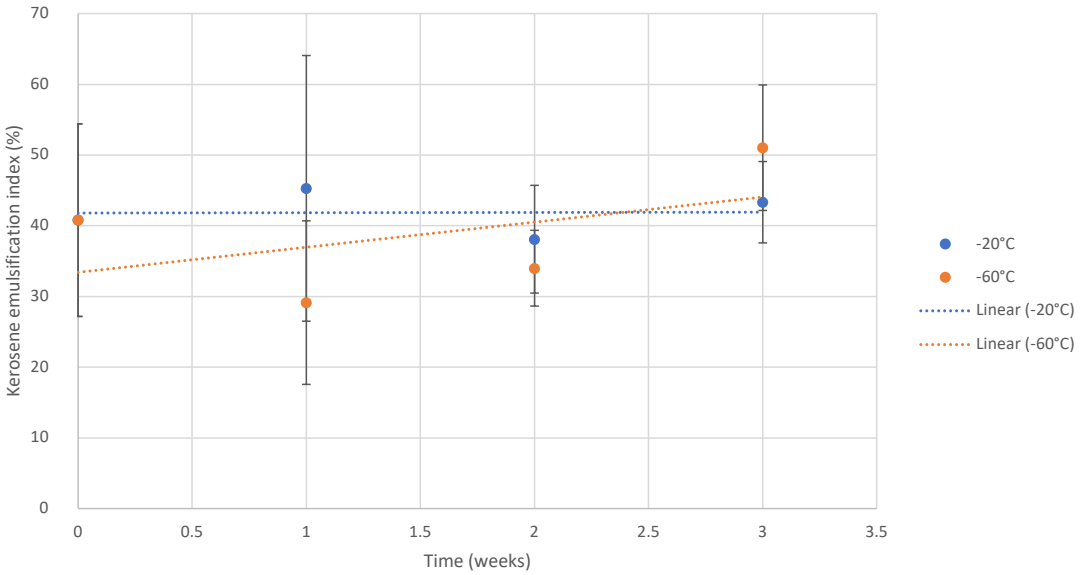

Figure D3. Mean kerosene emulsification index after 24 h for supernatant from *Colwellia psychrerythraea* strain 34H frozen for different periods of time (weeks). Dotted lines are linear regressions for incubations at –20°C (blue) and –60°C (orange). Error bars indicate standard deviation, n = 3.

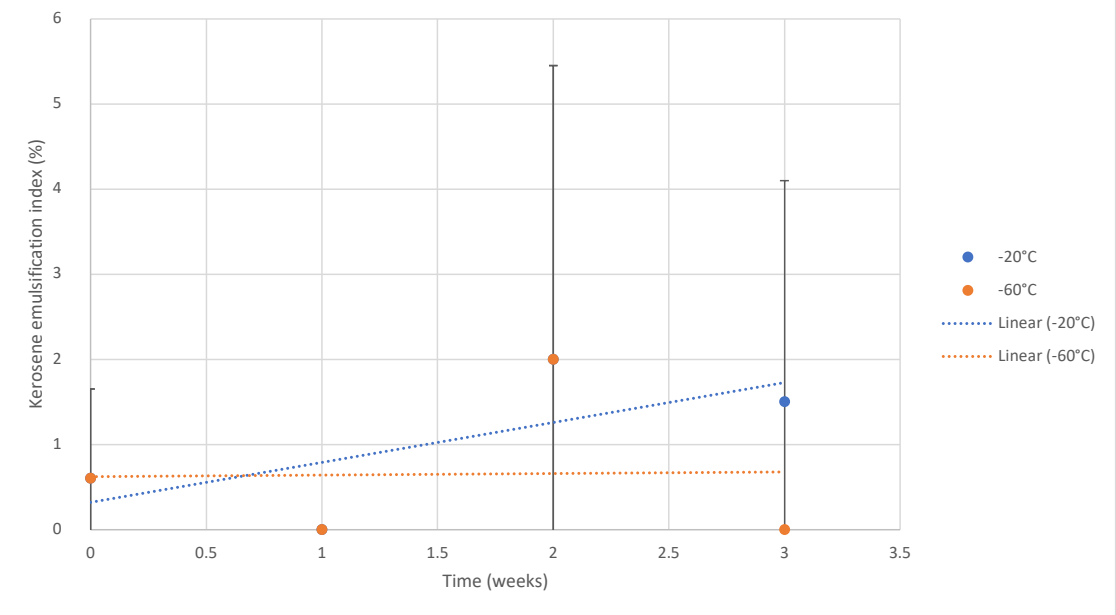

Figure D4. Mean kerosene emulsification index after 24 h for supernatants from *Pseudomonas putida* strain ATCC12633 frozen for different periods of time (weeks). Dotted lines are linear regressions for incubations at –20°C (blue) and –60°C (orange). Error bars indicate standard deviation, n = 3.

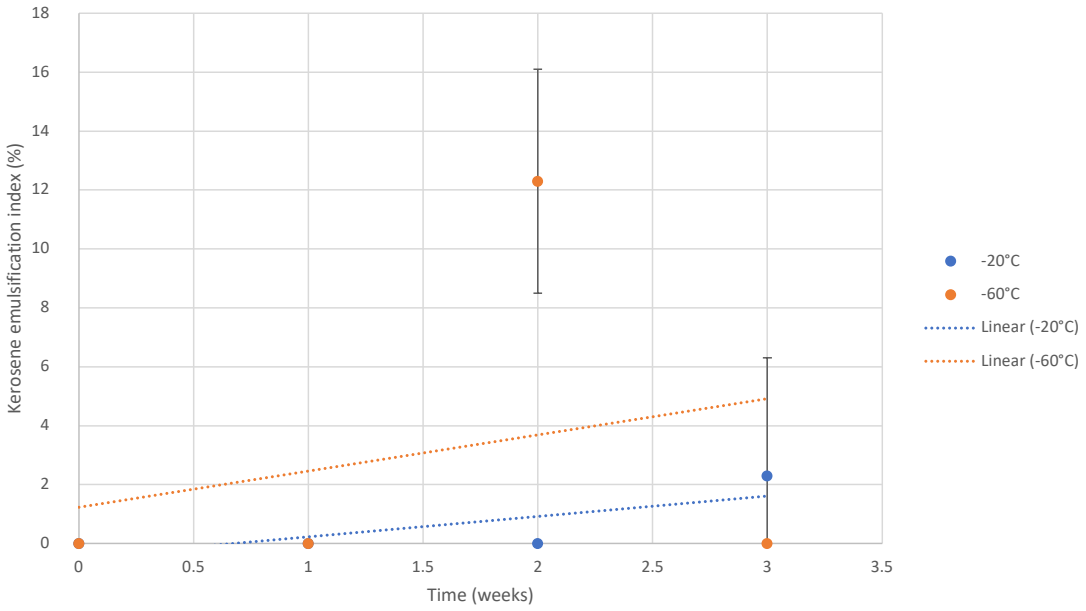

Figure D5. Kerosene emulsification index after 24 h of frozen TSB (media blank of *Pseudomonas* putida) over time. Dotted lines are linear regressions for incubations at –20°C (blue) and –60°C (orange). Error bars indicate standard deviation, n = 3.

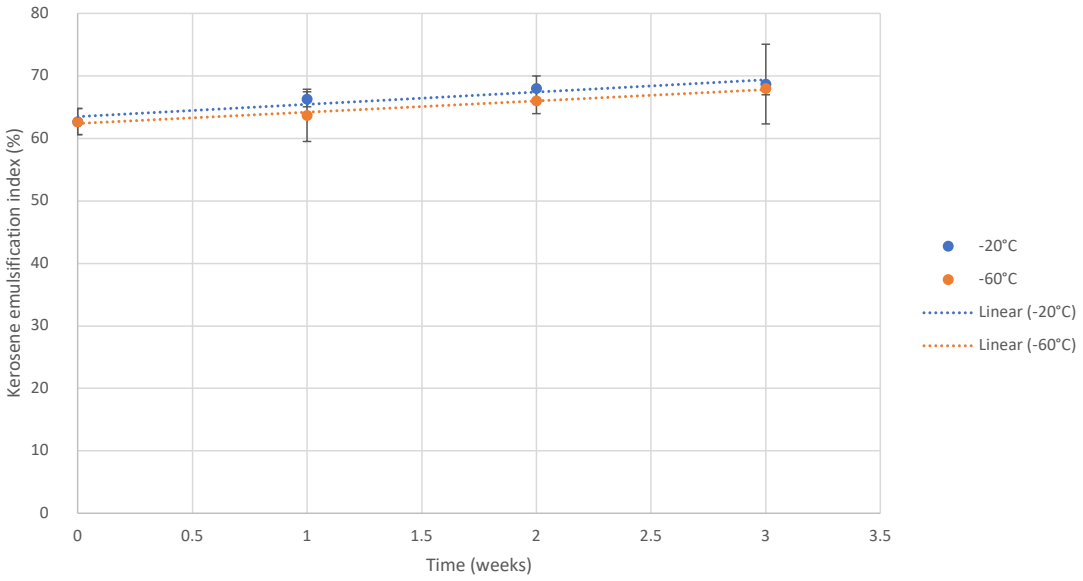

Figure D6. Mean kerosene emulsification index after 24 h for Triton-X 100 frozen for different periods of time (weeks), as controls. Dotted lines are linear regressions for incubations at –20°C (blue) and –60°C (orange). Error bars indicate standard deviation, n = 3.

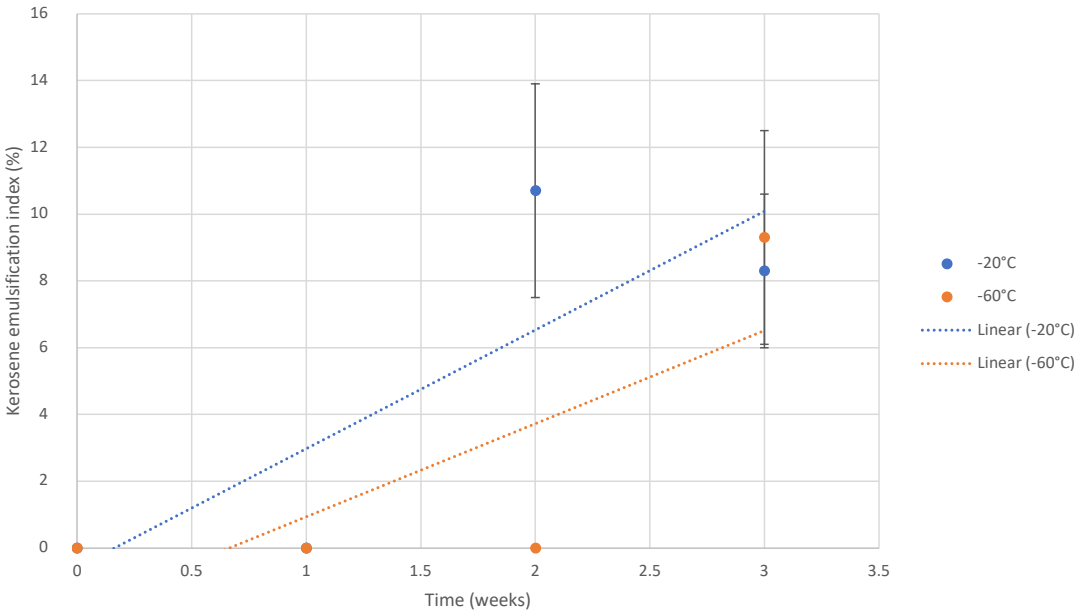

Figure D7. Mean kerosene emulsification index after 24 h for media blanks (Marine Broth 2216) frozen for different periods of time (weeks), as controls. Note that at some timepoints, vials broke despite sufficient headroom, leading to lack of replication. Error bars indicate standard deviation, n = 3.

Georges Kanaan

georges@gkanaan.com • https://gkanaan.com • Ge0rges
0000-0002-5721-1138

Education

University of Washington **Seattle, USA**
Dual-title PhD in Oceanography & Astrobiology *Dec 2025*
Energetics, epigenetics, and memory as acclimation strategies of marine bacteria in subzero brines.
Supervised by Dr. Jody Deming.

University of Washington **Seattle, USA**
Master of Oceanography *Feb 2023*
Focus in Biological Oceanography. Supervised by Dr. Jody Deming. Co-advised by Dr. Jodi Young.

University of Toronto **Toronto, CA**
Honours Bachelor of Computer & Cognitive Science *Jun 2021*
Triple-major equivalent with a double major in Computer Science. Completed courses in AI, NLP, CS Theory, Game Design, and Philosophy among others.

International College **Beirut, LB**
French Baccalaureate *Jun 2017*
Graduated with distinction. Science track with a focus in Biology.

Employment

École Normale Supérieure, University of Tromsø, Campbell & Bowler Lab **Paris, FR**
Post-doc *Expected Feb 2026*
- Expected to begin a post-doctoral position in February 2026 with Dr. Karley Campbell and Dr. Chris Bowler at the biological institute of the École Normale Supérieure in Paris and the University of Tromsø.

University of Washington, School of Oceanography **Seattle, USA**
Teaching Assistant, Ocean Sensors *Jan–Mar 2025*
- Supervised 36 hours of practical lab time where students built sensors from the ground up, including programming microcontrollers, assembling breadboard circuits, calibration, and data collection and analysis.
- Graded a class of 40 students on topics related to ocean sensors, their function and engineering, and their usefulness in ocean monitoring.

University of Washington, School of Oceanography **Seattle, USA**
Teaching Assistant, Hydrothermal Vents *Jan–Mar 2024*
- Graded a class of 77 students on topics related to hydrothermal vents, including their function in the ocean, underlying mechanisms, history, and discovery.

University of Washington, School of Oceanography **Seattle, USA**
Undergraduate Mentorship *Apr 2023–Apr 2025*
- Mentored several undergraduate students. Teaching and mentoring on sterile technique, bacterial culturing, epifluorescence microscopy, DNA extractions, spectrophotometric measurements, experimental design and planning, project management and academic orientation.
- One undergraduate student completed his senior thesis as part of my mentoring efforts with Dr. Jody Deming and was subsequently accepted into a doctoral program.
- Taught field sampling techniques as well as DNA extractions and epifluorescence microscopy, to an undergraduate student.

University of Washington **Seattle, USA**
Teaching Assistant, Marine Pollution *Apr–Jun 2022*
- Responsible for grading a class of 50 students on a wide range of marine pollution topics such as plastics, noise, light, etc.
- Guest lecturer on ocean acidification and guided an in-class paper discussion.

NASA Johnson Space Center **Houston, USA**
Extravehicular activity (EVA) Software Intern *Jun–Aug 2020*
- Cancelled due to COVID-19.
- Accepted to work on EVA informatics, specifically on EVA Operations System, a suite of decision support tools and capabilities for the creation, distribution, and utilization of operationally relevant EVA workflows and data for spacewalks.

NASA Goddard Space Flight Center **Greenbelt, USA**
Networking Intern *Jun–Aug 2019*
- Procured hardware for network emulation testing within a constrained budget.
- Developed and tested an emulation of a space network both at the hardware and software level to study the implementation of Delay/Disruption Tolerant Network (DTN) protocols, such as the Bundle Protocol.
- Developed a specialized network management tool that allows for monitoring DTNs, furthering NASA's goal to be a reliable space network provider. This tool was tested on the purpose-built DTN emulation hardware.
- Led the development of the network management tool. Including network overview, asynchronous management protocol interface, and visualizations for critical AMP data points. Resulted in an academic poster.

Anghami **Beirut, LB**
iOS Developer Intern *Jun–Aug 2017*
- Independently integrated the music syncing protocol from Airly, an app I developed, as a revenue generating feature for the service.
- Contributed to ongoing development of the mobile app in collaboration with the iOS engineering team.

PricewaterhouseCoopers **London, UK**
Cyber Security Intern *Jul 2016*
- Contributed to writing client side technical specifications which were used in key decision-making discussions.
- Attended company workshops pertaining to their cyber security consulting division, furthering my skills in that area.
- Shadowed professional pen testers for a day, immersing myself in a professional cybersecurity environment.

Saily **Beirut, LB**
iOS Developer Intern *May–Jul 2015*
- Assumed responsibility for design, implementation and testing of critical parts of the Saily App in a small team.
- Independently built the Saily Apple Watch app from the ground up.

961 Beer **Beirut, LB**
Contracted iOS Developer *Nov 2014–May 2015*
- Contracted to develop and manage an iOS app to locate storefronts selling the company's product.
- Responsible for design, implementation, maintenance and release of the app.
- Implemented network features to ensure constant availability of the database in the app.

FOO_ **Beirut, LB**
iOS Developer Intern *Jun–Jul 2014*
- Contributed to the development of ongoing projects for clients making use of various custom APIs.
- Built an in-house crash-reporting tool using custom APIs to transfer the crash logs to the company's database.
- Researched facial recognition technology demonstrating the OpenCV framework with the capability of recognizing facial features such as left eye, glasses, eyebrows.

Research Projects

Collaboration with Dr. Eric Pelletier **Génoscope**
Sea-ice Methods Optimization *Dec 2024–Ongoing*
- Helped design method benchmarks for ice-melting methods for use aboard Tara Polar Station.
- Currently optimizing DNA extraction methods for sea-ice samples.
- Currently optimizing sea-ice sampling protocols for genomics for use aboard the Tara Polar Station.

Collaboration with Dr. Marc Neveu **NASA**
Ice Plume Organics *Apr 2024–Ongoing*
- Part of an astrobiology research rotation at Goddard Space Flight Center.
- Cultured a model sea-ice bacterium and obtained extracellular polysaccharides from it.
- Injected the extracellular polysaccharides into a vacuum simulating Enceladus plume conditions.
- Assessed effect of vacuum on polysaccharide structure and detectability within the context of the search for life.

Collaboration with Dr. Ardith Bravenec, Caitling lab — **University of Washington**
Freezing Kinetics — *Jun 2023–Ongoing*
- Assessment of the effect of extracellular polysaccharides on freezing kinetics of water ice.
- Cultured and tested different model psychrophilic bacteria.
- Identified impact on rates and thresholds of vitrification and freezing based on the presence of extracellular polysaccharides using a differential scanning calorimeter.

Dissertation chapters with Dr. Jody W. Deming — **University of Washington**
DNA Methylation in Psychrophiles — *Feb 2023–Dec 2025*
- Planned and executed a sea-ice field campaign to collect sackhole brines from different sea-ice horizons.
- Developed a novel stepped-sackhole approach for brine collection from distinct sea-ice horizons.
- Sequenced environmental samples using Nanopore to obtain DNA methylation data.
- Designed an experiment to understand DNA methylation's role in a model sea-ice bacterium's stress response.
- Established a chemostat and growth system with continuous optical density and temperature measurements.

Dissertation chapter with Dr. Jody W. Deming and Dr. Jodi Young — **University of Washington**
Bacterial Energetics — *Sep 2022–Feb 2023*
- Developed a model to understand the required energetic input to support the bacterial community in subzero brine.
- Conducted a sensitivity analysis of the different inputs to characterize the accuracy of the model output.
- Manuscript published in a special volume of Frontiers in Microbiology 2023.
- Abstract accepted for a poster presented at Microenergy 2022.
- Participated in a workshop to co-author a synthesis paper on the larger cryopeg research project.

Collaboration with Dr. Laura Moore, Bundy Lab — **University of Washington**
Sea-ice Siderophores — *Feb 2022–Ongoing*
- Quantification and identification of siderophores produced by a model sea-ice bacterium.
- Assessment of the role siderophores play in iron cycling in the Arctic and within sea-ice.

Research with Dr. Jody W. Deming — **University of Washington**
Arctic Oil Bioremediation — *Sep 2021–Jan 2023*
- Proposed and received a grant to investigate novel bioemulsifiers produced by arctic sea-ice bacteria.
- Developed a plan to characterize the commercial viability of an identified bioemulsifier based on EPA requirements.
- Cultured multiple species of Arctic bacteria to survey their emulsification production capacity.
- Confirmed emulsification capacity on kerosene, then tested on crude oil.
- Mentored an undergraduate who continued work on this project for two months.

Research assistant to Dr. Miriam Diamond — **University of Toronto**
Machine Learning for Dark Matter Search in SuperCDMS — *May–Dec 2020*
- Grant from Arthur McDonald Canadian Astroparticle Physics Research Institute.
- Acquired a knowledge-base in particle physics in order to apply machine learning to physics problems.
- Researched and engineered both supervised and unsupervised machine-learning solutions to discriminate between single and multiple recoil events in the particle detector using HPC techniques on ComputeCanada supercomputers.
- Worked closely with physicists to understand the data and produce the adequate feature set through feature engineering, along with my fellow research assistant.

Independent — **University of Toronto**
Neural Plasticity & Unsupervised Learning — *Jul 2019–May 2020*
- Recruited and led a team of three undergraduate students.
- Researched and developed novel ideas to model neural plasticity in neural networks.
- Invited to present our research in a second-year cognitive science class at the University of Toronto.
- Published a preprint in a public computer science archive.

Research assistant to Dr. Steve Mann — **University of Toronto**
Brain Computer Interfaces — *May 2019–Apr 2020*
- Developed a working Brain-Computer interface with Muse EEG, Arduino and Raspberry Pi to perform Steady State Visually Evoked Potentials experiments.
- Captured the world's first image of vision and of multiple ayinographs, recording the eye's input as a camera using SSVEP, in line with the lab's sousveillance theme. Implemented possibly the first digital lock-in amplifier on iOS.
- Researched and developed a new way to treat prosopagnosia using a computer vision and mobile applications.

Research assistant to Dr. Ahamad Dhaini — **American University of Beirut**
Computer Aided Diagnostics — *May–Aug 2018*

- Rewrote and worked on adapting an existing optical coherence tomography scanning algorithm to different scanner formats.
- Used machine learning to identify valid corneal scan frames from the original video format.
- Used OpenCV to detect corneal haze contours and the corneal demarcation line.
- My contributions and findings directly resulted in a comparative study eligible for publication.

Field Work

microSHIFT 2025, Central Arctic, Arctic Ocean *May 2025–34 days*
- Participated in the microSHIFT 2025 expedition, led by Dr. Karley Campbell, as a scientist aboard R/V *Kronprins Haakon*.
- Planned and executed my own field campaign to optimize genomic methods for sea ice and to broadly characterize sea-ice and related microhabitats using metatranscriptomics.
- Led the genomics sampling for the microSHIFT project on behalf of Dr. Karley Campbell.

SCOPE 2025, Hokkaido, Japan *Jan 2025–12 days*
- Participated in the SCOPE 2025 international expedition, led by Dr. Daiki Nomura, as an invited researcher.
- Successfully planned and executed a field campaign for the collection of frost flowers from Lake Akana and sea-ice samples from Saroma-ko Lagoon.

BREATHE 2023, Yermack Plateau, Arctic Ocean *May 2023–19 days*
- Participated in the BREATHE 2023 expedition and field school, led by Dr. Karley Campbell, as an invited researcher aboard R/V Kronprins Haakon.
- Successfully planned and executed my own field campaign for the collection of sea ice brine for genomic work.

VISIONS'22, North Eastern Pacific Ocean *Aug 2022–10 days*
- Funded to participate on the first leg of the cruise, led by Dr. Deb Kelley, aboard the R/V *Thomas G. Thompson*.
- Led a 6-hour ROPOS dive to sample diffuse flow hydrothermal vent fluid at Axial seamount for Dr. Rika Anderson.

Biogeochemical Exchanges at Sea Ice Interfaces, Canadian Arctic *May 2022–14 days*
- Funded to attend the BEPSII summer field school in Cambridge Bay, Canada, in the Arctic.
- Attended over 30 hours of lecture on sea-ice physics, chemistry and biology.
- Learned fundamental field techniques for Arctic sampling: snow characterization, ice coring, sackhole brine sampling, seawater sampling, and photosynthetic active radiation measurements.

Publications

2025: Kanaan, G., Page-Roth, J., & Deming, J.W. *Drivers of bacterial community composition in an ice-covered geothermally heated lake*. (in prep).

2025: Deming, J.W., Cooper, Z.S., Eicken, H., Harrison, K., Iwahana, G., Kanaan, G., Rapp, J.Z., & Young, J.N. *Uncovering the mysteries of cryopegs: Geo-microbial evolution in subzero brines isolated geophysically within permafrost. Proceedings of the National Academy of Sciences*. (in prep).

2025: Cooper, Z.S., Carpenter, S.D., Kanaan, G., & Deming, J.W. *Cryomarinobacter cryopegasus, gen. nov., sp. nov, isolated from Arctic subzero cryopeg brine*. (in prep).

2025: Kanaan, G., Yang, Z., & Neveu, M. *Detectability of extracellular compounds from icy moon analogues under Enceladus plume conditions. Astrobiology* (submitted, in review).

2025: Kanaan, G., & Deming, J.W. *Multiple roles of DNA methylation in sea-ice bacterial communities and associated viruses. The ISME Journal*.

2023: Kanaan, G., Hoehler, T.M., Iwahana, G., & Deming, J.W. *Modeled energetics of bacterial communities in ancient subzero brines. Frontiers in Microbiology*.

2021: Kanaan, G., Zheng, K.W., & Fenaux, L. *A novel approach to lifelong learning: The plastic support structure. arXiv* 2106.06298.

2020: Mann, S., Pan, Z., Tao, Y., Gao, A., Tao, X., Garcia, D.E., Shi, D., & Kanaan, G. *Face Recognition and Rehabilitation: A Wearable Assistive and Training System for Prosopagnosia*. In *2020 IEEE In-*

ternational Conference on Systems, Man and Cybernetics (SMC'20), Toronto, ON, Canada, pp. 731-737. doi:10.1109/SMC42975.2020.9283058.

2019: Mann, S., Lam, D., Mathewson, K.E., Pierce, C., Stairs, J., Hernandez, J., Kanaan, G., Piette, L., Khokhar, H., & Mann, C. *The Human Eye as a Camera*. In *IEEE International Conference on E-health Networking, Application & Services (HealthCom'19)*, Bogota, Colombia, pp. 1-8. doi:10.1109/HealthCom46333.2019.9009592.

2019: Mann, S., Defaz, D., Pierce, C., Lam, D., Stairs, J., Hernandez, J., Li, Q., Xiang, Y.X., Kanaan, G., Chen, H., Aylward, G., Jorritsma, M., & Mann, C. *Keynote – Eye Itself as a Camera: Sensors, Integrity, and Trust*. In *5th ACM Workshop on Wearable Systems and Applications (WearSys'19)*, Association for Computing Machinery, New York, NY, USA, 1–2. `https://doi.org/10.1145/3325424.3330210`

Presentations & Posters

2025: Kanaan, G. & Deming, J.W. *Bacterial use of DNA methylation to acclimate to sea ice*. Poster, Gordon Research Conference on Polar Marine Sciences, March 9–14, Lucca (Barga), Italy.

2025: Kanaan, G. & Deming, J.W. *A sea-ice perspective on bacterial DNA methylation*. Talk, Gordon Research Seminar on Polar Marine Sciences, Lucca, Italy.

2024: Kanaan, G. & Deming, J.W. *Bacterial use of DNA methylation in sea ice*. Invited talk, Institut Biologique de l'École Normale Supérieure, Paris, France.

2025: Kanaan, G. & Deming, J.W. *Extremophile DNA methylation and epigenetic memory*. Special session: Pushing the frontiers of extreme microbiology. Poster, ISME19, 19th International Conference on Microbial Ecology, August 18–23, Cape Town, South Africa.

2025: Veseli, I., Schechter, M.S., Henoch, A., Trigodet, F., Sever, M., Kiefl, E., Klein, M.L., Kanaan, G., Salazar, V.W., Fink, I., Buck, M., Telatin, A., Watson, A.R., Deveaud, E., Utter, D.R., Fernandez-Guerra, A., Youngblut, N., Speth, D.R., Willis, A.D., Bartelme, R., Kananen, K., Quiles, C., Bradley, P.H., Miller, S.E., & Eren, A.M. *Making big data accessible to microbiologists: lessons from developing a versatile software ecosystem for multi-'omics analysis*. Talk, ISME19, 19th International Conference on Microbial Ecology, August 18–23, Cape Town, South Africa.

2024: Bravenec, A., Junge, K., Firth, E., Kanaan, G., & Catling, D.C. *Psychrophiles and the thermodynamic and kinetic aspects of brines: implications for icy worlds*. Poster, Astrobiology Science Conference, May 5–10, Providence, Rhode Island.

2023: Campbell, K., McKay, R., Keonig, Z., Osanen, J., Laber, C., Kanaan, G., Sadler, M., Van Niekerk, J., Brusselman, A., & Itkin, P. *BREATHE field school goes with the floe: Insights from an early-career training program*. Poster, The Nansen Legacy Symposium, November 7–9, Tromsø, Norway.

2023: Kanaan, G. & Deming, J.W. *Searching for memory: methylation in sea-ice bacteria*. Poster, Gordon Research Conference on Polar Marine Sciences, March 5–10, Ventura, California.

2023: Kanaan, G. & Deming, J.W. *The potential for microbial memory in sea ice*. Talk, Gordon Research Seminar on Polar Marine Sciences, March 5–10, Ventura, California.

2022: Kanaan, G., Hoehler, T.M., & Deming, J.W. *Understanding the microbial energetics of cold, salty, and isolated systems: Analogs for other icy worlds*. Poster, 4th International Workshop on Microbial Life under Extreme Energy Limitation, September 5–9, Sandbjerg Manor, Denmark.

Workshops

EBAME 8 Workshop on Computational Microbial Ecogenomics **Brest, FR**
Learned various bioinformatic techniques from Dr. Loïs Maignien, Dr. Tom Delmont, et al. *Oct 2024*

4th International Workshop on Microbial life under extreme energy limitation **Sønderborg, DK**
Presented calculations of the minimum metabolic requirements in isolated permafrost communities *Sep 2022*

Awards, Grants & Scholarships

Dissertation Completion Award **6,000 USD**
Washington NASA Space Grant Consortium *Fall 2025*
Awarded for academic excellence in support of dissertation writing.

Beatrice Crosby Booth Endowed Fellowship **9,000 USD**
University of Washington, School of Oceanography *Summer 2025*
Awarded for academic achievement.

Egtvedt Endowed Scholarship in Oceanography **1,000 USD**
University of Washington, School of Oceanography *Summer 2025*
Awarded for academic achievement.

Theodore H. and Marie M. Sarchin Endowed Fellowship in Oceanography **9,000 USD**
University of Washington, School of Oceanography *Fall 2025*
Awarded for academic achievement.

Scholar Mobility Fund **2,400 EUR**
ISME *May 2025*
Awarded to support participation in the microSHIFT 2025 expedition

Morse Scholar Exchange Program **2,000 USD**
Friday Harbor Labs *Jan 2025*
Awarded to fund a proposal sampling frost flowers at Lake Akan, Japan

Hall Conservation Genetics Award **10,000 USD**
University of Washington *Apr 2023*
Awarded to fund a proposal I developed on DNA methylation of sea-ice bacteria

Washington Space Grant **4,000 USD**
Washington NASA Space Grant Consortium *Sep 2022*
Awarded to fund a NASA Science Mission Directorate project, modeling bacterial energetics in the extreme environment of subzero brine

Leo Cup Award **40,000 USD**
University of Washington, School of Oceanography *Sep 2021*
Awarded to the best academic-year proposal for oceanographic research tackling marine pollution

Cross-Disciplinary Internship **10,000 USD**
Arthur B. McDonald Canadian Astroparticle Physics Research Institute *May 2020*
One semester of support for interdisciplinary research in particle physics

TPE Excellence Award
International College *Jun 2017*
Awarded to the student with the most original and best performing presentation on the national exam

WWDC Scholarship
Apple *Jun 2015*
Won a scholarship awarded to 350 students. Attended labs and sessions held by Apple engineers including the UI Design Labs. Met Apple engineers and discussed future technologies and ongoing personal projects

Hackathon–Runner Up (Move-Counter App)
AltCity *May 2014*
Designed, developed and pitched a working app in 12 hours with the help of a designer. Youngest participant. The app I built, Move-Counter, sported the capability of recording a given move, storing it as a hash then recognizing it.

Skills & Certificates

Medical certifications: Medically certified for a Winfly in Antarctica in 2023 to Palmer station for 6 months,

and for work on the Norwegian icebreakers in the high Arctic beyond the primary search and rescue zone.

Lab skills: Sterile technique, culturing, isolation, kerosene emulsification index assay, phenol sulfuric-acid assay, centrifugation, epifluorescence microscopy, nucleic acid extraction, spectrophotometry, differential scanning calorimetry, nanopore sequencing, media elaboration, extracellular polysaccharide isolation, GCMS analysis, chemostat operation

Bioinformatics Skills: Algorithm development, basecalling, alignments, mapping, manual binning, automatic binning, anvio, functional gene analysis, epigenetic analysis, machine learning

Field skills: Ice coring, sackhole brine sampling, PAR measurement, snow pits, seawater sampling, ROV operations, CTD operations, safety protocols.

Certificates: NAUI open water diving, NAUI drysuit diving, Norwegian polar institute survival suit use, Norwegian polar institute polar bear guard.

Programming languages: Objective-C/C, Swift, Python, PHP, Verilog, Bash, HTML, Markdown, CSS, C++, Java, Julia.

Computer science skills: Windows, Linux/Unix, macOS, Git, Unity, OpenCV, iOS/macOS SDK (Xcode), Spacy, VPS Deployment, Cydia Substrate, SciKit, Muse EEG, Tkinter, DTN, CORE, debuggers (gdb, lldb), PyTorch, HPC, Polars.

Language skills: Native speaker of French and English. Proficient in Arabic.

Volunteering

APECS
Project Group Co-Lead Podcast — *Sep 2024–Sep 2025*
- Organized and led the Polar Times science communication podcast for the Association of Polar Early Career Scientists.
- Oversaw a team of over 15 people divided into teams which produced different month-long topical deep dives.
- Supervised writing, editing, research, interviewing, marketing, recording, and publication.

APECS
Project Group Lead Mentorship Award — *Sep 2024–Sep 2025*
- Organized and led the international mentorship award project group for the Association of Polar Early Career Scientists.

Extremophiles
Journal Reviewer — *2024*
- Invited to review a subsequently published paper in the Extremophiles journal.

Graduate Climate Conference
Committee Member — *Sep 2023–Nov 2024*
- Member of the recordings and evaluation committee.
- Reviewed abstracts submitted for conference participation as an expert on polar regions, oceanography, and microbiology.

Pacific Science Center
Polar Science Day Volunteer — *Dec 2022, Mar 2024*
- Interpret and teach about Arctic Ocean salinity using a salinity taste test game.

Seattle Aquarium
Marine Science Interpreter — *May 2022–Ongoing*
- Interpret and animate various exhibits on local fauna and flora to thousands of guests.

Resilient Hearts Animal Sanctuary
Temporary Dog Foster — *May 2022–Ongoing*
- Fostered dogs for the local animal shelter.

UW Graduate Application Mentorship Program
Mentor — *Oct–Dec 2021*
- Guided two prospective international undergraduate students through the graduate student application process.

UW Academic & Recreational Graduate Oceanographers
Officer *Sep 2021–Ongoing*
- Social events coordinator for the School of Oceanography's graduate student organization.
- Planned and executed many social events for the graduate student body including park hangouts, barbecues, movie nights, and game nights. With my cohort, organized monthly social gatherings and a yearly graduate student retreat at Friday Harbor Labs on San Juan Island, Puget Sound, WA.

University of Washington CubeSat Team
Member *Sep 2021–May 2022*
- Worked on satellite communication infrastructure.

University of Washington Indoor Farming Project
Member *Sep 2021–May 2022*
- Club focused on hydroponics and sustainable farming. Produces food that is donated weekly to the university food bank.

University of Toronto Aerospace Team
Member *Sep 2019–May 2020*
- Developed a biological mission concept for the next SmallSat mission involving the study of herpes.
- Reached out to launch companies as well as agencies coordinating biological experiments on ISS to study the feasibility of conducting an experiment in space.

NeuroTech UofT
Director of Cortical Apps *Sep 2018–May 2019*
- Responsible for the coordination of the various teams building applications making use of brain computer interfaces.

Personal Projects

Server Hosting: DNS, VPN, & More *Nov 2012–Ongoing*
- Maintained a public facing ubuntu server hosting a myriad of services with 99.9% uptime.
- Hosted and configured a secure VPN based on OpenVPN, and later WireGuard.
- Hosted and configured a Minecraft server complete with automatic backups.
- Hosted and configured a personal DNS service using unbound, complete with ad-blocking capabilities using PiHole.
- Hosted and configured a private Siri proxy service used to get Siri on jailbroken iPhone 4.
- Hosted, configured and made my personal website.

Published 11 Apps & Tweaks
- Published 8 iOS Apps, 3 Tweaks (System modifications distributed through Cydia).
- 3 Tweaks received unprompted coverage from respectable review sources.
- Bloard (Tweak) received over a million downloads.
- Airly (App) improves on the Precision-Time-Protocol and allows precise music playback across devices.

Personal Experience

Lived in: Beirut, London, Toronto, Washington DC, Strasbourg, Seattle.

Well traveled (over 20 countries), and multilingual, I bring a diverse and unique background to any team.

Interests: music, history, running, skiing, biking, computational neuroscience, space, trains, sailing, chess, photography, backpacking, .

Self-taught: I am motivated by curiosity and my passion for science

Press Appearances

Article in the University of Washington's School of Oceanography about the BREATHE cruise in 2022.

Article in the University of Washington's School of Oceanography about the Leo Cup Award in 2021.

Article in the University of Toronto news, and national Lebanese news outlet l'Orient le Jour about my NASA internship in 2019.

Featured in a segment on young developers and entrepreneurs on a national television station in Lebanon.